Synthesis and Molecular Catalysis with Organo-Alkaline Earth Metal Complexes

by

Rohit Kumar

10CC17A26023

A thesis submitted to the
Academy of Scientific & Innovative Research
For the Award of the Degree of
DOCTOR OF PHILOSOPHY
in
SCIENCE

Under the supervision of

Dr. Sakya Singha Sen

CSIR-National Chemical Laboratory, Pune

Academy of Scientific and Innovative Research
AcSIR Headquarters, CSIR-HRDC campus
Sector 19, Kamla Nehru Nagar,
Ghaziabad, U.P.–201 002, India

August-2022

Certificate

This is to certify that the work incorporated in this Ph.D. thesis entitled, "*Synthesis and Molecular Catalysis with Organo-Alkaline Earth Metal Complexes*", submitted by *Rohit Kumar* to the Academy of Scientific and Innovative Research (AcSIR), in partial fulfillment of the requirements for the award of the Degree of *Doctor of Philosophy in Science*, embodies original research work carried-out by the student. We, further certify that this work has not been submitted to any other University or Institution in part or full for the award of any degree or diploma. Research material(s) obtained from other source(s) and used in this research work has/have been duly acknowledged in the thesis. Image(s), illustration(s), figure(s), table(s) etc., used in the thesis from other source(s), have also been duly cited and acknowledged.

(Signature of Student)
Rohit Kumar
Date: 05-08-2022

(Signature of Supervisor)
Dr. Sakya Singha Sen
Date: 05-08-2022

STATEMENTS OF ACADEMIC INTEGRITY

I , Rohit Kumar a Ph.D. student of the Academy of Scientific and Innovative Research (AcSIR) with Registration No. 10CC17A26023 hereby undertake that, the thesis entitled "Synthesis and Molecular Catalysis with Organo-Alkaline Earth Metal Complexes" has been prepared by me and that the document reports original work carried out by me and is free of any plagiarism in compliance with the UGC Regulations on *"Promotion of Academic Integrity and Prevention of Plagiarism in Higher Educational Institutions (2018)"* and the CSIR Guidelines for "*Ethics in Research and in Governance (2020)"*.

Signature of the Student
Date : 05-08-2022
Place : CSIR-NCL, Pune

It is hereby certified that the work done by the student, under my/our supervision, is plagiarism-free in accordance with the UGC Regulations on *"Promotion of Academic Integrity and Prevention of Plagiarism in Higher Educational Institutions (2018)"* and the CSIR Guidelines for "*Ethics in Research and in Governance (2020)"*.

NA

Signature of the Co-supervisor (if any)
Name :
Date :
Place :

Signature of the Supervisor
Name : Dr. Sakya Singha Sen
Date : 05-08-2022
Place : CSIR-NCL, Pune

This dissertation is dedicated to the almighty God

and all my family members

ACKNOWLEDGEMENTS

A Ph.D. journey explores who you are in many aspects; it's a singular experience that leads you along a formerly unexplored path to reach your ultimate destination. There are so many people whose support, encouragement, and inspiration are necessary. I owe those people for their kind wishes and blessings in finishing this journey because one can't succeed without the guidance and support of the research supervisor, friends, and well-wishers. I take this opportunity to acknowledge and express my deepest gratitude to everyone who has helped and supported me directly or indirectly throughout for making the research work described in this thesis possible.

First and foremost, I would like to take this opportunity to express my sincere gratitude to my research supervisor ***Dr. Sakya Singha Sen,*** *who has been patient enough to respect my personal life yet wise enough to push me when necessary. He has taught me a lot in the research field and about living a beautiful life which I never expected from a mentor. I have learned many things from him, mainly how to deal with scientific and real-life problems by being cool, calm, and composed. I have been deeply impacted by his excitement, integral view on research, and commitment to only delivering work of the higher impact. During the last five years from his interactions, I have learned extensively from him, including how to raise new possibilities, regard an old question from a new perspective, approach a problem through systematic thinking, data-driven decision making, and exploiting serendipity. I owe him lots of gratitude for having me shown this way of research. He constantly emphasizes inculcating the habit of critical thinking and teaches us about the dos and don'ts in science and life. I feel fortunate and privileged to be associated with him and part of his research group. I could never wish for a better supervisor. I'll miss the long conversation over at the group party, not only about the research but on several other topics. I will remain a great fan of his coolness, style, and excellent communication skills.*

This journey (Ph.D.) cannot be successful without the suggestions given by my Doctoral Advisory Committee (DAC) members during the DAC meetings. I express my sincere thanks to the Doctoral Advisory Committee members, ***Dr. E. Balaraman, Dr. Kumar Vanka, Dr. Subashchandrabose Chinnathambi,*** *and* ***Dr. T. Raja,*** *for their contribution in stimulating suggestions and encouragement during my Ph.D.*

I am grateful to ***Prof. Ashish Lele*** *(Director, CSIR-NCL),* ***Prof. A. K. Nangia*** *(Former Director, CSIR-NCL),* ***Dr. Shubhangi B. Umbarkar*** *(Head, Catalysis and Inorganic Chemistry Division),* ***Dr. D. Srinivas*** *and* ***Dr. C. S. Gopinath*** *(Former Head, Catalysis and Inorganic Chemistry Division), for giving me this opportunity and providing all necessary infrastructure and facilities to carry out my research work. I would like to acknowledge all the support from Catalysis and Inorganic Chemistry Division office staff. I am also highly thankful to the* ***Council of Scientific & Industrial Research*** *(****CSIR****), New Delhi, and the* ***Academy of Scientific and Innovative Research*** *(****AcSIR****), Ghaziabad, for the financial assistance and coursework facilities, respectively.*

My sincere thanks to ***Dr. Sayan Bagchi, Dr. Samir Chikkali, Dr. E Balaraman, Dr. C. V. Ramana, Dr. B. L. V. Prasad, Dr. Paresh Dhepe, Dr. Santosh Babu, Dr. Pradip Maity, Dr. Utpal Das, Dr. Arup Kumar Rath, Dr. Janardan Kundu, Mrs. Kohle, Mr. Iyer, Mr. Purushothaman, Library staff, Student academic office staff,*** *and all* ***other scientists of NCL*** *for their motivation, constant encouragement, and support.*

I am highly grateful to our collaborators ***Dr. Kumar Vanka*** *(CSIR-NCL, Pune) and his doctoral students,* ***Soumya Ranjan Dash****,* ***Dr. Shailja Jain****,* ***Vipin Raj K****,* ***Dr. Subhrashis Banerjee****,* ***Himanshu Sharma, Dr. Ruchi Dixit, Dr. Tamal Das*** *and* ***Dr. Debasis Koley*** *(IISER, Kolkata) and his doctoral students,* ***Dr. Sayan Datta****,* ***Praval Pratap Singh*** *for their essential support in DFT calculations,* ***Dr. Rajesh Gonnade*** *(CSIR-NCL, Pune) and his group members,* ***Dr. Ekta, Dr. Samir, Dr. Shridhar, Dr. Veer, Christy, Dr. Nitai, Tabrez, Debjani and Bhupender,*** *for single-crystal X-ray diffraction measurements, and for valuable suggestions and help at different parts of my research journey,* ***Dr. B. Shantakumari*** *and her students for the help in HRMS analysis, and* ***Mrs. Ansanas*** *for elemental analysis. I would also like to thank* ***Dr. Sapna Ravindranathan, Dr. Udaya Kiran Mareli, Dr. T. G. Ajithkumar,*** *and their team* ***Dinesh, Satish, Meenakshi, Deepali, Sherminaj,*** *and* ***Nita*** *for the NMR facilities. I am also grateful to our collaborator for introducing me to the luminescent field,* ***Joy Chatterjee*** *(IISER, Pune).*

I consider myself highly privileged to work and spend most of my day with the Sen Lab's wonderful and motivated young research team of colleagues. My experience studying through our group lectures has been fantastic. It is my pleasure to thank my labmates, ***Dr. Sanjukta Pahar****,* ***Gargi Kundu****,* ***VS Ajith Kumar****,* ***Biplab Mahata****,* ***Kajal Balayan*** *and former labmates*

Dr. Moumita Pait, ***Dr. Yuvaraj K.*** *for their kind support and suggestions during my research work. Special thanks to my labmates* ***Kritika Gour*** *and* ***Vishal Kumar Sharma*** *for always being supportive and helpful whenever I needed them. I would like to express my deepest gratitude to my former labmates,* ***Dr. Sandeep Yadav***, ***Dr. V. S. V. S. N. Swamy***, *and* ***Dr. Milan Bisai,*** *for instructing me in sensitive chemistry. Especially* ***Dr. Sandeep Yadav*** *for guiding me most of the time whenever it was needed.*

I am highly grateful to ***Dr. Shabana Khan*** *(from IISER-Pune) and her research group* ***Dr. Shiv Pal***, ***Dr. Neha***, ***Rajarshi***, ***Dr. Nasrina***, ***Nilanjana***, ***Jabed,*** *and* ***Moushakhi,*** *for their kind help during the different fragments of my research journey.*

Beyond the group, many well-wishers from CSIR-NCL made my journey more comfortable. I feel that this journey is incomplete without hostel life. I am thankful to ***Dr. Debu da, Dr. Ashish, Dr. Rangrajan, Dr. Reddy, Dr. Anupam Da, Neha, Chandan, Dr. Abhijit Da, Dr. Koushik da, Dr. Jaganath Da, Dr. Siba Da, Dr. Vinod, Dr. Manoj, Dr. Garima, Dr. Tapas da, Dr. Sushil, Samadhan, Srijan, Prem, Bharath, Viksit, Dr. Abdul, Dr. Ambrish, Ashish Da, Naru, Shibam, Chandu, Sonia, Dr. Rahul Jagtap, Dr. Satej, Sadhna, Dr. Shailaja, Dr. Subhrashis da, Dr. Anup, Dr. Arun Dadwal, Lavanya, Priya, Priyanka Walko, Priyanka Halder, Vinita, Mahesh Pol, Pinka, Singham, Vikash Chaturvedi, Ravi Ranjan, Himanshu, Akash, Dr. Neeta, Dr. Ravindar Phatke, Dr. Ruchi, Dr. Ayesha, Dr. Vinita, Dr. Tamal, Rashid, Anirban, Dr. Mahendar Power, Dr. Sibedatta, Mahendra Wagh, Shahbaz, Indrajeet, Dr. Shrikant, Dr. Shrikant Khake, Sandy, Sidharth, Santosh, Prashant Yadav, Rajni, Hari, Kranti, Smita, Ravi, Surya, Fayis, Pawan, Siddarth, Dr. Atish*** *from NCL for their kind help and support.*

I am lucky to have so many friends in and away from CSIR-NCL, whose company never allowed me to feel bored during the entire course of my work. I especially thank my brother cum friends, ***Rohit Kumar***, ***Golu Parte***, ***Dr. Kailas Pandhade***, ***Sachin Prajapati***, ***Dr. Nirshad Alam, Manish Prajapati***, ***Pawan Gurjar***, ***Dharmendra Singh,*** *for their kind support and love. Special thanks to* ***Kailash Singh(Baba), Devyani Dahare, Dr. Suman Devi***, ***Priyanka Katariya***, ***Lakshmi***, ***Gitanjali***, ***Dr. Govind Porwal, Sumanta, Kakde*** *and* ***Anirban*** *for making my initial days enjoyable at the hostel. I always enjoy their company, and they are my strength in many things. I am lucky to have such a big family at NCL. No words are sufficient to acknowledge my prized friends in and out of NCL who have helped me at various*

stages of my work at NCL. I wish to thank Mr. Mane, Mr. Koli, Ms. Nita, Mrs. Uma, Mr. Pathan, Mr. Deshmukh, Mr. Date, and all support staff whose names are not mentioned here, but had always been ready to understand my problem and helped me in all possible manners.

*My family is always a source of inspiration and great moral support for me in pursuing my education. I owe a lot to my beloved parents, who encouraged and helped me at every stage of my personal and academic life and longed to see this achievement come true. My sincere thanks to my beloved family members, my father '**Premchand**' and mother '**Satyaviri Devi**'. It would be incomplete without mentioning about my dear mother. I am fortunate to have my mother, who always lived for us and made countless sacrifices to improve our lives. I am glad to announce that today whatever I am, it is only because of my mother, and I can never even think of paying it back. My uncles **Satveer Tanwar**, **Balraj Tanwar, Rakesh Tanwar, Mukesh Kumar, Pappu Kumar, Billu Kumar,** my aunties **Santosh Devi, Sunita Devi, Sudesh Devi,** my sisters **Guddi**, **Soniya**, **Ritu, Bhawna, Ankita,** my brother-in-law **Kunwarpal**, my brothers **Krishna Kumar, Indraj Singh**, **Sushil, Sonu, Amit, Golu, Anuj, Praveen, Chintu, Naveen,** my sister-in-laws **Poonam, Neha, Manju** for their endless love, support, and sacrifice. I am very much indebted to my whole family, who supported me in every possible way to see the completion of this research work.*

*Special thanks to my CCSU(Chaudhary Charan Singh University, Meerut) campus teachers, **Meenu Teotia**, **Rakesh Soni**, **Nazia Tarannum**, **Shilpi Sexena,** friends, **Nishant**, **Manish, Sunny, Sachin, Saddam, Vishal, Himanshu, Raju, Ankur, Nitin,** and **Pankaj**. Further, I would like to thank my hometown and school friends **Rohit**, **Pankaj**, **Sonu**, **Rinku**, **Sankar**, **Sunil**, **Chote**, **Pradeep**, **Moolchand**, **Sumit**, **Bittu**, **Kapil, Aabid, Aarif, Vasim, Imran, Apsar, Javed, Asif, Akshay, Ankit** for the cherished friendships and creating a wonderful atmosphere around me outside the lab. I wish to thank all my teachers from nursery to college level, for their guidance and support whose names are not mentioned here.*

I wish to thank the wonderful scientific community, whose achievements are a constant source of inspiration for me. Above all, I extend my gratitude to the Almighty God for giving me the wisdom, health, and strength to undertake this research work and enabling me to complete it.

Rohit Kumar

Contents of the Thesis

Chapter 2:

Chapter 3:

Chapter 4:

Chapter 5:

Abbreviations

Units and standard terms

BDE	Bond Dissociation Energy
°C	Degree Centigrade
DFT	Density Functional Theory
mg	Milligram
h	Hour
Hz	Hertz
mL	Millilitre
min.	Minute
mmol	Millimole
NPA	Natural Population Analysis
ppm	Parts per million
%	Percentage
M.P.	Melting Point
B. P.	Boiling Point
Calcd.	Calculated
CCDC	Cambridge Crystallographic Data Centre
CIF	Crystallographic Information file

Chemical Notations

Ar	Aryl
MeCN	Acetonitrile
$CDCl_3$	Deuterated chloroform
C_6D_6	Deuterated benzene
DMSO-d_6	Deuterated dimethyl sulfoxide
Toluene-d_8	Deuterated toluene
DMF	N, N'-Dimethylformamide
DCM	Dichloromethane
DMSO	Dimethyl sulfoxide
EtOH	Ethanol
Me	Methyl
Et	Ethyl
Dipp	Di-isopropylphenyl
*i*Pr	Isopropyl
*t*Bu	Tertiary butyl
EtOAc	Ethyl Acetate
HBpin	Pinacolborane
MeOH	Methanol
py	Pyridine
THF	Tetrahydrofuran

Et_2O	Di-ethyl ether
TMSCN	Trimethylsilyl cyanide
*n*BuLi	*n*butyllithium

Other Notations

δ	Chemical shift
J	Coupling constant in NMR
Equiv.	Equivalents
HRMS	High Resolution Mass Spectrometry
NMR	Nuclear Magnetic Resonance
RT	Room temperature
UV	Ultraviolet
SC-XRD	Single Crystal X-Ray Diffraction

General remarks

- All chemicals were purchased from commercial sources and used as received.
- All reactions were carried out under inert atmosphere following standard procedures using Schlenk techniques and glovebox.
- Deuterated solvents for NMR spectroscopic analyses were used as received. All ^{1}H NMR and ^{13}C NMR analysis were obtained using a Bruker or JEOL 200 MHz, 400 MHz or 500 MHz spectrometers. Coupling constants were measured in Hertz. All chemical shifts are quoted in ppm, relative to TMS, using the residual solvent peak as a reference standard.
- HRMS spectra were recorded at UHPLC-MS (Q-exactive-Orbitrap Mass Spectrometer) using electron spray ionization [(ESI^{+}, +/− 5kV), solvent medium: acetonitrile and methanol] technique and mass values are expressed as *m/z*. GC-HRMS (EI) was recorded in Agilent 7200 Accurate-mass-Q-TOF.
- The solvent used were purified by an MBRAUN solvent purification system MBSPS-800 and further dried over activated molecular sieves prior to use.
- The preparation of sensitive NMR samples was carried out in a Glove box or under an inert atmosphere of argon applying standard Schlenk technique.
- Column chromatography was performed on silica gel (100-200 mesh size).
- LC-MS were obtained using a Q Exactive Thermo Scientific and an Agilent Technologies 6120.
- Chemical nomenclature (IUPAC) and structures were generated using ChemDraw Professional 20.1.

General remarks

- All chemicals were purchased from commercial sources and used as received.
- All reactions were carried out under inert atmosphere following standard procedures using Schlenk techniques and glovebox.
- Deuterated solvents for NMR spectroscopic analyses were used as received. All ^{1}H NMR and ^{13}C NMR analysis were obtained using a Bruker or JEOL 200 MHz, 400 MHz or 500 MHz spectrometers. Coupling constants were measured in Hertz. All chemical shifts are quoted in ppm, relative to TMS, using the residual solvent peak as a reference standard.
- HRMS spectra were recorded at UHPLC-MS (Q-exactive-Orbitrap Mass Spectrometer) using electron spray ionization [(ESI^{+}, +/− 5kV), solvent medium: acetonitrile and methanol] technique and mass values are expressed as *m/z*. GC-HRMS (EI) was recorded in Agilent 7200 Accurate-mass-Q-TOF.
- The solvent used were purified by an MBRAUN solvent purification system MBSPS-800 and further dried over activated molecular sieves prior to use.
- The preparation of sensitive NMR samples was carried out in a Glove box or under an inert atmosphere of argon applying standard Schlenk technique.
- Column chromatography was performed on silica gel (100-200 mesh size).
- LC-MS were obtained using a Q Exactive Thermo Scientific and an Agilent Technologies 6120.
- Chemical nomenclature (IUPAC) and structures were generated using ChemDraw Professional 20.1.

Synopsis of the Thesis to be submitted to the Academy of Scientific and Innovative Research for Award of the Degree of Doctor of Philosophy in Chemistry	
Name of the Candidate	**Mr. Rohit Kumar**
Degree Enrolment No. & Date	**PhD in Chemical Sciences (10CC17A26023); 07 Dec 2018**
Title of the Thesis	**Synthesis and Molecular Catalysis with Organo-Alkaline Earth Metal Complexes**
Research Supervisor	**Dr. Sakya S. Sen (CSIR-NCL, Pune)**

Keywords: *Alkaline Earth Metals, Catalysis, Homoleptic and Heteroleptic Complexes, Fluorescence, Quantum Yield, Hydroboration and Cyclotrimerization*

Chapter I: Introduction

Transition metal chemistry forms the heart of catalysis due to the availability of partially filled d-orbitals allows them for fast and reversible changes in the metal's oxidation states. However, these metals are expensive, and their byproducts are hazardous. The current trend in chemistry is to move towards cheaper alternatives. The last two decades have been witnessed that main group metal complexes, especially alkaline earth metal complexes, were used as the alternative to transition metal complexes because these metals are cheap in price and biocompatible in nature. The organo alkaline earth metal chemistry was started more than a century ago. In 1901, Grignard synthesized organomagnesium halides (Grignard reagents),[1] which proved to be a milestone in organometallic chemistry. Grignard reagents have been utilized as strong bases, nucleophiles, and alkyl and aryl transfer reagents.

Statement of problem:

As we move down the group 2, the higher analogs of Mg have not been studied extensively. The electro positivity increases as moving down the group, which leads to a rise in the metal-carbon bond polarity, making the metal-carbon bond weaker and a significant increase in reactivity. Therefore, the Grignard-like synthetic routes face the ether cleavage reactions and lead to the side

reactions like Wurtz-coupling; ($2RI + Ca \rightarrow R\text{-}R + CaI_2$).[2] In addition, the bigger challenge is the Schlenk equilibrium, where the homoleptic complexes are more favored than the heteroleptic complexes.[3] Over the last two decades, an array of heavy organocalcium metal compounds has been synthesized using various sterically demanding monoanionic ligand systems such as amidinate, guanidinate, and *β*-diketiminate.[4] The calcium chemistry is marked by its stable +2 oxidation state with d^0 electronic configuration. Their property resembles the trivalent and redox inactive lanthanides having d^0 electronic configuration. The chemistry of Ca is highly similar to that of Yb^{2+} in terms of Lewis acidity and size (Ionic radius: Yb^{2+}: 1.02 Å; Ca^{2+}: 1.00 Å). The reactivity of calcium compounds is similar to the ytterbium compounds in terms of catalytic activity for dehydrogenative silylation of amines.[5] The magnesium and calcium-based catalysts may be a key player in organometallic chemistry due to their cost effectiveness, large abundance, and biocompatibility. Despite these impressive headways, there is a scope to develop easy synthesizable magnesium and calcium-based catalysts with more stability and catalytic reactivity.

Objective: To synthesize soluble heteroleptic/monomeric magnesium and calcium complexes using suitable ligands that can provide metal steric and electronic protection and their exploration as a catalyst.

Methodology: It is based on the synthesis of soluble monomeric magnesium, calcium complexes and their utilization as a catalyst for hydroboration and cyclotrimerization. We have also studied the luminescent properties of fluorescent magnesium compounds.

Chapter II: **A Tale of Biphenyl and Terphenyl Substituents for Structurally Diverse Ketiminato Magnesium and Calcium Complexes**

There are various reports on the synthesis of amidinate, guanidinate, and *β*-diketiminate ligand stabilized magnesium and calcium complexes[4] but these metal complexes do not have the space for binding the substrate for catalysis. Hence, we have synthesized two less sterically demanding N,O-ketiminato ligands with biphenyl and terphenyl substituent on the nitrogen atom. So that metal can have the space for substrate binding in catalysis. But the reaction of the ligand with MgI_2 and CaI_2 leads to the formation of homoleptic complexes only due to Schlenk equilibrium (Scheme 1).

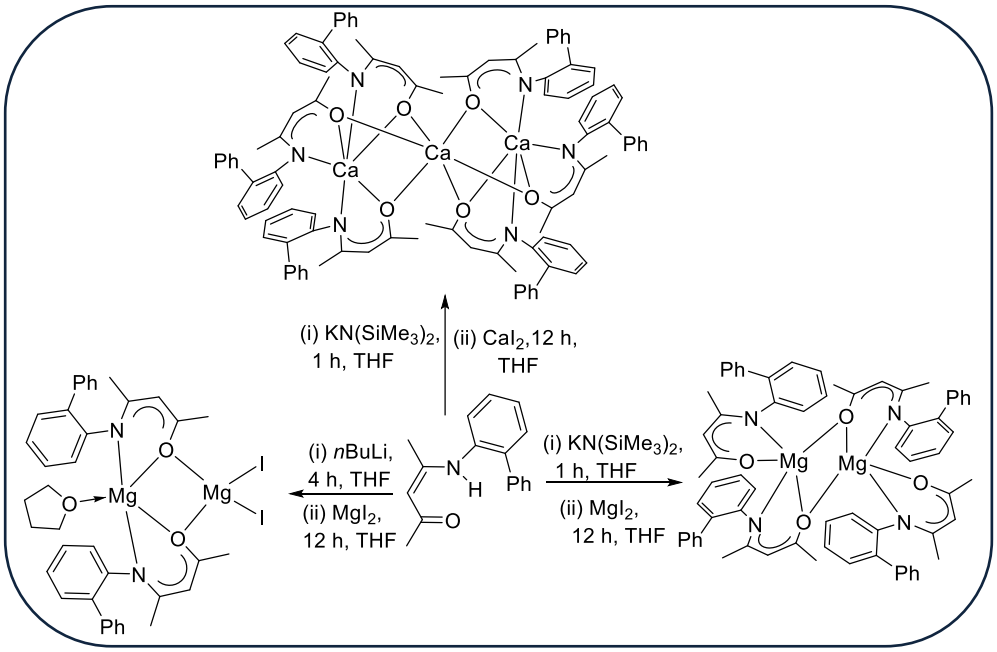

Scheme 1: Synthesis of magnesium and calcium complexes using biphenyl substituent ligand.

However, we could not isolate any chelating complex with terphenyl substituent ligand, and only oxygen bound magnesium and calcium adducts were isolated (Scheme 2). DFT studies were performed to understand this dissimilar behavior. All these complexes are characterized structurally.

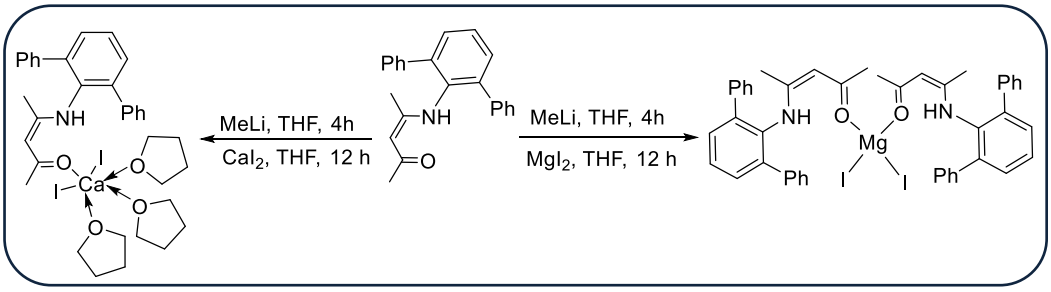

Scheme 2: Synthesis of magnesium and calcium complexes using terphenyl substituent ligand.

Chapter III: **Low Coordinate Monomeric Magnesium-Catalyzed Alkene and Alkyne Hydroboration**

Well-defined molecular magnesium compounds have achieved great advances in hydroboration of C=O or C=N bonds. By contrast, the magnesium-catalyzed hydroboration of alkenes and alkynes is scarce. Here, a series of low-coordinate monomeric magnesium alkyl (methyl, ethyl, isopropyl and butyl) complexes have been prepared using bis(phosphino)carbazole framework (Scheme 3) and among them magnesium methyl has been used as a catalyst for hydroboration of alkenes and alkynes with pinacolborane (Scheme 4).

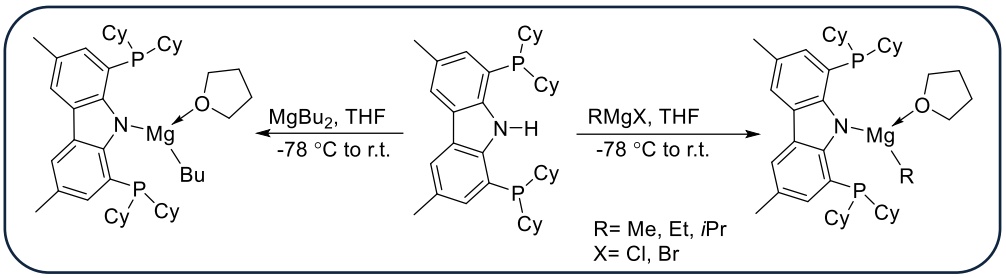

Scheme 3: Synthesis of magnesium alkyl complexes using bis(phosphino)carbazole ligand.

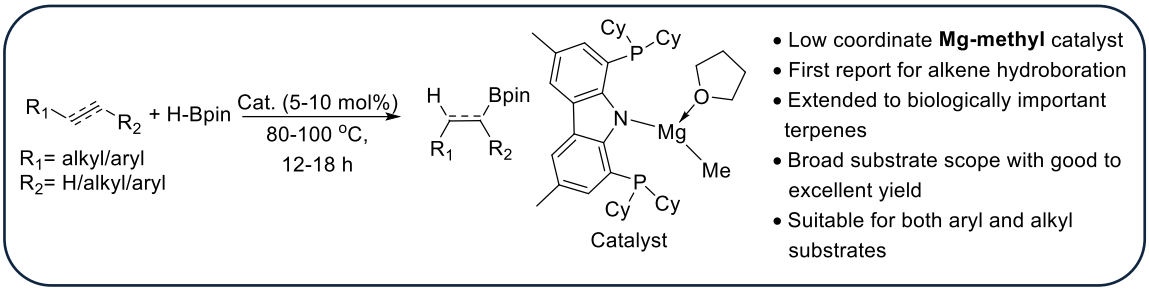

Scheme 4: Magnesium methyl complex as a catalyst for hydroboration of alkenes and alkynes.

Anti-Markovnikov regioselective hydroboration of alkenes and alkynes is achieved, which is confirmed by deuterium-labeling experiments. A wide variety of aromatic and aliphatic substrates were efficiently reduced. Experimental mechanistic investigations and DFT calculations provide insights into the reaction mechanism (Scheme 5). Finally, the hydroboration protocol has been extended to terpenes.

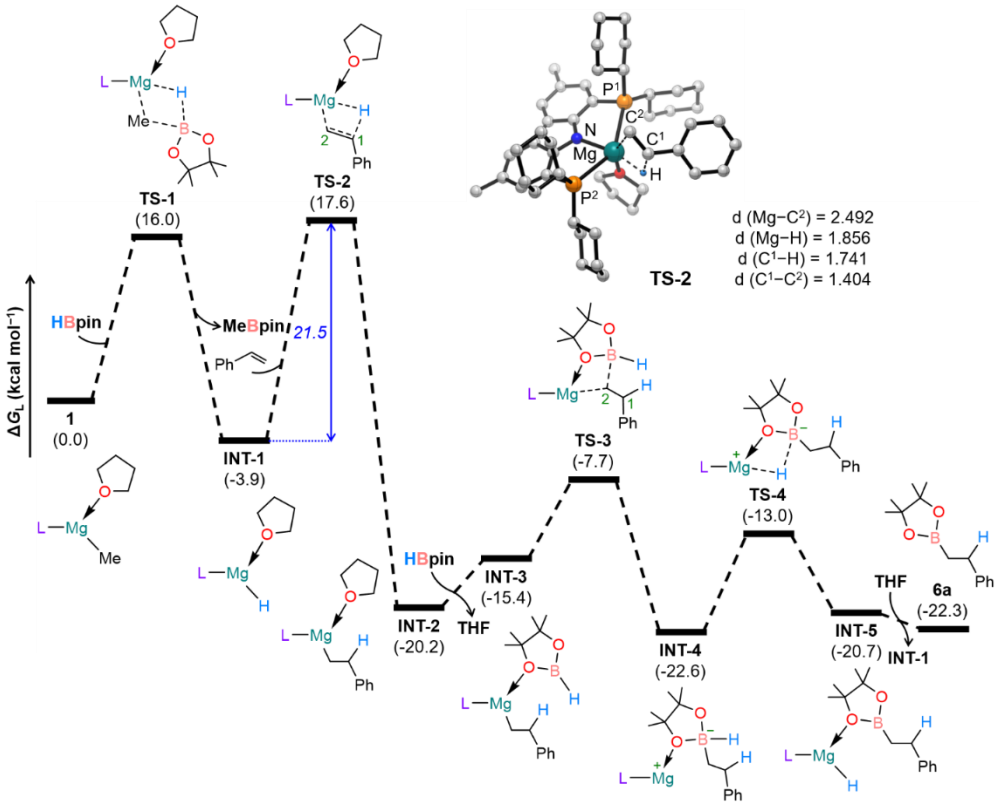

Scheme 5: DFT supported proposed mechanism for alkene hydroboration DFT.

Chapter IV: **Well-Defined Highly Luminescent Magnesium Complexes**

The synthesis, structure, and luminescent properties of two pyridylpyrrolide magnesium complexes are reported where one is dinuclear magnesium chloride complex, $(R_2PyrPyCl)_2Mg_2(THF)_3$ (R= Me) having two Cl-atoms in bridging between two metal centers stabilized by two ligand moieties and three THF molecules while another is homoleptic mononuclear magnesium complex, $(R_2PyrPy)_2Mg(THF)$ stabilized by two ligand moieties and a THF molecule (Scheme 6).

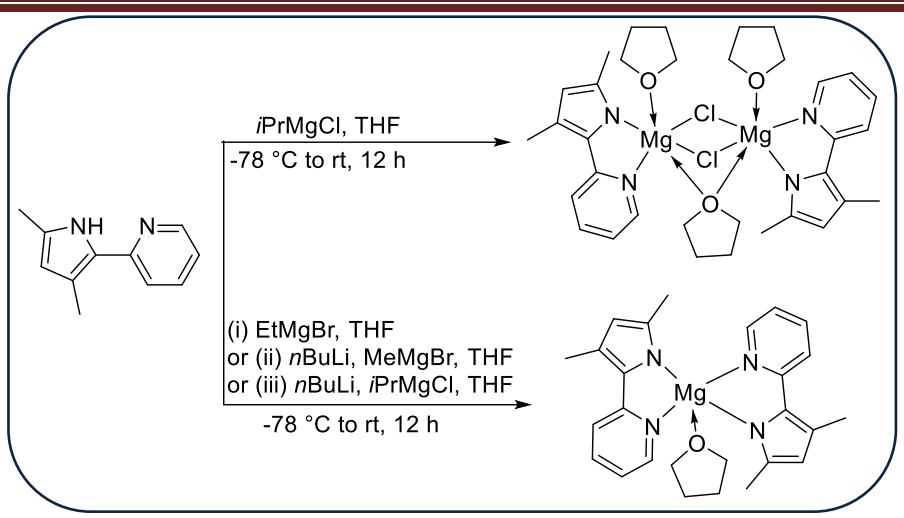

Scheme 6: Synthesis of pyridylpyrrolide magnesium compounds.

While dinuclear magnesium chloride complex shows absorption at 414 nm and emission at 505 nm, the mononuclear magnesium complex shows absorption at 412 nm and emission at 512 nm. The lifetime measurement reveals that both the compounds give double fitting value in nanoseconds which confirms the fluorescence. Quantum yield measurement indicates that these compounds are highly fluorescent and can be used for making light-emitting devices.

Chapter V: A Well-Defined Calcium Compound Catalyzes Trimerization of Arylisocyanates into 1,3,5-Triarylisocyanurates

We have used three different ligands in previous chapters, but none of them was found to be suitable for calcium until now. Hence, we have synthesized a new monoanionic tetradentate ligand with a diaminoethane core with phenolate and pyridine peripheral donors. Denticity of this ligand makes it more suitable for calcium which can overcome with the major Schlenk equilibrium issue. Using the ligand, we have synthesized a dinuclear potassium and calcium iodide complexes (Scheme 7). Furthermore, the calcium complex was screened as a potential catalyst for the cyclotrimerization of isocyanates to isocyanurates (Scheme 8). The reaction was performed in THF with 2 mol % of catalyst. Various substrate scope has been done with excellent isolated yield. Isocyanurates are used for the preparation of copolymer resins and activators for anionic polymerization.

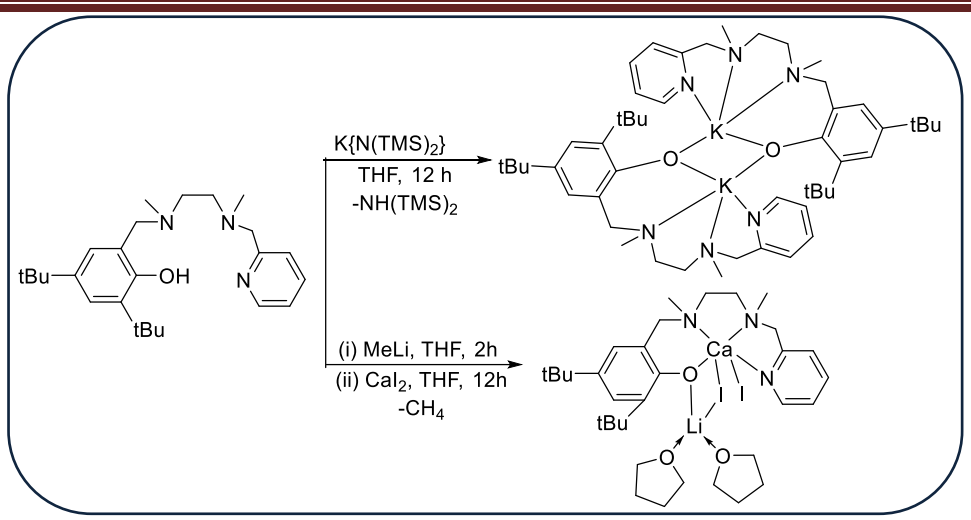

Scheme 7: Synthesis of potassium and calcium complexes bearing a tetradentate ligand.

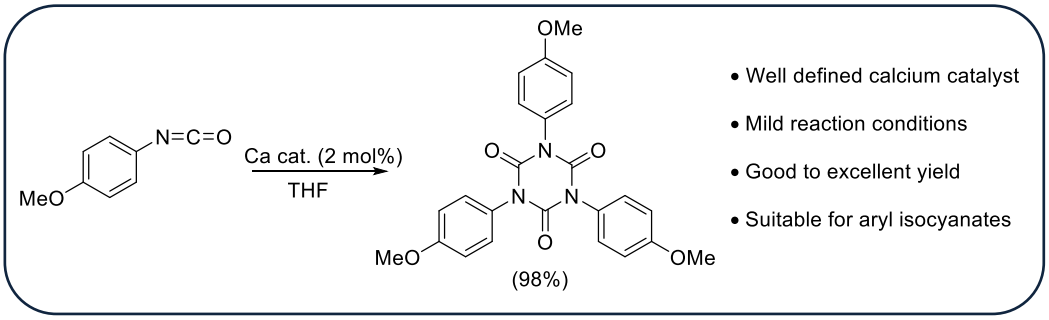

Scheme 8: Calcium complex as a catalyst for cyclotrimerization of isocyanates.

Surprisingly, when reaction was performed in C_6D_6, both dimerized and trimerized products were observed, characterized by single crystal-XRD and NMR spectroscopy. DFT calculations support the thermodynamics of proposed mechanism.

Summary:

This thesis deals with synthesizing alkaline earth metal-based complexes and their application in homogenous catalysis. It is divided into six chapters. The first chapter is the introduction wherein the evolution and importance of alkaline earth metal chemistry with recent literature precedence are described. The second to fifth chapters narrate our approach to the synthesis and catalytic activity of novel alkaline earth metal complexes. The second chapter describes the synthesis of organomagnesium and calcium complexes using two N,O-ketiminato ligands with biphenyl and

terphenyl substituent on the nitrogen atom, and DFT demonstrates the unusual reactivity of the ligand with terphenyl substituent. The third chapter contains the synthesis of a series of low coordinate magnesium alkyl complexes using bis(phosphino) carbazole-based PNP-donor ligand. The magnesium methyl complex has been used as a catalyst for the hydroboration of challenging substrates like alkenes, alkynes, and biologically important terpenes. Stoichiometric reactions and DFT calculations have investigated the catalytic cycle. The synthesis of well-defined pyridylpyrrolide magnesium complexes and their luminescent studies are included in fourth chapter. In the fifth chapter, synthesis and catalytic application of calcium complex bearing a monoanionic tetradentate ligand for cyclotrimerization of a variety of aromatic isocyanates under mild conditions is shown. The final chapter of the thesis describes the summary of Ph.D. work with the future outline.

Future Directives:

- Catalytic exploration of magnesium alkyl and calcium iodide complexes for other organic moieties.
- The use of fluorescent pyridylpyrrolide magnesium complexes for making light-emitting devices.

Details of Publications:

1. **R. Kumar**, S. Yadav, K. Gour, E. Sangtani, S. R. Dash, A. Raja, K. Vanka, R. G. Gonnade, and S. S. Sen* A Tale of Biphenyl and Terphenyl Substituents for Structurally Diverse Ketiminato Magnesium, Calcium and Germanium Complexes, *Chem. Asian. J.*, **2020**, *15*, 820. (**Thesis related**)
2. S. Yadav, **R. Kumar**, K. V. Raj, P. Yadav, K. Vanka and S. S. Sen*, Amidinato Germylene-Zinc Complexes: Synthesis, Bonding, and Reactivity, *Chem. Asian. J.*, **2020**, *15*, 3116.
3. **R. Kumar**, M. Bisai, S. Jain, K. Vanka, S. S. Sen*, Deoxygenative hydroboration of primary and secondary amides: a catalyst-free and solvent-free approach, *Chem Comm*., **2021**, *57*, 10596.
4. **R. Kumar**, V. Sharma, S. Jain, K. Vanka, S. S. Sen*, A Well-Defined Calcium Compound Catalyzes Trimerization of Arylisocyanates into 1,3,5-Triarylisocyanurates, *ChemCatChem*, **2022**, (DOI: 10.1002/cctc.202101788). (**Thesis related**)

5. **R. Kumar**, S. Datta, V. Sharma, R. G. Gonnade, D. Koley, S. S. Sen*, Low Coordinate Monomeric Magnesium-Catalyzed Alkene and Alkyne Hydroboration (Manuscript submitted). (**Thesis related**)

References:

[1] V. Grignard, *Compt. rend. Hebd. Séances Acad. Sci*. **1900**, *130*, 1322

[2] R. Fischer, M. Gärtner, H. Görls, M. Westerhausen, *Angew. Chem. Int. Ed.* **2006**, *45*, 609.

[3] W. Schlenk, *Ber. Dtsch. Chem. Ges*., **1929,** *62*, 920.

[4] S.-O. Hauber, F. Lissner, G. B. Deacon, M. Niemeyer, *Angew. Chem. Int. Ed.* **2005**, *44*, 5871; H. M. El-Kaderi, M. J. Heeg, C. H. Winter, *Polyhedron* **2006**, *25*, 224; S. P. Sarish, A. Jana, H. W. Roesky, T. Schulz, D. Stalke, *Organometallics*, **2010**, *29*, 2901; A. Causero, H. Elsen, G. Ballmann, A. Escalona, S. Harder, *Chem. Commun*., **2017**, *53*, 10386.

[5] T. Kamata, Y. Miura, T. Shishido, K. Takehira, K. Takaki, *J. Org. Chem*., **1999**, *64*, 3891; F. Buch, S. Harder, *Organometallics*, **2007**, *26*, 5132.

Rohit Kumar

(Dr. Sakya S. Sen)
Supervisor

Chapter 1: Introduction

Abstract:

The first chapter briefly explains the discovery of alkaline earth metals. A general introduction to the generation of the first well-defined organo-magnesium and calcium complexes. In addition, a summary of the fundamental interest and formidable synthetic difficulty surrounding the synthesis of compounds with alkaline earth metals is provided. Further, a brief overview of a few crucial compounds in this field of chemistry is also explained, along with their catalytic applications. At last, the purpose and findings of this contribution are discussed.

1: Introduction:

1.1: An overview of the alkaline earth metals' history

The alkaline earth metals' names are primarily derived from their oxides, which were once known by the names beryllia, magnesia, lime, strontia, and baryta. The "alkaline" (basic) nature of their oxides is due to the formation of metal oxides after reaction with water. While "earth" was only a term given by the early chemists to nonmetallic substances, those are partially soluble/insoluble in water and resistant to heating properties shared by these oxides. These alkaline earths were not the elements, but these compounds were first realized by chemist, Antoine Lavoisier. This was mentioned in his textbook 'Traité Élémentaire de Chimie (Elements of Chemistry)' written in French in 1789, and later translated into English by Robert Kerr in 1790, in which he named them salt-forming earth elements. This book was considered to be the first modern 'chemical textbook'.[1] Later, he suggested that these alkaline earths might be metal oxides, but he later acknowledged that this was just speculation. In 1808, using Lavoisier's idea, Humphry Davy obtained samples of the metals by electrolysis of their molten earths,[2] thus supporting Lavoisier's hypothesis and causing the group to be named the alkaline earth metals. The alkaline earth metals Be, Mg, Ca, Sr and Ba are all silvery shining metals (Figure 1.1).

(a) (b) (c) (d) (e)

Figure 1.1: Elemental form of alkaline earth metals. (a) Beryllium crystals (b) Magnesium crystals (c) Crystals of calcium under argon gas (d) Crystals of strontium drifting in paraffin oil and (e) Crystals of barium under argon gas.

Similar to the other first element of the periodic table in the main group, Beryllium shows completely different reactivity compared to heavier analogs, and beryllium compounds are toxic. Strong interactions between the atoms can explain it due to a better orbital overlap. Hence, the chemistry of Be is mainly covalent due to the small size and high electronegativity. At the same time, heavier analogs become more ionic due to their large size and less electronegativity.

Interestingly, magnesium and calcium are non-toxic and two of the most earth-abundant elements as magnesium is the 8th and calcium is the 5th in the list. These are essential minerals in the human body and function as the enzyme co-factors,[3] which makes them a central component of the bone structure.[4] In contrast, strontium and barium are significantly less earth-abundant and the barium compounds are highly toxic. Hence, In my thesis work, I have worked mainly on magnesium and calcium, and therefore, I will give a brief introduction to the synthesis and applications of their organometallic complexes.

1.2: A brief history of organo-magnesium and organo-calcium complexes

The last two decades have been witnessed for the shift of the larger scientific community towards green and sustainable chemistry or transition metal-free chemistry, which is mainly driven by the main group elements especially alkaline earth metals due to environmental friendliness, biocompatibility and abundance. The use of abundant, sustainable, and biocompatible elements has been the primary objective of chemists for modern organic synthesis.[5] Compared to transition metals (Pd, Ni, Rh, etc.), these metals are redox inactive, making it challenging to progress via oxidative addition or reductive elimination. Despite this, chemists have been devoted to utilizing alkaline earth metals in organic synthesis due to their abundance, biocompatibility, and potent chemical activities.[6-7] The first breakthrough was made by Victor Grignard(1901), who synthesized alkyl/aryl magnesium halides, commonly known as Grignard reagents, which have been widely used in synthetic chemistry.[8-9]

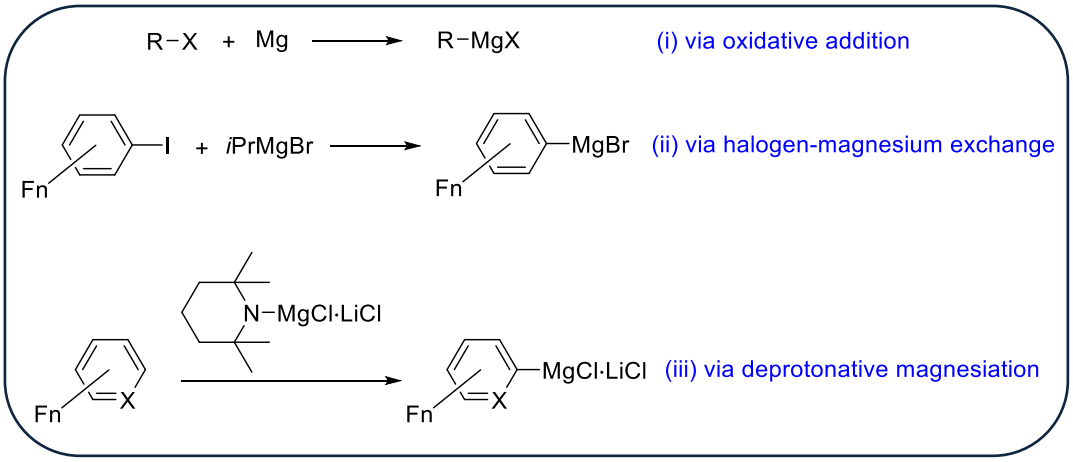

Scheme 1.1: General synthetic methods of organo-magnesium halide reagents.

These reagents can be prepared via oxidative addition of organic halides to magnesium metal {Scheme 1.1(i)}[10] or via halogen–magnesium exchange between halo(hetero)arenes and alkyl-magnesium reagents {Scheme 1.1(ii)}.[11–15] Deprotonative magnesiation of (hetero)arenes has also been developed to prepare aryl magnesium reagents directly. At the same time, it commonly needs pre-functionalization at a suitable position of the (hetero)arene substrates {Scheme 1.1(iii)}.[16-17] Strong bases, nucleophiles, as well as alkyl-aryl transfer reagents have all been employed with these organo-magnesium halides.[18-19] However, if we move down the group, the heavier elements elaborate substantial synthetic challenges; hence, the chemistry of heavier elements has not been studied extensively. Various attempts have been made to synthesize heavier alkaline earth organometallics, which only recently led to success. The common assumption that the heavier alkaline earth metals react similarly to magnesium chemistry has hampered their progress, and their chemistry is unclear. Moving down the group, the electro-positivity increases along with the size, leading to a rise in the metal-carbon bond's polarity and ionicity and a substantial enhancement in reactivity.[20] Hence, The Grignard-type synthesis methods run into ether cleavage reactions, which cause side reactions such as Wurtz coupling; ($2RI + Ca \rightarrow R\text{-}R + CaI_2$).[21-22] Therefore, these degrading reactions must be avoided during low-temperature maintenance. Furthermore, a lot of difficulties and hurdles were encountered in the synthesis and characterization of organo-alkaline complexes. Here is a description of one of the most significant synthetic challenge.

1.2.1: Schlenk equilibrium

The Schlenk equilibrium, which favours homoleptic complexes over heteroleptic complexes, is one of the major difficulties in the chemistry of alkaline earth metals.[23] According to Schlenk, the significant ionic interaction between the ligand and metal causes the ligand scrambling to occur in these complexes, which results in an equilibrium between the homoleptic and heteroleptic species(Scheme 1.2). Due to their ability to coordinate, ethereal solvents like Et_2O and THF can stabilize heteroleptic compounds and avoid unwanted homoleptic compounds.[24]

Scheme 1.2: The continuous halide and alkyl group mixing.

Consequently, the Schlenk equilibrium hinders the formation of heavier metal complexes. The ligand scrambling causes an equilibrium shift toward homoleptic complexes, resulting in the precipitation of an insoluble MX_2 complex and high lattice energy. These heavier metals have a major problem with solubility in organic solvents. Ionic radii increases as you move down the group (Ca^{2+}, 1.00 Å; Sr^{2+}, 1.18 Å; and Ba^{2+}, 1.35 Å; specially with coordination number 6 complexes), making the coordination saturation difficult.[25] These issues can be avoided by fulfilling the steric demands of large ionic radii having alkaline earth metals using bulky and multidentate ligands, co-ligand incorporation, and/or secondary interactions to inhibit the association of the molecules and sustain solubility. Contempt synthetic efforts to reduce association, various complexes show widespread aggregation, creating substantial solubility problems in molecular alkaline earth metal chemistry.

1.2.2: Organocalcium chemistry: The beginning with carbon-based ligands

Organo-calcium chemistry started to develop in 1950 when Stucky and coworkers synthesized the first organo-alkaline earth metallocene, i.e., calcocene, $Ca(C_5H_5)_2$ (**1.1**) and $Ca(C_5H_5)_2(THF)_2$(**1.2**) (Scheme 1.3). The cyclopentadiene and activated calcium metal reaction was used to manufacture both of these compounds.[26] Due to the unique coordinating capability of the cyclopentadiene ring, the first well-defined organo-calcium complex was isolated and characterized structurally. Further, the introduction of the steric groups to the ligand systems, especially the cyclopentadienyl ring, permitted the isolation of distinct compounds, signifying the advantages of the steric support of bulky groups to avoid aggregation.[27] Till the report of Lappart and coworkers for the synthesis of $[Ca\{CH(SiMe_3)_2\}_2(1,4\text{-dioxane})_2]$(**1.3**)[28], Ca-C σ-bond chemistry has not yet been studied in detail, unlike metallocenes. The co-condensation of calcium vapors and $[(SiMe_3)_2CHBr]$ in THF first, then dioxane at 77 K leads to forming of the first Ca–C σ bonded complex (**1.3**). Compound **1.3** displays the Ca-C bond length of 2.483(5) Å. The expected product was calcium analogue of Grignard reagent i.e., RCaBr(THF)*n*, but it forms compound **1.3** due to the major issue of Schlenk equilibrium.[23]

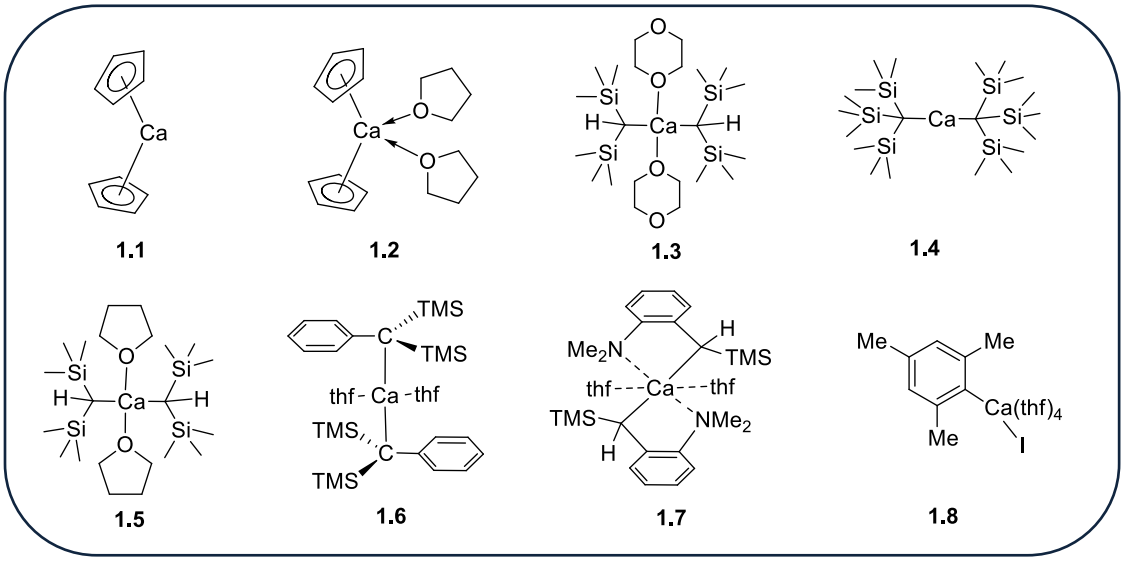

Scheme 1.3: The outline of the journey for organo-calcium complexes.

Quite a few years later, potassium bis{tris(trimethylsilyl)methanide} [$KC(SiMe_3)_3$] was treated with CaI_2 in benzene, leads to the formation of calcium bis{tris(trimethylsilyl)methanide} [$Ca\{C(SiMe_3)_3\}_2$](**1.4**).[29a] Molecular structure of **1.4** shows the additional steric stabilization due to the agostic interaction of calcium with H-atoms of the trimethyl silyl group, and this agostic interaction results in the formation of the first solvent coordination-free calcium complex. The bond length of the Ca-C bond was 2.459(9) Å, which is a little shorter than the sum of their covalent radii, and bond angle was 149.7(6)°, which suggests that the compound **1.4** adopts bent geometry. When an excess amount of diethyl ether (Et_2O) was treated with **1.4** then it forms a parent hydrocarbon of potassium bis{tris(trimethylsilyl)methanide} and calcium ethanolate which indicates the rapid reaction time of organo-calcium compounds. A similar compound was synthesized by Hill and coworkers where they treated [$K\{CH(SiMe_3)_3.(THF)$] with CaI_2 in a 2:1 ratio in THF solvent to synthesize [$Ca\{CH(SiMe_3)_2\}_2$]$(THF)_2$ (**1.5**).[29b] In 2000, The first benzyl organocalcium complex [$\{PhC(SiMe_3)_2Ca\}_2$](**1.6**) was reported by Harder and coworkers, by the reaction of potassium *α,α*-bis(trimethylsilyl)benzyl and CaI_2 in THF.[29c] In continuation of this work, the same group slightly modified the potassium *α,α*-bis(trimethylsilyl)benzyl part by attaching the di-methylamino group to the benzyl group and substituting hydrogen for one of the TMS moiety. Further, they synthesized bis(2-NMe_2-α-Me_3Si-benzyl)calcium$(THF)_2$(**1.7**) using

the same reaction conditions as **1.6**.[29d] However, synthesizing heavier analogs of Grignard reagent, i.e., alkyl or aryl calcium halide, remained challenging for scientists. Beckmann reported that PhCaI, the first aryl calcium iodide in 1905, which was synthesized via reacting aryl halide and calcium metal in diethyl ether.[30] However, the lack of characterization evidence and the generation of diethyl ether coordinated calcium iodide complex from repeat reactions could not prove the synthesis of aryl calcium iodide,[31] and these remained uncharacterized. Several research groups have made various efforts to synthesize these elusive compounds, but these efforts led to extensively clashing reports about their preparedness and efficiency. By reacting (2,6-dimethoxy phenyl)potassium with CaI_2 in THF, Harder and coworkers attempted to make an aryl calcium iodide in 2005. Still, they ended up getting a tetranuclear cluster of composition [2,6-$(MeO)_2C_6H_3]_6Ca_4O$].[32] After one year or so, Westerhausen and coworkers reported the first well-defined higher analog of Grignard's reagent, i.e., (2,4,6-trimethyl phenyl) calcium iodide; [MesCaI$(THF)_4$](**1.8**), by the reaction of activated calcium with aryl iodide in THF.[33] They claimed that the other aryl calcium iodide compounds are also synthesized like [PhCaI$(THF)_4$], [(*p*-tolyl)CaI$(THF)_4$], and [PhCaBr$(THF)_4$], but they could not able to characterize them structurally like **1.8**. Interestingly, the excellent solubility of compound **1.8** in aromatic hydrocarbons and ethers makes it an alternative to Grignard's reagent, but crystalline **1.8** starts decomposing above -10 °C; however, it was completely decomposed at – 30 °C in solution. Compound **1.8** exhibits two signals for the mesityl group in ^{1}H NMR spectra with a 3:2 integration ratio, most likely as a result of the Schlenk equilibrium, which results in $CaMes_2$ and MesCaI at 250 K. In contrast, it shows only one signal, probably due to $CaMes_2$ at 310 K. All of these calcium iodide complexes have one thing in common: the metal centre is hexa-coordinated, and the anion is arranged in trans position. One thing to note here, all these structurally characterized compounds, **1.1** to **1.8** are inactive towards further functionalization because of the homoleptic nature and solubility issues. Even Grignard reagents also suffered from solubility/stability issues as these reagents always come as molar solvents in THF/ether. If these reagents are kept for a longer time, they start decomposing. Hence, the scientific community tried to solve this issue by designing various N-atom-based ligands to synthesize the heteroleptic alkaline earth metal complexes by σ-bond metathesis.

1.2.3: Organo-magnesium and calcium chemistry: The beginning with nitrogen-based ligands

Various monoanionic nitrogen-based ligands such as amidinate,[34a,b] guanidinate,[34c-i] triazenide,[34j] ^{Dipp}Nacnac,[34j-q] diboxmethanide,[34r-t] silylated aminopyridinate,[34u-v] aminotroponiminate,[34w] tridentate Schiff base,[34x] carbazole mesoionic carbene,[34y] etc. have been used to synthesize organo-magnesium and calcium compounds, considering the steric and electronic demands of alkaline earth metals (scheme 1.4). Among all these ligands amidinate, guanidinate, and ^{Dipp}Nacnac, ligands have been used to stabilize monomeric alkaline earth amides to dimeric hydrides. Despite enormous synthetic challenges, organomagnesium and calcium complexes show very interesting reactivity and mimic transition metal complexes in various catalytic applications; it ushers in a new era of homogeneous catalysis employing earth-abundant metal complexes.

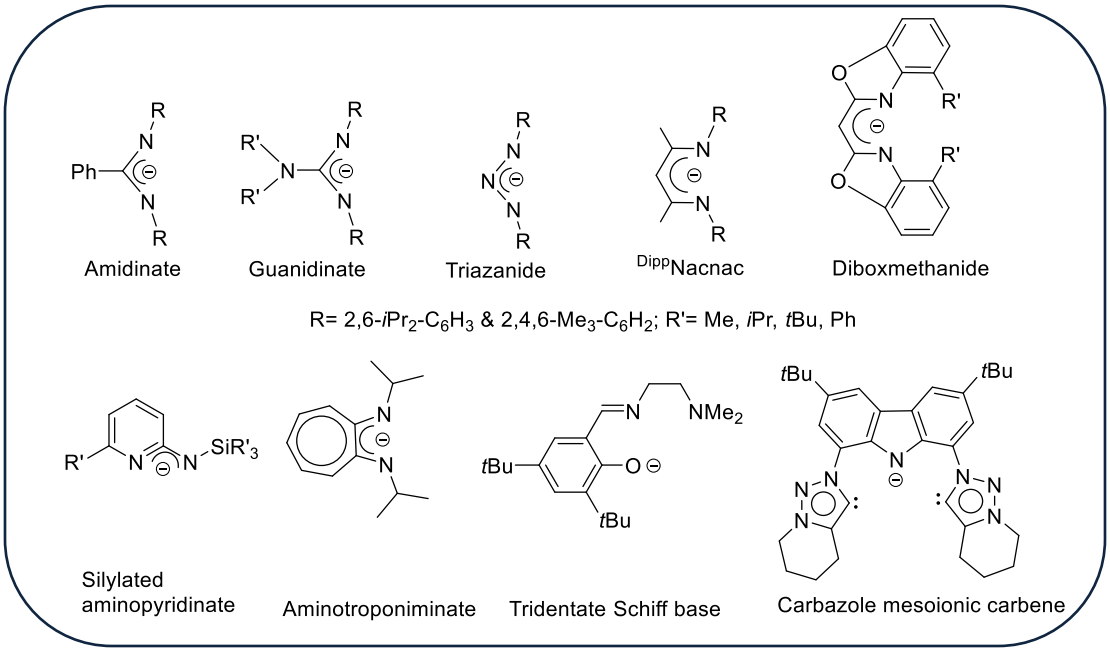

Scheme 1.4: Previously reported monoanionic ligands used for stabilizing alkaline earth metal complexes.

1.2.4: Similar reactivity of Mg-Zn and Ca-Yb

The redox inactive nature of alkaline earth metals makes them tidy with their +2 oxidation state with d^0 electronic configuration. Interestingly, the properties of magnesium match with zinc due

to their similar size and redox inactive nature. Recently, Harder and coworkers have compared the reactivity of magnesium and zinc in cationic π-arene and halobenzene complexes.[35a,b] Similarly, the properties of calcium somewhat match the particularly redox-inactive and trivalent lanthanides with d^0 electronic configuration with Yb^{+2}.[36] This is due to the size similarity of calcium and ytterbium (small size due to lanthanide contraction). In terms of Lewis acidity, alkaline earth metals behave similarly to lanthanides. The two basic mechanistic processes that link calcium reactivity to lanthanide chemistry are polarisation insertion and σ-bond metathesis. The substrate polarity drives the catalytic path of the reaction. Protonolysis is caused by the prototic Y–H bond and results in an L–La–Y (La: Lanthanide metal) fragment. The initial step of a protic Y-H catalytic cycle, L-La-Y, undergoes insertion into the unsaturated bond. Following further protonolysis by Y-H, L-La-Y moiety regeneration and the anti-Markovnikov product was formed(Scheme 1.5).

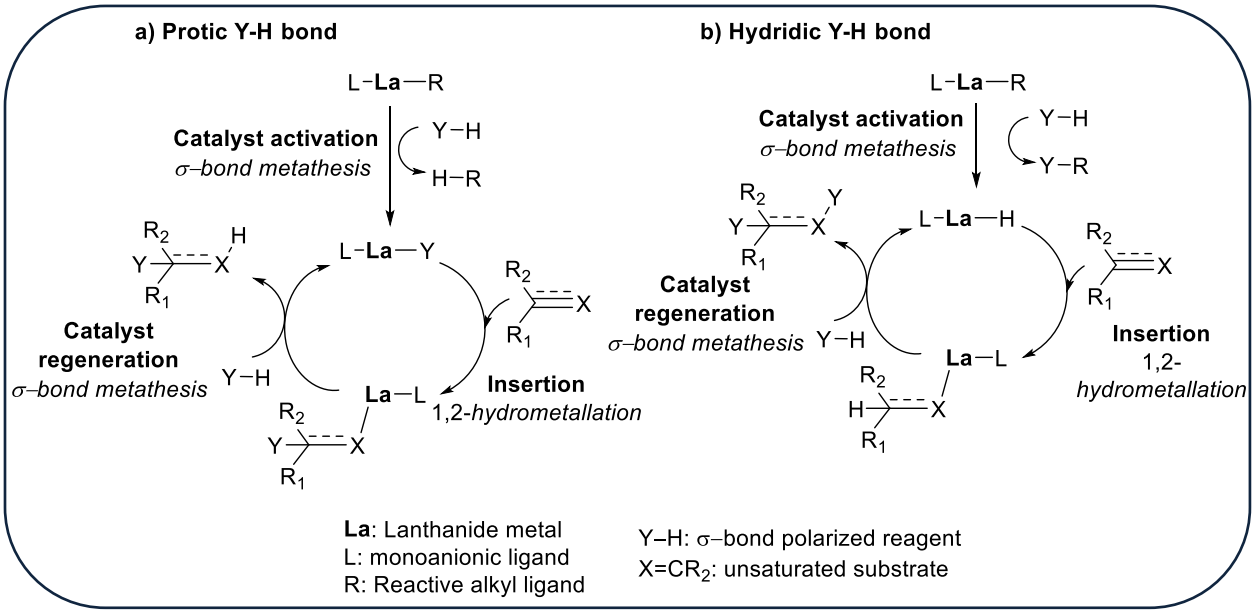

Scheme 1.5: General lanthanide metal-mediated proposed catalytic cycles in heterofunctionalisation of unsaturated compounds.

In contrast, the hydridic Y–H bond produces a metal hydride L–La–H that functions as an active catalyst. The unsaturated substrate is inserted into the lanthanide metal hydride bond (Scheme 1.5), and then it undergoes further σ-bond metathesis to generate Markonikov product

and active catalyst.[37,38] These proposed mechanisms support a number of organo-lanthanide catalysed processes, including olefin polymerization, hydroalkoxylation of alkenes, hydrophosphination, hydrosilylation, hydroamination, and hydrogenation.[39-68]

1.2.5: Unique electrophilicity/nucleophilicity of organocalcium reagents

Organocalcium reagents exhibit nucleophilicity and electrophilicity in a range between group 3 and group 1 elements (Scheme 1.6). The calcium metal exhibits strong Lewis acidity, a property common to group 3 elements, and nucleophilic reactivity, a property common to group 1 elements.

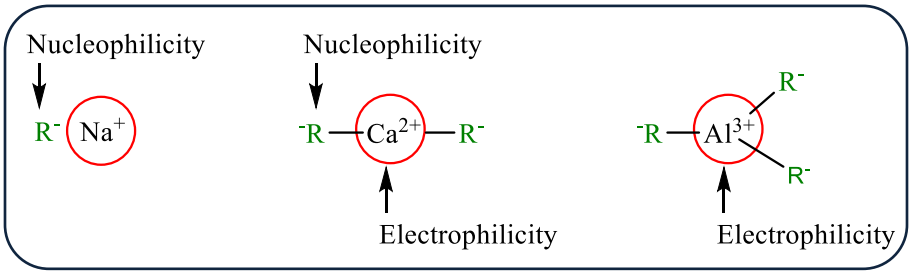

Scheme 1.6: Comparison of the organocalcium reagents with group 1 and 3 reagents.

1.3: Advantages of organo-magnesium and calcium complexes in catalysis

The advantages of using organomagnesium and calcium complexes in catalysis are: a) Transition metals including Rh, Ir, Ru, Os, Pd, and Pt are the primary building blocks for industrial catalysts. Both magnesium and calcium metal can be a capable contender to achieve the aim of "cheap metals for noble task" because they are the 8th and 5th most earth-abundant.[69] b) Consumption of calcium and magnesium are considered safe in the human body, making them biocompatible and advantageous in developing polymers suitable for biodegradable materials and medical applications. It can easily convert to carbnates and hydroxids, which perfectly fits the present trend of preparing the less non-toxic metal catalyst.[70] c) Organo-magnesium and calcium chemistry is in its initial phase and started only a decade ago, making it a significant and intriguing area from a theoretical/academic perspective.

1.4: Organo-magnesium and calcium complexes for catalysis

Various reports in the literature indicate organo-magnesium and calcium reagents have been used as catalysts. Here we have shown some of them related to the thesis work.

1.4.1: Organo-magnesium and calcium catalyzed hydroboration reactions

Brown *et al.* discovered the hydroboration in 1956 [71], which involves B-H bond addition to C=C, C≡C, C=N, and C≡N bonds. It is a interesting and atom-economic transformation for synthesizing organoboranes. The addition of boranes (HBR_2) across the C=O or the C=N leads to forming a B−O or B−N bond-containing compound (Scheme 1.7), and further hydrolysis gives a product equivalent to a two-step reduction process.[72-73]

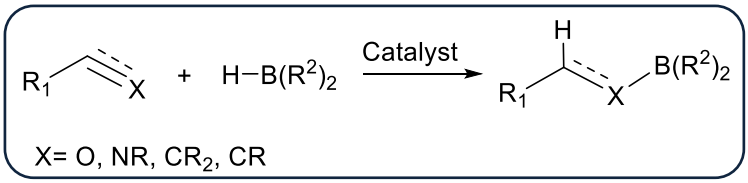

Scheme 1.7: Hydroboration of unsaturated bonds using boranes in the presence of a catalyst.

Furthermore, adding boranes to the C−C multiple bonds such as alkenes and alkynes results in synthesizing a C−B bond appropriate for consecutive conversions such as carbon-carbon couplings[74], similar to the Suzuki coupling reaction.[75-76] The high Lewis acidity of organo-magnesium and calcium complexes makes them suitable catalysts for hydroboration reactions.

Some of the organo-magnesium and calcium compounds have been shown in scheme 1.8. These complexes have been used as catalysts in the multiple hetero-functionalization reactions related to this work.

Hill group introduced a versatile catalyst ^{Dipp}Nacnac-magnesium butyl [{HC-$(C(Me)_2N$-2,6-$i Pr_2C_6H_3)_2$}Mg-Bu(THF)](**1.9**) for smooth hydroboration of various functional groups such as pyridines,[77] imines,[78] aldehyde-ketones,[79] isonitriles,[80] nitriles,[81] carbodiimides[82] and isocyanates[83] (Scheme 1.9).

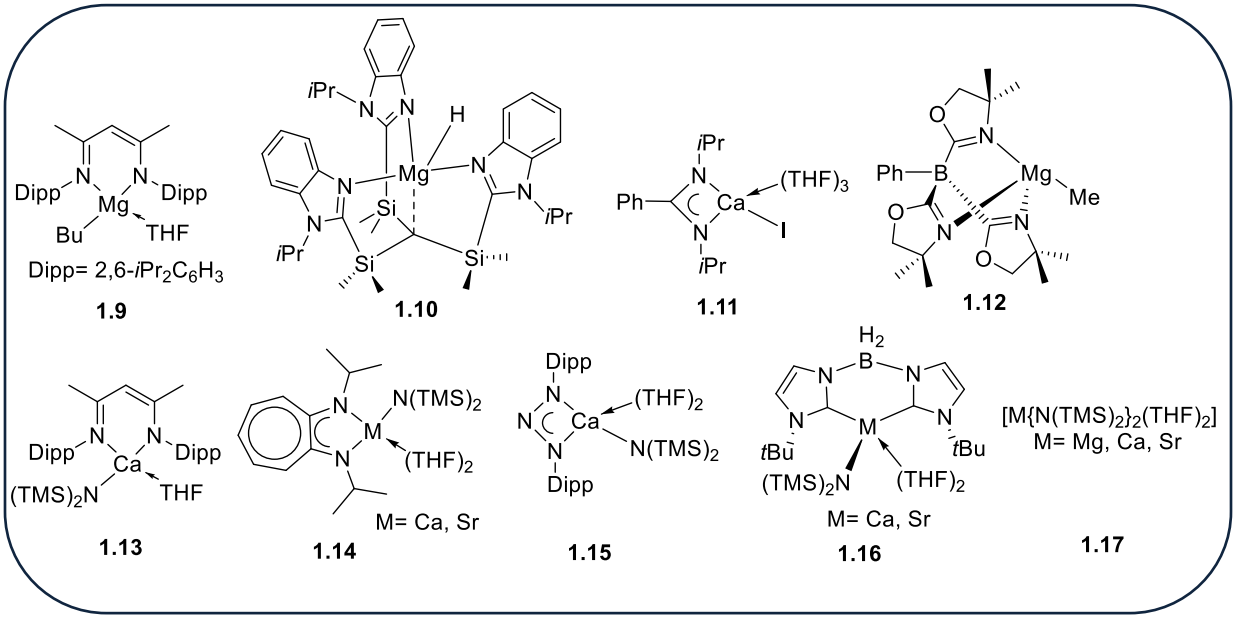

Scheme 1.8: Examples of precatalysts used in this work's relevant alkaline earth metal-mediated catalysis.

The reaction conditions required 5-10 mol% catalyst loading, and the completion time was 1-24 h at 50-70 ºC. All these catalytic reactions were performed for all the substrates in deuterated solvents, i.e., benzene-d_6 or toluene-d_8. More importantly, the author has claimed that **1.9** act as a pre-catalyst in all the cases, and ^{Dipp}Nacnac-Mg-H acts as an active catalyst generated during the reaction with HBpin.

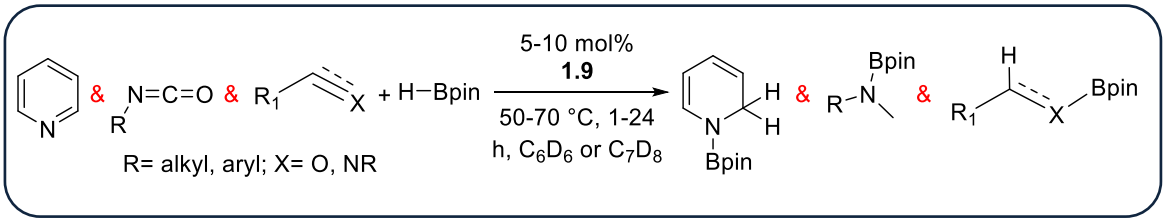

Scheme 1.9: Hydroboration of pyridines, imines, aldehyde-ketones, isonitriles, nitriles, carbodiimides, and isocyanates in the presence of ^{Dipp}Nacnac-MgBu catalyst.

A few years later, Rueping group described the Mg-catalyzed hydroboration of terminal and internal alkynes[84] for the first time(Scheme 1.10). They used the commercially available catalyst Mg-Bu_2.

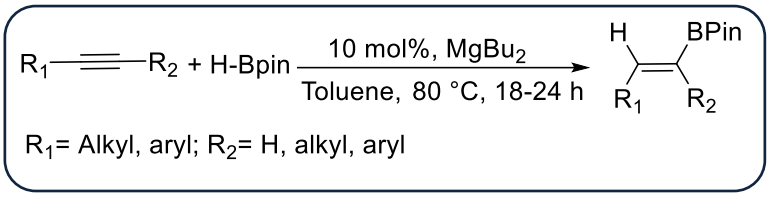

Scheme 1.10: Hydroboration of internal and terminal alkynes using Mg-Bu_2 as catalyst.

Rueping also claimed that Mg-Bu_2 is not the active catalyst. During the reaction with HBpin, it forms Mg-H, which acts as an active catalyst. Based on the generation of active catalyst, metal hydride, and consequent hydrometalation, a general catalyst cycle is given in scheme 1.11. However, this catalytic cycle can vary due to the nature of the metal and ligand. Moreover, this catalytic cycle is only for the hydroboration given by an alkaline earth metal catalyst bearing a monoanionic ligand. It is not for the catalyst bearing a di-anionic ligand or cationic complex, which may occur via different pathways.[85]

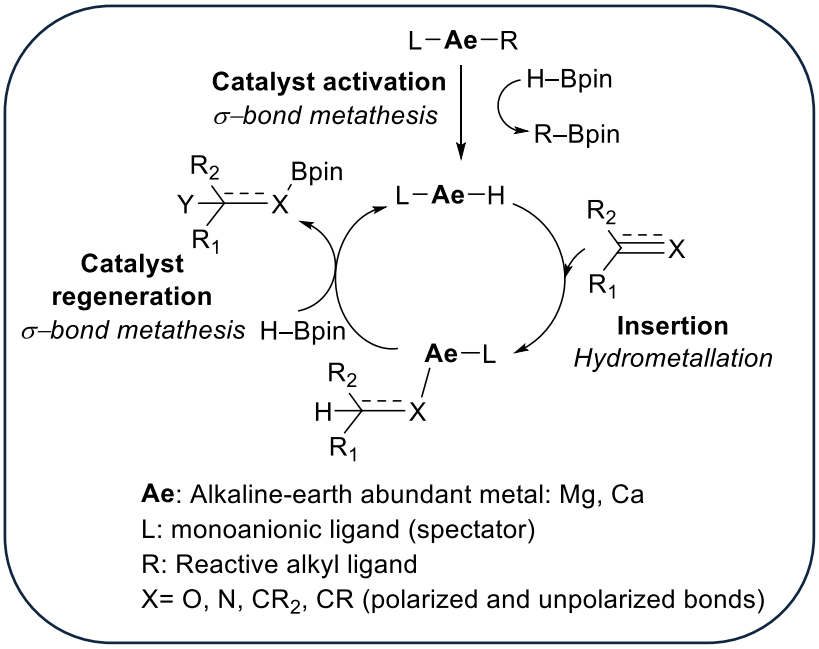

Scheme 1.11: A basic catalytic cycle for the hydroboration of polarised and unpolarized functional groups by alkaline earth metal complexes.

More importantly, there is no report on hydroboration of alkenes using a magnesium catalyst apart from the report of Perkin and coworkers. They used magnesium hydride [Tism^{Pri}Benz]Mg-H (**1.10**)

as a catalyst for the hydroboration of styrene. However, they did not elaborate the substrate scope for alkenes.[86]

Our group introduced a heteroleptic calcium complex [{Ph-C(N-*i*Pr$_2$)$_2$}Ca-I(THF)$_3$] (**1.11**) and utilized it to catalyze the hydroboration of ketone and aldehydes.[87] The catalyst is very efficient as it took only 40 minutes to complete the reaction for aldehydes with 0.5 mol% catalyst loading. In contrast, slightly more catalyst loading and time were required up to 3 mol % and 5 hours, respectively, for ketones (Scheme 1.12).

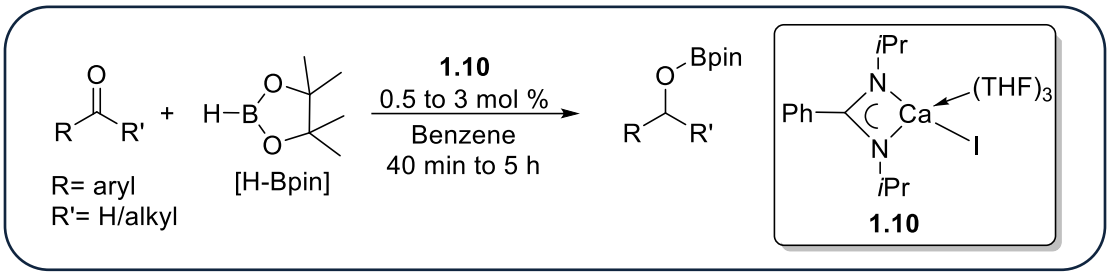

Scheme 1.12: Amidinate-Ca iodide complex catalyzed hydroboration of ketones and aldehydes.

In 2011, Harder group reported the hydroboration of alkenes using ^{Dipp}Nacnac-Ca hydride dimer as catalyst. But detailed mechanistic studies reveal that BH_3 catalyzes the reaction, which is generated in situ from the reaction of ^{Dipp}Nacnac-Ca hydride with HBcat (catechol borane).[88] similar to Burgess' report for Nb-mediated alkene hydroboration.[89]

1.4.2: Magnesium and calcium catalyzed hydroamination reactions

The insertion of an N-H bond across C=C, C≡C, C=N, and C≡N bonds results in the atom-efficient process known as hydroamination.[90] The hydroamination process is thermodynamically favorable; however, it is kinetically unfavorable because of the strong attraction in between nitrogen lone pair and unsaturated bond. Interestingly, because of their high Lewis acidity, both organo-magnesium and calcium compounds can act as catalysts in hydroamination reactions. Sadow group synthesized a boron-based ligand stabililzed monomeric magnesium methyl complex To^{M}MgMe (**1.12** To^M = tris(4,4-dimethyl-2-oxazolinyl)phenylborate) and further used it as a catalyst for intra-molecular hydroamination/cyclization of aminoalkenes.[91] Similarly, Hill group used ^{Dipp}Nacnac-calcium amide (**1.13**) as a catalyst for the intramolecular hydroamination of *α, ω*-

aminoalkene.[92] Afterward, the calcium amide combination of aminotroponate and aminotropniminate (**1.14**) was utilized for inert terminal amino alkenes to be hydroaminated intramolecularly under mild reaction conditions reported by Roesky and coworkers.[93] Later, for intramolecular hydroamination, the Hill group utilised the triazenide calcium complex (**1.15**) and bis(imidazolin-2-ylidene-1-yl)borate calcium amide [{$H_2B(Im^tBu)_2$}M{$N(SiMe_3)_2$}(THF)n] (M=Ca, n=1; M=Sr, n=2)(**1.16**).[94] It was determined that these reactions adhere to Baldwin's ring formation rule, indicating that heterocycles with five and six members are better inaccessible than those with seven members.[95] A five-membered ring converts more quickly than a six-membered ring, which converts more quickly compared to a troublesome seven-membered one. Substitution significantly affects the conversion rate of amino alkenes. The Thorpe-Ingold effect generally causes the big geminal substitution to speed up the reaction rate, while the terminal substitution significantly reduces the reaction rate.[96] Using a chiral *β*-diketimine calcium complex, Harder group made an effort for the alkene intramolecular hydroamination and enantioselective catalytic hydrosilylation.[97] Due to the Schlenk equilibrium, which allowed the homoleptic calcium complex and the heteroleptic calcium complex should be in equilibrium, very little enantiomeric excess was produced throughout the reaction. The active catalyst in the reaction may be this achiral homoleptic calcium complex. Afterwards, the Hill group demonstrated by theoretical and experimental research that under ambient reaction conditions, the homoleptic alkaline earth metal complex [$MN(SiMe_3)_2]_2$ [M = Ca, Sr](**1.17**) can function as the precatalyst for the intermolecular hydroamination of vinyl arene and dienes(Scheme 1.13).[98]

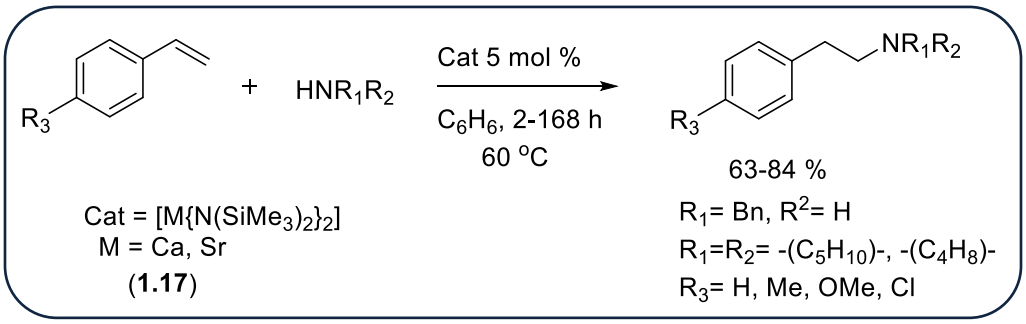

Scheme 1.13: Alkaline earth metal complexes are used to catalyze the intermolecular hydroamination of activated alkenes.

According to the reaction kinetics, the conversion rate is first order in the case of amine and alkene but second order in the case of catalyst. The total reaction turns into a pseudo-first-order reaction as the excess alkene is added, maintaining the catalyst concentration constant. The bond metathesis between the catalyst and amine to produce metal amide as precatalyst species is the first step in the alkaline earth metal catalysed hydroamination reaction, which is similar to the mechanism of the organolanthanides.

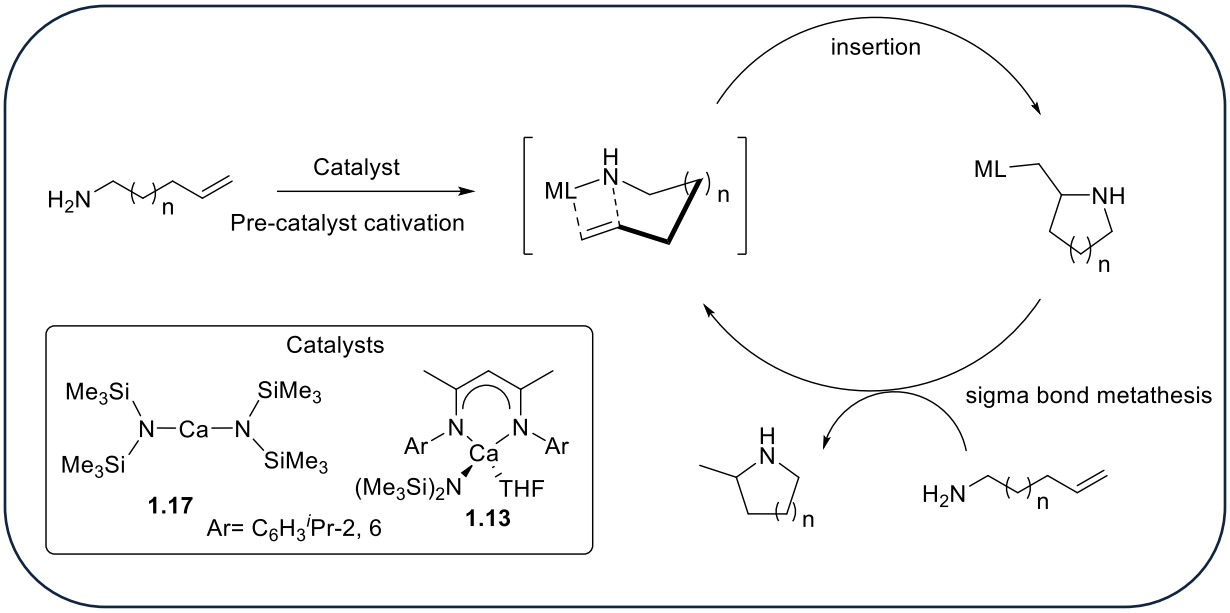

Scheme 1.14: A suggested catalytic cycle for the intramolecular hydroamination by calcium catalyst.

The alkene insertion to the Ca-N bond occurs in second step due to the intramolecular nucleophilic attack. Finally, the hydroamination product and active catalyst are produced by the σ-bond metathesis between the second amine molecule and the calcium alkyl. (Scheme 1.14).[99]

In 2008, the production of ureas and guanidines from respective isocyanates and carbodiimides, was further expanded using alkaline earth metal catalysed hydroamination.

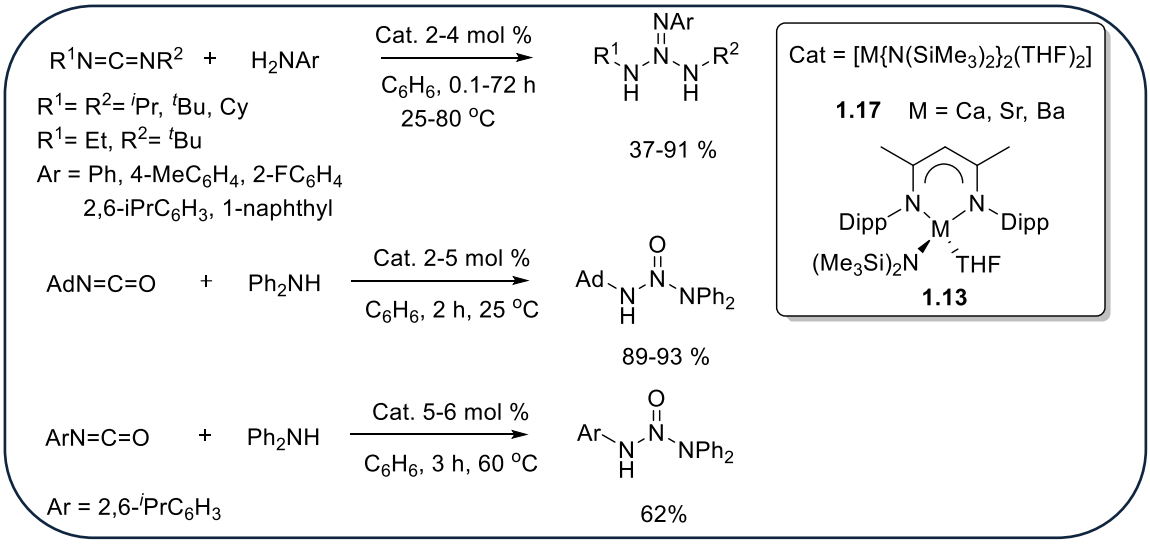

Scheme 1.15: Alkaline earth metal complexes catalyzed hydroamination of carbodiimides and isocyanates.

This was done using heteroleptic calcium amide complex (**1.13**) and [M{N(SiMe$_3$)$_2$}$_2$(THF)$_n$] (M = Ca, Sr, Ba; n = 0, 2) (**1.17**) the homoleptic alkaline earth metal series as precatalysts (Scheme 1.8).[100] In comparison to calcium and barium complexes, strontium complexes were discovered to have the highest turnover frequency.

1.4.3: Organo-magnesium and calcium-mediated hydrophosphination reactions

The insertion of a phosphine P-H bond into an unsaturated C=C bond is known as hydrophosphination. Harder et al. reported the hydrophosphination of alkynes using potent Lewis acidic cationic magnesium complex (**1.18**) to enlarge the hydroelementation. (Scheme 1.16).[101] Phenylacetylene can be hydrophosphinated with diphenylphosphine in the 10 mol % catalytic amount of **1.18**, which can act as a frustrated Lewis pair (FLP). It is interesting to note that the *Z*-isomer is the only product of hydrophosphination of terminal alkynes. However, internal alkynes did not react in this initial trial, and dialkylphosphine usage produced only traces of product.

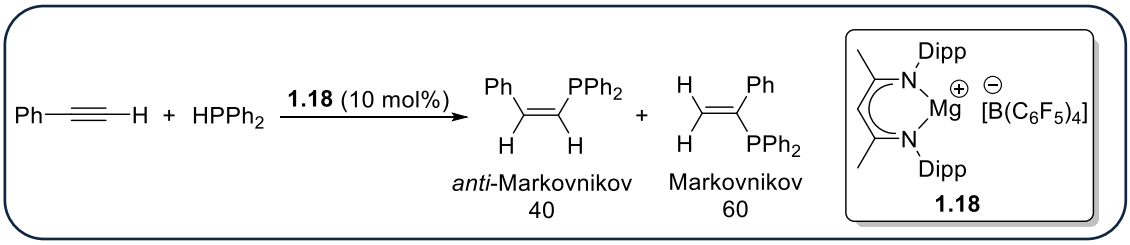

Scheme 1.16: ^{Dipp}Nacnac-magnesium cation catalyzed hydrophosphination of alkynes.

For the intermolecular hydrophosphination of activated alkenes and alkynes, Hill and coworkers used monomeric calcium as a catalyst (Scheme 1.17).[102] By adding a stereoselective P-H bond across the unsaturated alkene C-C bond, the reaction was carried out via the anti-Markovnikov pathway. The first step involves a calcium amide-diphenylphosphine σ-bond metathesis, which produces a ^{Dipp}Nacnac stabilised diphenylphosphine moiety (Scheme 1.18). Similarly, Westerhausen and coworkers have extensively explored the stoichiometric σ bond metathesis of homoleptic metal phosphides from alkaline earth metal amides.[103] The diphenylphosphine moiety stabilized by *β*-diketiminato subsequently underwent insertion of unsaturated C-C bond to generate $LCaCH_2CH(Ph)PR_2$ through syn-addition. In order to produce a phosphinated product and an active catalyst, the final catalytic step involves σ-bond metathesis with diphenylphosphine.

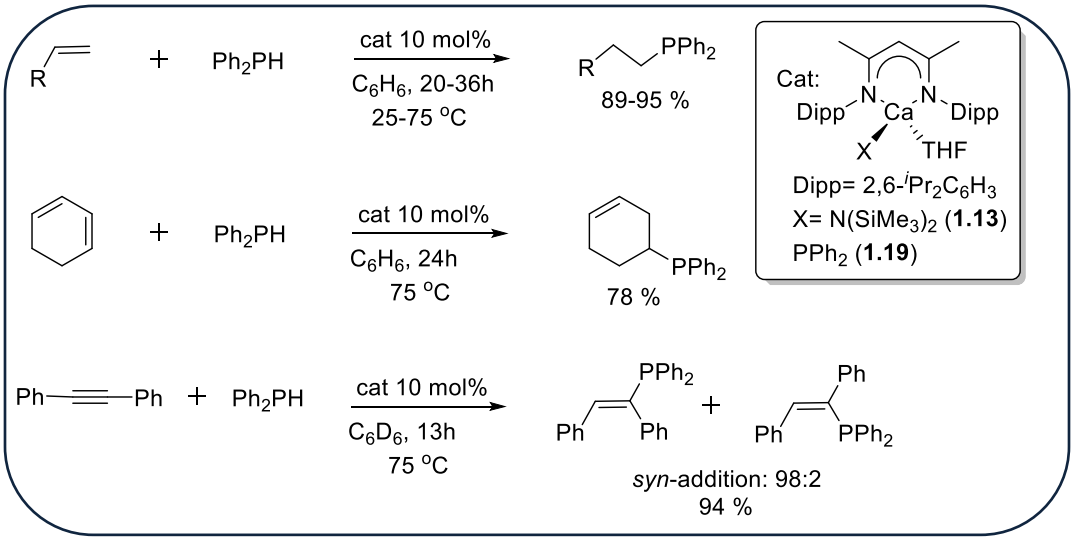

Scheme 1.17: Intermolecular hydrophosphination catalyzed by an organo-calcium complex.

Later, a homoleptic calcium complex $[(thf)_4Ca(PPh_2)_2]$ was used as catalyst by Westerhausen and coworkers for the hydrophosphination of phenyl substituted alkyne.[104] The hydrophosphination method based on alkaline earth metals was also extended to cabodiimides. In order to hydrophosphinate both symmetric and unsymmetric carbodiimide, a variety of alkaline earth amide complexes $[[M\{N(SiMe_3)_2\}_2(THF)_2]$, M = Ca, Sr, Ba] (**1.17**) were employed.[105]

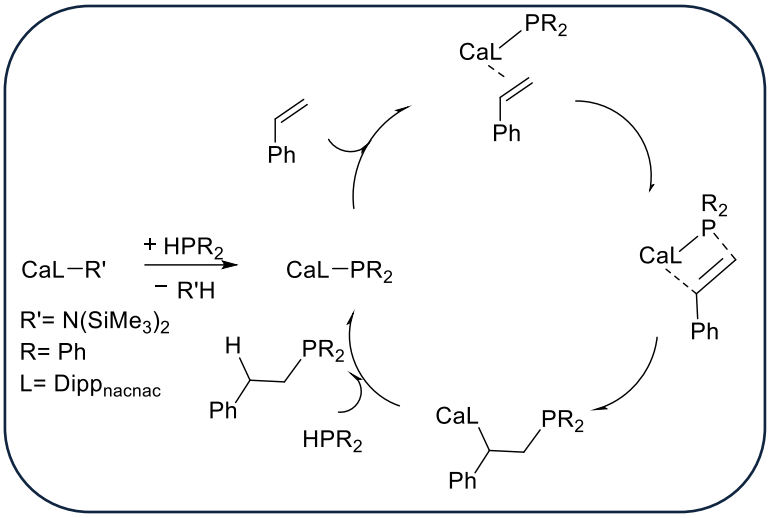

Scheme 1.18: Plausible mechanism for catalyzing alkene hydrophosphination.

The reaction proceeds by inserting the carbodiimide moiety into the metal-phosphide link, much like the hydroboration of carbodiimides. The active catalyst and phosphaguanidine are produced by adding more carbodiimide. The Westerhausen and Hill group then published the calcium phosphide compound [$(THF)_4Ca(PPh_2)_2$], and ^{Dipp}Nacnac supported calcium amide incorporation using carbodiimides.[106] Later, aldehydes and inactive ketones were selectively hydrophosphonylated, according to Sarazin and colleagues.[107]

1.5: Organo-magnesium hydride complexes and their application

Throughout the 1970s, Ashby and coworkers conducted several ground-breaking research on magnesium hydrides with an emphasis on the production of a wide variety of amide, alkoxide, halide, and hydrocarbyl hydridomagnesium derivatives, [HMgX] (X= Cl, Br, OR, NR_2, and R; R= alkyl, aryl, or cyclopentadienyl).[108] However, these were poorly defined structures, and were most likely oligomeric or polymeric. These compounds were synthesized by reacting the appropriate MgX_2 precursor with activated magnesium hydride (Scheme 1.19).[109]

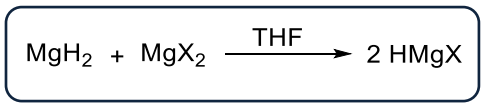

Scheme 1.19: Synthesis of hydridomagnesium derivatives by reacting MgX_2 with activated magnesium hydride.

In course of their comprehensive research on similarly coordinated molecular Mg(I) derivatives,[110,111] Jones and coworkers 2007 used a silane ($PhSiH_3$) metathesis reaction to produce the ^{Dipp}Nacnac-magnesium(II) hydride, [(^{Dipp}Nacnac)Mg(μ-H)]$_2$ (**1.20**, ^{Dipp}Nacnac= HC(MeCNDipp)$_2$]).[112] Specifically, [(^{Dipp}Nacnac)MgBu] was reacted with $PhSiH_3$ to produce compound **1.20** in a moderate yield then THF was added to produce the THF adduct [(^{Dipp}Nacnac)Mg(THF)(μ-H)]$_2$ (**1.21**) (Scheme 1.20).

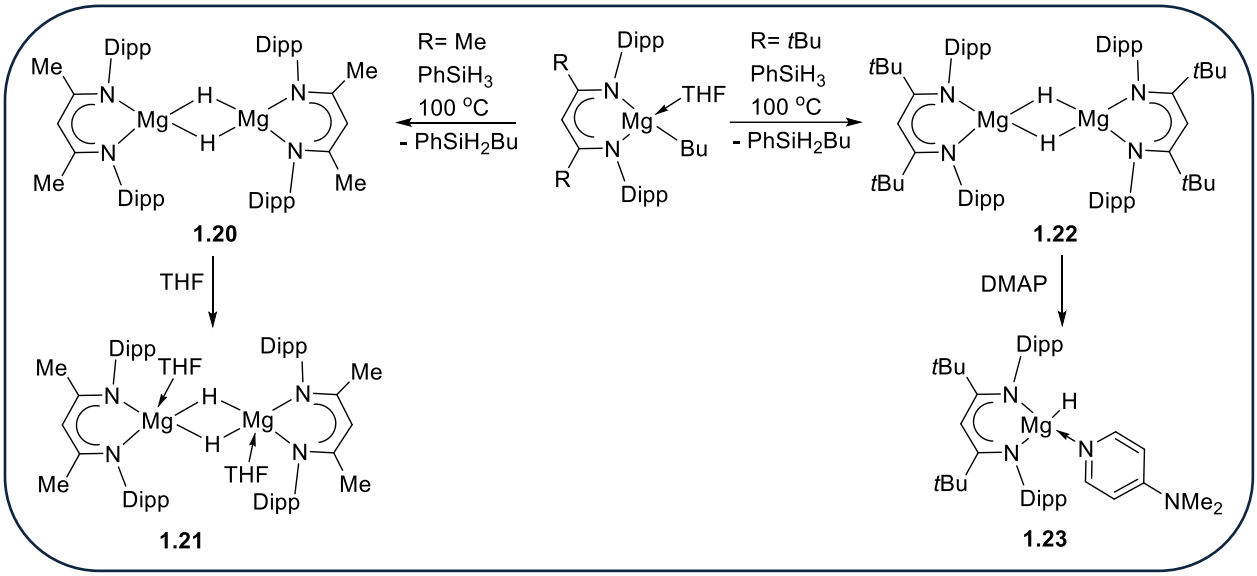

Scheme 1.20: Synthetic ways for ^{Dipp}Nacnac-magnesium hydrides **1.20**–**1.23**.

Hydride resonances were clearly detected at 4.03 (sharp) and 4.21 (wide) ppm in the ^{1}H NMR spectra of **1.20** and **1.21** in C_6D_6. Jones and Stasch continued their investigation by reporting that a tert-butyl-substituted counterpart of **1.20**, [($^{tBu/Dipp}$Nacnac)Mg(μ-H)]$_2$ [**1.22**, $^{tBu/Dipp}$Nacnac={HC-(*t*BuCNDipp)$_2$}$^-$], was attainable by the same technique, although under harsh reactions conditions (100 °C up to 16 h, Scheme 1.21).[113] Compound **1.22**, according to the same study, failed to produce an efficient THF adduct, but treatment with 4-dimethylamidopyridine (**4**-DMAP) yielded the monomeric complex of magnesium hydride [($^{tBu/Dipp}$Nacnac)Mg-(H)(DMAP)] (**1.23**), the first structural description of a terminal Mg–H bonding (Scheme 1.21). Further, Jones and coworkers showed that Mg(I) complexes, [(^{Dipp}Nacnac)Mg–Mg(^{Dipp}Nacnac)] (**1.24**) and [(^{Dep}Nacnac)- Mg–Mg(^{Dep}Nacnac)] (**1.25**), underwent oxidative hydrogenation with 1,3-cyclohexadiene which

produce quantitative amount of Mg(II) hydride **1.20** and its counterpart, [(^{Dep}Nacnac)Mg(μ-H)]$_2$ (**1.26**), respectively (Scheme 1.21).[114]

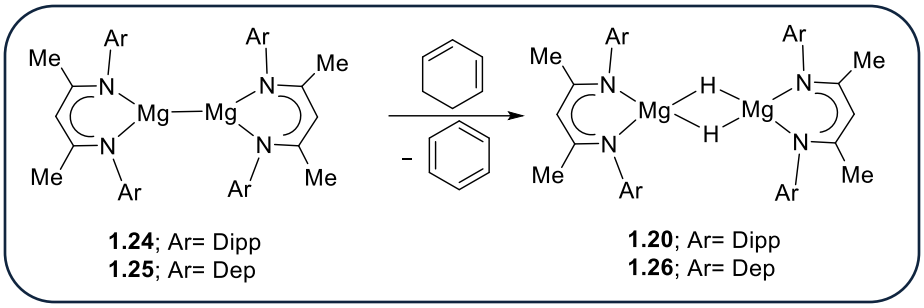

Scheme 1.21: Oxidative hydrogenation of Mg(I) compounds **1.25** and **1.26**.

Hill and coworkers utilized ^{Dipp}Nacnac-magnesium hydride; **1.20** for alkene insertion and as a potential catalyst for hydrosilylation of alkenes.[115a] The reaction of **1.20** with 1-hexene at 80 ºC leads to the formation of ^{Dipp}Nacnac-magnesium n-hexyl derivative; **1.27**.

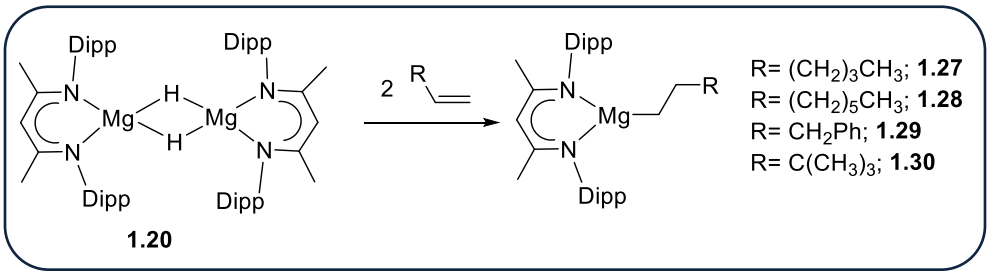

Scheme 1.22: Synthesis of the magnesium alkyl compounds **1.27**–**1.30** *via* alkene insertion.

Similarly, treatment of **1.20** with 1-octene, 3-phenyl-1-propene and 3,3-dimethyl-1-butene give their corresponding magnesium derivatives(**1.28-1.30**), respectively (Scheme 1.22). Further, they have utilized compound **1.20** as a catalyst for the hydrosilylation of alkenes using $PhSiH_3$. Hydrosilylated products were produced with good to outstanding yield, although reaction conditions were harsh as it took 4-30 days at 60-80 ºC to complete the reaction(Scheme 1.23).

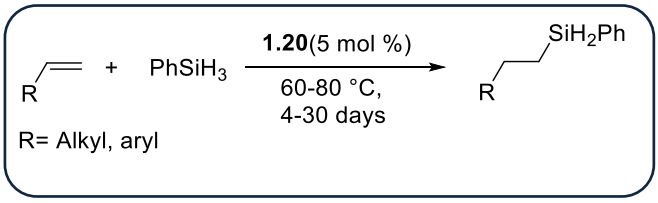

Scheme 1.23: Hydrosilylation of alkenes catalyzed by **1.20**.

1.6: Organo-calcium hydride complexes and their application

The existence of a heteroleptic calcium hydride species for the first time was noted by Harder and coworkers during the alkene hydrosilylation catalytic cycle utilising $[Ca(DMAT)_2(THF)_2]$ (**1.7**) as a catalyst.[115b] However, this organocalcium hydride could not be separated because of its significant instability. Subsequently, Harder and coworkers isolated the first organocalcium hydride $[(^{Dipp}Nacnac)CaH]_2$(**1.31**) complex by the reaction of $[^{Dipp}Nacnac$-$CaN(SiMe_3)_2(thf)]$ with $PhSiH_3$ in hexane (Scheme 1.24).[116] A singlet resonance at δ=4.45 ppm confirms calcium hydride in the ^1H NMR, and the Ca-H bond distances were 2.09(4)-2.21(3) Å.

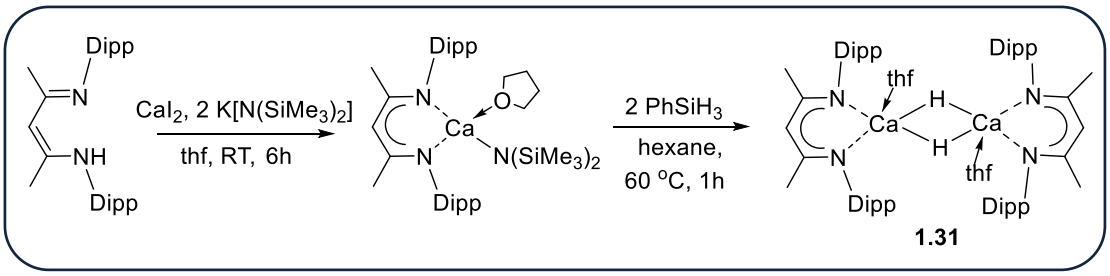

Scheme 1.24: Synthesis of first well-defined organocalcium hydride $[Dipp_{nacnac}$-$CaH(THF)]_2$.

In another procedure that involves the reaction of chelating N-macrocyclic ligand Me_3TACD-H and the Ca-$N(SiMe_3)_2$ precursor, Okuda and his colleagues isolated a cationic calcium hydride complex $[(Me_3TACD)_3Ca_3(\mu_3\text{-}H)_2]$(**1.32**).[117]

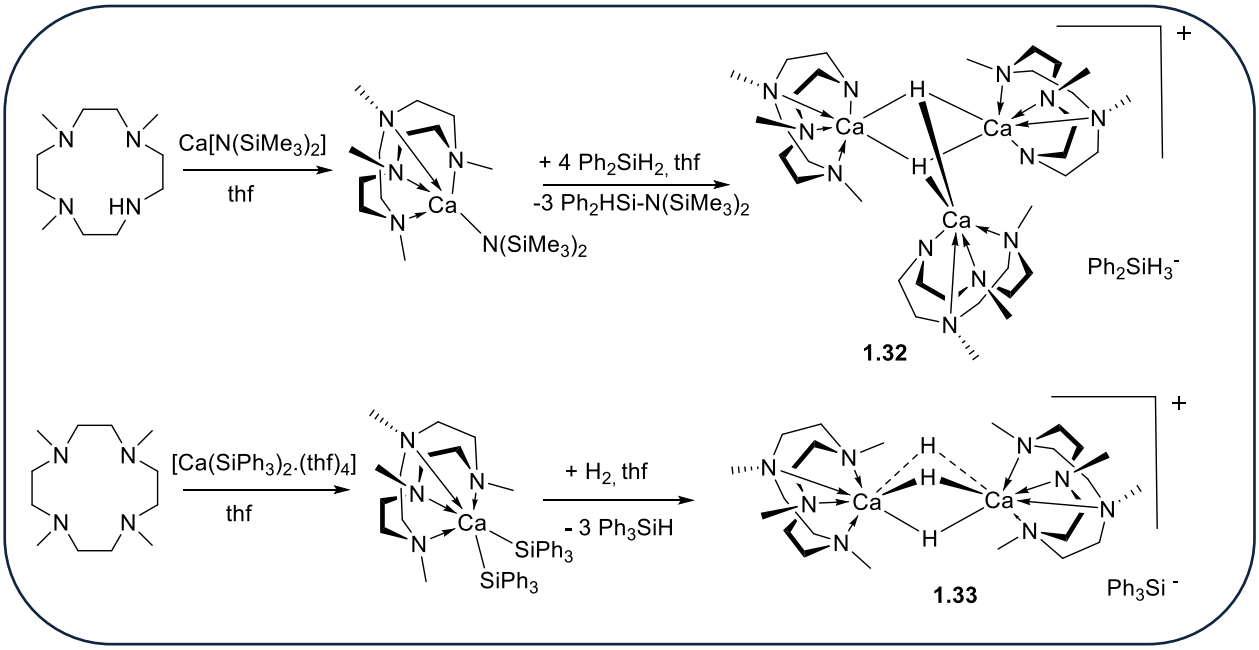

Scheme 1.25: The procedures used to produce the cationic calcium hydride compound.

The same group also published a dimeric calcium hydride complex $[Ca_2H_3(Me_4TACD)_2](SiPh_3)$(**1.33**), utilizing a neutral N-macrocyclic ligand, Ca-SiR_3 precursor, and H_2 (Scheme 1.25).[118] Another effort by Harder and colleagues involved precisely modified amidinate ligands to produce calcium hydride complexes (**1.34**).[119] By altering the substitution on the nitrogen atoms, and the amidinate system's core substituents, several amidinate ligands were studied. Only the nitrogen-substituted Dipp (2,6-diisopropylphenyl) was found resistant to ligand exchange. The *t*Bu and adamantyl groups on the backbone of the amidiante system made it easier to reach the compounds of dimeric calcium hydride (Scheme 1.26). The compound was also significantly stabilized by the aryl…Ca interaction.

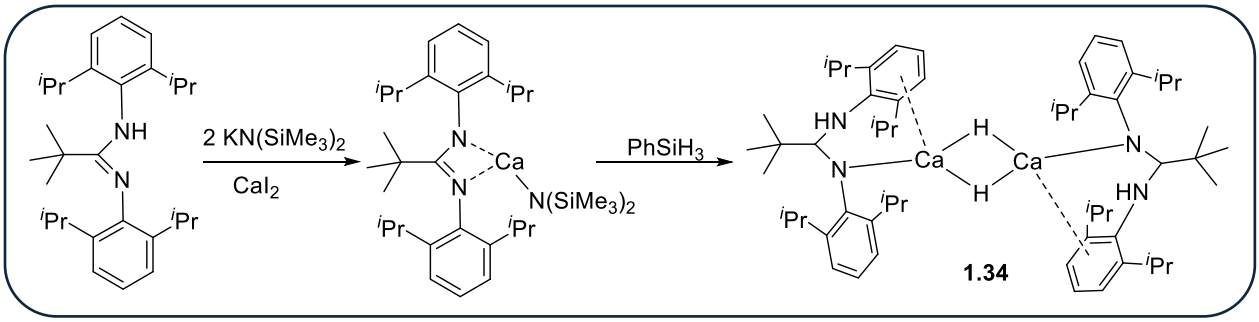

Scheme 1.26: Calcium hydride compounds are synthesized by modifying the amidinate ligand system.

The catalytic hydrogenation of conjugated alkenes for the first time using (^{Dipp}NacnacCaH)$_2$.THF and dibenzylcalcium complex was reported by Harder and coworkers.[120] These catalysts work well in moderate environments (20 ºC, 20 bar). The stoichiometric reaction between the catalyst and alkene proved that the initial step involved the addition of (^{Dipp}NacnacCaH)$_2$.THF to alkene. The σ-bond metathesis between organocalcium intermediate and H_2 took place in the second stage of the catalytic cycle (Scheme 1.27).

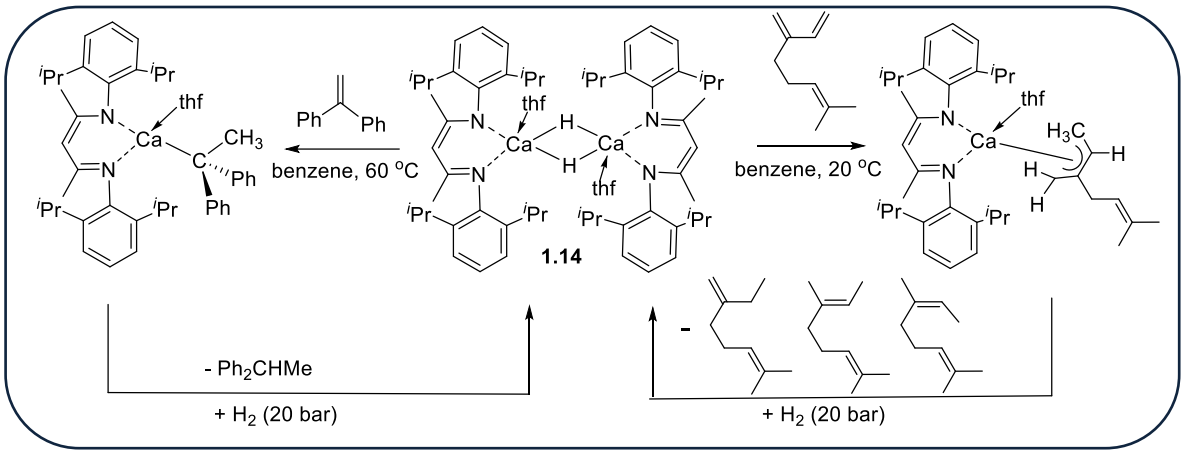

Scheme 1.27: Hydrogenation of activated alkenes catalyzed by calcium hydride.

The anticipated calcium benzylic complex was produced by the stoichiometric reaction of (^{Dipp}NacnacCaH)$_2$.THF with 1,1-diphenylethylene (DPE). It then passes through the protonation with H_2 to produce hydrogenated DPE. Polar solvents are used to expedite the reaction, however they can also cause unwanted oligomerization events.

1.7: Luminescent properties of organo-alkaline earth metal complexes

Electron-rich metals from the second or third row of the transition metal series are often coupled with electron-deficient ligands to form molecular photosensitizers.[121-123] A metal-to-ligand charge transfer (MLCT) is enabled by such a combination, which results in long-lasting emissive excited states. However, attention has switched to creating photosensitizers based on abundant elements in Earth's crust due to the rising emphasis on ecological and economic systems. Chandrasekhar and coworkers reported the first well-defined trinuclear luminescent magnesium complex (**1.35**) stabilized by a phosphorus-based tris-hydrazone ligand.[124] In the presence of triethylamine, the tris-hydrazone ligand interacts in a 2:3 stoichiometric ratio with $MgCl_2 \cdot 6H_2O$ to produce **1.35** (Scheme 1.28).

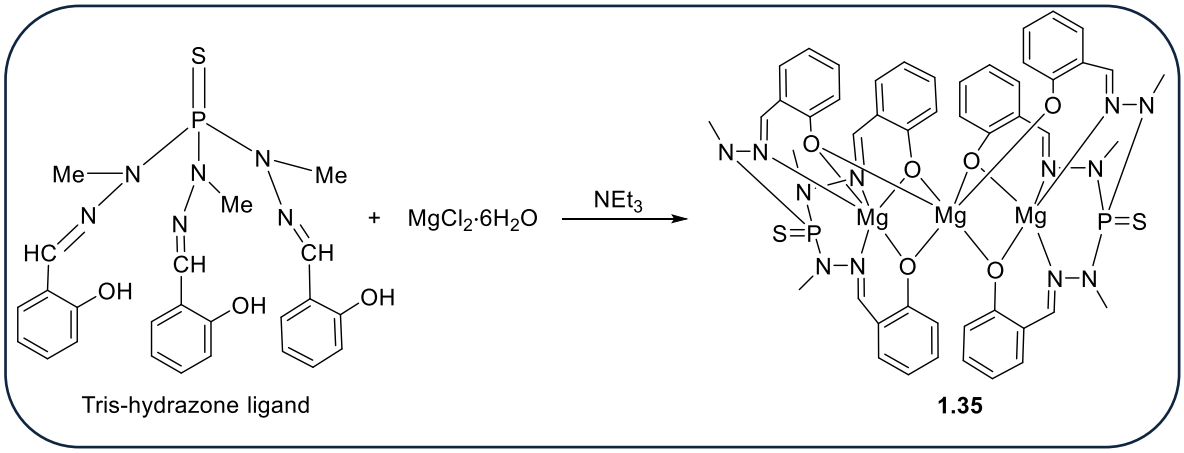

Scheme 1.28: Synthesis of first trinuclear luminescent magnesium complex (**1.35**).

Roesky and coworkers used diamidophosphine ligand to stabilize magnesium, calcium and strontium complexes.[125] The reaction of diamidophosphine ligand with Mg-(nBu)$_2$ in toluene leads to the formation of bimetallic species [(PNNP)Mg]$_2$ (**1.36**). While reaction with potassium bis(trimethylsilyl)amide and subsequent addition of metal iodide in THF at 60 ºC gives monometallic calcium [(PNNP)Ca(THF)$_3$] and strontium [(PNNP)Ca(THF)$_3$] complexes(Scheme 1.29).

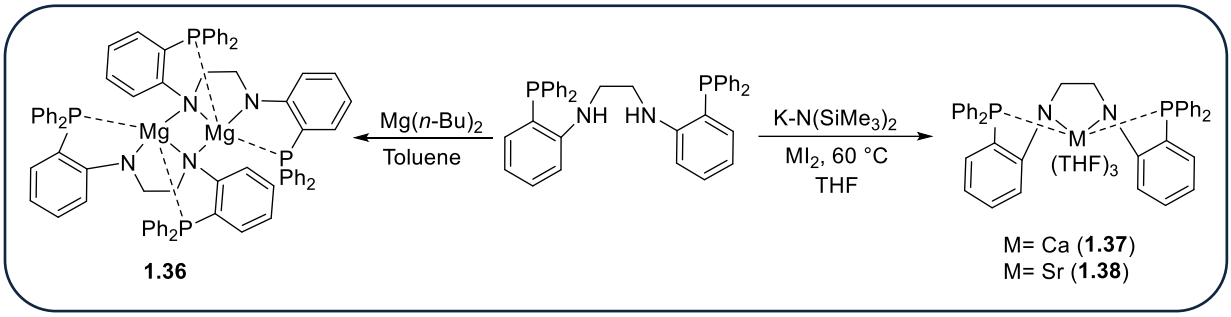

Scheme 1.29: Synthesis of diamidophosphine ligand stabilized alkaline earth metal complexes (**1.36-1.38**).

Further, photoluminescent studies for magnesium complex reveal that the complex is intensely fluorescent and shows 27% and 34% quantum yield in solid and liquid states, respectively. Similarly, calcium and strontium complexes show 14% & 21% and 12% & 25% quantum yield in solution and solid states, respectively. Last but not the least, Munz and coworkers showed that lithium and magnesium complexes based on carbazolide bridged mesoionic bis-carbene pincer

ligand exhibit bright luminescence with quantum yields of up to 14%,[34y] however the magnesium compound was not structurally authenticated, presumably due to solubility issues.

1.8: Organo-magnesium and calcium catalyzed cyclotrimerization of isocyanates

Cyclotrimerization of isocyanate derivatives is an important and atom-economical transformation to access isocyanurates, which have industrial and commercial applications, as they have excellent thermal stability and flame resistance properties. Therefore, adding isocyanurate frameworks to polymer networks could improve the physical qualities of polyurethanes, copolymer resins, plastics, and coating materials, including water resistance, transparency, impact resistance, higher heat and chemical resistance.[126,127] Additionally, isocyanurates are necessary building blocks in the production of microporous (poly)isocyanurate, which has been used as a support in heterogeneous catalysis.[128] There is no report on cyclotrimerization of isocyanates using organo-magnesium complex as a catalyst apart from the report fromHarder and coworkers, who synthesized a calcium carbene complex (**1.39**) by the reaction of (DIPP-N=(Ph_2)P)$_2CH_2$ with (*para*-*t*Bu-benzyl)$_2$Ca·(THF)$_4$ (Scheme 1.30). However, no further substrate scope was studied.

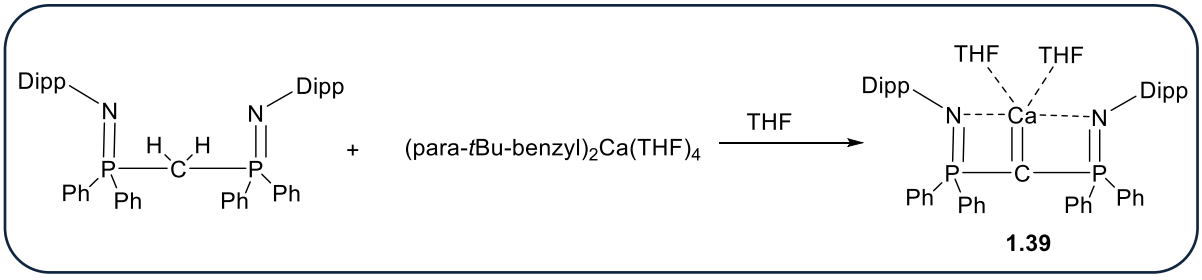

Scheme 1.30: Synthesis of calcium carbene complex (**1.39**).

Further they utilized **1.39** as a catalyst for the trimerization of PhNCO.[129] However, they did not explore substrate scope

1.9: Aim and outline of this thesis

There are five chapters in the thesis. While this chapter describes the advances of alkaline earth metal chemistry toward catalysis and luminescence studies, the other four chapters will showcase our contribution. The thesis aims to increase our knowledge of the structural characteristics,

reactivity, and synthesis of organo-magnesium and calcium complexes. The work on the thesis was primarily focused on the following points:

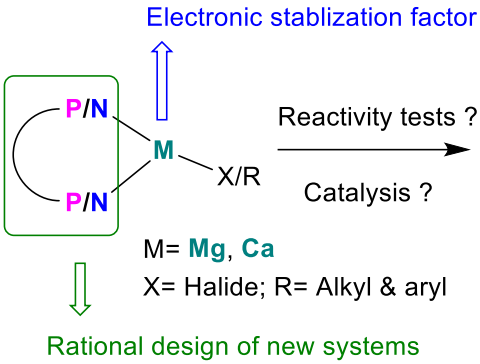

1) Designing novel monoanionic N- and P-donor-based multidenate ligands to eliminate Schlenk equilibrium.

2) Preparation of the hydrocarbon soluble monomeric/heteroleptic organo-magnesium and calcium complexes.

3) The application of these soluble organo-magnesium and calcium complexes in homogenous catalysis such as hydroboration of various functional groups and cyclotrimerization of isocyanates.

4) To study the photophysical properties of luminescent organo-magnesium complexes.

5) To conduct experimental and theoretical investigations on the proposed catalytic mechanisms.

Chapter 2 presents the synthesis and characterization of N,O-ketiminato ligand stabilized homoleptic and heteroleptic magnesium and calcium complexes. Single crystal XRD studies determined the structural and the bonding arrangement of all the complexes. DFT studies support the different reactivity of two N,O-ketiminato ligands with biphenyl and terphenyl substituents on the nitrogen atom.

Chapeter 3 contains the synthesis of various monomeric magnesium alkyl complexes using bis(phosphino)carbazole framework, and among them magnesium-methyl complex has been utilised as a hydroboration catalyst fors alkenes and alkynes with pinacolborane (HBpin). A broad variety of aromatic and aliphatic alkenes and alkynes were efficiently reduced. Anti-Markovnikov regioselective hydroboration of alkenes and alkynes was achieved, which was confirmed by deuterium-labelling experiments. The work represents the first example of the use of magnesium in homogeneous catalytic hydroboration of alkene with broad substrate scope. DFT calculations and experimental mechanistic exploration provided an understanding of the reaction's mechanism. Finally, the hydroboration methodology was extended to terpenes.

Chapter 4 covers the structural characterization and synthesis of well-defined 2,2'-pyridylpyrrolide (PyPyrH) ligand supported two magnesium complexes. Both complexes show bright luminescence with a quantum yield of 22% and 16% in the solid state. Theoretical calculations reveal that the emissive propoerties is originated from the intra- and inter ligand charge transfer.

Chapter 5 accounts the synthesis of a calcium complex bearing a tetradentate monoanionic ligand with a diaminoethane core and phenolate and pyridine peripheral donors. Single crystal X-ray studies on calcium complex revealed that LiI was also co-crystallized, leading to a four-membered ring with four different elements. Further, calcium complex was found to be an efficient catalyst for the cyclotrimerization of a variety of aromatic isocyanates under mild conditions.

1.10: References

[1] a) See Lavoisier, Antoine (1789), Traité Élémentaire de Chimie, présenté dans un ordre nouveau, et d'après des découvertes modernes; b) Lavoisier, Antoine (1790), Elements of Chemistry in New Systematic Order, Containing All Modern Discoveries, illustrated with 13 Copperplates, translated from the French by Robert Kerr (1 ed.), Edinburgh: William Creech, retrieved 2012-04-15.

[2] R. E. Krebs (2006). The history and use of our earth's chemical elements: a reference guide. Greenwood Publishing Group. pp. 65–81. ISBN 0-313-33438-2.

[3] J. A. Cowan, *Chem. Rev*., **1998**, *98*, 1067–1088.

[4] K. D. Cashman, *British Journal of Nutrition*, **2007**, *87*, S169–S177.

[5] B. M. Trost, *Science*, **1991**, *254*, 1471–1477.

[6] S. Harder, *Chem. Rev*., **2010**, *110*, 3852–3876.

[7] A. G. M. Barrett, M. R. Crimmin, M. S.Hill, P. A. Procopiou, *Proc. R. Soc. London, Ser. A*, **2010**, *466*, 927–963.

[8] (a) V. Grignard, *Ann. Chim*., **1901**, *24*, 433-490; (b) D. Seyferth, *Organometallics*, **2009**, *28*, 1598–1605.

[9] *The Chemistry of Organomagnesium Compounds*, ed. Z. Rappaport and I. Marek, Wiley-VCH, Weinheim, Germany, **2008**.

[10] J. F. Garst, M. P. Soriaga, *Coord. Chem. Rev*., **2004**, *248*, 623–652.

[11] S. D. Robertson, M. Uzelac, R. E. Mulvey, *Chem. Rev*., **2019**, *119*, 8332–8405.

[12] D. Tilly, F. Chevallier, F. Mongin, P. C. Gros, *Chem. Rev*., **2014**, *114*, 1207–1257.

[13] T. Klatt, J. T. Markiewicz, C. Sämann, P. Knochel, J. Org. Chem., **2014**, *79*, 4253–4269.

[14] H. Ila, O. Baron, A. J. Wagner, P. Knochel, *Chem. Lett.*, **2006**, *35*, 2–7.

[15] P. Knochel, W. Dohle, N. Gommermann, F. F. Kneisel, F. Kopp, T. Korn, I. Sapountzis, V. A. Vu, *Angew. Chem., Int. Ed*., **2003**, *42*, 4302–4320.

[16] M. Balkenhohl, P. Knochel, *SynOpen*, **2018**, *2*, 78–95.

[17] P. Knochel, M. A. Schade, S. Bernhardt, G. Manolikakes, A. Matzger, F. M. Piller, C. J. Rohbogner and M. Mosrin, *Beilstein J. Org. Chem*., **2011**, *7*, 1261–1277.

[18] C. Elschenbroich, A. Salzer, *Organometallics*: A Concise Introduction, 2nd ed., Weinheim, VCH, **1992**; Grignard Reagents New Developments (Ed.: H. G. Richey) *Wiley*, Chichester, **2000**.

[19] (a) J. J. Eisch, *Organometallics*, **2002**, *21*, 5439–5463; (b) B. J. Wakefield, *Organomet. Chem. Rev*. **1966**, *1*, 131−156; (c) H. Normant, *Bull. Soc. Chim. Fr.*, **1972**, 2161−2175.

[20] C. Lambert, P. v. R. Schleyer, *Angew. Chem., Int. Ed.*, **1994**, *33*, 1129−1140.

[21] (a) J. S. Alexander, K. Ruhlandt-Senge, *Angew. Chem., Int. Ed*., **2001**, *40*, 2658−2660; (b) J. S. Alexander, K. Ruhlandt-Senge, H. Hope, *Organometallics*, **2003**, *22*, 4933−4937.

[22] (a) R. Fischer, M. Gärtner, H. Görls, M. Westerhausen, *Organometallics*, **2006**, *25*, 3496−3500; (b) J. S. Alexander, K. Ruhlandt-Senge, *Chem. Eur. J*., **2004**, *10*, 1274−1280.

[23] (a) P. R. Markies, T. Nomoto, G. Schat, O. S. Akkerman, F. Bickelhaupt, W. J. J. Smeets, A. L. Spek, *Organometallics*, **1991**, *10*, 3826−3837; (b) M. Gaertner, H. Goerls, M. Westerhausen, *Synthesis*, **2007**, 725−730.

[24] W. Schlenk, W. Jr. Schlenk, *Chem. Ber.*, **1929**, *B62*, 920.

[25] R. D. Shannon, *Acta Crystallogr.*, **1976**, *A32*, 751.

[26] R. Zerger, G. Stucky, *J. Organomet. Chem*., **1974**, *80*, 7−17.

[27] (a) S. C. Sockwell, T. P. Hanusa and J. C. Huffman, *J. Am. Chem. Soc.*, **1992**, *114*, 3393–3399; (b) M. J. Harvey and T. P. Hanusa, *Organometallics*, **2000**, *19*, 1556–15566; (c) H. Sitzmann, T. Dezember and M. Ruck, *Angew. Chem., Int. Ed.*, **1998**, *37*, 3113–3116; (d) J. S. Overby and T. P. Hanusa, *Organometallics*, **1996**, *15*, 2205–2212; (e) G. Moesges, F. Hampel and P. v. R. Schleyer, *Organometallics*, **1992**, *11*, 1769–1770; (f) S. Harder, M.

Lutz and A. W. G. Straub, *Organometallics*, **1997**, *16*, 107–113; (g) N. Leyser, K. Schmidt and H.-H. Brintzinger, *Organometallics*, **1998**, *17*, 2155–2161; (h) D. J. Burkey and T. P. Hanusa, *Organometallics*, **1996**, *15*, 4971–4976; (i) P. S. Tanner, R. A. Williams and T. P. Hanusa, *Inorg. Chem.*, **1993**, *32*, 2234–2235.

[28] F. G. N. Cloke, P. B. Hitchcock, M. F. Lappert, G. A. Lawless, B. Royo, *J. Chem. Soc. Chem. Commun*., **1991**, 724−726.

[29] (a) C. Eaborn, S. A. Hawkes, P. B. Hitchcock, J. D. Smith, *Chem. Commun*., **1997**, 1961−1962; (b) M. R. Crimmin, A. G. M. Barrett, M. S. Hill, D. J. MacDougall, M. F. Mahon, P. A. Procopiou, *Chem. Eur. J.*, **2008**, *14*, 11292−11295; (c) F. Feil, S. Harder, *Organometallics*, **2000**, *19*, 5010−5015; (d) S. Harder, F. Feil, A. Weebe, *Organometallics*, **2001**, *20*, 1044−1046.

[30] E. Beckmann, *Ber. Dtsch. Chem. Ges*., **1905**, *38*, 904−906.

[31] H. Gilman, F. Schulze, *J. Am. Chem. Soc*., **1926**, *48*, 2463−2467.

[32] C. Ruspic, S. Harder, *Organometallics*, **2005**, *24*, 5506−5508.

[33] R. Fischer, M. Gaertner, H. Goerls, M. Westerhausen, *Organometallics*, **2006**, *25*, 3496−3500.

[34] (a) G. J. Moxey, F. Ortu, L. G. Sidley, H. N. Strandberg, A. J. Blake, W. Lewis, D. L. Kays, *Dalton Trans.,* **2014**, *43*, 4838−4846; (b) R. J. Schwamm, B. M. Day, N. E. Mansfield, W. Knowelden, P. B. Hitchcock, M. P. Coles, *Dalton Trans*., **2014**, *43*, 14302−14314; (c) B. M. Day, W. Knowelden, M. P. Coles, *Dalton Trans*., **2012**, *41*, 10930−10933; (d) J. Schwamm, M. P. Coles, *Organometallics*, **2013**, *32*, 5277–5280; (e) B. M. Day, N. E. Mansfield, M. P. Coles, P. B. Hitchcock, *Chem. Commun*., **2011**, *47*, 4995–4997; (f) C. Jones, *Coord. Chem. Rev.*, **2010**, *254*, 1273−1289; (g) C. Glock, C. Loh, H. Goerls, S. Krieck, M. Westerhausen, *Eur. J. Inorg. Chem.*, **2013**, 3261−3269; (h) M. K. Barman, A. Baishya, S. Nembenna, *J. Organomet. Chem.,* **2015**, *785*, 52−60; (i) S.-O. Hauber, F. Lissner, G. B. Deacon, M. Niemeyer, *Angew. Chem., Int. Ed.,* **2005**, *44*, 5871−5875; (j) A. G. M. Barrett, M. R. Crimmin, M. S. Hill, P. B. Hitchcock, G. Kociok-Köhn, P. A. Procopiou, *Inorg. Chem.,* **2008**, *47*, 7366−7376; (k) S. Nembenna, H. W. Roesky, S. Nagendran, A. Hofmeister, J. Magull, P.-J. Wilbrandt, M. A. Hahn, *Angew. Chem., Int. Ed.,* **2007**, *46*, 2512−2514; (l) A. G. M. Barrett, M. R. Crimmin, M. S. Hill, P.

B. *Hitchcock*, P. A. Procopiou, *Angew. Chem., Int. Ed.,* **2007**, *46*, 6339−6342; (m) C. Ruspic, S. Harder, *Inorg. Chem.,* **2007**, *46*, 10426−10433; (n) M. Westerhausen, M. H. Digeser, C. Gückel, H. Nöth, J. Knizek, W. Ponikwar, *Organometallics*, **1999**, *18*, 2491−2496; (o) S. P. Sarish, A. Jana, H. W. Roesky, T. Schulz, M. John, D. Stalke, *Inorg. Chem.,* **2010**, *49*, 3816−3820; (p) S. P. Sarish, S. Nembenna, S. Nagendran, H. W. Roesky, *Acc. Chem. Res.,* **2011**, *44*, 157−170; (q) F. Ortu, G. J. Moxey, A. J. Blake, W. Lewis, D. L. Kays, *Inorg. Chem.,* **2013**, *52*, 12429−12439; (r) I. Koehne, R. Herbst-Irmer, D. Stalke, *Eur. J. Inorg. Chem.,* **2017**, 3322–3326; (s) I. Koehne, S. Bachmann, T. Niklas, R. Herbst-Irmer, D. Stalke, *Chem. Eur. J.* **2017**, *23*, 13141–13149; (t) I. Koehne, N. Graw, T. Teuteberg, R. Herbst-Irmer, D. Stalke, *Inorg. Chem.*, **2017**, *56*, 14968−14978; (u) F. Ortu, G. J. Moxey, A. J. Blake, W. Lewis, D. L. Kays, *Inorg. Chem.*, **2013**, *52*, 12429−12439; (v) N. Sen, S. Pal, V. V. Khade, S. Khan, *Eur. J. Inorg. Chem.*, **2019**, *41*, 4450–4454; (w) S. Datta, P. W. Roesky, S. Blechert, *Organometallics*, **2007**, *26*, 4392-4394; (x) D. J. Darensbourg, W. Choi, C. P. Richers, *Macromolecules*, **2007**, *40*, 3521-3523; (y) P. Pinter, C. M. Schüßlbauer, F. A. Watt, N. Dickmann, R. Herbst-Irmer, B. Morgenstern, A. Grünwald, T. Ullrich, M. Zimmer, S. Hohloch, D. M. Guldi, D. Munz, *Chem. Sci*., **2021**, *12*, 7401–7410.

[35] (a) A. Friedrich, J. Eyselein, J. Langer, S. Harder, *Organometallics,* **2021**, *40*, 448−457; (b) A. Friedrich, J. Pahl, J. Eyselein, J. Langer, N. van Eikema Hommes, A. Görling, S. Harder, *Chem. Sci*., **2021**, *12*, 2410–2418.

[36] S. Harder, *Angew. Chem., Int. Ed*., **2004**, *43*, 2714−2718.

[37] S. Hong, T. J. Marks, *Acc. Chem. Res*., **2004**, *37*, 673−686.

[38] A. Molander, J. A. C. Romero, *Chem. Rev*., **2002**, *102*, 2161−2186.

[39] Y. W. Li, T. J. Marks, *Organometallics*, **1996**, *15*, 3770−3772.

[40] M. R. Gagné, T. J. Marks, *J. Am. Chem. Soc.*, **1989**, *111*, 4108−4109.

[41] S. W. Hong, S. Tian, M. V. Metz, T. J. Marks, *J. Am. Chem. Soc.*, **2003**, *125*, 14768−14783.

[42] S. D. Wobser, C. J. Stephenson, M. Delferro, T. J. Marks, *Organometallics*, **2013**, ***32,*** 1317−1327.

[43] B. D. Stubbert, T. J. Marks, *J. Am. Chem. Soc.*, **2007**, *129*, 4253−4271.

[44] X. H. Yu, S. Seo, T. J. Marks, *J. Am. Chem. Soc.*, **2007**, *129*, 7244−7245.

[45] A. Dzudza, T. J. Marks, *Org. Lett.*, **2009**, *11*, 1523−1526.

[46] P. W. Roesky, U. Denninger, C. L. Stern, T. J. Marks, *Organometallics*, **1997**, *16*, 4486−4492.

[47] A. Motta, I. L. Fragala, T. J. Marks, *Organometallics*, **2005**, *24*, 4995−5003.

[48] A. M. Kawaoka, M. R. Douglass, T. J. Marks, *Organometallics*, **2003**, *22*, 4630−4632.

[49] S. Y. Seo, X. H. Yu, T. J. Marks, *J. Am. Chem. Soc.*, **2009**, *131*, 263−273.

[50] S. Hong, A. M. Kawaoka, T. J. Marks, *J. Am. Chem. Soc.*, **2003**, *125*, 15878−15892.

[51] M. R. Douglass, C. L. Stern, T. J. Marks, *J. Am. Chem. Soc.*, **2001**, *123*, 10221−10238.

[52] C. J. Weiss, S. D. Wobser, T. J. Marks, *Organometallics*, **2010**, *29*, 6308−6320.

[53] A. Dzudza, T. J. Marks, *J. Org. Chem.*, **2008**, *73*, 4004−4016.

[54] S. Seo, T. J. Marks, *Chem. Eur. J.*, **2010**, *16*, 5148−5162.

[55] C. J. Weiss, T. J. Marks, *Dalton Trans.*, **2010**, *39*, 6576−6588.

[56] A. M. Seyam, B. D. Stubbert, T. R. Jensen, J. J. O'Donnell, C. L. Stern, T. J. Marks, *Inorg. Chim. Acta*, **2004**, *357*, 4029−4035.

[57] A. Motta, I. L. Fragala, T. J. Marks, *Organometallics*, **2006**, *25*, 5533−5539.

[58] V. M. Arredondo, S. Tian, F. E. McDonald, T. J. Marks, *J. Am. Chem. Soc.*, **1999**, *121*, 3633−3639.

[59] Y. W. Li, T. J. Marks, *J. Am. Chem. Soc.*, **1998**, *120*, 1757−1771.

[60] J. S. Ryu, T. J. Marks, F. E. McDonald, *J. Org. Chem.*, **2004**, *69*, 1038−1052.

[61] A. M. Kawaoka, T. J. Marks, *J. Am. Chem. Soc.*, **2005**, *127*, 6311−6324.

[62] J. S. Ryu, G. Y. Li, T. J. Marks, *J. Am. Chem. Soc.*, **2003**, *125*, 12584−12605.

[63] X. H. Yu, T. J. Marks, *Organometallics*, **2007**, *26*, 365−376.

[64] L. Jia, X. M. Yang, A. M. Seyam, I. D. L. Albert, P. F. Fu, S. T. Yang, T. J. Marks, *J. Am. Chem. Soc.*, **1996**, *118*, 7900−7913.

[65] S. Seo, X. H. Yu, T. J. Marks, *Tetrahedron Lett.*, **2013**, *54*, 1828−1831.

[66] G. Jeske, H. Lauke, H. Mauermann, H. Schumann, T. J. Marks, *J. Am. Chem. Soc.*, **1985**, *107*, 8111−8118.

[67] G. Jeske, H. Lauke, H. Mauermann, P. N. Swepston, H. Schumann, T. J. Marks, *J. Am. Chem. Soc.*, **1985**, *107*, 8091−8103.

[68] A. S. Dudnik, V. L. Weidner, A. Motta, M. Delferro, T. J. Marks, *Nature Chem.*, **2014**, *6*, 1100−1107.

[69] A. Yaroshevsky, *Geochem. Int*., **2006**, *44*, 48−55.

[70] Anastas, P. T.; Crabtree, R. H. *Handbook of Green Chemistry*; Wiley- VCH: Weinheim, Germany, **2009**; Vol. 1.

[71] H. C. Brown, B. C. Subba Rao, *J. Am. Chem. Soc*., **1956**, *78*, 5694−5695.

[72] C. Chong, R. Kinjo, *ACS Catal*., **2015**, *5*, 3238−3259.

[73] M. L. Shegavi, S. K. Bose, *Catal. Sci. Technol*., **2019**, *9*, 3307−3336.

[74] D. Leonori, V. K. Aggarwal, *Angew. Chem., Int. Ed.*, **2015**, *54*, 1082−1096.

[75] N. Miyaura, A. Suzuki, *Chem. Rev*., **1995**, *95*, 2457−2483.

[76] A. Suzuki, *Angew. Chem., Int. Ed*., **2011**, *50*, 6722−6737.

[77] M. Arrowsmith, M. S. Hill, T. Hadlington, G. Kociok-Köhn, C. Weetman, *Organometallics*, **2011**, *30*, 5556−5559.

[78] M. Arrowsmith, M. S. Hill, G. Kociok-Köhn, *Chem. Eur. J*., **2013**, *19*, 2776–2783.

[79] M. Arrowsmith, T. J. Hadlington, M. S. Hill, G. Kociok-Köhn, *Chem. Commun.*, **2012**, *48*, 4567–4569.

[80] C. Weetman, M. S. Hill, M. F. Mahon, *Chem. Commun.*, **2015**, *51*, 14477–14480.

[81] C. Weetman, M. D. Anker, M. Arrowsmith, M. S. Hill, G. Kociok-Köhn, D. J. Liptrot, M. F. Mahon, *Chem. Sci*., **2016**, *7*, 628–641.

[82] C. Weetman, M. S. Hill, M. F. Mahon, *Chem. Eur. J*., **2016**, *22*, 7158–7162.

[83] Y. Yang, M. D. Anker, J. Fang, M. F. Mahon, L. Maron, C. Weetmanb, M. S. Hill, *Chem. Sci*., **2017**, *8*, 3529–3537.

[84] M. Magre, B. Maity, A. Falconnet, L. Cavallo, M. Rueping, *Angew. Chem., Int. Ed.* **2019**, *58*, 7025–7029.

[85] M. Magre, M. Szewczyk, M. Rueping, *Chem. Rev*., **2022**, *122*, 8261−8312.

[86] M. Rauch, S. Ruccolo, G. Parkin, *J. Am. Chem. Soc*. **2017**, *139*, 13264−13267.

[87] S. Yadav, S. Pahar, S. S. Sen, *Chem. Commun.*, **2017**, *53*, 4562−4564.

[88] S. Harder, J. Spielmann, *J. of Organometal. Chem.*, **2012**, *698*, 7−14.

[89] K. Burgess, M. Jaspars, *Tet. Lett.*, 1993, 34, 6813−6816.

[90] (a) A. Togni, H. Grutzmacher, *Catalytic Heterofunctionalization*; VCH: Weinheim, Germany, **2001**; (b) M. Nobis, B. Driessen-Hölscher, *Angew. Chem., Int. Ed.*, **2001**, *40*, 3983−3985; (c) G. A. Molander, J. A. C. Romero, *Chem. Rev.,* **2002**, *102*, 2161−2186; (d) S. Hong, T. J. Marks, *Acc. Chem. Res.,* **2004**, *37*, 673−686; (e) R. Severin, S. Doye, *Chem. Soc. Rev.,* **2007**, *36*, 1407−1420; (f) T. E. Müller, K. C. Hultzsch, M. Yus, F. Foubelo, T. Tada, *Chem. Rev.*, **2008**, *108*, 3795−3892; (g) P. W. Roesky, *Angew. Chem. Int. Ed.*, **2009**, *48*, 4892−4894.

[91] J. F. Dunne, D. B. Fulton, A. Ellern, A. D. Sadow, *J. Am. Chem. Soc.* **2010**, *132*, 17680–17683.

[92] M. R. Crimmin, I. J. Casely, M. S. Hill, *J. Am. Chem. Soc.*, **2005**, *127*, 2042−2043.

[93] S. Datta, P. W. Roesky, S. Blechert, *Organometallics*, **2007**, *26*, 4392−4394.

[94] (a) A. G. M. Barrett, M. R. Crimmin, M. S. Hill, P. B. Hitchcock, G. Kociok-Köhn, P. A. Procopiou, *Inorg. Chem.*, **2008**, *47*, 7366−7376.; (b) M. Arrowsmith, M. S. Hill, G. Kociok-Köhn, *Organometallics*, **2009,** *28*, 1730−1738.

[95] J. E. Baldwin, *J. Chem. Soc., Chem. Commun.*, **1976**, 734−736.

[96] M. E. Jung, G. Piizzi, *Chem. Rev.*, **2005**, *105*, 1735−1766.

[97] F. Buch, S. Harder, *Z. Naturforsch.*, **2008**, *63b*, 169−177.

[98] A. G. M. Barrett, C. Brinkmann, M. R. Crimmin, M. S. Hill, P. Hunt, P. A. Procopiou, *J. Am. Chem. Soc.*, **2009**, *131*, 12906−12907.

[99] M. R. Crimmin, M. Arrowsmith, A. G. M. Barrett, I. J. Casely, M. S. Hill, P. A. Procopiou, *J. Am. Chem. Soc.*, **2009**, *131*, 9670−9685.

[100] (a) A. G. M. Barrett, T. C. Boorman, M. R. Crimmin, M. S. Hill, G. Kociok-Köhn, P. A. Procopiou, *Chem. Commun*., **2008**, 5206−5208; (b) J. Lachs, A. Barrett, M. Crimmin, G. Kociok-Köhn, M. Hill, M. Mahon, P. Procopiou, *Eur. J. Inorg. Chem.*, **2008**, 4173−4179.

[101] J. Pahl, T. E. Stennett, M. Volland, D. M. Guldi, S. Harder, *Chem. Eur. J*., **2019**, *25* 2025–2034.

[102] M. R. Crimmin, A. G. M. Barrett, M. S. Hill, P. B. Hitchcock, P. A. Procopiou, *Organometallics*, **2007,** *26*, 2953−2956.

[103] T. M. A. Al-Shboul, H. Görls, M. Westerhausen, *Inorg. Chem. Commun.*, **2008**, *11*, 1419−1421.

[104] T. M. A. Al-Shboul, V. K. Pálfi, L. Yu, R. Kretschmer, K. Wimmer, R. Fischer, H. Görls, M. Reiher, M. Westerhausen, *J. Organomet. Chem.*, **2011**, *696* , 216−227.

[105] M. R. Crimmin, A. G. M. Barrett, M. S. Hill, P. B. Hitchcock, P. A. Procopiou, *Organometallics*, **2008,** *27*, 497−499.

[106] T. M. A. Al-Shboul, G. Volland, H. Gorls, M. Westerhausen, *Zeit. Anorg. Allg. Chem*. **2009**, *635*, 1568−1572.

[107] B. Liu, J.-F. Carpentier, Y. Sarazin, *Chem. Eur. J.*, **2012**, *18*, 13259−13264.

[108] (a) E. C. Ashby, A. B. Goel, *J. Chem. Soc., Chem. Commun.*, **1977**, 169; (b) E. C. Ashby, A. B. Goel, *J. Am. Chem. Soc*., **1977**, *99*, 310−311; (c) E. C. Ashby, J. J. Lin, A. B. Goel, *J. Org. Chem.* **1978**, *43*, 1557−1560; (d) E. C. Ashby, J. J. Lin, A. B. Goel, *J. Org. Chem*., **1978**, *43*, 1560−1563; (e) E. C. Ashby, S. A. Noding, A. B. Goel, *J. Org. Chem.*, **1980**, *45*, 1028−1035; (f) E. C. Ashby, A. B. Goel, *Inorg. Chem.*, **1978**, *17*, 1862−1866; (g) E. C. Ashby, A. B. Goel, *Inorg. Chem.*, **1979**, *18*, 1306−1311; (h) A. B. Goel, E. C. Ashby, *J. Organomet. Chem*., **1981**, *214*, C1−C6.

[109] (a) E. C. Ashby, R. D. Schwartz, *Inorg. Chem.*, **1971**, *10*, 355−357; (b) R. G. Beach, E. C. Ashby, *Inorg. Chem*., **1971**, *10*, 906−910.

[110] S. P. Green, C. Jones, A. Stasch, *Science*, **2007**, *318*, 1754−1757.

[111] C. Jones, *Nat. Rev. Chem.*, **2017**, *1*, 0059.

[112] S. P. Green, C. Jones, A. Stasch, *Angew. Chem., Int. Ed.*, **2008**, *47*, 9079−9083.

[113] S. J. Bonyhady, C. Jones, S. Nembenna, A. Stasch, A. J. Edwards, G. J. McIntyre, *Chem. Eur. J.*, **2010**, *16*, 938−955.

[114] R. Lalrempuia, C. E. Kefalidis, S. J. Bonyhady, B. Schwarze, L. Maron, A. Stasch, C. Jones, *J. Am. Chem. Soc.*, **2015**, *137*, 8944−8947.

[115] (a) L. Garcia, C. Dinoi, M. F. Mahon, L. Maron, M. S. Hill, *Chem. Sci*., **2019**, *10*, 8108–8118; (b) F. Buch, J. Brettar, S. Harder, *Angew. Chem. Int. Ed.*, 2006, 45, 2741–2745.

[116] S. Harder, J. Brettar, *Angew. Chem., Int. Ed.,* **2006**, *45*, 3474−3478.

[117] P. Jochmann, J. P. Davin, T. P. Spaniol, L. Maron, J. Okuda, *Angew. Chem., Int. Ed.*, **2012**, *51*, 4452−4455.

[118] V. Leich, T. P. Spaniol, J. Okuda, *Angew. Chem., Int. Ed.,* **2016**, *55*, 4794−4797.

[119] A. Causero, G. Ballmann, J. Pahl, H. Zijlstra, C. Färber, S. Harder, *Organometallics*, **2016**, *35*, 3350−3360.

[120] J. Spielmann, F. Buch, S. Harder, *Angew. Chem., Int. Ed*., **2008**, *47*, 9434−9438.

[121] A. Juris, V. Balzani, F. Barigelletti, S. Campagna, P. Belser, A. v. Zelewsky, *Coord. Chem. Rev.* **1988**, *84*, 85–277.

[122] V. Balzani, A. Juris, *Coord. Chem. Rev.*, **2001**, *211*, 97–115.

[123] I. M. Dixon, J.-P. Collin, J.-P. Sauvage, L. Flamigni, S. Encinas, F. Barigelletti, *Chem. Soc. Rev.*, **2000**, *29*, 385–391.

[124] V. Chandrasekhar, R. Azhakar, J. F. Bickley, A. Steiner, *Chem. Commun*., **2005**, 459–461.

[125] S. Bestgen, C. Schoo, B. L. Neumeier, T. J. Feuerstein, C. Zovko, R. Köppe, C. Feldmann, P. W. Roesky, *Angew. Chem., Int. Ed.*, **2018**, *57*, 14265–14269.

[126] Z. Wirpsza, *Polyurethanes: Chemistry, Technology and Application*, Ellis Horwood, London, **1993**.

[127] (a) T. S. Leu, *J. Appl. Polym. Sci.*, **2006**, *102*, 2470–2480; (b) G. Q. Xiao, S. Q. Gao, X. L. Xie, M. C. Xu, *Polym. Adv. Technol.*, **2009**, *20*, 1157–1162; (c) W. Sun, X. Yan, X. Zhu, *J. Appl. Polym. Sci.*, **2011**, *122*, 2359–2367.

[128] Y. Zhang, S. N. Riduan, J. Y. Ying, *Chem. Eur. J.*, **2009**, *15*, 1077–1081.

[129] L. Orzechowski, S. Harder, *Organometallics*, **2007**, *26*, 2144–2148.

Chapter 2: A Tale of Biphenyl and Terphenyl Substituents for Structurally Diverse Ketiminato Magnesium and Calcium Complexes

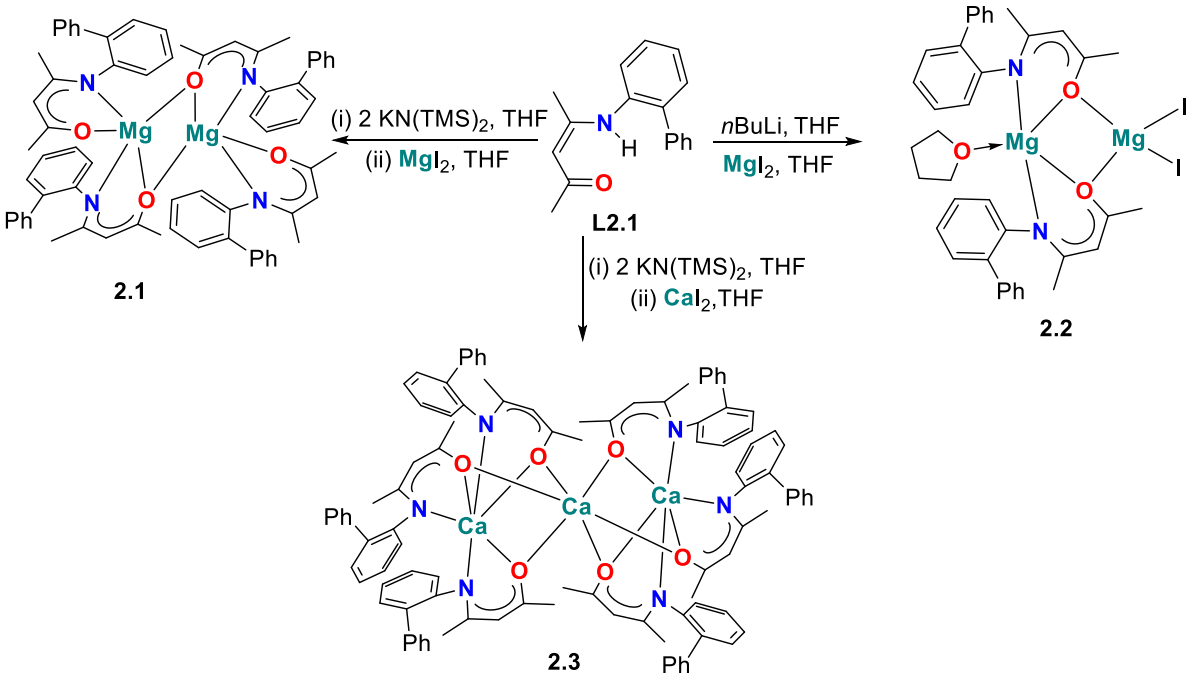

Abstract:

This chapter includes the use of two N, O-ketiminato ligands (**L2.1** and **L2.2**) with biphenyl and terphenyl substituent on the nitrogen atom. Deprotonation of **L2.1** with $KN(SiMe_3)_2$, and subsequent reaction with MgI_2 led to a homoleptic dinuclear magnesium complex (**2.1**) with a Mg_2O_2 four-membered ring. Deprotonation with *n*BuLi, and subsequent reaction with MgI_2 afforded an unusual dinuclear magnesium complex (**2.2**) with a Mg_2O_2 ring. Extension of the ligand for calcium resulted in a trinuclear calcium complex (**2.3**) with six four-membered Ca_2O_2 rings. We could not isolate any chelating complex when **L2.2** was used as a ligand, and only oxygen bound magnesium (**2.4**) and calcium (**2.5**) adducts were isolated. DFT studies were performed to understand this dissimilar behavior.

2.1: Introduction

The main group metal chemistry has been driven by the use of monoanionic bidentate ligand systems such as amidinate $[RC\{NR\}_2]^-$, guanidinate $[RNC(NR_2)NR]^-$,[1] trizenide $[(R_2N_3)]^-$,[2] *β*-diketiminate $[(R)NC(Me)C(H)C(Me)N(R)]^-$,[3] diboxmethanide[(4,6-R-$NCOC_6H_2)_2CH]^-$, [4,5] silylatedaminopyridinato $[(2\text{-}R_3SiNH\text{-}6\text{-}MeC_5H_3N)]^-$ [6] (Scheme 2.1). The strong binding efficiency to the metal center, good adjustability, tunable steric, and electronic property of these ligands have been used to stabilize various main group complexes.

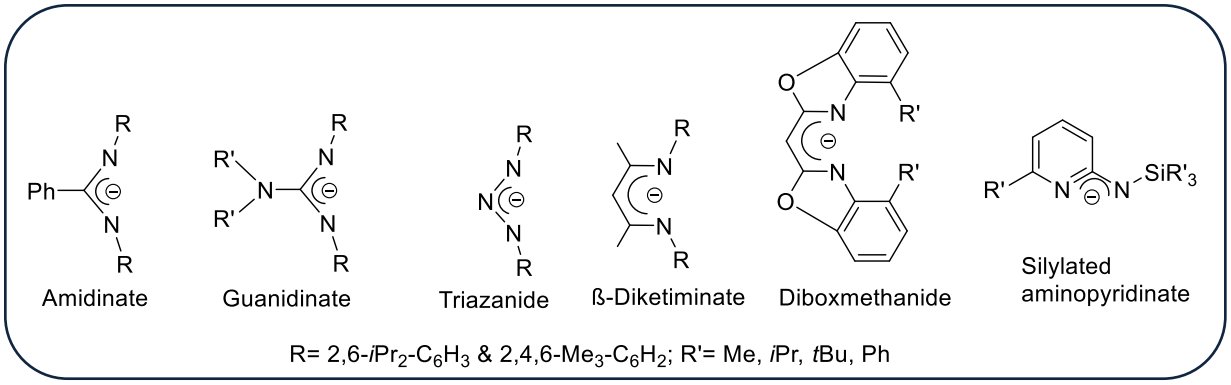

Scheme 2.1: Previously reported monoanionic ligands used for main group elements.

In *β*-diketiminate ligand system, further replacement of an NDipp moiety (Dipp= 2,6-$iPr_2C_6H_3$) with an oxygen atom leads to the formation of a N,O-ketiminato ligand. This replacement reduces the steric protection from the ligand system, but provides a more open side to the metal center. The ketiminato moieties have not been found expanding use as ligands to stabilize the main group complexes. Nevertheless, following the initial studies on the preparation of aluminum and magnesium ketiminato complexes and their reactivity towards ring-opening polymerization of *ε*-caprolactone by Huang and coworkers,[7-8] the synthesis of main group complexes using N,O-ketiminato ligand has received renewed interest. Recently, Reddy and coworkers reported magnesium and aluminium complexes of γ-phosphino-ketiminates as dual-purpose catalysts for CO_2/epoxide coupling and the ring-opening polymerization of ε-caprolactone.[9] Subsequently, the synthesis of aluminum, gallium, and especially zinc complexes containing N,O-ketiminato ligands and their applications in ring-opening polymerization of lactides have been accomplished.[8-12] The isolation of alkaline earth metal

complexes with N, O-ketiminato ligands were also achieved, credit to extensive works derived from groups of Huang, Reddy, Wang, and others.[13-18]

In this chapter,, we shall report the preparation of a new N, O-ketiminato ligand (**L2.1**) by introducing "biphenyl" moiety on the nitrogen atoms and prepared structurally diverse complexes with magnesium (**2.1** and **2.2**), and calcium (**2.3**). Furthermore, to investigate the influence of the steric on the structures of the corresponding complexes, the substitution of the "biphenyl" group with "terphenyl" moiety was accomplished (**L2.2**). In contrast, both magnesium and calcium do not form a chelating complex with **L2.2**.

2.2: Synthesis and characterization of ligand L2.1 and magnesium complexes(2.1-2.2)

Ligand **L2.1** was prepared by reacting 1:1 ratio of 2,4-pentanedione and 2-phenylaniline in toluene with a catalytic amount of *p*-toluenesulfonic acid (Scheme 2.2). The formation of **L2.1** was confirmed by single-crystal X-ray studies (Figure 2.1) and NMR spectroscopy. Two methyl groups resonate at δ 1.56 and 1.91 ppm, while the γ proton resonates at δ 4.93 ppm. **L2.1** crystallizes in the triclinic space group *P*ī.

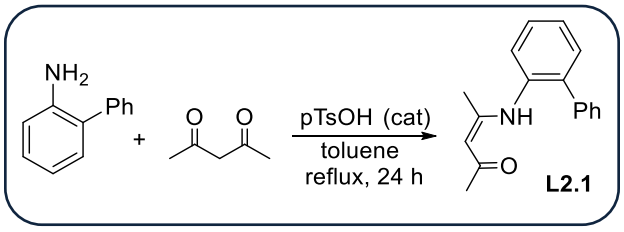

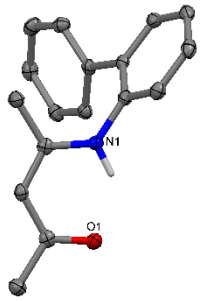

Scheme 2.2: Synthesis of ligand, **L2.1** (left) and **Figure 2.1:** The molecular structure of **L2.1** with the parameters of anisotropic displacement shown at the 50% level of probability. Atoms of hydrogen are left out for simplicity (except the one bound to N). CCDC number-1886689.

Deprotonation of **L2.1** with $KN(SiMe_3)_2$ in THF at room temperature and subsequent reaction with MgI_2 led to a homoleptic complex of composition **L2.1**$_4Mg_2$ (**2.1**) (Scheme 2.3) containing a four-membered Mg_2O_2 ring, where the oxygen atoms of the two ligands participate in the ring formation. **2.1** crystallizes in the triclinic space group *P*ī.[19]

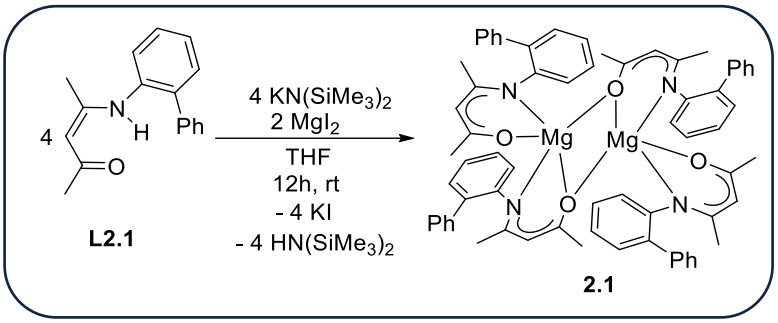

Scheme 2.3: Synthesis of dinuclear magnesium complex, **2.1**.

Each magnesium atom is connected by two ligand moieties and another oxygen atom of the third ligand, resulting a penta-coordinate magnesium atom with a distorted square pyramidal geometry. The η^2-ketiminato ligands coordinate to the magnesium atom with a bite angle of 87.89(8)°, which is lower than that reported by Huang and coworkers, presumably due to ring strain.[13] The Mg-$O_{Ketiminato}$ bond lengths are 1.9436(19), 2.0263(18), and 2.0433(19) Å (Figure 2.1.2), which are longer than those reported by Huang and coworkers (1.8955(15) Å).[15]

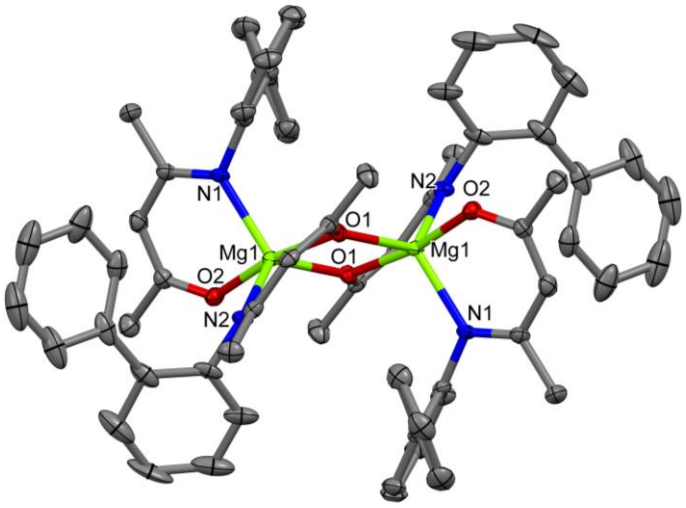

Figure 2.2: Molecular structure of complex **2.1** with parameters of anisotropic displacement shown at the 50% level of probability. Hydrogen atoms are left out for simplicity. Symmetry generator *: 1−x, 1−y, 1−z. Selected bond lengths [Å] or angles [deg]: Mg1−O2 1.9436(19), Mg1−O1 2.0263(18), Mg1−O1 2.0433(19), Mg1−N1 2.148(2), Mg1−N2 2.154(2),), O1−Mg1 2.0433(19); O2−Mg1−O1 96.16(8) and 170.48(8), O1−Mg1−O1 78.16(8), O2−Mg1−Mg1 134.59(7), O1−Mg1−Mg1 38.89(5) and 39.28(5), N1−Mg1−Mg1 117.59(7), N2−Mg1−Mg1 106.86(7), Mg1−O1−Mg1 101.84(8). CCDC number-1885674.

The methine protons of the ketiminato backbones exhibit a singlet resonance at about 5.03 ppm in the ^{1}H NMR spectrum of **2.1**, which has been shifted downfield compared to the free ketimine ligands (δ 4.93 ppm). In addition, complex **2.1** exhibits two singlet resonances for the methyl groups at δ 1.68 and 2.02 ppm of the ketiminato backbones integrating each for 12 protons. This indicates that the four ligands attached to the magnesium centers are equivalent, but the two methyl groups on a particular ligand are not equivalent. In the HRMS, only half fragment was detected at *m/z* 525.2520 with the highest intensity. Due to the sensitivity of the system, we could never obtain a very clean ^{13}C NMR and always accompanied by free ligand resonances.

Next, we lithiated **L2.1** with *n*BuLi in THF, and subsequently added this solution to the MgI_2 suspension in THF. The reaction led to an unusual magnesium compound (**2.2**) with a four-membered Mg_2O_2 cycle (Scheme 2.4). However, the coordination environment of the two magnesium atoms is different. Although a similar dinuclear Zn complex with two differently coordinated Zn atoms was previously reported, [20] analogous alkaline earth metal complexes are unknown to our knowledge. **2.2** is extremely sensitive to air and moisture. Despite several attempts, a full spectroscopic characterization of **2.2** could not be obtained. Most of the time, the resonance for the NH peak was observed, resulting presumably from the decomposition of **2.2**. However, in the HRMS, the molecular ion peak with the highest intensity at *m/z* 803.0468 was detected.

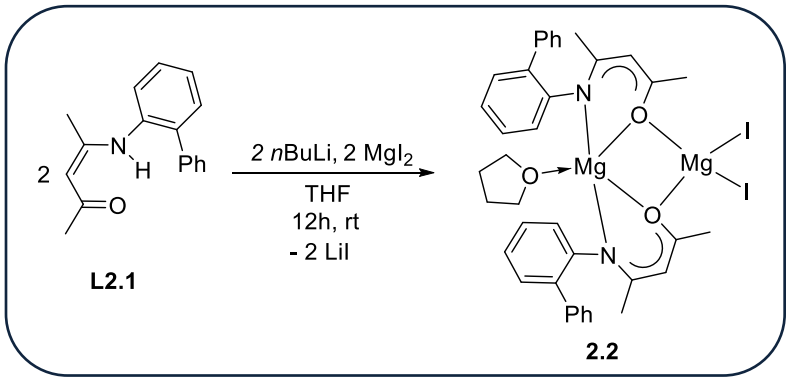

Scheme 2.4: Synthesis of complex **2.2**, where two Mg centers are differently coordinated.

A single-crystal X-ray study authenticated the constitution, which suggests the orthorhombic space group $P2_12_12_1$ for **2.2**. The relevant bond length and angles are given in the tale of Figure 2.3. One magnesium atom is coordinated to two ligand moieties and one THF

molecule. It has the tau parameter value τ_5=0.497, indicating the geometry around the Mg is intermediate between the idealized square-pyramidal and trigonal-bipyramidal. [21] The Mg–O_{thf} bond length is 2.092(3) Å, which is longer than the other Mg–O bonds (2.012(3) and 2.039(3) Å). The second magnesium center is connected to the two oxygen atoms of the ligand systems and two iodine atoms, giving tau parameter value τ_4=0.832, which indicates a tetrahedral geometry around the Mg center. [22] No THF molecule is coordinated to the second magnesium atom.

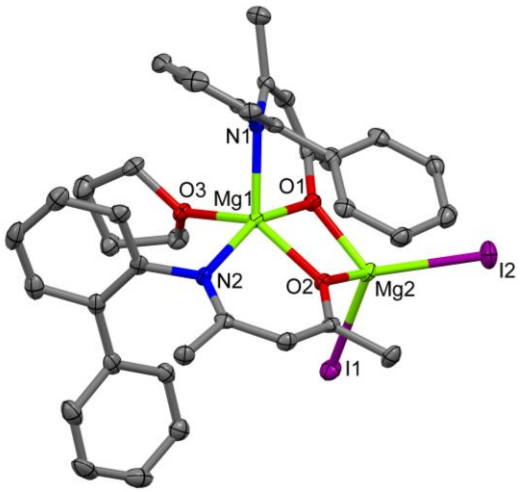

Figure 2.3: The molecular structure of complex **2.2**·toluene in the solid-state with parameters of anisotropic displacement shown at the 50% level of probability. Hydrogen atoms and toluene molecule are left out for simplicity. Selected bond lengths [Å] or angles [deg]: I1−Mg2 2.6909(12), I2−Mg2 2.6643(13), Mg1−O2 2.012(3), Mg1−O1 2.039(3), Mg1−O3 2.092(3), Mg1−N1 2.123(3), Mg1−N2 2.162(3), Mg1−Mg2 3.0782(17), Mg2−O1 1.958(3), Mg2−O2 1.985(3); O2−Mg1−O1 77.24(11), O2−Mg1−O3 134.13(11), O1−Mg1−O3 87.92(11), O2−Mg1−Mg2 39.32(8), O1−Mg1−Mg2 38.68(8), O3−Mg1−Mg2 110.23(8), N1−Mg1−Mg2 116.45(10), N2−Mg1−Mg2 120.44(10), O1−Mg2−O2 79.77(11), O2−Mg2−Mg1 39.95(8),), I1−Mg2−Mg1 107.53(5), Mg2−O2−Mg1 100.73(12). CCDC number-1885678.

The Mg–O bond lengths 1.958(3) and 1.985(3) Å) are shorter than the Mg–O bond lengths in compound **2.1**. The Mg-I bond lengths in **2.2** are 2.6643(13) and 2.6909(12) Å, which coincide well with those found in the four-coordinate $(Et_2O)_2MgI_2$ (2.654(3) Å), independently reported by the groups of Schnöckel and Eaborn. [23,24] The Mg–I bond length is shorter than that in the solid-state structure of MgI_2 (2.9183(5) Å) [25] but longer than the Mg–I bond length in di-coordinate

magnesium diiodide in the gas phase (2.52 ± 0.03 Å), [26] as measured by electron diffraction studies.

2.3: Synthesis and characterization of calcium complex(2.3)

Subsequently, we treated **L2.1** with $KN(SiMe_3)_2$ and reacted with CaI_2. The reaction led to an interesting trinuclear calcium complex (**2.3**) stabilized by six N, O-ketiminato ligands (Scheme 2.5). **2.3** crystallizes in the triclinic system space group Pī.

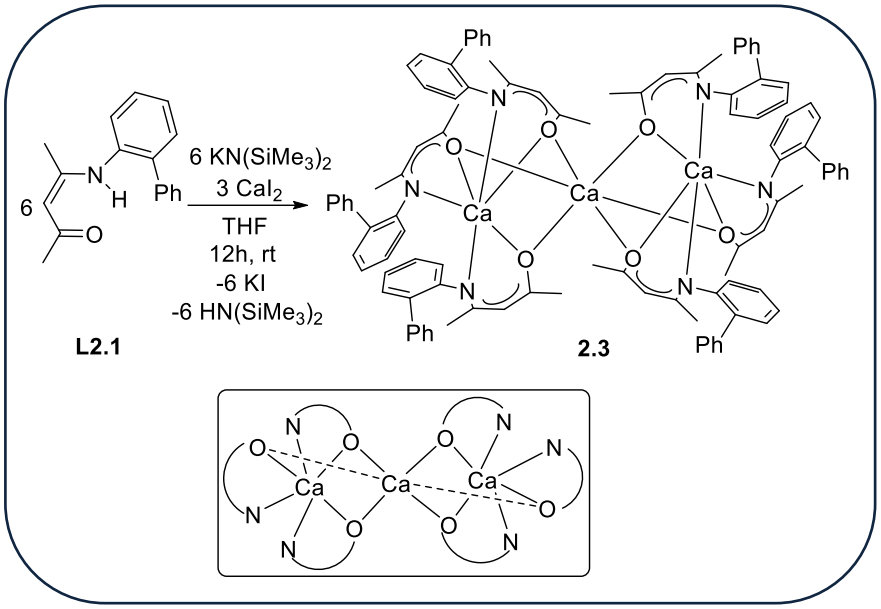

Scheme 2.5. Synthesis of trinuclear calcium complex, **2.3**.

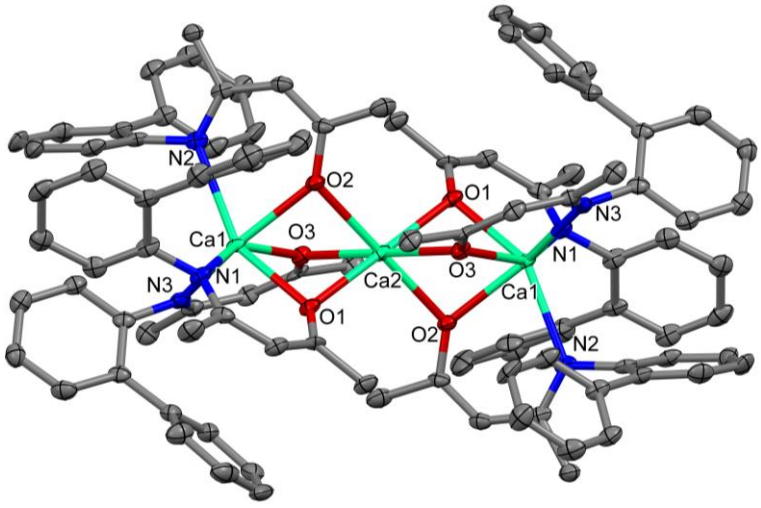

Figure 2.4: The molecular structure of complex **2.3** in the solid-state with parameters of anisotropic displacement shown at the 50% level of probability. Hydrogen atoms are left out for simplicity. Selected bond lengths [Å] or angles [deg]: Ca2−O3 2.315(4) and 2.316(4), Ca2−O2 2.347(4) and 2.347(4), Ca2−O1 2.361(4) and 2.361(4), Ca2−Ca1 3.3307(12), Ca1−O2 2.333(4), Ca1−O1 2.342(4), Ca1−O3 2.359(4); O3−Ca2−O3 180.0, O3−Ca2−O2 105.26(13) and 74.74(13), O2−Ca2−O2 180.0, O3−Ca2−O1 104.09(13), 105.24(13), 74.76(13) and 75.91(13), O3−Ca2−O1 75.91(13) and 104.09(13), O2−Ca2−O1 74.76(13) and 105.24(13), O1−Ca2−O1 180.0, , Ca1−Ca2−Ca1 180.0, O2−Ca1−O1 75.35(14), O2−Ca1−O3 74.17(13), O1−Ca1−O3 75.43(13). CCDC number-1885782.

The single-crystal X-ray diffraction studies showed that the two calcium atoms are connected with three ligand moieties in the usual ketiminate bonding mode, leading to an octahedral geometry around the calcium atoms (Figure 2.4). However, the octahedral coordination sphere of the third calcium atom is saturated by the oxygen atom of each six ligands. The γ-H for all six ligands appears at δ 5.03 ppm, while the methyl groups resonate at δ 1.68 and 2.02 ppm. Despite numerous attempts, only comparatively poor crystals of **2.3** could be produced via crystallization. Even though the X-ray diffraction investigation proves the constitution, the bond precision is limited. Therefore, the absolute values for the bond lengths might not be as reliable as their standard deviations, so we refrain from discussing any structural parameters.

2.4: Synthesis and characterization of ligand L2.2, 2.4, magnesium(2.5) and calcium complexes(2.6)

Subtle modification in the ligand skeletons may have a striking influence on the structure of the corresponding complexes. We modified the ligand by replacing the biphenyl group with the terphenyl moiety to see if the extra phenyl group stabilized the heteroleptic alkaline earth metal complexes. The synthesis of ligand **L2.2** was accomplished by the following method shown in Scheme 2.6. The state-of-the-art spectroscopic tools characterized **L2.2**. The reaction of **L2.2** with *n*BuLi led to 75-80 % deprotonation. Hence, we have deprotonated **L2.2** with MeLi at -78 °C to get the lithiated compound (**2.4**) in almost quantitative yield (Scheme 2.6). **2.4** is a dimeric compound with a Li_2O_2 four-membered ring (Figure 2.5) and having a Li-N bond length 2.020(3) Å, which is slightly less than the sum of covalent radii of Li and N i.e., 2.09 Å and Li2-O3 1.993(3) Å. The Li atoms in **2.4** are tetracoordinate with one nitrogen and one oxygen atom of the ketiminato

ligand, one oxygen atom from another ketiminato ligand, and one oxygen atom of the coordinated THF molecule, and this arrangement leads to a distorted tetrahedral geometry around them. The ^{1}H NMR shows two singlet peaks for methyl protons at δ 1.45 ppm and 1.55 ppm, while the γ-proton appears at δ 4.56 ppm, which comes slightly upfield compared to ligand i.e., 4.66 ppm, due to coordination of the solvent to the lithium atom.

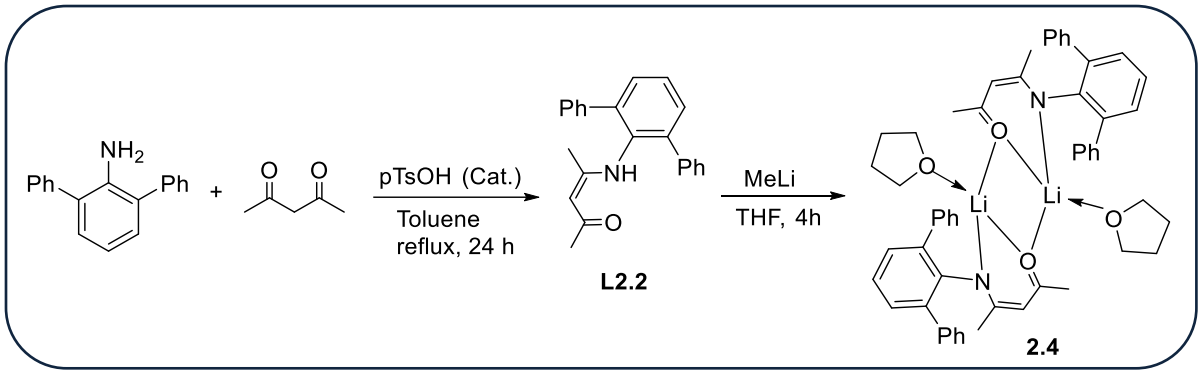

Scheme 2.6: Synthesis of ligand (**L2.2**) and complex **2.4**.

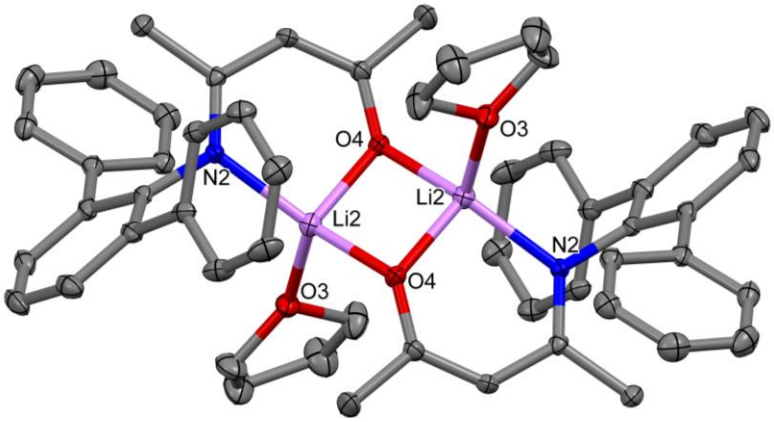

Figure 2.5: The molecular structure of **2.4** in the solid-state with parameters of anisotropic displacement shown at the 50% level of probability. Hydrogen atoms are left out for simplicity. Selected bond lengths [Å] or angles [deg]: C24-O3 1.436(2), C24-C25 1.511(3), C27-O3 1.427(2), C33-O4 1.2864(18), C36-N2 1.3068(19), Li2-O4 1.892(3), Li2-O3 1.993(3), Li2-N2 2.020(3), O4-Li2-O4$^{\#1}$92.80(13), O4-Li2-O3 109.78(15), O4$^{\#1}$-Li2-O3 100.88(13), O4-Li2-N2 95.42(13), O4-Li2-N2 95.42(13), O4$^{\#1}$-Li2-N2 144.98(17), O3-Li2-N2 108.11(14), O4-Li2-Li2$^{\#1}$ 46.99(9), O4$^{\#1}$-Li2-Li2$^{\#1}$ 45.81(9). CCDC number-1958801.

Consequently, we have sought to prepare magnesium and complexes with **L2.2**. The reaction of **2.4** with MgI_2/CaI_2 or metalation with $KN(SiMe_3)_2$ and subsequent reaction with MgI_2/CaI_2 led to **2.5** and **2.6**, where magnesium and calcium are found to bind with the oxygen atom of the ligand without entering into the ligand pocket (Scheme 2.7). This is presumably due to the sterics of the additional phenyl ring that inhibits the chelation. It is also assumed that an unintended hydrolysis is taking place during the reaction or crystallization. It is surprising though that when no base is used, the adduct formation was not observed, even after heating conditions. However, even after several attempts, we could not prevent hydrolysis.

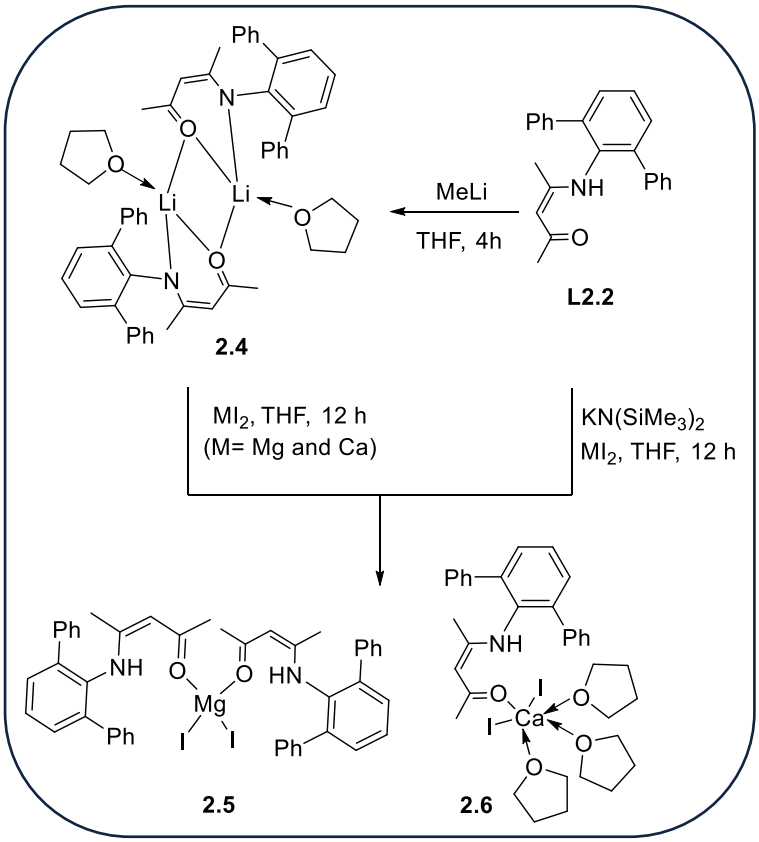

Scheme 2.7: Synthesis of complex **2.5** and **2.6** from ligand **L2.2** and complex **2.4**.

Both **2.5** and **2.6** have been structurally characterized. While the magnesium atom in **2.5** exhibits a tetrahedral geometry, the calcium atom in **2.6** possess an octahedral geometry. The difference in their coordination geometries can be attributed to their difference in the ionic radii.

Two tetrahydrofuran molecules make up the unit cell of compound **2.5**; squeeze/Platon has considered these molecules a diffuse contribution to the total scattering without exact atomic locations. [27] However, it has been considered in the molecular formula unit for correct molecular weight, crystal density and F(000) computations. The solid-state structure of **2.5** is depicted in Figure 2.6. The Mg-I bond lengths are 2.6898(12) and 2.7022(11) Å, which are in good agreement with those in **2.2**. The molecular structure of **2.6** is depicted in Figure 2.7. The Ca-I bond lengths are 3.136(2) and 3.099(2) Å, which coincide well with the length of the Ca-I bond in [(thp)$_4$Ca(I)(Ph)] (thp=tetrahydropyran). [28]

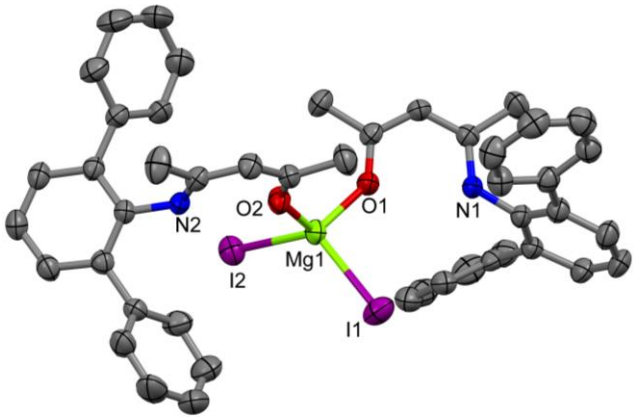

Figure 2.6: The molecular structure of complex **2.5** with the parameters of anisotropic displacement shown at the 50% level of probability. Hydrogen atoms are left out for simplicity. Selected bond lengths [Å] or angles [deg]: Mg1-I1 2.6898(12), Mg1-I2 2.7022(11), Mg1-O2 1.936(2), Mg1-O1 1.945(2), N1-C4 1.326(3), N2-C27 1.321(3), O1-C2 1.279(3), O2-C25 1.280(3), O2-Mg1-O1 110.45(9), O2-Mg1-I1 109.98(8), O1-Mg1-I1 100.17(6), O2-Mg1-I2 99.58(7), O1-Mg1-I2 115.00(7), I1-Mg1-I2 121.76(4), C4-N1-C6 124.8(2), C4-N1-H1 117.6, C6-N1-H1 117.6, C27-N2-C29 124.1(2). CCDC number-1959123.

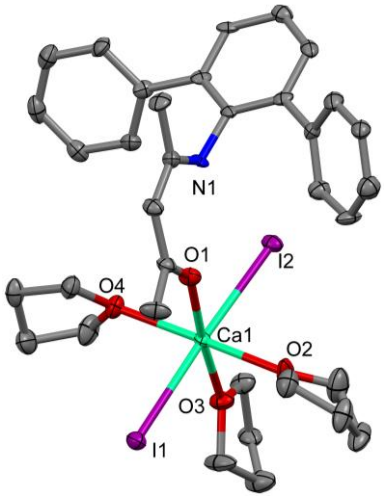

Figure 2.7: The molecular structure of **2.6** with parameters of anisotropic displacement shown at the 50% level of probability. Hydrogen atoms are left out for simplicity. Selected bond lengths [Å] or angles [deg]: Ca1-I1 3.136(2), Ca1-I2 3.099(2), Ca1-O1 2.312(8), Ca1-$O2_{thf}$ 2.334(8), Ca1-$O3_{thf}$ 2.404(8), Ca1-$O4_{thf}$ 2.367(7), O1-C1 1.257(13), N1-C3 1.313(14), C1-C2 1.438(13), O1-Ca1-O2 89.4(3), O1-Ca1-O4 87.4(3), O2-Ca1-O4 175.4(3), O1-Ca1-O3 175.4(3), O2-Ca1-O3 88.9(4), O4-Ca1-O3 94.5(3), O1-Ca1-I2 85.57(18), O2-Ca1-I2 89.0(2), O4-Ca1-I2 93.9(2), O3-Ca1-I2 90.15(19), O1-Ca1-I1-95.84(19), O2-Ca1-I1 88.9(2), O4-Ca1-I1 88.2(2), O3-Ca1-I1 88.38(19), I2-Ca1-I1 177.53(7). CCDC number-1958776.

2.5: DFT calculations

DFT calculations were carried out to find the possibility of chelated binding models of Mg and Ca with the ligand **L2.2**. **2.5A**, **2.6A,** and **2.6B** were the plausible structures for the bonding of Mg and Ca with ligand **L2.2**, respectively (Scheme 2.8).

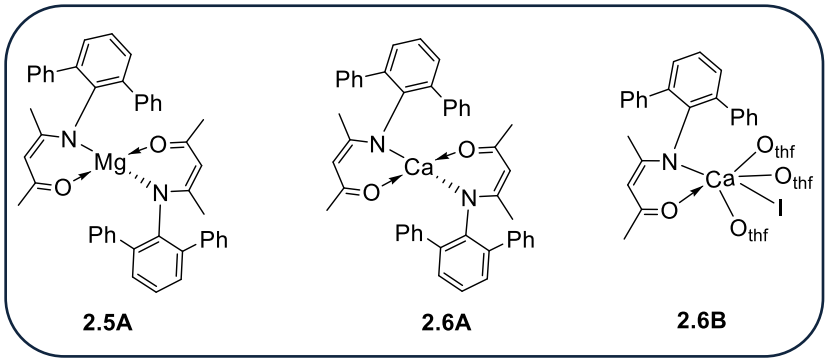

Scheme 2.8: Possible chelated model complexes of Mg (**2.5**) and Ca (**2.6**).

However, all these model complexes were found to be higher in energy than **2.5** and **2.6**. For example, **2.5A** was +44.9 kcal/mol higher in energy than compound **2.5**. Similarly, **2.6A** and **2.6B** were +52.9 kcal/mol and +33.0 kcal/mol higher than **2.6**, respectively. The energy difference can be attributed to the presence of the extra phenyl group, which sterically hinders the complex formation and does not permit the metal ion to be in a position for chelation with both nitrogen and oxygen.

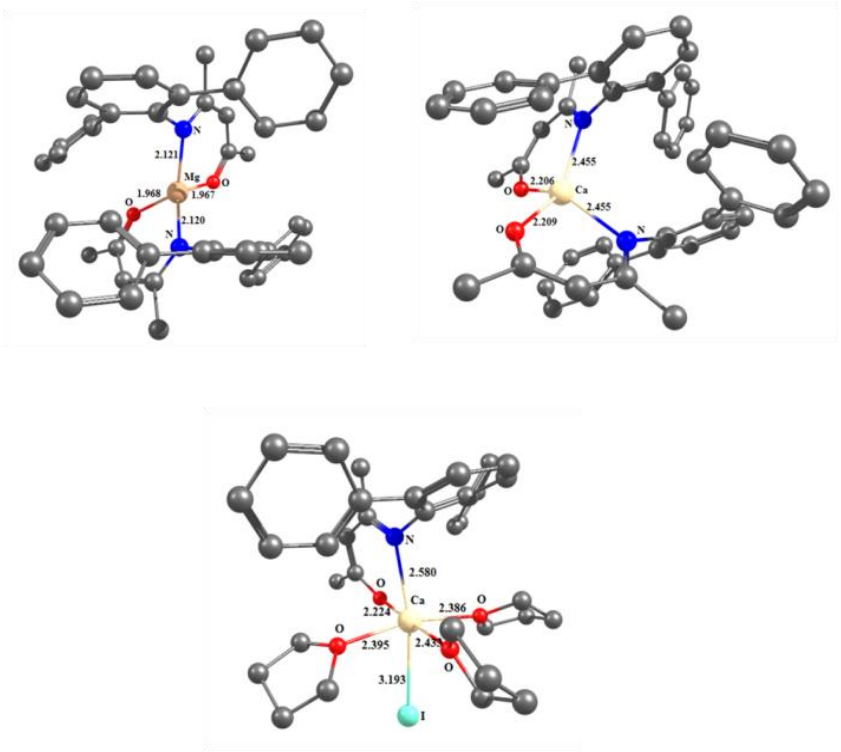

Figure 2.8: Probable chelated models for Mg and Ca with ligand **L2.2: 2.5A** (above left), **2.6A** (above right), and **2.6B** (below) (Optimized using Turbomole 7.1 by employing pbe functional and def-TZVP basis set).

The steric crowding upon probable chelation can be clearly observed in the optimized models (Figure 2.8).

2.6: Conclusions

N, O-ketiminato ligand (**L2.1**) featuring sterically demanding 2-biphenyl substituent on the nitrogen atom has been used to stabilize structurally diverse magnesium (**2.1** and **2.2**) and calcium complexes (**2.3**). We have also attempted several catalytic reactions using **2.1**-**2.3** such as hydrosilylation, Tischenko reaction etc., however due to their homoleptic nature, they are found to be catalytically impotent. A slightly modified ligand (**L2.2**) was prepared by substituting the "biphenyl" group with the "terphenyl" moiety, and it has a profound effect on the structures of the corresponding complexes. Magnesium and calcium only form O-bound adducts (**2.5** and **2.6**) with **L2.2**. DFT studies shed light on why **L2.1** forms chelated complexes and **L2.2** forms simple adducts. Comparing the previous reports on N, O-ketiminate main group compounds with our results, it can be said that the coordination environment of the resulting main group compounds can be varied by changing the substituents on the nitrogen atom of the ligand.

2.7: References

[1] (a) G. J. Moxey, F. Ortu, L. G. Sidley, H. N. Strandberg, A. J. Blake, W. Lewis, D. L. Kays, *Dalton Trans.*, **2014**, *43*, 4838–4846; (b) R. J. Schwamm, B. M. Day, N. E. Mansfield, W. Knowelden, P. B. Hitchcock, M. P. Coles, *Dalton Trans*., **2014**, *43*, 14302–14314; (c) B. M. Day, W. Knowelden, M. P. Coles, *Dalton Trans*., **2012**, *41*, 10930–10933; (d) J. Schwamm, M. P. Coles, *Organometallics*, **2013**, *32*, 5277–5280; (e) S. Yadav, V. S. V. S. N. Swamy, R. G. Gonnade, S. S. Sen, *ChemistrySelect*, **2016**, *1*, 1066–1071; (f) B. M. Day, N. E. Mansfield, M. P. Coles, P. B. Hitchcock, *Chem. Commun*., **2011**, *47*, 4995–4997; (g) C. Jones, *Coord.Chem. Rev.*, **2010**, *254*, 1273–1289; (h) C. Glock, C. Loh, H. Goerls, S. Krieck, M. Westerhausen, *Eur. J. Inorg. Chem.*, **2013**, 3261–3269; (i) M. K. Barman, A. Baishya, S. Nembenna, *J. Organometal. Chem.*, **2015**, *785*, 52–60.

[2] (a) S.-O. Hauber, F. Lissner, G. B. Deacon, M. Niemeyer, *Angew. Chem., Int. Ed.* **2005**, *44*, 5871–5875; (b) A. G. M. Barrett, M. R. Crimmin, M. S. Hill, P. B. Hitchcock, G. Kociok-Köhn, P. A. Procopiou, *Inorg. Chem.*, **2008**, *47*, 7366–7376; (c) H. S. Lee, S.-O. Hauber, D. Vinduš, M. Niemeyer, *Inorg. Chem.*, **2008**, *47*, 4401–4412; (d) A. R. Leverett, V. Diachenko, M. L. Cole, A. I. McKay, *Dalton Trans.*, **2019**, *48*, 13197–13204.

[3] (a) S. Nembenna, H. W. Roesky, S. Nagendran, A. Hofmeister, J. Magull, P.-J. Wilbrandt, M. A. Hahn, *Angew. Chem., Int. Ed.*, **2007**, *46*, 2512–2514; (b) A. G. M.Barrett, M. R. Crimmin, M. S. Hill, P. B. Hitchcock; P. A. Procopiou, *Angew. Chem., Int. Ed.*, **2007**, 46, 6339–6342; (c) C. Ruspic, S. Harder, *Inorg. Chem.*, **2007**, *46*, 10426–10433; (d) M. Westerhausen, M. H. Digeser, C. Gückel, H. Nöth, J. Knizek, W. Ponikwar, *Organometallics*, **1999**, *18*, 2491–2496; (e) S. P. Sarish, A. Jana, H. W. Roesky, T. Schulz, M. John, D. Stalke, *Inorg. Chem.*, **2010**, *49*, 3816–3820; (f) S. Yadav, R. Dixit, M. K. Bisai, K. Vanka, S. S. Sen, *Organometallics*, **2018**, *37*, 4576–4584; (g) S. P. Sarish, S. Nembenna, S. Nagendran, H. W. Roesky, *Acc. Chem. Res.*, **2011**, *44*, 157–170.

[4] (a) I. Koehne, R. Herbst-Irmer, D. Stalke, *Eur. J. Inorg. Chem.*, **2017**, 3322–3326; (b) I. Koehne, S. Bachmann, T. Niklas, R. Herbst-Irmer, D. Stalke, *Chem. Eur. J.*, **2017**, *23*, 13141 –13149.

[5] I. Koehne, N. Graw, T. Teuteberg, R. Herbst-Irmer, D.Stalke, *Inorg. Chem.*, **2017**, *56*, 14968−14978.

[6] (a) F. Ortu, G. J. Moxey, A. J. Blake, W. Lewis, D. L. Kays, *Inorg. Chem.*, **2013**, *52*, 12429−12439; (b) N. Sen, S. Pal, V. V. Khade, S. Khan, *Eur. J. Inorg. Chem.*, **2019**, *41*, 4450–4454.

[7] R.-C. Yu, C.-H. Hung, J.-H. Huang, H.-Y. Lee, J.-T. Chen, *Inorg. Chem.*, **2002**, *41*, 6450–6455.

[8] H.-C. Huang, B. Wang, X.-L. Chen, L. Pan, Y.-S.Li, *J. Polymer. Chem. A.*, **2019**, *57*, 973–981.

[9] B. Jana, W. Uhl, *Inorg. Chim.Acta*, **2017**, *455*, 61–69.

[10] C. C. Roberts, B. R. Barnett, D. B. Green, J. M. Fritsch, *Organometallics*, **2012**, *31*, 4133–4141.

[11] C. Di Iulio, M. Middleton, G. Kociok-Köhn, M. D. Jones, A. L. Johnson, *Eur. J. Inorg. Chem.*, **2013**, 1541–1554.

[12] C. Scheiper, D. Dittrich, C. Wölper, D. Bläser, J. Roll, S. Schulz, *Eur. J. Inorg. Chem.*, **2014**, 2230–2240.

[13] W.-Yi Lee, H.-H. Hsieh, C.-C. Hsieh, H. M. Lee, G.-H. Lee, J.-H. Huang, T.-C. Wu, S.-H. Chuang, *J. Organomet. Chem.*, **2007**, *692*, 1131–1137.

[14] S.−M. Ho, C.−S. Hsiao, A. Datta, C. H. Hung, L.−C. Chang, T.−Y. Lee, J.−H. Huang, *Inorg. Chem.*, **2009**, *48*, 8004–8011.

[15] L.-F. Hsueh, N.-T. Chuang, C.-Y. Lee, A. Datta, J.-H. Huang, T.-Y. Lee, *Eur. J. Inorg. Chem.*, **2011**, 5530–5537.

[16] B. Raghavendra, P. V. S. Shashank, M. K. Pandey, N. D. Reddy, *Organometallics*, **2018**, *37*, 1656−1664.

[17] X.-L. Chen, B. Wang, L. Pan, Y.-S. Li, Appl. *Organomet. Chem*., **2019**, *33*, 4770–4781.

[18] J. Gao, D. Zhu, W. Zhang, G. A. Solan, Y. Ma, W.-H. Sun, *Inorg. Chem. Front.*, **2019**, *6*, 2619–2652.

[19] (a) T. Kottke, D. Stalke, *J. Appl. Crystallogr.*, **1993**, *26*, 615–619; (b) D. Stalke, *Chem. Soc. Rev.*, **1998**, *27*, 171–178; (c) T. Schulz, K. Meindl, D. Leusser, D. Stern, J. Graf, C. Michaelsen, M. Ruf, G. M. Sheldrick, D. Stalke, *J. Appl. Crystallogr.*, **2009**, *42*, 885−891; (d) L. Krause, R. Herbst-Irmer, G. M. Sheldrick, D. Stalke, *J. Appl. Crystallogr.*, **2015**, *48*, 3−10; (e) L. Krause, R. Herbst-Irmer, D. Stalke, *J. Appl. Crystallogr.*, **2015**, *48*, 1907–1913.

[20] R. Olejnik, M. Bilek, Z. Růžičkova, Z. Hoštalek, J. Merna, A. Růžička, *J. Organomet. Chem.*, **2015**, *794*, 237–246.

[21] L. Yang, D. R. Powell, R. P. Houser, *Dalton Trans.*, **2007**, 955–964.

[22] A. W. Addison, T. N. Rao, J. Reedijk, J. v. Rijn, G. C. Verschoor, *J. Chem. Soc. Dalton Trans.*, **1984**, 1349–1356.

[23] A. Ecker, C. Üffing, H. Schnöckel, *Chem. Eur. J.*, **1996**, *2*, 1112–1114.

[24] C. Eaborn, P. B. Hitchcock, A. Kowalewska, Z.-R. Lu, D. J. Smith, W. A. Stanczyk, *J. Organomet. Chem.*, **1996**, *521*, 113–120.

[25] M. A. Brogan, A. J. Blake, C. Wilson, D. H. Gregory, *Acta Crystallogr.*, **2003**, *C59*, i136–i138.

[26] P. A. Akishin, V. P. Spiridonov, *Zh. Fiz. Khim.*, **1958**, *32*, 1682–1683.

[27] A. L. Spek, *Acta Cryst*., **2015**, *C71*, 9–18.

[28] J. Langer, S. Krieck, R. Fischer, H. Görls, M. Westerhausen, *Z. Anorg. Allg. Chem.*, **2010**, *636*, 1190−1198.

Chapter 3: Low-Coordinate Monomeric Magnesium-Catalyzed Alkene and Alkyne Hydroboration

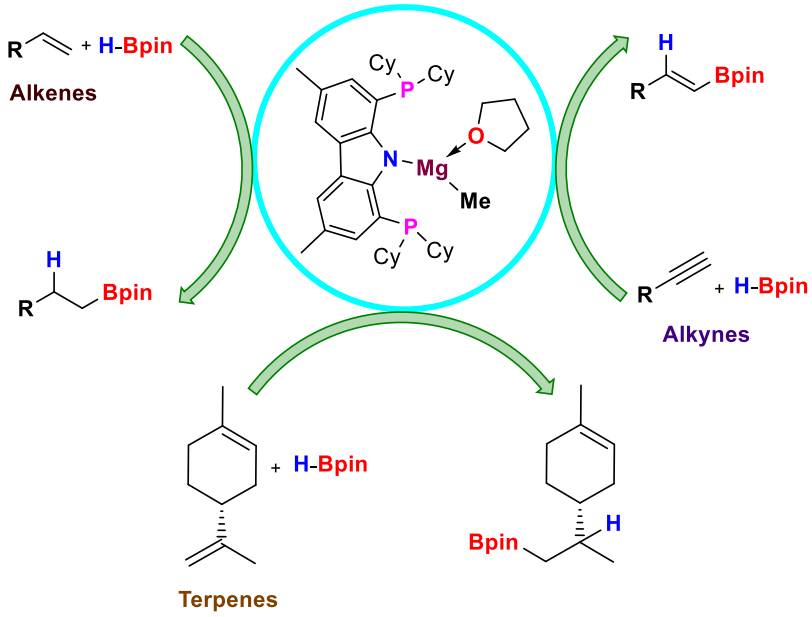

- Monomeric **Mg-methyl** catalyst
- First report for alkene hydroboration
- Extended to biologically important terpenes
- Broad substrate scope with good to excellent yield
- Suitable for both aryl and alkyl substrates
- Mechanistic investigation with DFT studies

Abstract:

Well-defined molecular magnesium compounds have achieved great advances in hydroboration of C=O or C=N bonds. By contrast, the magnesium-catalyzed hydroboration of alkenes and alkynes is very scarce. Here, a series of low-coordinate monomeric magnesium alkyl complexes (**3.1**-**3.4**) have been prepared using bis(phosphino)carbazole framework and among them **3.1** has been used as a catalyst for hydroboration of alkenes and alkynes with pinacolborane (HBpin). A broad variety of aromatic and aliphatic alkenes and alkynes was efficiently reduced. Anti-Markovnikov regioselective hydroboration of alkenes and alkynes is achieved, which is confirmed by deuterium-labelling experiments. This represents the first example of the use of magnesium in homogeneous catalytic hydroboration of alkene with broad substrate scope. Experimental mechanistic investigations and DFT calculations provide insights into the reaction mechanism. Finally, the hydroboration protocol has been extended to terpenes.

3.1: Introduction

Increased focus on sustainable catalytic methods has brought a shift of emphasis toward catalysis with more earth-abundant elements.[1] In this regard, the alkaline-earth metal-based compounds have recently come forth as alternatives to the traditional transition metal or lanthanide-based catalysts for the hydroelementation of the unsaturated bonds. Magnesium is the eighth most abundant element in the Earth's crust, magnesium compounds are readily accessible, and their byproducts are easily decomposed, and non-hazardous. The well-defined magnesium compounds have achieved remarkable advances as homogeneous catalysts in recent years for the hydroboration of polarized unsaturated bonds such as aldehydes, ketones, nitriles, isonitriles carbodiimides, isocyanates, carbonates, thanks to ground-breaking works from the groups of Hill, Sadow, Okuda, Rueping and others.[2-14] By contrast, the hydroboration of alkynes and alkenes, which has applications in fine chemicals, perfumes, medicines etc.,[15] lags far behind in implementing magnesium-based catalysts. The reason can be attributed to the less/non-polarized nature of the C–C multiple bonds. Stoichiometric hydroboration of functionalized alkynes and alkenes using excess pinacolborane (HBpin) was reported by the group of Knochel,[16] and in recent years several catalysts based on *p*-block elements have been reported to mediate this transformation, thanks to stimulating works by the groups of Thomas, Ingleson, Roesky, Melen and others.[17] However, it was only recently that Rueping and coworkers reported the hydroboration of terminal and internal alkynes catalyzed by Bu_2Mg (Scheme 3.1).[18] The only report of magnesium-catalyzed hydroboration of alkenes came from Parkin and coworkers, who

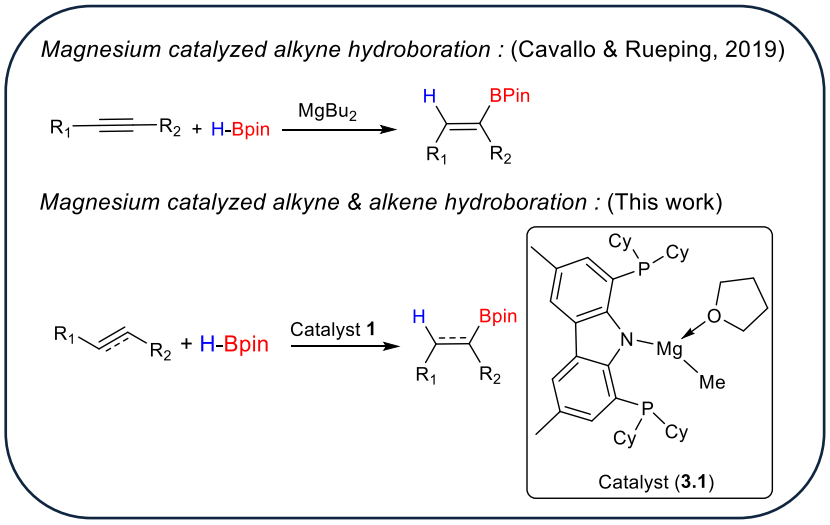

Scheme 3.1: Mg-catalyzed hydroboration of alkyne (known) and alkenes (unknown).

employed a five-coordinate magnesium hydride, [TismPriBenz]MgH [TismPriBenz=tris[(1-isopropylbenzimidazol-2-yl)-dimethylsilyl)]methyl] as a catalyst for hydroboration of styrene,[19a] however the substrate scope was not elaborated. Besides, in a seminal work Harder and coworkers described that in $[DIPPnacnacCaH\cdot(THF)]_2$ catalyzed alkene hydroboration, the organocalcium compound catalyzes the decomposition of HBcat to mainly $B_2(cat)_3$ and BH_3 (or B_2H_6), and the latters are the bonafide catalysts.[19b] Despite the synthetic utility and widespread application of Grignard reagents, only a handful of well-defined magnesium alkyl complexes are known to date and a closer look at their molecular structures reveals that the magnesium center in these compounds is mostly four or higher coordinate.[20] In this chapter, we describe the preparation of a series of monomeric magnesium alkyl complexes using bis(phosphino)carbazolido ligand, and their activity as catalysts for the hydroboration of alkenes and alkynes.

3.2: Synthesis of ligand (L3.1) and magnesium alkyl complexes (3.1-3.4)

For the design of well-defined magnesium alkyl complexes, we have turned our attention towards bis(phosphino)carbazole-based frameworks due to the push–pull electronic environment provided by a π-acidic phosphine and a π-donating carbazolido ligand. Moreover, these scaffolds combine ‘‘hard’’ amido and ‘‘soft’’ phosphine donors. Particularly interesting to us in this regard the recent report by Munz and coworkers, who have isolated a luminescent magnesium bromide complex supported by carbazolyl bridged pincer-type NHC. However, the compound was not structurally authenticated presumably due to solubility issue.[21] We have developed here a new and convenient synthetic procedure to access bis(phosphino)carbazole ligand. We could start with relatively cheap di-*p*-tolylamine instead of 3,6-bromo-9*H*-carbazole and avoid the use of hazardous *tert*-butyllithium.

The preparation of **L3.1** requires only two steps in comparison to multi-step synthesis reported by Gibson and coworkers[22]: (i) bromination of di-p-tolyl amine using bromine in acetic acid and (ii) lithiation of the brominated compound using *n*BuLi and subsequent addition of chlorodicyclohexyl phosphine in diethyl ether, which led to the formation of a PNP-donor ligand (Scheme 3.2). Treatment of **L3.1** with Grignard reagents such as MeMgBr, EtMgBr, *i*PrMgCl or $MgBu_2$ in THF gives corresponding magnesium methyl (**3.1**), ethyl (**3.2**), isopropyl (**3.3**), and butyl (**3.4**) complexes (Scheme 3.2).

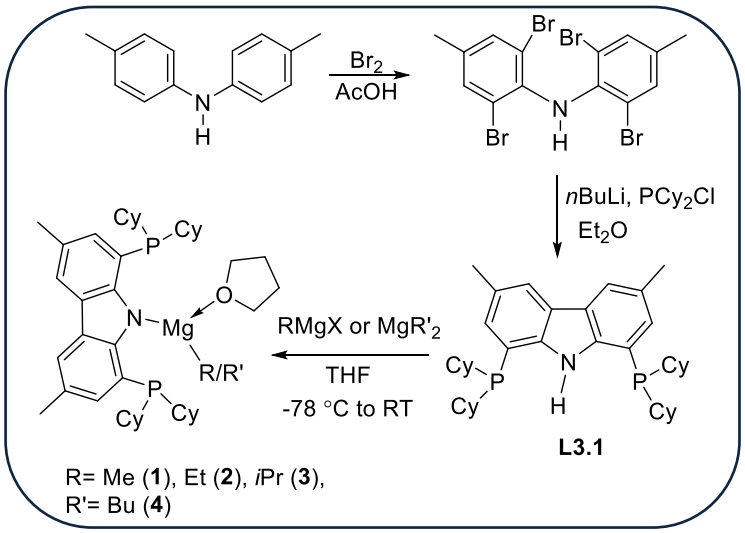

Scheme 3.2: Synthesis of **3.1**-**3.4** starting from di-p-tolylamine.

The ^{1}H NMR of **3.1** show the chemical shift for the methyl protons bound to Mg at -0.74 ppm. It must be stated here that despite repeated attempts, we are unable to get very pure spectra of **3.2** and **3.3** mainly due to solubility issue. The additional peaks in their respective spectrum originate from the coordinated THF molecules and toluene solvent which has been used during work up and sometimes isooctane (in case of **3.2**). Single-crystal X-ray diffraction studies have determined the molecular structures of **3.1**-**3.4**, demonstrating that they exist as monomeric species with a terminal alkyl ligand (Figure 3.1 and 3.2).

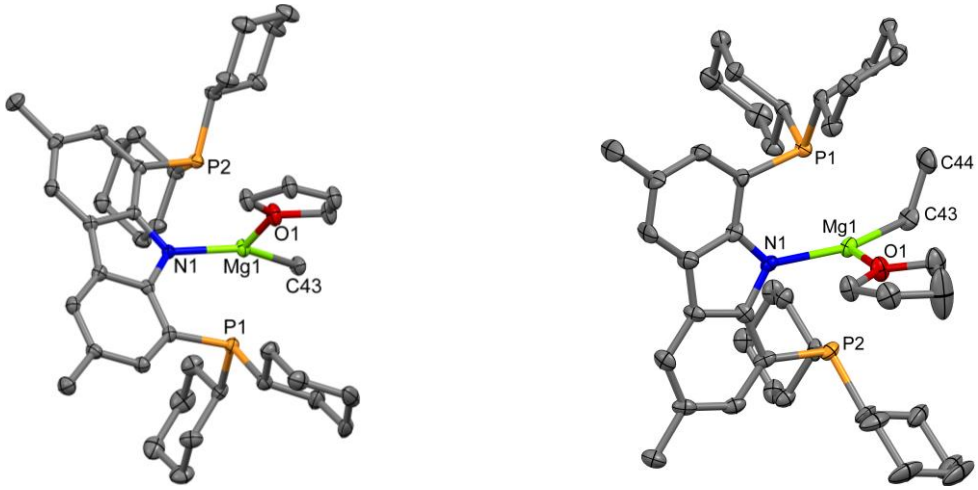

Figure 3.1: The molecular structures of **3.1** (left) and **3.2** (right) with parameters of anisotropic displacement shown at the 50% level of probability. Hydrogen atoms are left out for simplicity. Selected distances (Å) and angles (deg) for **3.1**: P1–Mg1 2.8461(13), P2–Mg1 2.8094(13), Mg1–

O1 2.027(3), Mg1–N1 2.081(3), Mg1–C43 2.164(3); O1–Mg1–N1 98.56(10), O1–Mg1–C43 112.87(12), N1–Mg1–C43 148.50(13), O1–Mg1–P2 96.43(8), N1–Mg1–P2 74.75(7), C43–Mg1–P2 102.65(9), O1–Mg1–P1 96.19(8), N1–Mg1–P1 74.30(7), C43–Mg1–P1 99.33(9), P2–Mg1–P1 147.94(5); **3.2**: P1–Mg1 2.859(2), P2–Mg1 2.824(2), Mg1–O1 2.039(4), Mg1–N1 2.088(5), Mg1–C43 2.142(6); O1–Mg1–N1 97.04(17), O1–Mg1–C43 111.9(2), N1–Mg1–C43 151.0(2), O1–Mg1–P2 97.20(13), N1–Mg1–P2 74.59(13), C43–Mg1–P2 101.90(17), O1–Mg1–P1 96.31(13), N1–Mg1–P1 74.02(13), C43–Mg1–P1 100.65(17), P2–Mg1–P1 147.05(8). **CCDC** number- 2144879 for **3.1** and 2144880 for **3.2**.

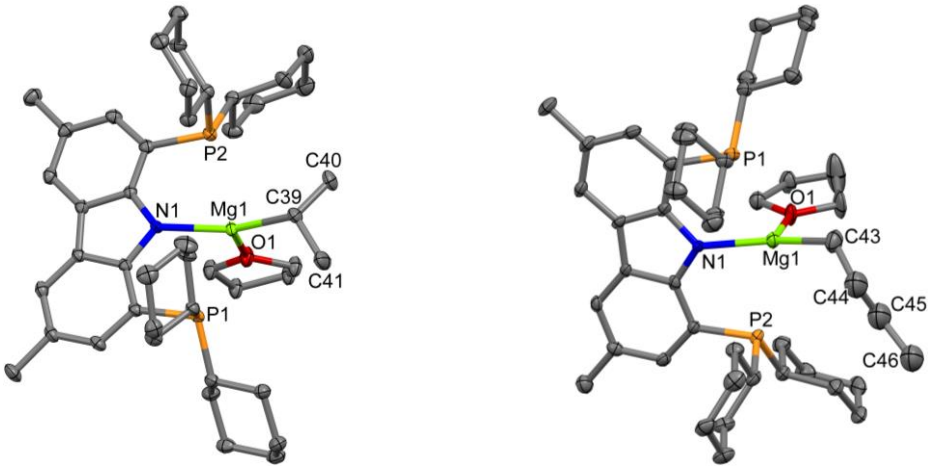

Figure 3.2: The molecular structures of **3.3** (left) and **3.4** (right) with parameters of anisotropic displacement shown at the 50% level of probability. Hydrogen atoms are left out for simplicity. Selected distances (Å) and angles (deg) for **3.3**: P1–Mg1 2.8358(9), P2–Mg1 2.8439(9), Mg1–O1 2.0382(18), Mg1–N1 2.0867(19), Mg1–C39 2.151(2); O1–Mg1–N1 97.18(8), O1–Mg1–C39 113.57(8), N1–Mg1–C39 149.23(9), O1–Mg1–P1 96.82(6), N1–Mg1–P1 74.65(5), C39–Mg1–P1 101.38(7), O1–Mg1–P2 96.53(6), N1–Mg1–P2 74.21(5), C39–Mg1–P2 100.30(7), P1–Mg1–P2 147.35(3); **3.4**: P1–Mg1 2.8307(18), P2–Mg1 2.8428(18), Mg1–O1 2.031(3), Mg1–N1 2.085(3), Mg1–C43 2.142(5); O1–Mg1–N1 97.80(13), O1–Mg1–C43 111.05(18), N1–Mg1–C43 150.63(19), O1–Mg1–P1 98.09(11), N1–Mg1–P1 74.16(10), C43–Mg1–P1 95.80(15), O1–Mg1–P2 95.03(11), N1–Mg1–P2 74.30(10), C43–Mg1–P2 107.33(15), P1–Mg1–P2 147.14(6). **CCDC** number- 2144881 for **3.3** and 2144882 for **3.4**.

The phosphine moieties do not coordinate to the magnesium centers of compounds **1-4**. The Mg–P interactions in these compounds vary within the range of 2.8094(13) – 2.8428(18) Å, which are longer than the predicted covalent value (2.65 Å) and other mononuclear and dinuclear

magnesium phosphanides e.g. $Mg[P\{CH(SiMe_3)_2\}\{C_6H_4\text{-}2\text{-}CH_2NMe_2\}]_2$ (2.556(1) Å) and $[BuMg\{P(CH(SiMe_3)_2)(C_6H_4\text{-}2\text{-}OMe)\}]_2$ (2.5760(8) and 2.5978(8) Å), $[Mg\{[O,O'\text{-}(Me_2PCH_2)_2C_6H_3]_2\}_2]$ 2.761(1) and 2.770(1) Å).[23] However, there might be weak interaction between the phosphorus and magnesium atom as the angles N1-Mg1-C43, N1-Mg1-O1, O1-Mg1-C43 are 148.5°, 98° and 112°. The $Mg–N_{carbazole}$ bond lengths are 2.081(3) and 2.085(3) Å in compounds **3.1**-**3.4**, which are longer than Mg–N bond lengths in *β*-diketiminato magnesium complexes[20b] and those of three-coordinate amido magnesium alkyl complexes [1.997(3), 1.9973(12), 2.046(2) Å] reported by Ma and coworkers.[20h] During the preparation of our manuscript, the groups of Westerhausen and Tan independently reported carbazolyl Hauser bases, where the Mg–N bonds were determined to be 2.045(3) and 1.977(4) Å.[24] The slightly elongated Mg-N bond lengths in compounds **3.1**-**3.4** are more in line with the quasi-coordination of the phosphine units to the Mg centers. The terminal Mg–C bond lengths in **3.1**-**3.4** are 2.164(3) and 2.142(5) Å, which are in harmony with those mentioned by Ma [2.114(4), 2.1844(16), 2.173(4) Å].[20h]

3.3: Magnesium methyl complex as catalyst for hydroboration of alkynes

Having established simple strategies to obtain magnesium alkyl complexes based on bis(phosphino)carbazolido ligand, the catalytic utility of these derivatives was further studied. Because hydroboration by compounds with main-group elements has become a hot topic in recent years, hydroboration of alkyne was chosen for further investigation. Initial catalyst evaluation for the hydroboration of alkynes was carried out with **3.1**-**3.4** and phenyl acetylene as model substrate and HBpin. Results suggest that compound **3.1** shows better catalytic activity than the remaining three magnesium compounds. Performing the reaction with **3.1** at 80 °C for 18 h afforded the corresponding (E)-vinyl boronate **3.5a** in 91% yield and excellent selectivity. Using the optimized reaction conditions (Table 3.1 for optimization), the incredible efficiency of the catalyst was demonstrated by the good to outstanding yields of hydroboration for both aliphatic and aromatic alkynes to produce the appropriate vinyl-boronates (Scheme 3.3).

Table 3.1: Table of optimization for the 3.1 catalyzed hydroboration of phenylacetylene.

Entry	Catalyst; 3.1 (Mol%)	Equiv. of HBpin	Solvent	Temperature (°C)	Time (h)	NMR Yield (%)
1.	2	1.1	Neat	60	12	24
2.	2	1.1	Neat	60	18	31
3.	5	1.1	Neat	60	18	38
4.	5	1.1	Neat	70	12	44
5.	5	1.1	Neat	70	18	60
6.	5	1.1	Neat	80	12	76
7.	5	1.1	Neat	80	18	91

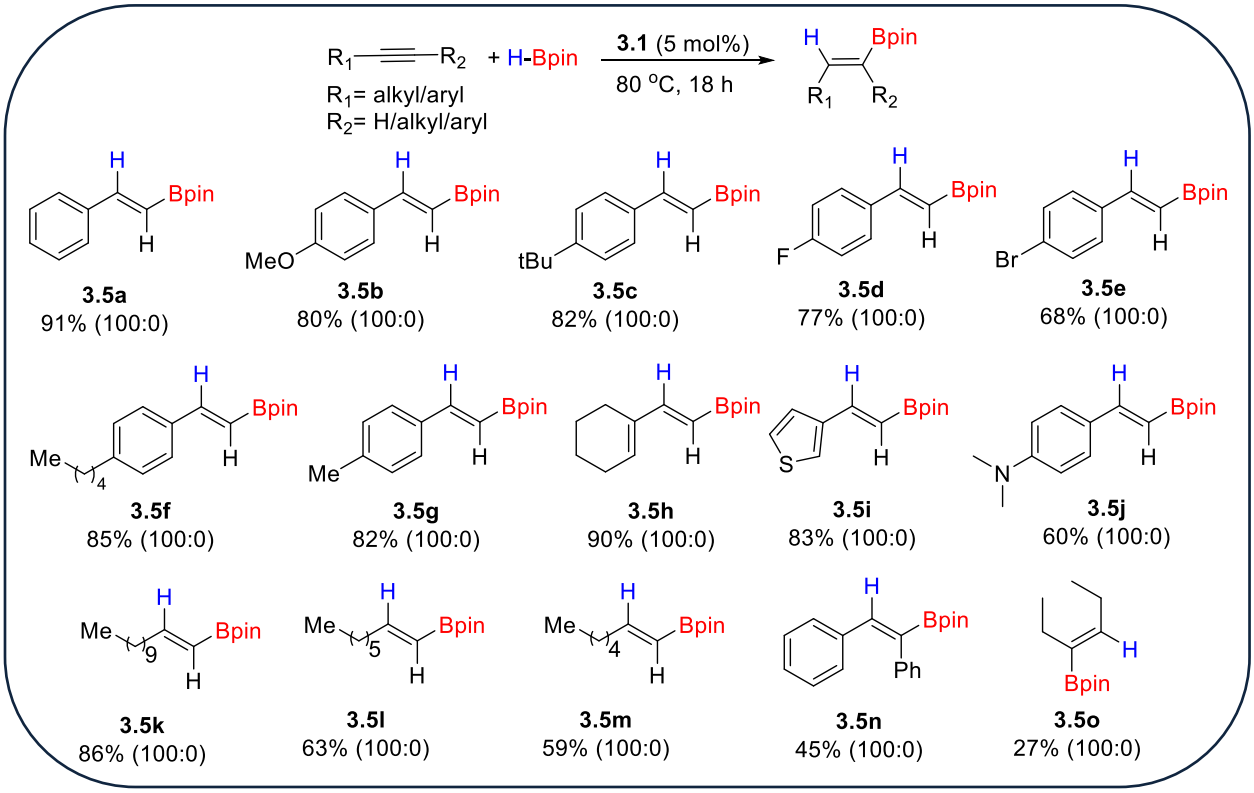

Scheme 3.3: Hydroboration Scope with alkyne substrates. Reaction conditions: Alkyne (0.25 mmol), HBpin (0.275 mmol, 1.1equiv), 5 mol% catalyst, 18 h reaction at 80 °C temperature in neat condition. The ^{1}H NMR integration with respect to mesitylene was used to calculate yields. Regioisomer distribution is reported by ratios in parenthesis (linear vs. branched).

Smooth hydroboration of aromatic alkynes with electron-donating (**3.5b**, **3.5c**, **3.5f**, **3.5g**) or -withdrawing (**3.5d** and **3.5e**) substituents was observed. 1-ethenyl cyclohexene was found to react exclusively with the alkyne functionality in good yield (**3.5h**), with no apparent reduction of the alkene moiety. Overall, the protocol is comparable with that reported by Rueping and coworkers,[18] though in our case the catalyst mol% is less, and no solvent is needed. In fact, scaling up the reaction to 5 mmol for phenylacetylene revealed almost no drop in yield. Internal alkynes such as diphenyl acetylene and 3-hexyne underwent hydroboration (**3.5n** and **3.5o**), though in moderate yields.

3.4: Deuterium labeling experiment for diastereoselectivity

Deuterium labeling experiments were carried out to understand the diastereoselectivity (Scheme 3.4). The *cis* orientation of the deuterium and phenyl ring is shown by a resonance at 6.20 ppm in the ^{2}H NMR for the catalytic hydroboration of PhC≡CD with HBpin(Scheme 3.4, above). Likewise, the reaction of PhC≡CH and DBpin (Scheme 3.4, below) exhibits a resonance at δ 7.24 ppm in the ^{2}H NMR spectrum (see Figures 3.3-3.4), demonstrating evidence in favor of a 1,2-*cis*-hydroboration.

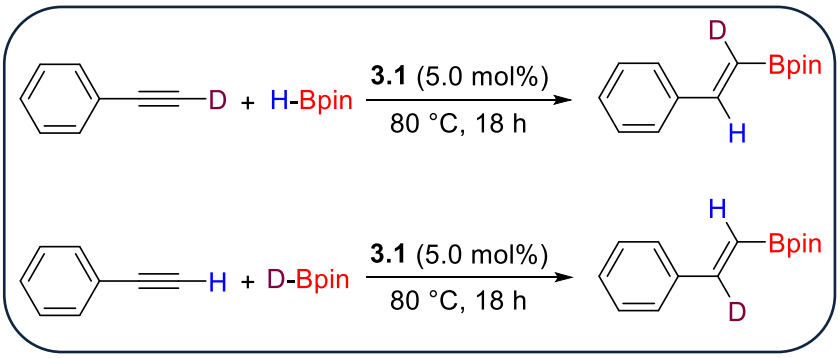

Scheme 3.4. Experiment with deuterium labelling: Phenylacetylene-D hydroboration with HBpin (top) and (b) phenylacetylene hydroboration with DBpin (below).

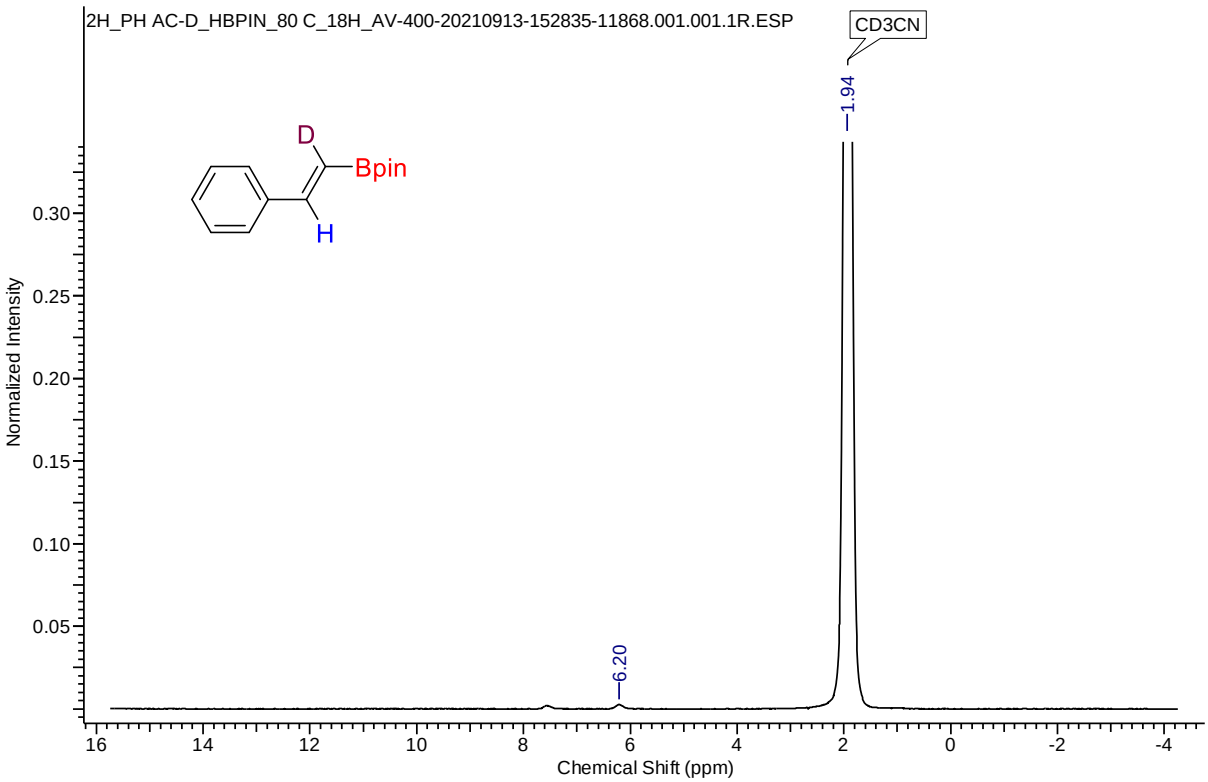

Figure 3.3: ^{2}H NMR spectrum of the reaction of PhC≡CD with HBpin in the presence of **3.1** (CD_3CN, 61.42 MHz, 298 K).

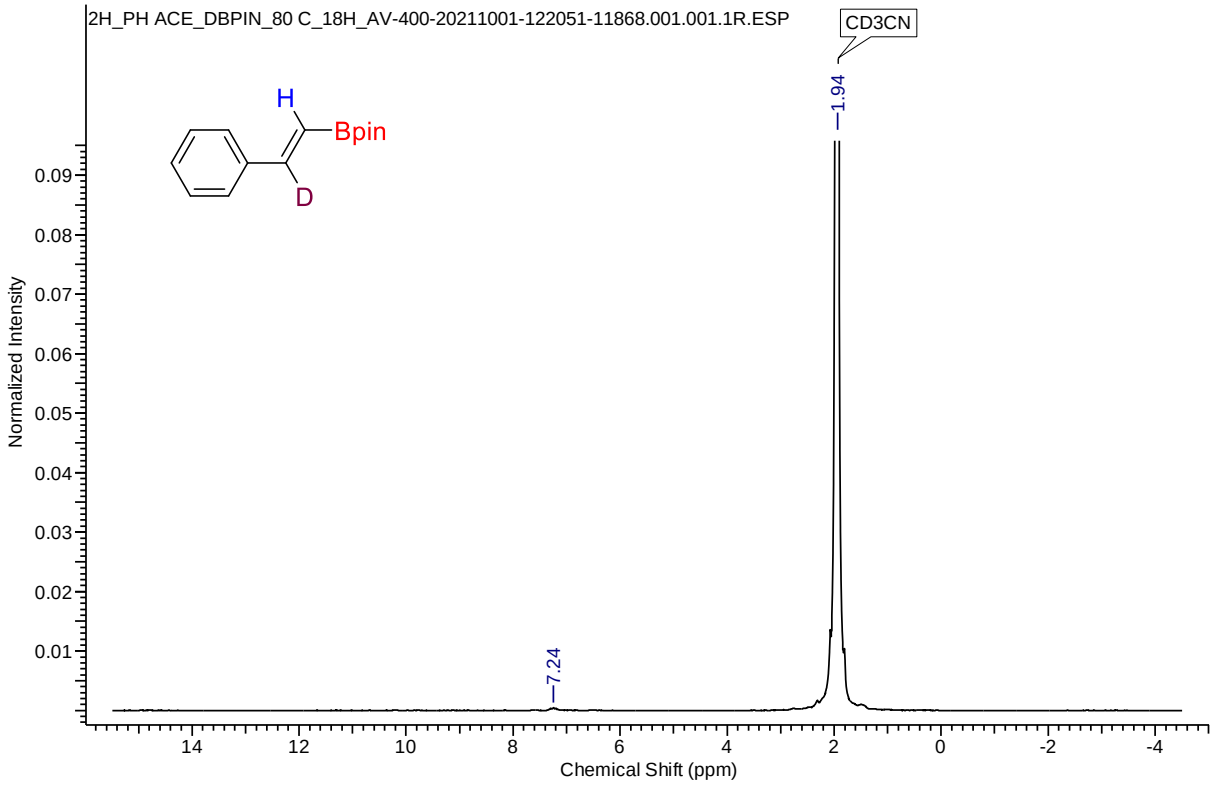

Figure 3.4: ^{2}H NMR spectrum of the reaction of DBpin with PhC≡CH in the presence of **3.1** (CD_3CN, 61.42 MHz, 298 K).

3.5: Magnesium methyl complex(3.1) as a catalyst for hydroboration of alkenes

Subsequently, we were interested in the hydroboration of alkenes, which is more challenging compared to alkynes. For hydroboration of alkenes, catalyst loadings were increased up to 10 mol%, and the reactions were completed around 12 h upon heating at 100 °C leads to 93 % yield (see Table 3.2). Simple aryl- and alkyl-substituted terminal alkenes proceeded to the hydroboration products (Scheme 3.5).

Table 3.2: Styrene hydroboration optimization table with catalyst 3.1.

Entry	Catalyst; 3.1 (Mol%)	Equiv. of HBpin	Solvent	Temperature (ºC)	Time (h)	NMR Yield (%)
1.	5	1.1	Neat	60	18	20
2.	5	1.1	Neat	70	18	28
3.	5	1.1	Neat	80	18	36
4.	5	1.1	Neat	100	13	75
5.	5	1.1	Neat	100	18	84
6.	10	1.1	Neat	80	18	76
7.	10	1.1	Neat	90	18	85
8.	10	1.1	Neat	100	12	93

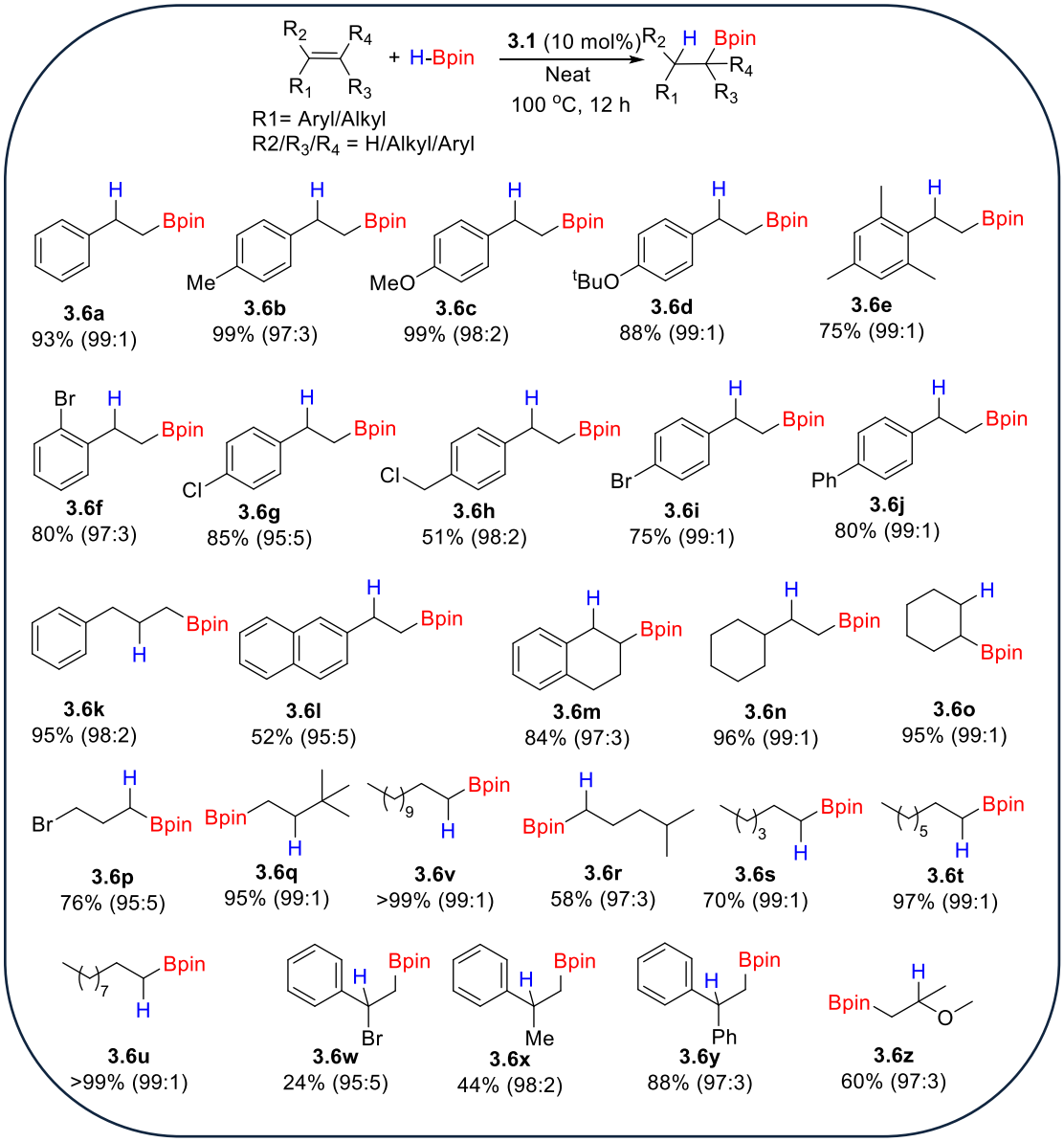

Scheme 3.5: Hydroboration Scope with alkene substrates. Reaction conditions: Alkene (0.25 mmol), HBpin (0.275 mmol, 1.1equiv), 10 mol% catalyst, 12 h reaction at 100 °C temperature in neat condition. The ^{1}H NMR integration with respect to mesitylene was used to calculate yields. Regioisomer distribution is reported by ratios in parenthesis (linear vs. branched).

Notably, the isomer ratio for all substrates was 95-99:5-1 towards the anti-Markovnikov product. The substrate scope revealed that the reduction of both electron-rich styrene derivatives (**3.6b**-**3.6e**) and electron-poor derivatives (**3.6f**, **3.6g**, **3.6i**) afforded the corresponding boronates in excellent yields. Sterically encumbered 2,4,6-trimethylphenyl substituted styrene performed well (**3.6e**), explicating that the steric parameters have little effect on the catalyst activity. Analysis of

the scope for aliphatic alkenes has shown high reactivity for a large number of alkyl substrates. While a recently reported Mn(I) catalyst was unreactive towards hydroboration of cyclohexene,[25] **3.1** can selectively reduce cyclohexene (**3.6o**) in quantitative yield. Similarly, Oestreich and coworkers found only traces for hydroboration of 4-methoxy styrene[17i] with BAr^F_3 (Ar^F=3,5-bis(trifluoromethyl)phenyl), while **3.1** gives quantitative yield for the same. In case of internal alkenes, the reactions were sluggish with *α*-bromo (**3.6w**) and *α*-methyl (**3.6x**) groups. However, the reaction was smooth for *α*-phenyl styrene, which gives 88% conversion (**3.6y**). Gratifyingly, the alkene hydroboration reaction was also scaled up to 5 mmol under the same conditions with almost no compromise of the yields.

Recently Thomas and cowokers have shown that nucleophiles such as NaO*t*Bu,[26] *n*BuLi,[27] nBu_2Mg[18] etc., actually promote the formation of BH_3 from HBpin and the generated BH_3 does the catalysis.[28,29] To ascertain whether BH_3 was involved in hidden catalysis, we have carried out the same reaction in the presence of 10 mol% TMEDA, which led to the formation of the corresponding borylated alkane with 86% yield for styrene with a 7% yield drop.

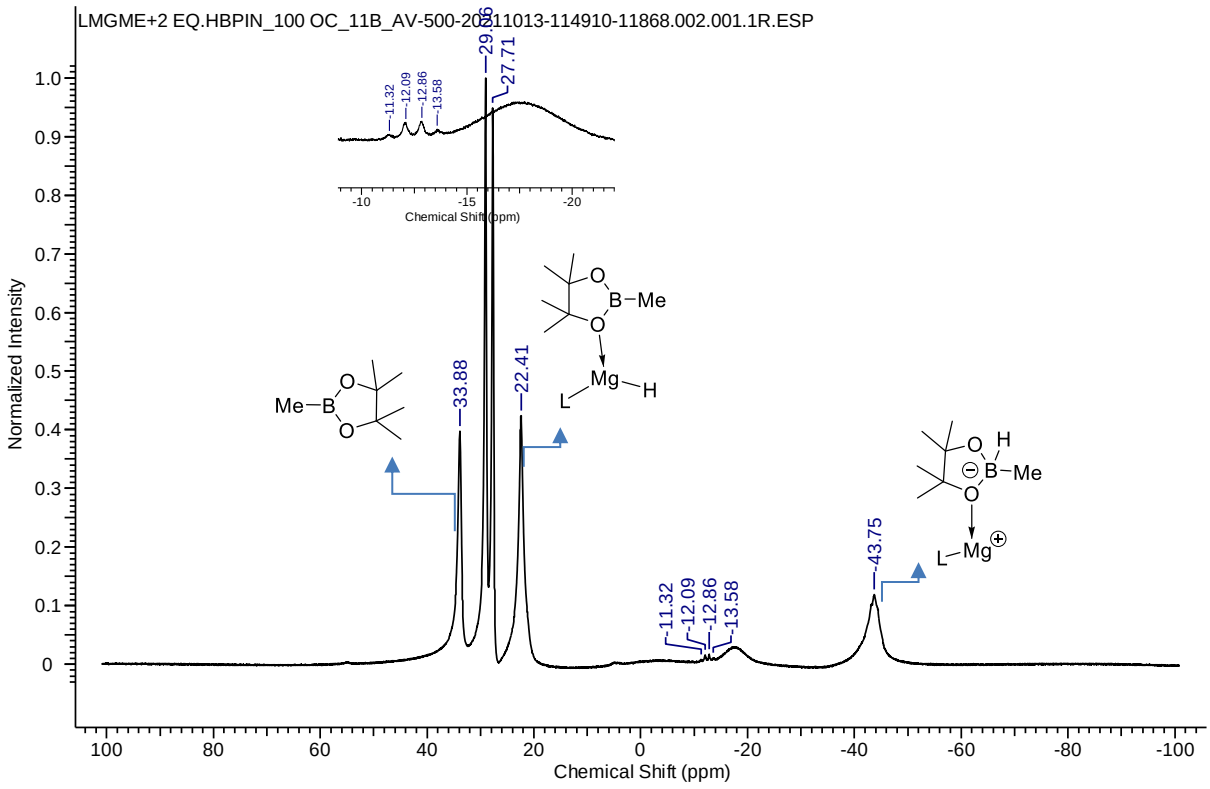

Figure 3.5: ^{11}B NMR spectrum of the reaction of **3.1** with HBpin.

The ^{11}B NMR of the reaction in the presence of TMEDA reveals no prominent resonance at -10 ppm, which is characteristic for TMEDA·BH_3 adduct.[28] However, the inspection of the ^{11}B NMR spectrum arising from the reaction of HBpin with **3.1** reveals the generation of BH_3 in a very minor quantity (Figure 3.5). Hence, we cannot unequivocally exclude the possibility of hidden borohydride catalysis.[28-30]

3.6: Magnesium methyl complex(3.1) as a catalyst for hydroboration of terpenes

In a bid to expand the scope of catalysis by **3.1**, naturally occurring terpenes such as R- or S-limonene, myrcene and *β*-pinene have been subjected to the selective reduction of their olefinic bond. Interestingly, good yields were observed for all cases with excellent selectivity (Scheme 3.6), which could not be afforded with our previously reported lithium-based catalyst.[31] In case of limonene, only terminal double bond was selectively reduced.[32] Interestingly, Ritter and coworkers reported the analogous hydroboration of myrcene with HBpin, which was catalyzed by the iminopyridine−iron(II) complex (5 mol%) in the presence of magnesium metal (10%),[33] while in our case no transition metal or elemental magnesium is needed.

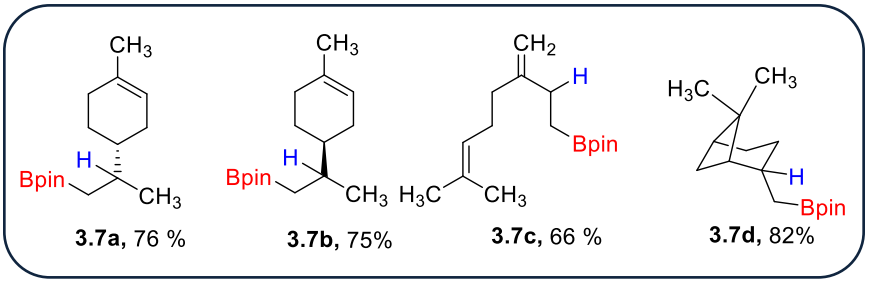

Scheme 3.6: Selective alkene hydroboration for terpenes: *R*- or *S*- limonene, myrcene, and *β*-pinene.

3.7: Competitive experiments for chemoselective hydroboration

A series of experiments were carried out to further evaluate the chemoselective hydroboration (Scheme 3.7). The competing study used a combination of (i) acetophenone and styrene and (ii) ethyl benzoate and styrene resulted in almost quantitative hydroboration of ketone/ester and complete recycle of styrene. Similarly, equimolar amounts of acetophenone or ethyl benzoate and phenylacetylene were reacted with HBpin to produce the corresponding boronate esters of ketone or ester. Similar chemoselectivity was observed for nitriles over alkene and alkyne.

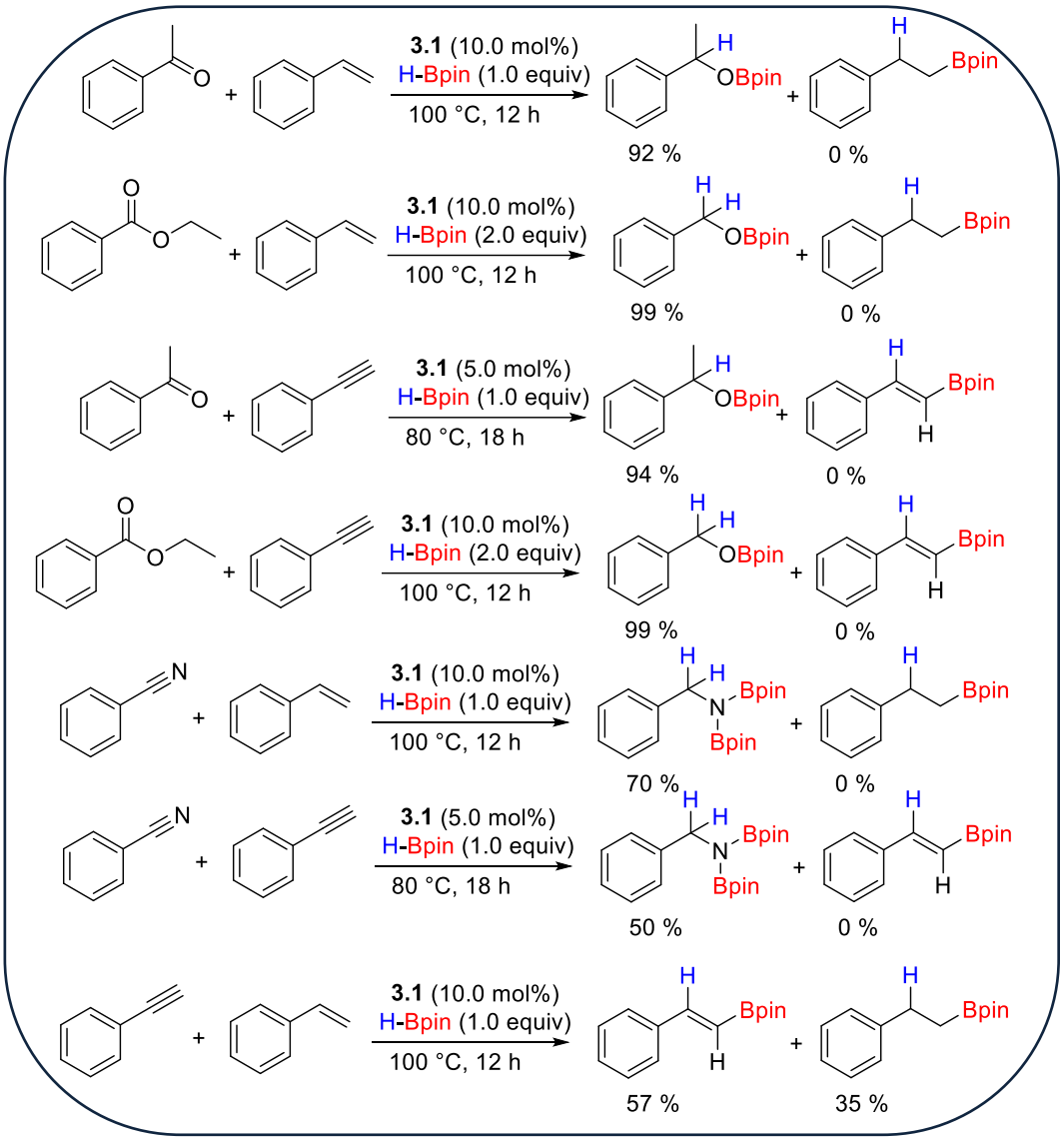

Scheme 3.7: Competitive experiments for chemoselective hydroboration.

In another competition study, where equimolar styrene and phenylacetylene are allowed to compete for 1.0 equiv of HBpin, marginal preference for alkyne hydroboration was witnessed, reaching 57% conversion of phenylacetylene and only 35% conversion of styrene. The details of the competitive experiments are given in the appendix section 6.3.11.

3.8: Mechanistic investigation

The stoichiometric reaction of catalyst 3.1 and HBpin:

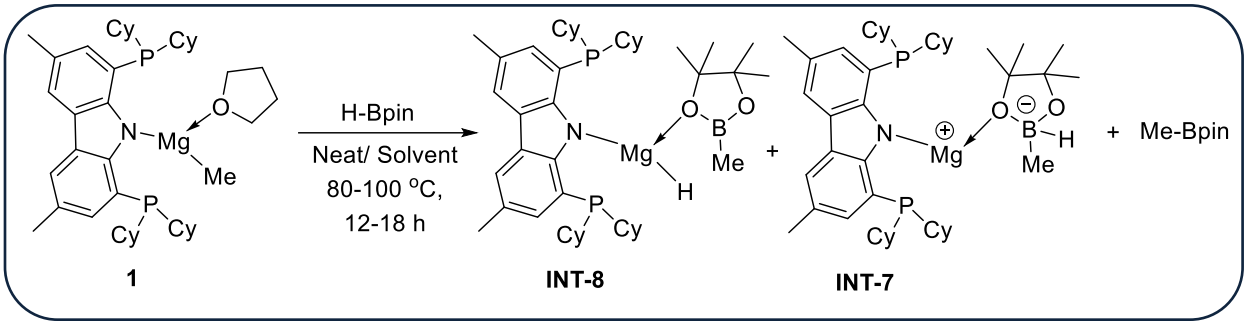

Scheme 3.8: Stoichiometric reaction of **3.1** with HBpin.

A solution of HBpin (64/128 mg, 0.50/1.0 mmol) in THF/C_6D_6 was added to the THF/C_6D_6 solution of **3.1** (315 mg, 0.50 mmol) at room temperature inside the glove box. The reaction mixture was allowed to stirr/heat overnight at 80 °C. The reaction mixture was subjected for characterization. ^{1}H NMR (C_6D_6, 400 MHz, 298 K): ^{1}H NMR spectra is not very clean but one new peak is generated at 4.54 ppm, which can be assigned as a Mg-H further ^{11}B NMR (C_6D_6, 128 MHz, 298 K): δ 33.38 (s, Me-Bpin), 29.06-27.71 (d, for unreacted HBpin), 22.41 (s, Mg-*H*), 43.75 (s, for zwitter ionic species) ppm (Figure 3.5).

3.9: Kinetic experiments

The hydroboration of styrene with **3.1** was monitored *in situ* by ^{1}H NMR spectroscopy. Reactions were initially carried out employing identical concentrations of **3.1** and different styrene concentrations. A graph of ln[styrene] versus time (Figure 3.6), revealed that the reaction is first order with respect to styrene. The same sets of experiments were performed with varying concentration of HBpin and the resulting plot indicated first-order rate dependence with respect to HBpin (Figure 3.7). The overall rate law for the hydroboration is presented in equation below:

Rate= k[Styrene][HBpin]

Further Arrhenius analysis afforded an activation of ca. 13 (+/- 6) kcal.mol^{-1} (Figure 3.8).

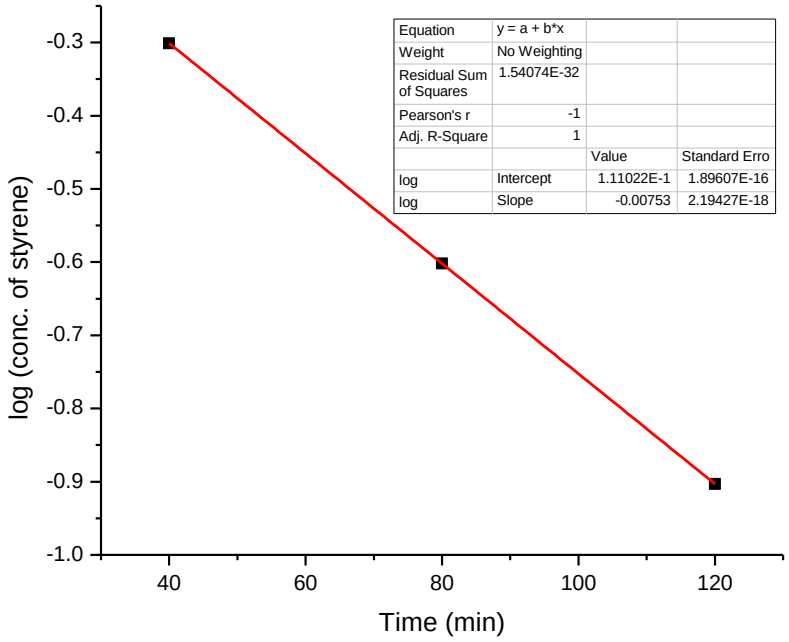

Figure 3.6: Plot of log (conc. of styrene) vs. time (min.). This shows first order dependence over styrene.

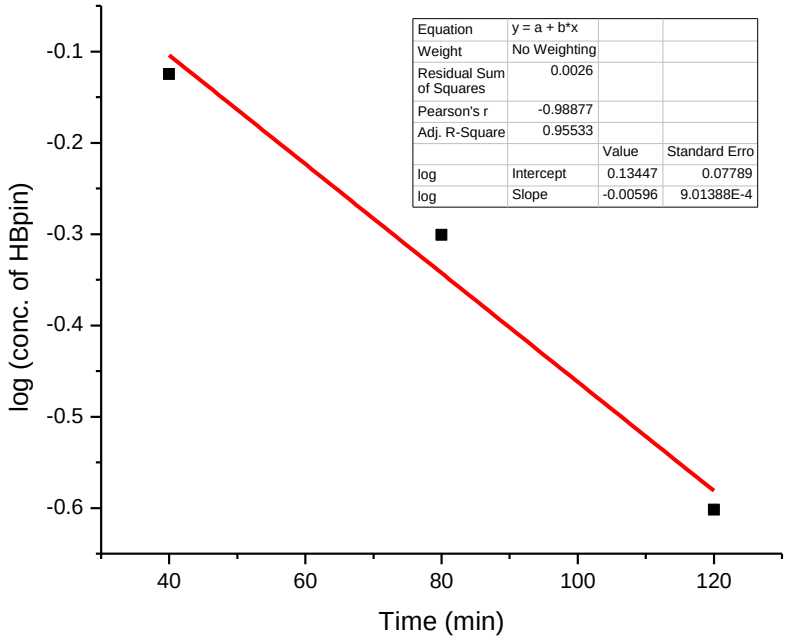

Figure 3.7: Plot of log (conc. of HBpin) vs. time (min.). This shows first order dependence over HBpin.

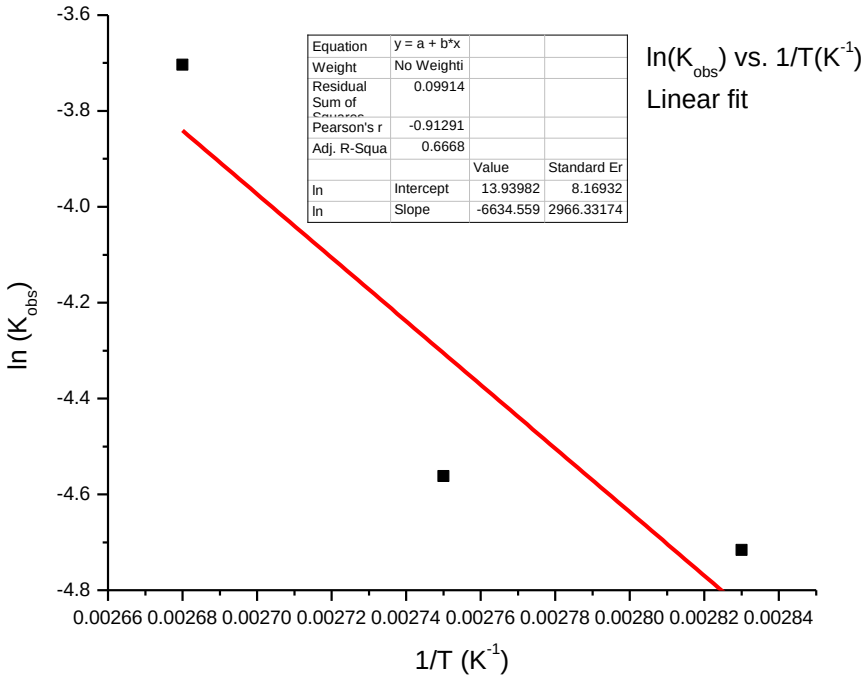

Figure 3.8: Arrhenius plot of $\ln(K_{obs})$ *vs.* 1/T (K^{-1}).

Slope of Arrhenius plot = -6634.56

-Ea/R = -6634.56; Ea = 55.16 kJ/mol or 13.2 kcal/mol

3.10: **DFT studies**

A detailed theoretical exploration of the catalytic efficiency of the monomeric magnesium alkyl complexes in hydroboration reactions is performed to unravel the complete mechanistic scenario. Quantum chemical calculations were performed at the R-M06-2X-D3/def2-TZVP//R-BP86/def2-SVP level[34] to explore the mechanistic avenues in Mg-catalyzed hydroboration of styrene. Theoretical calculations suggest the initiation of the reaction with σ-bond metathesis between the H−Bpin and Mg−Me bonds following *Pathway-A* via the transition state **TS-1** (Figure 4), leading to the formation of a slightly more stable intermediate **INT-1** that serves as the active catalyst. This step needs to overcome an energy barrier of 16.0 kcal.mol^{-1}. The insertion of styrene into the Mg−H bond in **INT-1** furnishes an appreciably stable intermediate **INT-2**, surmounting the rate-limiting energy barrier of 21.5 kcal.mol^{-1}. The substitution of the coordinated THF in **INT-2** with HBpin followed by the nucleophilic migration of the phenethyl group to the boron center results in the zwitterionic intermediate **INT-4**. The generation of **INT-4** is supported by the

^{11}B NMR resonance at -43.75 ppm arising from the stoichiometric reaction of **1** and HBpin (Figure 3.5, above), which is in good agreement with that reported by Cavallo and Rueping.[18] The subsequent hydride transfer from boron to magnesium generates **INT-5** via **TS-4**. Finally, the desired hydroboration product (**6a**) is liberated from **INT-5** to regenerate the active catalyst **INT-1** for the next catalytic cycle.

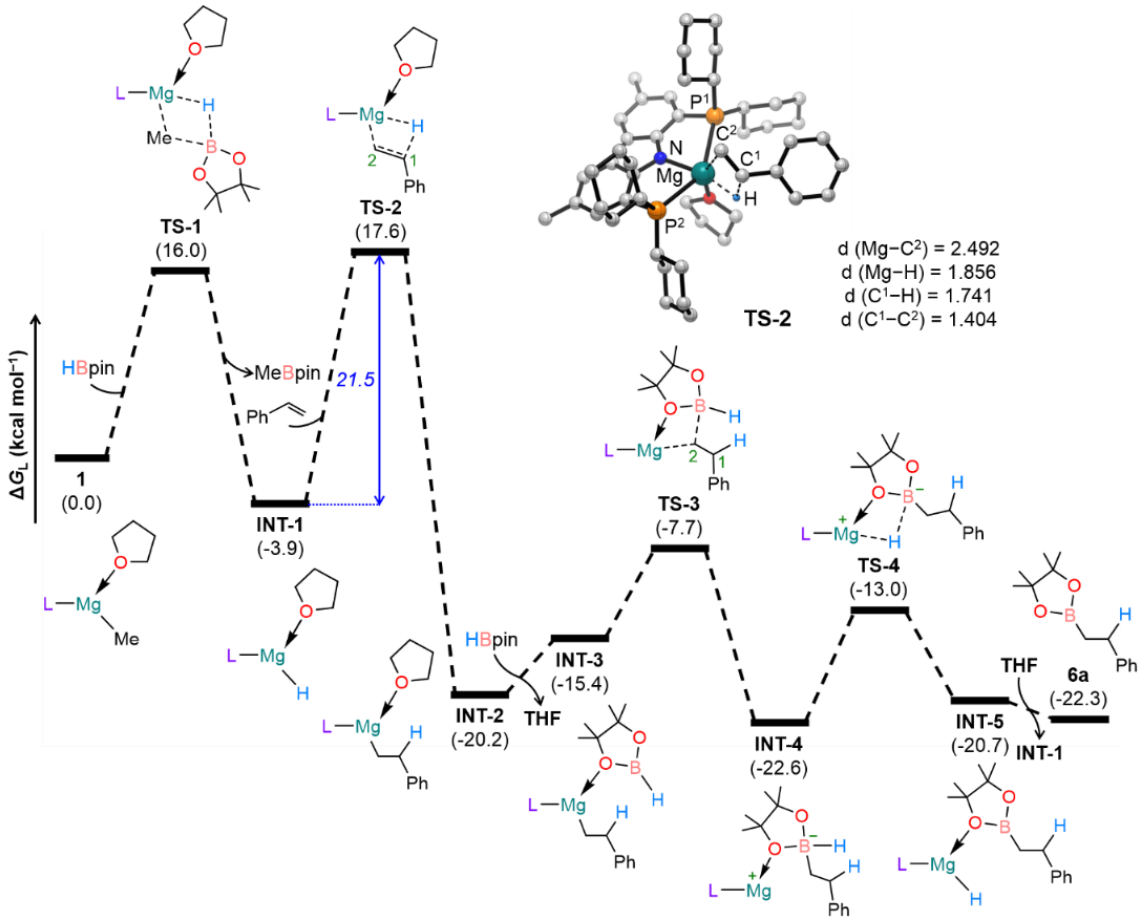

Figure 3.9: Energy profile for the Mg-catalyzed hydroboration of styrene following *Pathway-A*. Optimized geometry of the transition state **TS-2** with important geometrical parameters is also provided. Bond distances (d) are in angstroms (Å). Only key hydrogen atom is shown for clarity. L = 1,8-bis(phosphino)carbazolide anion.

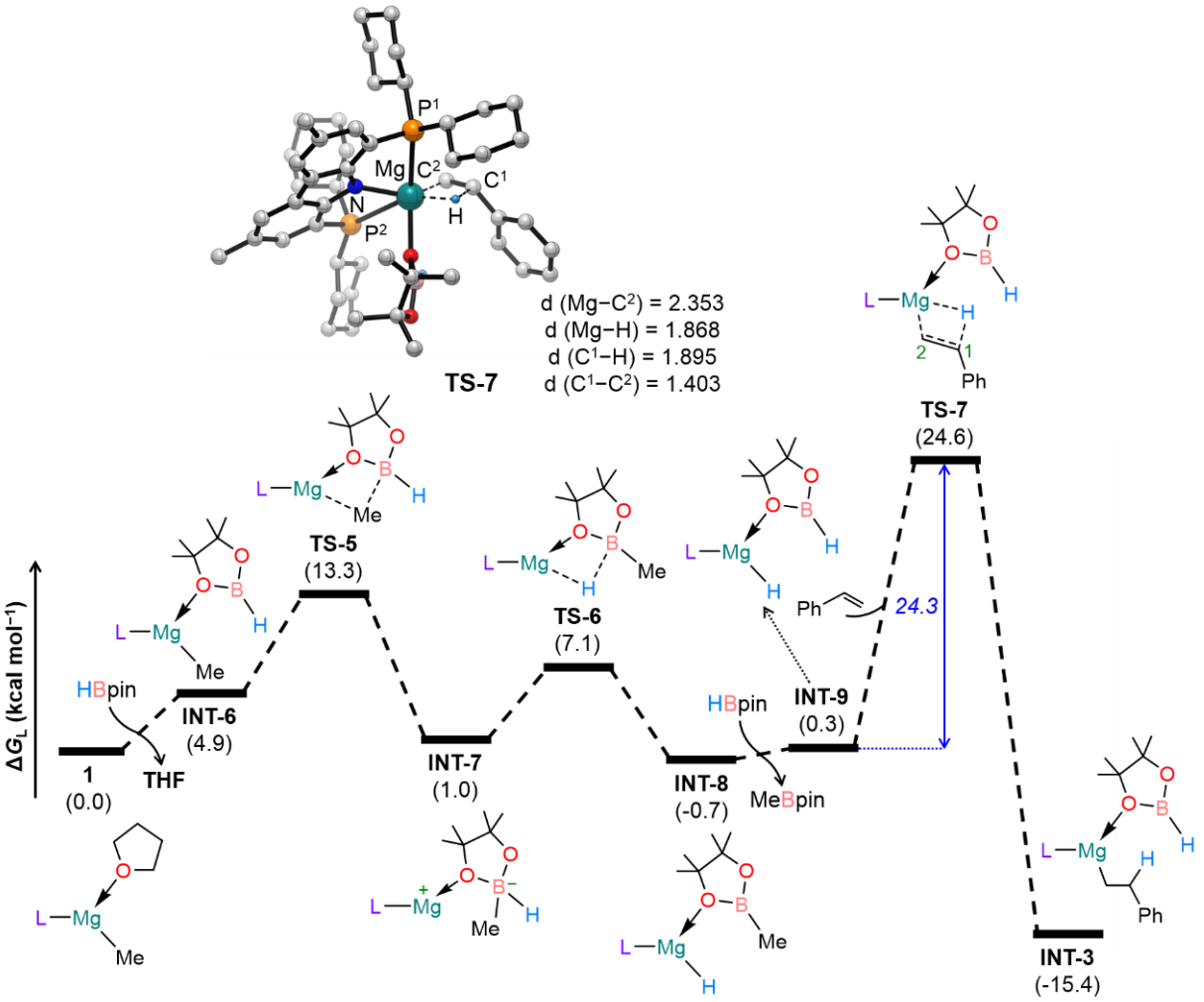

Figure 3.10: Energy profile for the Mg-catalyzed hydroboration of styrene following *Pathway-B*. Optimized geometry of the transition state **TS-7** with important geometrical parameters is also provided. Bond distances (d) are in angstroms (Å). Only key hydrogen atoms are shown for clarity. L = 1,8-bis(phosphino)carbazolide anion.

We have also investigated the alternative route, *Pathway-B*, concerning the HBpin coordinated magnesium hydride species (**INT-9**) as the active catalyst (Figures 5). [18] Though the generation of **INT-9** demands an appreciably lower energy barrier than that of **INT-1** by 2.7 kcal.mol^{-1}, similar insertion of styrene into the Mg−H bond in **INT-9** requires a slightly higher energy barrier of 24.3 kcal.mol^{-1} to afford **INT-3**. Hence, of the two competing routes for the generation of **INT-3**, *Pathway-A* prevails over *Pathway-B* on the kinetic ground. However, monitoring the stoichiometric reaction of **1** with HBpin by ^{11}B NMR revealed three resonances at 33.9 (MeBpin),[29a] 22.4 (**INT-8**), and -43.7 (zwitterionic species **INT-7**) ppm (Figure 3), which

are in line with those that were reported by Cavallo and Rueping.[18] Additionally, given the fact that HBpin was used in stoichiometric amount, **INT-9** may dominate the reaction course. These data prefer *Pathway-B* over *Pathway-A*. Furthermore, distortion–interaction analyses[35] of the key transition states **TS-2**/**TS-7** considering **INT-1**/**INT-9** and styrene as the interacting fragments reveal the activation barriers to be solely governed by the distortion energies of the **INT-1**/**INT-9** fragments (Tables S6 and S7).[36] We have also investigated *Pathway-C* involving direct insertion of styrene into the B−H bond in **INT-6**, as depicted in Figure S131. However, the corresponding transition state **TS-9** exhibits a drastically high energy barrier of 44.2 kcal.mol^{-1}; therefore, this route can be safely discarded.

3.11: Conclusions

In conclusion, we have introduced bis(phosphino)carbazolido ligand to develop monomeric magnesium alkyl species through a convenient synthetic route. We have further demonstrated that the easily prepared magnesium methyl compound **3.1** may be applied to the efficient hydroboration of a variety of alkenes and alkynes as well as few biologically important terpenes. The methodology proceeds with the syn addition of HBpin and good regioselectivity for unsymmetrical alkenes and alkynes. Extensive DFT Studies have been conducted to have an insight the mechanism.

3.12: References

[1] R. M. Bullock, J. G. Chen, L. Gagliardi, P. J. Chirik, O. K. Farha, C. H. Hendon, C. W. Jones, J. A. Keith, J. Klosin, S. D. Minteer, R. H. Morris, A. T. Radosevich, T. B. Rauchfuss, N. A. Strotman, A. Vojvodic, T. R. Ward, J. Y. Yang, Y. Surendranath, *Science* **2020**, *369*, eabc3183 (1-10).

[2] M. Arrowsmith, T. J. Hadlington, M. S. Hill, G. Kociok-Köhn, *Chem. Commun.*, **2012**, *48*, 4567–4569.

[3] M. Arrowsmith, M. S. Hill, G. Kociok-Köhn, *Chem. Eur. J.*, **2013**, *19*, 2776−2783.

[4] D. Mukherjee, A. Ellern, A. D. Sadow, *Chem. Sci.*, **2014**, *5*, 959–964.

[5] C. Weetman, M. S. Hill, M. F. Mahon, *Chem. Commun.*, **2015**, *51*, 14477–14480.

[6] N. L. Lampland, M. Hovey, D. Mukherjee, A. D. Sadow, *ACS Catal.*, **2015**, *5*, 4219–4226.

[7] C. Weetman, M. D. Anker, M. Arrowsmith, M. S. Hill, G. Kociok-Köhn, D. J. Liptrot, M. F. Mahon, *Chem. Sci.*, **2016**, *7*, 628–641.

[8] D. Mukherjee, S. Shirase, T. P. Spaniol, K. Mashima, J. Okuda, *Chem. Commun.*, **2016**, *52*, 13155–13158.

[9] Y. Yang, M. D. Anker, J. Fang, M. F. Mahon, L. Maron, C. Weetman, M. S. Hill, *Chem. Sci.*, **2017**, *8*, 3529–3537.

[10] S. Yadav, R. Dixit, M. K. Bisai, K. Vanka, S. S. Sen, *Organometallics*, **2018**, *37*, 4576–4584.

[11] Y. K. Jang, M. Magre, M. Rueping, *Org. Lett.*, **2019**, *21*, 8349–8352.

[12] M. Szewczyk, M. Magre, V. Zubar, M. Rueping, *ACS Catal.*, **2019**, *9*, 11634–11639.

[13] M. S. Hill, D. J. Liptrot, C. Weetman, *Chem. Soc. Rev.*, **2016**, *45*, 972–988.

[14] M. Magre, M. Szewczyk, M. Rueping, *Chem. Rev.* **2022**, *122*, 9, 8261–8312.

[15] J. V. Obligacion, P. J. Chirik, *Nat Rev Chem*, **2018**, *2*, 15–34.

[16] C. E. Tucker, J. Davidson, P. Knochel, *J. Org. Chem.*, **1992**, *57*, 3483–3485.

[17] Selected references for alkyne hydroboration by compounds with p-block elements, please see: (a) Z. Yang, M. Zhong, X. Ma, K. Nijesh, S. De, P. Parameswaran, H. W. Roesky, *J. Am. Chem. Soc.*, **2016**, *138*, 2548–2551. (b) A. Bismuto, S. P. Thomas, M. J. Cowley, *Angew. Chem. Int. Ed.*, **2016**, *55*, 15356–15359. (c) J. S. McGough, S. M. Butler, I. A. Cade, M. J. Ingleson, *Chem. Sci.*, **2016**, *7*, 3384–3389. (d) J. R. Lawson, L. C. Wilkins, R. L. Melen, *Chem. Eur. J.*, **2017**, *23*, 10997−11000. (e) J. L. Carden, L. J. Gierlichs, D. F. Wass, D. L. Browne, R. L. Melen, *Chem. Commun.*, **2019**, *55*, 318–321. (f) S. Pahar, V. Sharma, S. Tothadi, S. S. Sen, *Dalton Trans.*, **2021**, *50*, 16678–16684. (g) A. Harinath, I. Banerjee, J. Bhattacharjee, T. K. Panda, *New J. Chem.*, **2019**, *43*, 10531-10536. For alkene hydroboration: (h) A. Prokofjevs, A. Boussonnihre, L. Li, H. Bonin, E. Lacite, D. P. Curran, E. Vedejs, *J. Am. Chem. Soc.*, **2012**, *134*, 12281–12288. (i) Q. Yin, S. Kemper, H. F. T. Klare, M. Oestreich, *Chem. Eur. J.*, **2016**, *22*, 13840−13844. (j) A. Bismuto, M. J. Cowley, S. P. Thomas, *ACS Catal.*, **2018**, *8*, 2001–2005.

[18] M. Magre, B. Maity, A. Falconnet, L. Cavallo, M. Rueping, *Angew. Chem., Int. Ed.*, **2019**, *58*, 7025–7029.

[19] (*a*) M. Rauch, S. Ruccolo, G. Parkin, *J. Am. Chem. Soc.*, **2017**, *139*, 13264–13267. (b) S. Harder, J. Spielmann, *J. Organometal. Chem.*, **2012**, *698*, 7–14.

[20] (*a*) P. Ghosh, G. Parkin, *Inorg. Chem.*, **1996**, *35*, 1429–1430. (*b*) V. C. Gibson, J. A. Segal, A. J. P. White, D. J. Williams, *J. Am. Chem. Soc.*, **2000**, *122*, 7120–7121. (*c*) A. P. Dove, V. C. Gibson, P. Hormnirun, E. L. Marshall, J. A. Segal, A. J. P. White, D. J. Williams, *Dalton Trans.*, **2003**, 3088–3097. (*d*) L. F. Sánchez-Barba, A. Garcés, M. Fajardo, C. Alonso-Moreno, J. Fernández-Baeza, A. Otero, A. Antiñolo, J. Tejeda, A. Lara-Sánchez, M. I. López-Solerag, *Organometallics*, **2007**, *26*, 6403–6411. (*e*) S. E. Baillie, V. L. Blair, T. D. Bradley, W. Clegg, J. Cowan, R. W. Harrington, A. Hernan-Gómez, A. R. Kennedy, Z. Livingstonea, E. Hevia, *Chem. Sci.*, **2013**, *4*, 1895–1905. (*f*) V. Balasanthiran, M. H. Chisholm, K. Choojun, C. B. Durr, P. M. Wambua, *Polyhedron*, **2016**, *103*, 235–240. (*g*) S. Ruccolo, M. Rauch, G. Parkin, *Chem. Sci*., **2017**, *8*, 4465–4474. (*h*) M. Ma, J. Li, X. Shen, Z. Yu, W. Yao, S. A. Pullarkat, *RSC Adv.*, **2017**, *7*, 45401–45407. (*i*) J. Langer, I. Kosygin, R. Puchta, J. Pahl, S. Harder, *Chem. Eur. J.*, **2016**, *22*, 17425–17435.

[21] P. Pinter, C. M. Schüßlbauer, F. A. Watt, N. Dickmann, R. Herbst-Irmer, B. Morgenstern, A. Grünwald, T. Ullrich, M. Zimmer, S. Hohloch, D. M. Guldi, D. Munz, *Chem. Sci.*, **2021**, *12*, 7401–7410.

[22] V. C. Gibson, S. K. Spitzmesser, A. J. P. White, D. J. Williams, *Dalton Trans.*, **2003**, 2718–2727.

[23] a) S. Blair, K. Izod, W. Clegg, R. W. Harrington, *Eur. J. Inorg. Chem.* **2003**, 3319–3324; b) S. Blair, K. Izod, W. Clegg, *Inorg. Chem.* **2002**, *41*, 3886–3893; c) A. Pape, M. Lutz, G. Müller, *Angew. Chem.* **1994**, *106*, 2372–2375; *Angew. Chem., Int. Ed. Engl.* **1994**, *33*, 2281–2284; d) M. M. Meinholz, S. K. Pandey, S. M. Deuerlein, D. Stalke, *Dalton Trans.* **2011**, *40*, 1662–1671.

[24] a) j) P. Schüler, S. Sengupta, S. Zaubitzer, F. Fiesinger, S. Dongmo, H. Görls, M. Wohlfahrt-Mehrens, M.v.d. Borg, D. Gaissmaier, S. Krieck, M. Marinaro, T. Jacob, M. Westerhausen, *Eur. J. Inorg. Chem.* **2022**, e202200149 (1-6); b) J. Pan, L. Zhang, Y. He, Q. Yu, G. Tan, *Organometallics* **2021**, *40*, 3365−3369.

[25] S. Weber, D. Zobernig, B. Stöger, L. F. Veiros, K. Kirchner, *Angew. Chem.* **2021**, *133*, 24693–24697; *Angew. Chem. Int. Ed.* **2021**, *60*, 24488–24492.

[26] J. H. Docherty, J. Peng, A. P. Dominey, S. P. Thomas, *Nat. Chem.* **2017**, *9*, 595−600.

[27] Z.-C. Wang, M. Wang, J. Gao, S.-L. Shi, Y. Xu, *Org. Chem. Front*. **2019**, *6*, 2949−2953.

[28] A. D. Bage, T. A. Hunt, S. P. Thomas, *Org. Lett.* **2020**, *22*, 4107–4112.

[29] A. D. Bage, K. Nicholson, T. A. Hunt, T. Langer, S. P. Thomas, *ACS Catal*. **2020**, *10*, 13479–13486.

[30] N. W. J. Ang, C. S. Buettner, S. Docherty, A. Bismuto, J. R. Carney, J. H. Docherty, M. J. Cowley, S. P. Thomas, *Synthesis* **2018**, *50*, 803−808.

[31] M. K. Bisai, S. Yadav, T. Das, K. Vanka, S. S. Sen, *Chem. Commun.* **2019**, *55*, 11711–11714.

[32] W. N. Palmer, T. Diao, I. Pappas, P. J. Chirik, *ACS Catal.* **2015**, *5*, 622–626.

[33] J. Y. Yu. B. Moreau, T. Ritter, *J. Am. Chem. Soc.* **2009**, *131*, 12915–12917.

[34] a) D. Sarkar, S. Dutta, C. Weetman, E. Schubert, D. Koley, S. Inoue, *Chem. Eur. J.* **2021**, *27*, 13072–13078; b) S. Dutta, K. Singh, D. Koley, *Chem. Asian J.* **2021**, *16*, 3492–3508.

[35] a) K. Kitaura, K. Morokuma, *Int. J. Quantum Chem.* **1976**, *10*, 325–340. b) F. M. Bickelhaupt, K. N. Houk, *Angew. Chem.* **2017**, *129*, 10204–10221; *Angew. Chem., Int. Ed.* **2017**, *56*, 10070–10086.

[36] S. Dutta, S. De, S. Bose, E. Mahal, D. Koley, *Eur. J. Inorg. Chem.* **2020**, 638–655.

Chapter 4: Well-Defined Highly Luminescent Magnesium Complexes

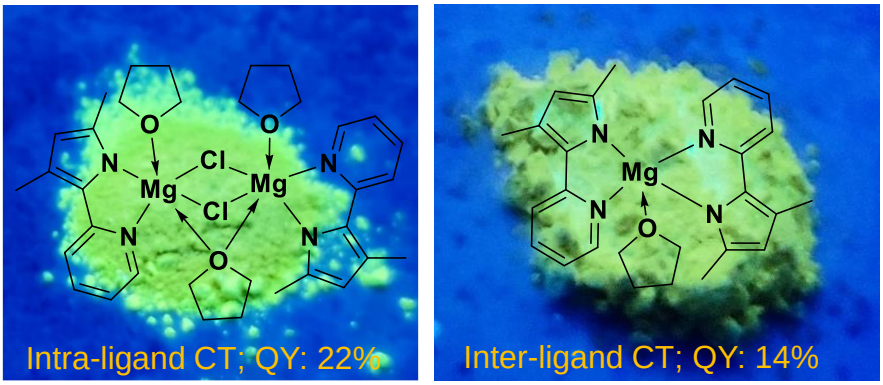

Abstract:

In this chapter, we report 2,2'-pyridylpyrrolide ligand (PyPyrH) supported two magnesium complexes (**4.1** & **4.2**). For **4.1**, the emission decay profile has two components with the lifetime values of 4.14 and 9.37 ns having relative contribution of 0.63 and 0.38, respectively. For **4.2**, the emission transient is composed of two components, 6.20 and 8.12 ns, having a relative contribution of 0.64 and 0.33, respectively. Both complexes show bright luminescence with a quantum yield of 22% and 14% in the solid state. Theoretical calculations reveal that the emissive properties are originated from the intra- and inter-ligand charge transfer.

4.1: Introduction

The molecular photosensitizers typically consist of electron-rich metals from the 2nd or 3rd row of the transition metal series, combined with electron-deficient ligands.[1-3] Such a combination allows metal-to-ligand charge transfer (MLCT), leading to long-lived emissive excited states. However, increased emphasis on sustainable and economic systems has shifted the focus to developing photosensitizers based on earth-abundant elements. Keeping the photo-induced charge separation by MLCT intact, a range of 1st row late transition metals have been explored to replace the precious metals.[4] In the same vein, luminescent magnesium complexes are desirable targets due to the high abundance of magnesium in the Earth's crust, and they are primarily non-toxic and inexpensive. However, due to the magnesium's electron- deficient nature, it can be conceived that they need an electron-rich ligand and rely on alternative mechanisms such as ligand to metal charge transfer (LMCT) or ligand to ligand or intra ligand charge transfer (LLCT/ILCT). While there are some reports on luminescent group 1 metal complexes,[5-7] analogous well-defined magnesium complexes have remained largely underexplored despite the first report that came in 2005 from the group of Chandrasekhar.[8] However, two recent landmark studies on luminescent magnesium species by the groups of Roesky[9] and Munz[7] could revolutionize the field. Roesky's team reported N-supported phosphine complexes of magnesium with a quantum yield of 27-34%.[9]

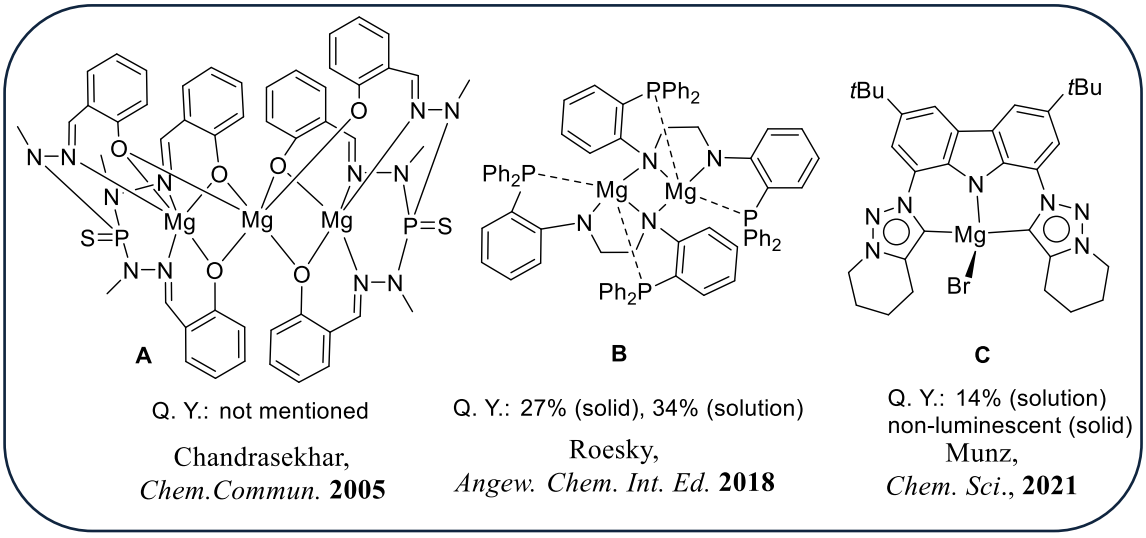

Scheme 4.1: Reported luminescent magnesium complexes.

Munz and coworkers showed that lithium and magnesium complexes based on carbazolide bridged mesoionic bis-carbene pincer ligand exhibit bright luminescence with quantum yields of up to 14%,[7] however the magnesium compound was not structurally authenticated, presumably due to solubility issues.

In order to search for an electron-rich ligand, we turned our attention toward 2,2'-pyridylpyrrolide (PyPyrH) moiety as a promising ligand system to support the photoluminescence through LMCT. Inspiration comes from the increased fluorescent properties shown by a good number of transition metal complexes such as Zn, Pd, Ir, Hf, and Zr based on this ligand display, [10-13] while the ligand itself is slightly fluorescent. The fluorescent properties in most cases emanate from the π-π* transition (HOMO–LUMO). It is striking that main-group compounds composed of the 2,2'-pyridylpyrrolide system have been less explored,[14] and we assume that it could be due to the lack of kinetic support provided by the ligand. Nonetheless, we have recently prepared a series of germanium and tin compounds using this system.[15,16] Here, we have prepared two magnesium complexes (**4.1** and **4.2**) based on the 2,2'-pyridylpyrrolide ligand. Interestingly, both **4.1** and **4.2** are luminescent, and their luminescent properties are originated from the inter/intra-ligand charge transfer. The quantum yields of **4.1** and **4.2** are 22% and 14% in the solid state, which are significantly more than that of **C**, but less than **B**.

4.2: Synthesis of magnesium complexes (4.1-4.2)

The synthetic procedure of the **PyPyrH** ligand involves the condensation of 2-aminomethylpyridine and 1,3-diketone.[17] Treatment of **PyrPyH** with *i*PrMgCl in THF gives a chloride bridged dimeric magnesium complex (**4.1**) (Scheme 4.1). The dimerization presumably takes place to satiate the electrophilicity of the magnesium centres; a phenomenon common in alkaline earth metal chemistry.[18] Here it is important to mention that the group of Kays performed the same reaction with MeMgI in the presence of TMEDA, which led to green coloured monomeric magnesium iodide complex due to chelation from TMEDA,[14] however, it has not been studied spectroscopically so far. **4.1** crystallizes in the *C*2/c space group of the monoclinic crystal system and the magnesium centres adopt a distorted octahedral geometry (Figure 4.1). The Mg–Cl bond lengths found for **4.1** are 2.48-2.50 Å, slightly longer than the nacnac-based magnesium chloride dimer,

i.e., 2.3926-2.4091 Å.[14] The Mg–N bond lengths are 2.063–2.075 Å, marginally shorter than the Mg–N bond lengths in *β*-diketiminato magnesium complexes.[15] Interestingly, there are three THF molecules in the asymmetric unit. Each magnesium center is coordinated by a THF molecule. The third THF molecule coordinates to both magnesium atoms and plays the role of a bridging ligand.

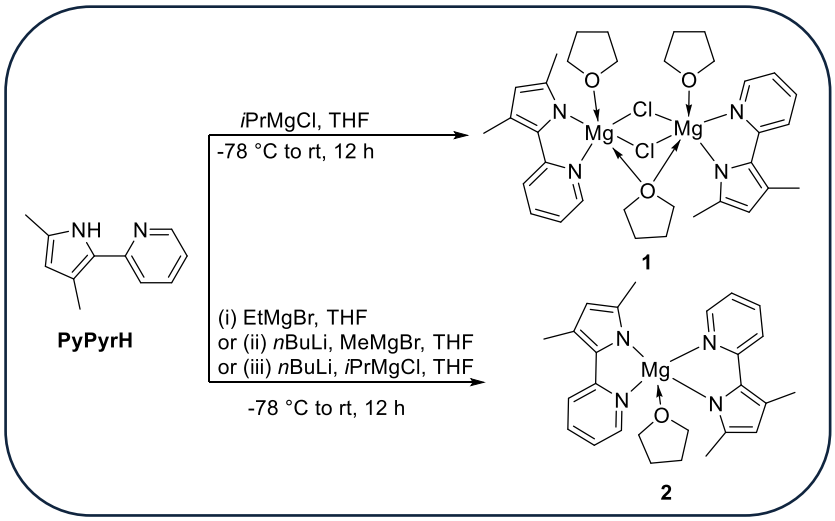

Scheme 4.2: Synthesis of magnesium complexes **4.1** and **4.2**.

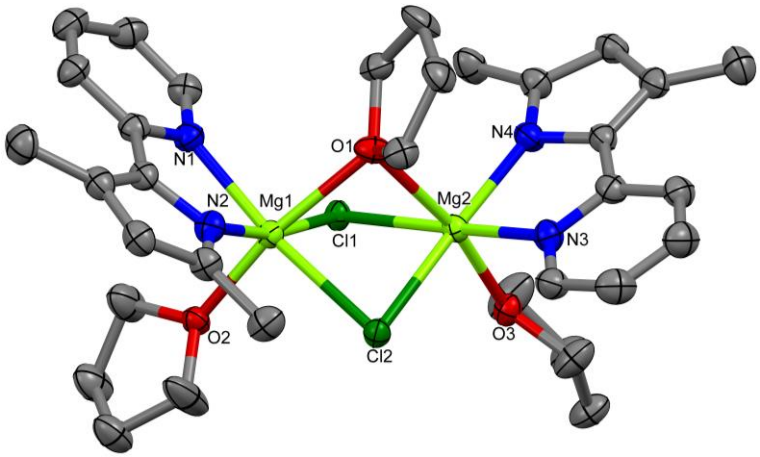

Figure 4.1. At the 50% probability level, the solid-state structure of **4.1** is shown with anisotropic displacement parameters. For simplicity, hydrogen atoms are not displayed. Selected bond lengths (Å) and bond angles (°): Cl1 Mg2 2.4874(17), Cl1 Mg1 2.4956(17), Cl2 Mg1 2.4881(17), Cl2 Mg2 2.4936(17), Mg1 N2 2.072(4), Mg1 O2 2.074(3), Mg1 N1 2.176(4), Mg1 O1 2.328(4), Mg2 N4 2.069(4), Mg2 O3 2.077(3), Mg2 N3 2.174(4), Mg2 O1 2.343(4); Mg2 Cl1 Mg1 80.09(5), Mg1 Cl2 Mg2 80.12(5), N2 Mg1 O2 93.52(15), N2 Mg1 N1 78.93(16), O2 Mg1 N1 94.34(14),

N2 Mg1 O1 95.73(15), O2 Mg1 O1 168.87(14), N1 Mg1 O1 93.51(15). CCDC number-2189747.

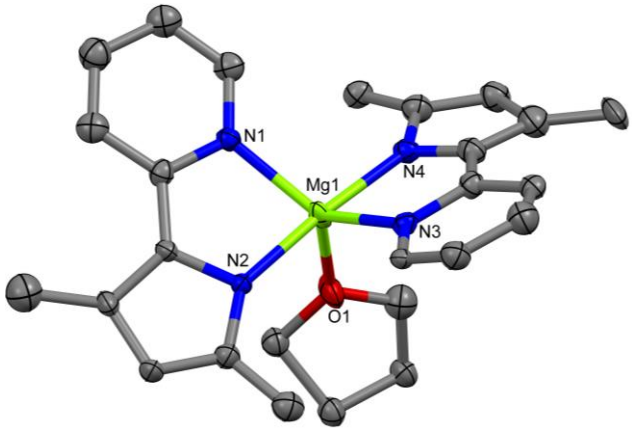

Figure 4.2. At the 50% probability level, the solid-state structure of **4.2** is shown with anisotropic displacement parameters. For simplicity, hydrogen atoms are not displayed. Selected bond distances (Å) and bond angles (deg): Selected bond lengths (Å) and bond angles (°): N1 Mg1 2.083(14), N2 C9 1.34(3), N2 C6 1.44(2), N2 Mg1 2.02(2), Mg1 N4 2.07(5), Mg1 O1 2.078(5), Mg1 N3 2.107(14); C1 N1 Mg1 128.6(13), C5 N1 Mg1 111.5(12), C9 N2 C6 103.3(16), C9 N2 Mg1 144.0(13), C6 N2 Mg1 110.8(13), N2 C6 Mg1 41.2(10). CCDC number-2189748

Replacement of *i*PrMgCl with less bulky EtMgX (X=Cl, Br) led to the formation of a homoleptic magnesium complex (**4.2**), where two PyPyr moieties stabilize the magnesium center along with one THF molecule (Scheme 4.2). **4.2** crystallizes in P_2/c space group of monoclinic crystal system and the magnesium center adopts a distorted trigonal bipyramidal geometry (Figure 4.2). The Mg–N bond lengths are 2.080–2.087 Å, which are longer than those in **4.1**. When the **PyPyrH** was deprotonated with *n*BuLi, and subsequently treated with MeMgBr and *i*PrMgCl, it only led to compound **4.2**.

4.3: Photophysical investigations

Solid-state absorption studies reveal that both **4.1** and **4.2** display a broad absorption band with a peak at 413 nm (Figure 3a, b). Due to the closed-shell electronic configuration of Mg^{2+}, the possibility of MLCT can be safely excluded for these complexes.[10,19] Hence, the broad absorption peaks are reasoned to be originated from the intra-ligand and/or inter-ligand π-π* and n-π* transitions. Similar interligand charge transfer was reported by Wagler and coworkers for hexa-coordinate silicon complexes.[20] Emission spectra of both the complexes show peaks at ~515 nm

(Figure 3a, b) with a significant difference in the full-width-half-maxima (FWHM) value. FWHM of the emission bands were found to be 112 nm and 71 nm for **4.1** and **4.2**, respectively.

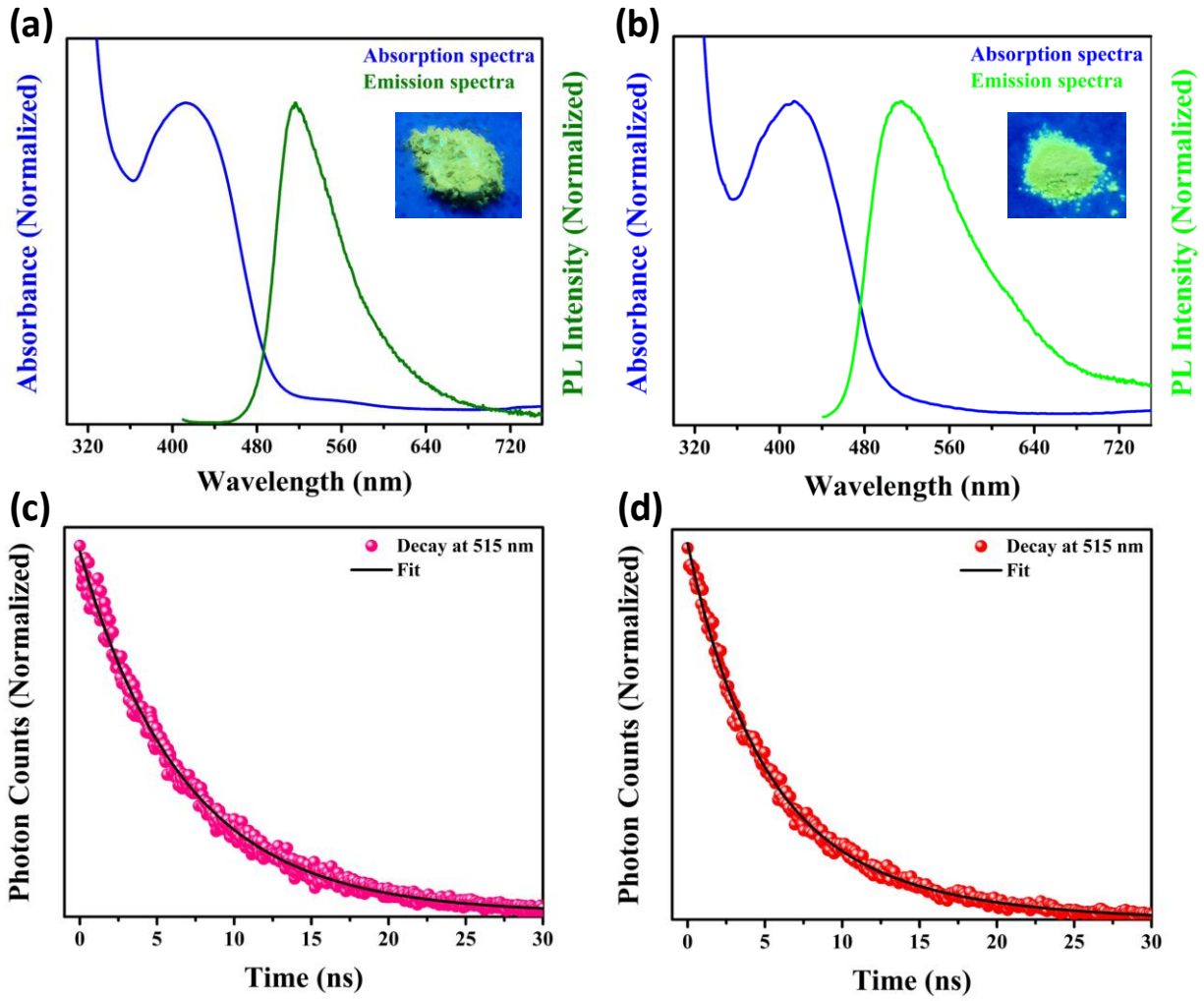

Figure 4.3: (a) Absorption spectra and emission spectra (excited at 400 nm) of **4.1** along with solid state compound photo under UV light, (b) Absorption spectra and emission spectra (excited at 400 nm) of **4.2** along with solid state compound photo under UV light (c) emission decay profile of **4.1**, (d) emission decay profile of **4.2**.

4.4: DFT calculations

In order to carry out molecular level investigation, TD-DFT calculations were performed at different level of theories (Table 4.1). The orbitals were generated from the TDDFT calculation at the M06-2X/def2-TZVPP//B3LYP-D3/def2-SVP level of theory, where the highest occupied

molecular orbital (HOMO) and the lowest unoccupied molecular orbital (LUMO) has been shown in Figure 4.4 with corresponding energy levels. For the ligand, the HOMO has a larger electron density at the pyrrole moiety, and the LUMO shares a larger electron density over the pyridine moiety (Figure 4.4a).

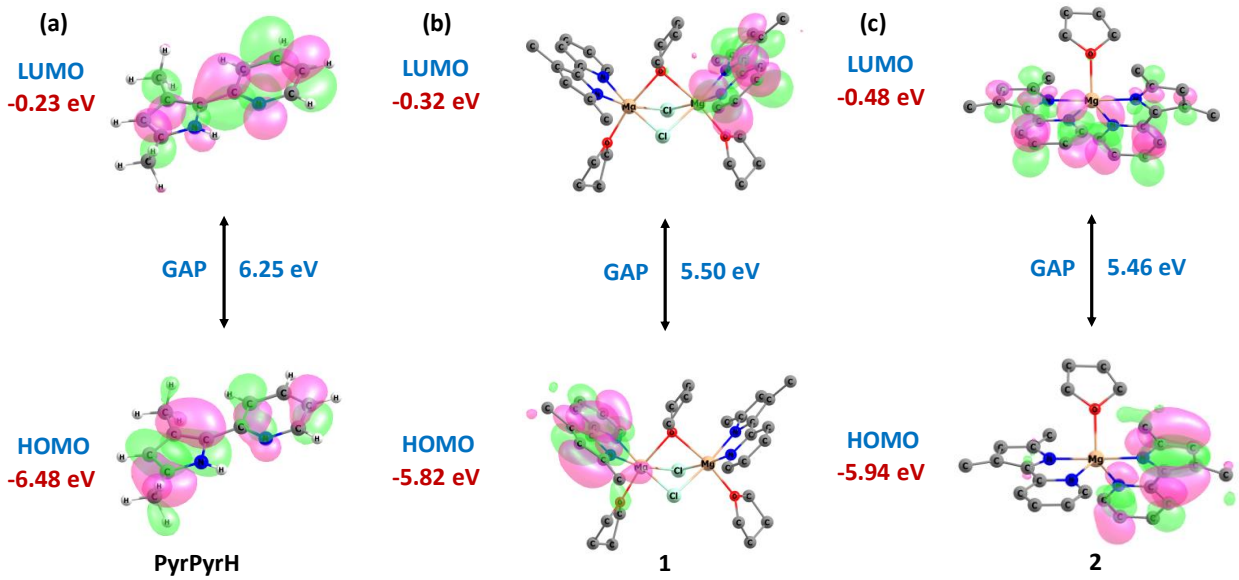

Figure 4.4: HOMO-LUMO diagram and associated energy values generated from the TDDFT calculation at the M06-2X/def2-TZVPP//B3LYP-D3/def2-SVP level of theory for; (a) **PyPyrH** ligand, (b) complex **4.1**, and (c) complex **4.2**.

Both the orbital has reasonable spatial overlap with each other. However, in the complexes, the HOMO-LUMO transition exhibits a significant charge flow from one coordinated ligand to another. Interestingly, complex **4.2** shares a larger HOMO-LUMO overlap (Figure 4.4c), and complex **4.1** has significant spatial separation between HOMO and LUMO (Figure 4.4b). To further elaborate on the nature of the excited state processes in the complexes, and to obtain the emission spectra, the first excited states (S_1) were optimized, and natural transition orbital (NTO) calculations were evaluated for S_1-S_0 transition in both complexes. It was observed that for **4.2**, during the emission (S_1 to S_0 transition) h-NTO shares a large electron density localized over one coordinated ligand, and in e-NTO the electron density is distributed over another ligand (Figure 4.5b). It indicates the formation of an emissive inter-ligand charge transfer excited state. This was also predicted from the excitation to the S_1 state involving the HOMO to LUMO transition (Table

4.1) for **4.2** (f^{osc} = 0.1040, $^{calcd}\lambda^{abs}$ = 361 nm, $^{exp}\lambda^{abs}$ = 413 nm). On the other hand, for complex **4.1**, the electron density distribution is entirely different in the first excited state (S_1). In this case, during the emission process (S_1 to S_0 transition) e-NTO has a larger electron density on the pyridine moiety of one ligand, and h-NTO has a higher electron density on the pyrrole moiety of the same ligand (Figure 4.5a).

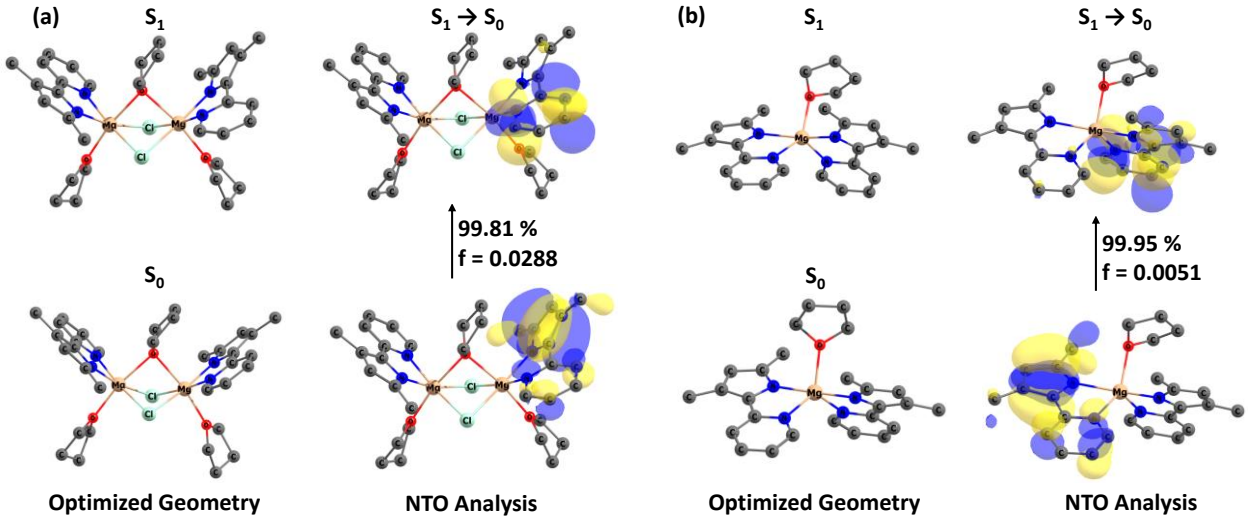

Figure 4.5: (a) Optimized geometry of **4.1** in the ground state and excited state along with NTO analysis for emission, (b) Optimized geometry of **4.2** in the ground state and excited state along with NTO analysis for emission.

As the electron density during the emission gets shifted within the same ligand, the S_1 to S_0 transition here is regarded as emission from an intra-ligand charge transfer excited state. Similar behavior was also predicted from the excitation to the S_1 state involving the HOMO-1 to LUMO transition (Figure 4.6, Table 4.1) for **4.1** (f^{osc} = 0.0115, $^{calcd}\lambda^{abs}$ = 355 nm, $^{exp}\lambda^{abs}$ = 413 nm).

The different charge-transfer excited states for **4.1** and **4.2** can also be characterized from the emission bandwidth. Band broadening in solid state emission significantly depends upon the reorganization energy, charge transfer character of the complexes and the electron-phonon scattering.[21,22] Bandwidth of individual vibrational coarse structure in the emission spectra increases with increasing charge transfer character of the complex, leading towards a structureless broad emission.[23] To explain the difference between emission bandwidths of two complexes

excited state energies need to be investigated. Hence, the reorganization energies (λ^{RE}) were calculated at the M06-2X/def2-TZVPP//B3LYP-D3/def2-SVP level of theory (Table 4.1). It was observed that **4.1** has a higher reorganization energy (20.8 kcal/mol) compared to that of **4.2** (15.5 kcal/mol), which explains why the emission spectrum of **4.1** has a larger bandwidth than that of **4.2**.[24-26]

Table 4.1: Absorption spectra (λ^{abs}) obtained from TD-DFT calculation at the triple-ζ (def2-TZVPP) level of theory with different functionals (wavelength in nm, f=oscillator strength and the orbitals involved in the transition).

λ^{abs}	Exp	B3LYP	BP86	cam-B3LYP	M06-2X	ωB97XD	PBE0	B97D3
4.1	413 nm	402.14 nm f=0.0088 HOMO-1 to LUMO	540.29 nm f=0.0003 HOMO to LUMO+1	354.48 nm f=0.0120 HOMO-1 to LUMO	355.33 nm f=0.0115 HOMO-1 to LUMO	350.42 nm f=0.0121 HOMO-1 to LUMO	388.01 nm f=0.0092 HOMO-1 to LUMO	536.89 nm f=0.0003 HOMO to LUMO+1
4.2	413 nm	415.60 nm f=0.0255 HOMO to LUMO	537.23 nm f=0.0019 HOMO to LUMO	358.60 nm f=0.1053 HOMO to LUMO	360.76 nm f=0.1040 HOMO to LUMO	353.69 nm f=0.1133 HOMO to LUMO	396.05 nm f=0.0436 HOMO to LUMO	534.21 nm f=0.0018 HOMO to LUMO

The calculated emission from the S_1 state for **4.1** (f^{osc} = 0.0288, $^{calcd}\lambda^{em}$ = 479 nm, $^{exp}\lambda^{em}$ = 515 nm) and for **4.2** (f^{osc} = 0.0051, $^{calcd}\lambda^{em}$ = 447 nm, $^{exp}\lambda^{em}$ = 515 nm) was also found to be in good agreement with the experimental observation (Table 4.2). This also gives insights to the higher quantum yield of **4.1 (**22%) than **4.2** (14%) (Figure 4.6), which can be attributed to approx. 5.6 times higher oscillator strength (f) of **4.1** than that of **4.2** (Figure 5a, b). In TDDFT calculations, the higher oscillator strength of S_1 to S_0 transition in **4.1** can be explained in terms of electron density of e-NTO and h-NTO.

Table 4.2: Fluorescence spectra (λ^{em}) obtained from TD-DFT calculation at the triple-ζ (def2-TZVPP) level of theory with different functionals (wavelength in nm, f=oscillator strength).

λ^{em}	Exp	B3LYP	cam-B3LYP	M06-2X	ωB97XD	PBE0
4.1	515 nm	656.23 nm f=0.0146	474.65 nm f=0.0321	479.50 nm f=0.0288	457.61 nm f=0.0348	611.82 nm f=0.0166
4.2	515 nm	744.81 nm f=0.0003	427.32 nm f=0.0069	447.36 nm f=0.0051	388.80 nm f=0.0352	666.70 nm f=0.0004

4.5: Quantum yield measurement

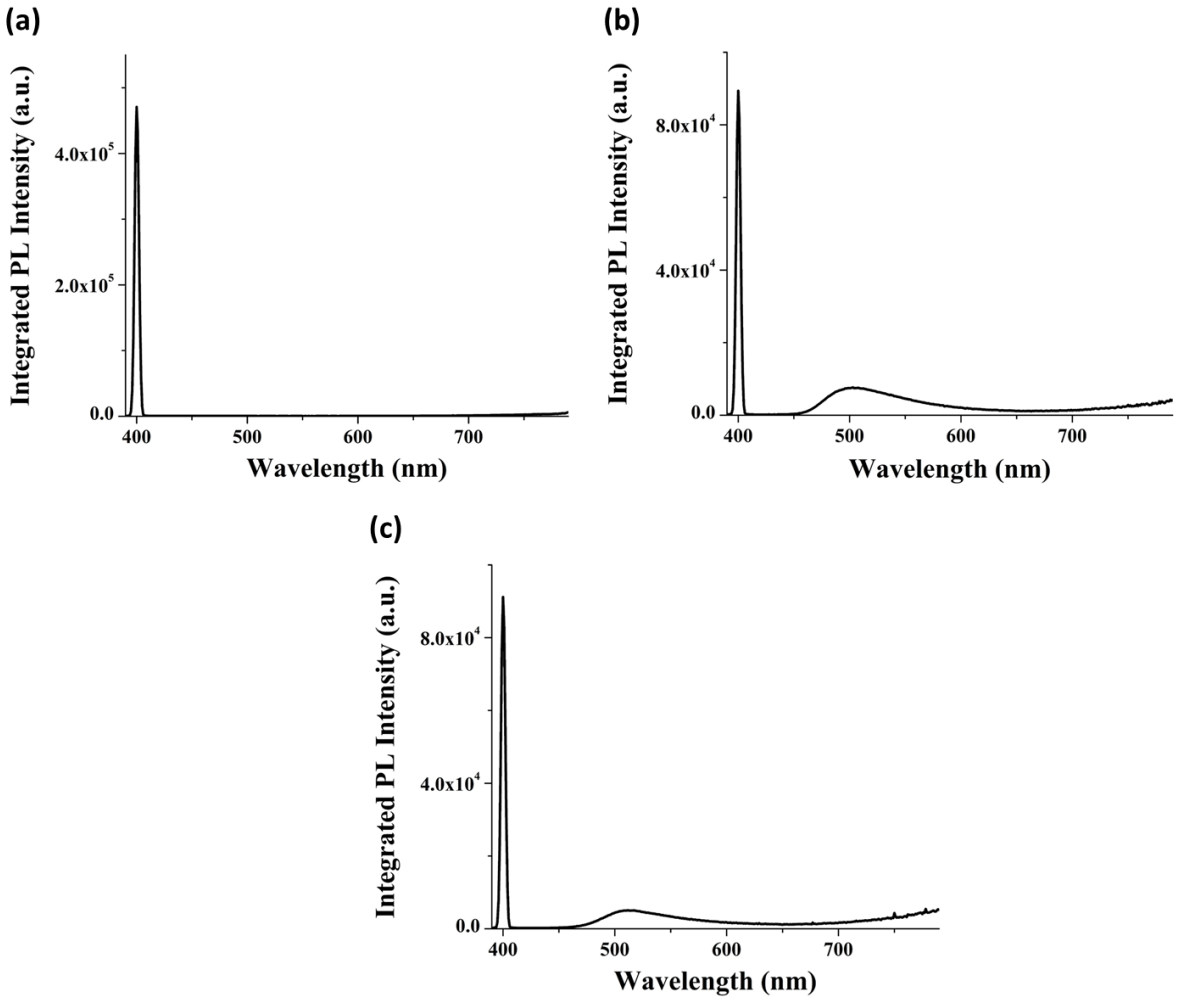

Figure 4.6: (a) Integrated scattering for the reference, (b) Integrated scattering and emission spectra of compound **4.1**, (c) Integrated scattering and emission spectra of compound **4.2**.

Calculated absolute quantum yield for compound **4.1** ~ 22.73%

Relative error = ± 0.00157

Absolute error = ± 0.036.

Calculated absolute quantum yield for compound **4.2** ~ 14.47%

Relative error = ± 0.00235

Absolute error = ± 0.034.

4.6: Life-time measurement

In this case, the extent of spatial overlap between e-NTO and h-NTO is greater due to its intra-ligand charge transfer character (Figure 4.5a). On the other hand, due to the inter-ligand charge transfer process being predominant in **4.2**, the spatial overlap between e-NTO and h-NTO becomes minimal (Figure 4.5b). Therefore, S_1 to S_0 transition probability is higher in **4.1**, and so is the oscillator strength and the quantum yield. Moreover, Intra-ligand charge transfer in **4.1** may increase the vibronic coupling among the excited states,[27] thereby enhancing the internal conversion (IC). However, excited state lifetimes for both complexes were found to be similar. For **4.1**, the emission decay profile has two components with the lifetime values of 4.14 and 9.37 ns having relative contribution of 0.63 and 0.38, respectively (Figure 4.3c, Table 4.2), while for **4.2**, the emission transient is composed of two components, 6.20 and 8.12 ns, having a relative contribution of 0.64 and 0.33, respectively (Figure 4.3d, Table 4.3). As the lifetime of the complexes lies within a few nanosecond ranges, the possibility of delayed emission or phosphorescence is eliminated and the phenomenon is associated predominantly with fluorescence emission.

Table 4.3: Lifetime fitting parameters of compounds **4.1** and **4.2** obtained from TCSPC.

Sample	α_1	τ_1 (ns)	α_2	τ_2 (ns)	$\langle\tau\rangle$ (ns)
4.1	0.63	4.14	0.38	9.37	7.16
4.2	0.64	6.20	0.33	8.12	6.98

As we have observed an intra-ligand charge transfer in **4.1** having a minimal role of Mg^{2+}, it is also important to carry out a comparative study of the ligand. The ligand shows broad emission features with a peak at ~420 nm (Figure 4.7). It is pertinent to mention that despite a ligand restricted charge transfer in both **4.1** and **4.2**, their emissive behaviours are entirely different. TDDFT studies were performed to address this intriguing observation.

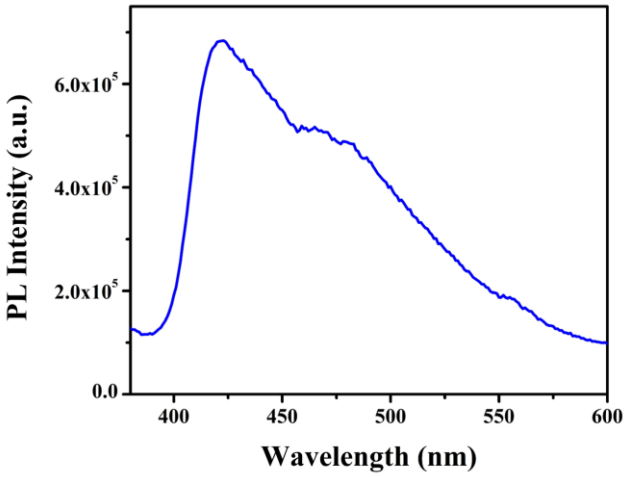

Figure 4.7: Solid state emission spectra of PyPyrH ligand (Excited at 340 nm).

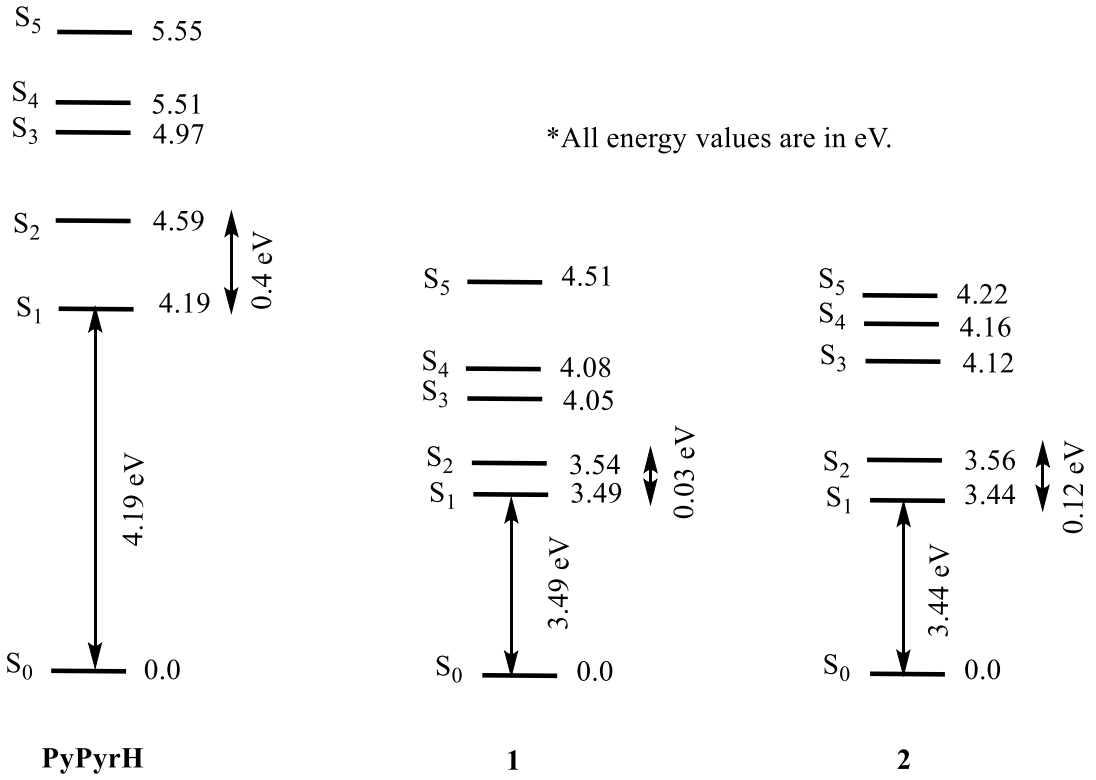

Figure 4.8: Franck-Condon (FC) energy levels associated with the excited states as obtained from the single point TD-DFT calculations at the theory level M06-2X/def2-TZVPP using the optimized ground state (S_0) obtained at B3LYP-D3/def2-SVP level of theory.

We observed that in the case of ligand, the frontier orbital transition contributing to the S_1 state is HOMO to LUMO with excitation energy of 4.19 eV (S_0 to S_1). On the other hand, in **4.1**, the S_1 is mainly comprised of HOMO to LUMO+1 (46.65%) and HOMO-1 to LUMO (51.52%) transitions with an excitation energy of 3.49 eV (S_0 to S_1). This illustrates that the electronic structure of the emissive state in PyPyrH has been modulated upon complex formation. Franck-Condon (FC) energy for **4.1** was decreased by 4.19-3.49=0.6 eV (Figure 4.8). The decrease in the FC energy also accounts for the large emission band shift of **4.1** compared to the free ligand.

4.7: Conclusions

In conclusion, we have employed the PyPyrH ligand, usually not considered as an appropriate ligand for alkaline earth metals, to obtain two well-defined pyridylpyrrole magnesium complexes (**4.1** and **4.2**). Both complexes exhibit fluorescence with emission lifetimes in a nanosecond range and luminescence quantum yields of 22% and 14% in the solid-state. Detailed theoretical studies rationalize that the luminescent properties arise due to inter- and intra-ligand charge transfer.

4.8: References

[1] A. Juris, V. Balzani, F. Barigelletti, S. Campagna, P. Belser, A. von Zelewsky, *Coord. Chem. Rev.*, **1988**, *84*, 85–277.

[2] V. Balzani, A. Juris, *Coord. Chem. Rev.*, **2001**, *211*, 97–115.

[3] I. M. Dixon, J.-P. Collin, J.-P. Sauvage, L. Flamigni, S. Encinas, F. Barigelletti, *Chem. Soc. Rev.*, **2000**, *29*, 385–391.

[4] C. Wegeberg, O. S. Wenger, *JACS Au*, **2021**, *1*, 1860−1876

[5] O. Back, C. Förster, T. Basché, K. Heinze, *Chem.–Eur. J.*, **2019**, *25*, 6542.

[6] T. J. Feuerstein, B. Goswami, P. Rauthe, R. Köppe, S. Lebedkin, M. M. Kappes, P. W. Roesky, *Chem. Sci.*, **2019**, *10*, 4742.

[7] P. Pinter, C. M. Schüßlbauer, F. A. Watt, N. Dickmann, R. Herbst-Irmer, B. Morgenstern, A. Grünwald, T. Ullrich, M. Zimmer, S. Hohloch, D. M. Guldi, D. Munz, *Chem. Sci*., **2021**, *12*, 7401–7410.

[8] V. Chandrasekhar, R. Azhakar, J. F. Bickley, A. Steiner, *Chem. Commun*., **2005**, 459–461.

[9] S. Bestgen, C. Schoo, B. L. Neumeier, T. J. Feuerstein, C. Zovko, R. Köppe, C. Feldmann, P. W. Roesky, *Angew. Chem., Int. Ed.*, **2018**, *57*, 14265–14269.

[10] J. J. Klappa, S. A. Geers, S. J. Schmidtke, L. A. MacManus-Spencer, K. McNeill, *Dalton Trans*., **2004**, 883–891.

[11] A. Ionescu, N. Godbert, R. Termine, M. La Deda, M. Amati, F. Lelj, A. Crispini, A. Golemme, M. Ghedini, P. Garcia-Orduña, I. Aiello, *Inorg. Chem*., **2021**, *60*, 9287–9301.

[12] Y. Zhang, N. G. Akhmedov, J. L. Petersen, C. Milsmann, *Chem. Eur. J*., **2019**, *25*, 3042–3052.

[13] P. M. N. Đỗ, N. G. Akhmedov, J. L. Petersen, B. S. Dolinar, C. Milsmann, *Chem. Commun*., **2020**, *56*, 5397–5400.

[14] A. C. A. Ried, L. J. Taylor, A. M. Geer, H. E. L. Williams, W. Lewis, A. J. Blake, D. L. Kays, *Chem. Eur. J.*, **2019**, *25*, 6840–6846.

[15] S. Pahar, V. S. V. S. N. Swamy, T. Das, R. G. Gonnade, K. Vanka, S. S. Sen, *Chem. Commun.*, **2020**, *56*, 11871–11874.

[16] S. Pahar, V. Sharma, S. Tothadi, S. S. Sen, *Dalton Trans*., **2021**, *50*, 16678–16684.

[17] J. J. Klappa, A. E. Rich, K. McNeill, *Org. Lett.*, **2002**, ***4***, 435–437.

[18] S. P Sarish, S. Nembenna, S. Nagendran, H. W. Roesky, *Acc. Chem. Res.*, **2011**, *44*, 157–170.

[19] Y. Hai, J.-J. Chen, P. Zhao, H. Lv, Y. Yu, P. Xu, J.-L. Zhang, *Chem. Commun*., **2011**, *47*, 2435–2437.

[20] J. Wagler, D. Gerlach, U. Böhme, G. Roewer, *Organometallics,* **2006,** *25*, 2929-2933.

[21] J.-W. Huang, Y.-C. Hsu, X. Wu, S. Wang, X.-Q. Gan, W.-Q. Zheng, H. Zhang, Y.-Z. Gong, W.-Y. Hung, P.-T. Chou, W. Zhu, *J. Mater. Chem. C*, **2022**, *10*, 7866–7874.

[22] X.-K. Chen, V. Coropceanu, J.-L. Bredas, *Nature Communications*, **2018**, *9*, 5295 (1–10).

[23] X. Wen, P. Yu, Y.-R. Toh, X. Ma, S. Huang, J. Tang, *Nanoscale*, **2013**, *5*, 10251–10257.

[24] F. Liu, Z. Cheng, L. Wan, Z. Feng, H. Liu, H. Jin, L. Gao, P. Lu, W. Yang, *Small*, **2022**, *18*, 2106462(1-9).

[25] X.-F. Song, Z.-W. Li, W.-K. Chen, Y.-J. Gao, G. Cui, *Inorg. Chem.*, **2022**, *61*, 7673−7681.

[26] Z. Pei, Q. Ou, Y. Mao, J. Yang, A. d. l. Lande, F. Plasser, W. Liang, Z. Shuai, Y. Shao, *J. Phys. Chem. Lett.*, **2021**, *12*, 2712−2720.

[27] W.-C. Chen, P.-T. Chou, Y.-C. Cheng, *J. Phys. Chem. C*, **2019**, *123*, 10225−10236.

Chapter 5: A Well-Defined Calcium Compound Catalyzes Trimerization of Arylisocyanates into 1,3,5-Triarylisocyanurates

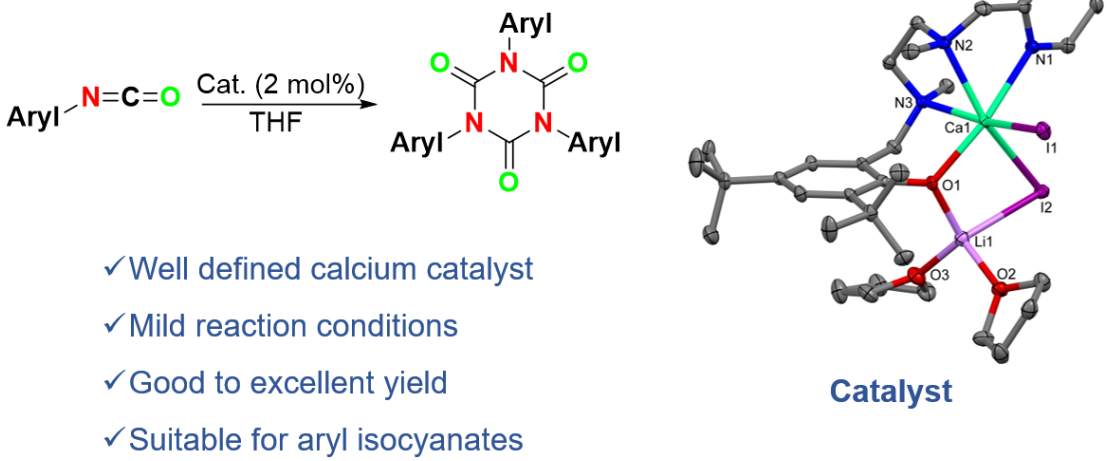

Abstract:

Ligand systems play a crucial role in stabilizing main group metal complexes, mainly alkaline earth metal complexes, as alkaline earth metals follow the Schlenk equilibrium issue. Hence, we have synthesized a tetradentate ligand to stabilize these complexes to avoid the Schlenk equilibrium. Here, we report the synthesis of homoleptic potassium (**5.1**) and heteroleptic calcium complex (**5.2**) bearing a tetradentate monoanionic ligand with a diaminoethane core and phenolate and pyridine peripheral donors. Single crystal X-ray studies on **5.2** revealed that LiI was also co-crystallized, leading to a four-membered ring with four different elements. **5.2** was found to be an efficient catalyst for the cyclotrimerization of various aromatic isocyanates under mild conditions.

5.1: Introduction

There has been a trend in chemistry for some time to use compounds with main-group elements in the place of transition metals (Ru, Os, Rh, Ir, Pd, and Pt) for molecular catalysis.[1,2] The primary factor driving this trend to switch from transition metals is their expense and low-terrestrial abundance. Besides, there is growing apprehension about the health and environmental impact of the residual metal that is retained in the products. Among main-group elements, calcium complexes have attracted considerable attention due to their high terrestrial abundance (3.4 wt %; calcium is the fifth most abundant element) and biocompatibility of calcium. Organocalcium compounds have been shown to catalyze important organic transformations such as hydroamination, hydrophosphination, hydrosilylation, hydroboration, hydrogenation, the cyanosilylation of unsaturated organic compounds, as well as polymerization.[3-6]

Cyclotrimerization of isocyanate derivatives is an essential and atom-economical transformation to access isocyanurates, which have industrial and commercial applications, as they have excellent thermal stability and flame resistance properties. As a result, adding isocyanurate frameworks to polymer networks may improve the physical qualities of polyurethanes, copolymer resins, plastics, and coating materials by enhancing their heat and chemicals resistance, transparency, water and impact resistance.[7,8] Besides, isocyanurates are essential units for the synthesis of a microporous (poly)isocyanurate, which has been applied as support in heterogeneous catalysis.[9] Examples of catalysts that have been used for this important transformation include transition metals,[10-14] rare earth metals,[15-18] and Lewis bases like N-heterocyclic carbenes,[19] phosphines,[20] and N-heterocyclic olefins.[21] However, less attention has been paid to employing main-group elements, though there are some recent reports on the cyclotrimerization of isocyanates by K, Al, Ge, and Sn compounds [22-24] (Scheme 5.1). Despite such progress, these approaches have significant limitations, including high temperatures, prolonged reaction time, by-product formation, and subsequent difficulties in separation. In 2007, Orzechowski and Harder reported the catalytic trimerization of PhNCO by a calcium carbene complex with iminophosphorane ligands.[25] However, no further substrate scope was studied. Herein, we report the synthesis of an {ONNN}-type tetradentate ligand-based new heteroleptic calcium iodide (**5.2**), which is found to be quite an efficient catalyst for the trimerization reaction.

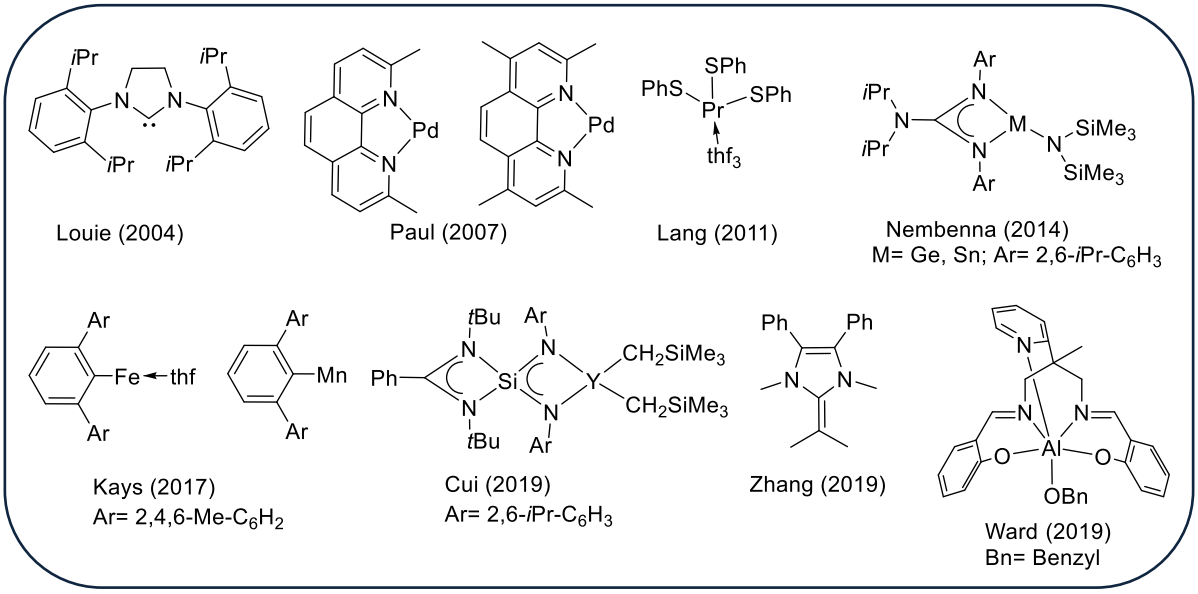

Scheme 5.1: Previously reported catalysts for cyclotrimerization of isocyanates.

5.2: Synthesis of ligand (L5.1), potassium (5.1) and calcium (5.2) complexes

In the previous chapters, I have used bidentate and tridentate ligand systems, and both were able to stabilize heteroleptic magnesium complexes. But none of them has worked for calcium due to different reactivity and large size of calcium compared to magnesium. Hence, we have decided to increase the coordination number around the calcium center and synthesized a tetradentate ligand. The tetradentate ligand (**L5.1**) was prepared according to the literature procedure.[26]

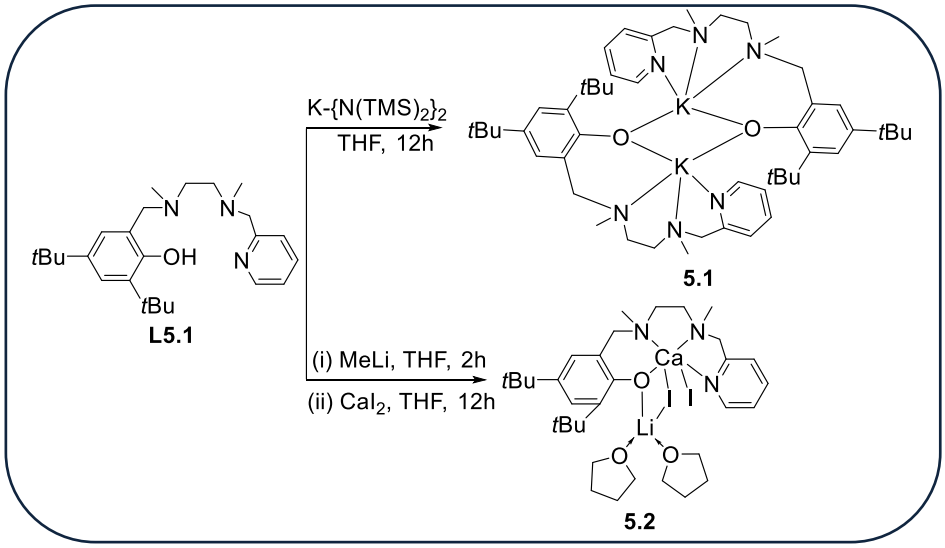

Scheme 5.2: Synthesis of complexes **5.1**-**5.2** using ligand **L5.1**.

The ligand consists of a diaminoethane group as core, and pyridine and di-*tert*-butyl-phenolate as peripheral moieties. We reasoned that such a ligand might be appropriate for the calcium atom, because it provides a high coordination number around the metal center, and thereby could hinder the formation of a homoleptic compound.[27,28] The reaction between **L5.1** and $KN(TMS)_2$ in THF led to a dimeric potassium complex (**5.1**) (Scheme 5.2). Lithiation of the ligand by MeLi, with the subsequent addition of CaI_2, afforded a hexacoordinate calcium complex (**5.2**) (Scheme 5.2).

Both **5.1** and **5.2** were characterized by NMR spectroscopy and single-crystal X-ray analysis. Compound **5.1** features a dimeric centrosymmetric structure, where the two halves of the dimer are linked through a four-membered K_2O_2 ring (Figure 5.1). The potassium atoms are penta-coordinated with a distorted trigonal pyramidal geometry. The K–O and K–N bond lengths are 2.55-2.59 Å and 2.85-2.86 Å, respectively, which are shorter than the sum of their covalent radii. Compound **5.2** contains a hexacoordinated calcium center and adopts a distorted octahedral geometry. Interestingly, lithium iodide is also co-crystallized along with calcium iodide (Figure 5.2), resulting in an unprecedented Ca-O-Li-I four-membered ring with four different atoms. The terminal Ca–I bond distance in **5.2** is 3.078(5) Å, that is marginally shorter than the previously described terminal Ca–I bond (3.084(3) – 3.166 Å).[29-31]

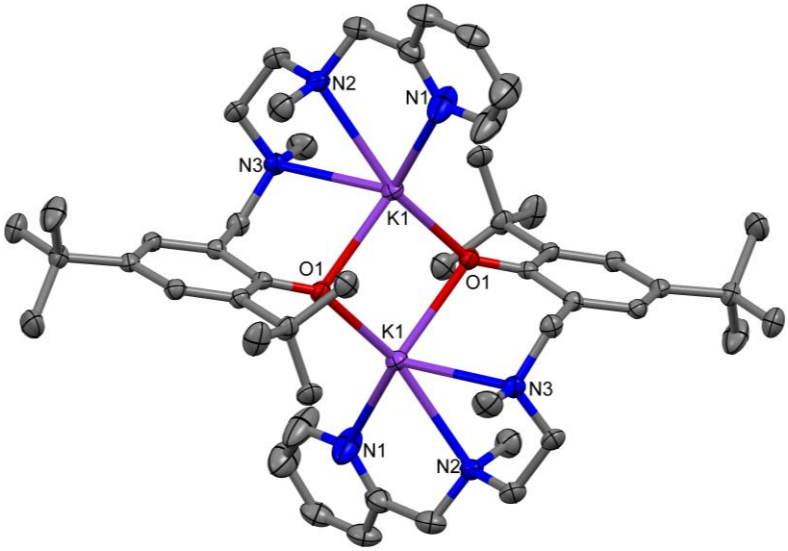

Figure 5.1: The solid-state structures of **5.1** with parameters of anisotropic displacement shown at the 50% level of probability. Hydrogen atoms are left out for simplicity. Selected distances (Å)

and angles (deg): K1–O1, 2.5589(17); K1–O1, 2.5997(15); K1–N1, 2.851(2); K1–N3 2.8605(18); K1–N2, 2.8792(18); K1–C1, 3.367(2); K1–C16, 3.423(2); K1–C19, 3.496(3); K1–K1 3.7291 and O1–K1–O1, 87.41(5); O1–K1–N1, 120.38(6); O1–K1–N1, 130.48(7); O1–K1–N3, 111.33(5); O1–K1–N3, 73.31(5), N1–K1–N3, 121.89(6); O1–K1–N2, 159.84(4). CCDC number- 2111877.

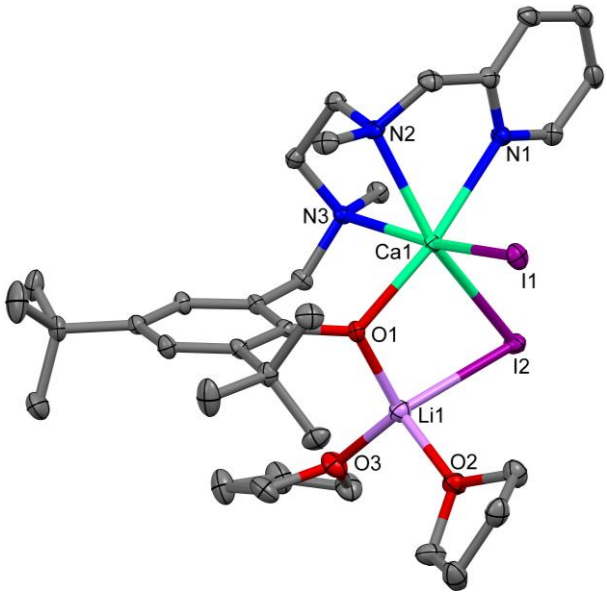

Figure 5.2: The solid-state structures of **5.2** with parameters of anisotropic displacement shown at the 50% level of probability. Hydrogen atoms are left out for simplicity. Selected distances (Å) and angles (deg): Ca1–O1, 2.2529(17); Ca1–N2, 2.507(2); Ca1–N1 2.522(2); Ca1–N3, 2.527(2); Ca1–I1, 3.0780(5); Ca1–I2, 3.0814(5); Ca1–Li1, 3.298(5); I2–Li1, 2.877(5); Li1–O1, 1.921(5); Li1–O2, 1.937(5); Li1–O3, 1.952(5) and C15–N3–Ca1, 108.35(14); C1–O1–Li1, 115.5(2); C1–O1–Ca1, 126.58(15); Li1–O1–Ca1, 104.09(16); C30–O2–C33 106.8(2); C30–O2–Li1, 124.7(2); C33–O2–Li1, 126.5(2). CCDC number- 2111874.

5.3: Calcium complex (5.2) as a catalyst for cyclotrimerization of isocyanates

Furthermore, compound **5.2** was screened as a potential catalyst for the cyclotrimerization of isocyanates (Scheme 5.3). No reaction was observed in the absence of the catalyst. The reaction was performed in THF with 2 mol % of catalyst loading. Compound **5.2** was found to be effective for aryl isocyanates, but in the case of alkyl isocyanates, no cyclotrimerization was observed due to the absence of C=N bond activation by the conjugation of the aryl ring like in aryl isocyanates. The mass spectra and NMR results show that the mixture of the crude product is entirely pure (only trimer is observed), and single-crystal X-ray diffraction was a characteristic of the bulk

product in the cases of 4-methoxyphenyl isocyanate (**5.3a**), 4-bromophenyl isocyanate (**5.3b**), 4-cyano phenyl isocyanate (**5.36i**), and 4-fluorophenyl isocyanate (**5.36k**).

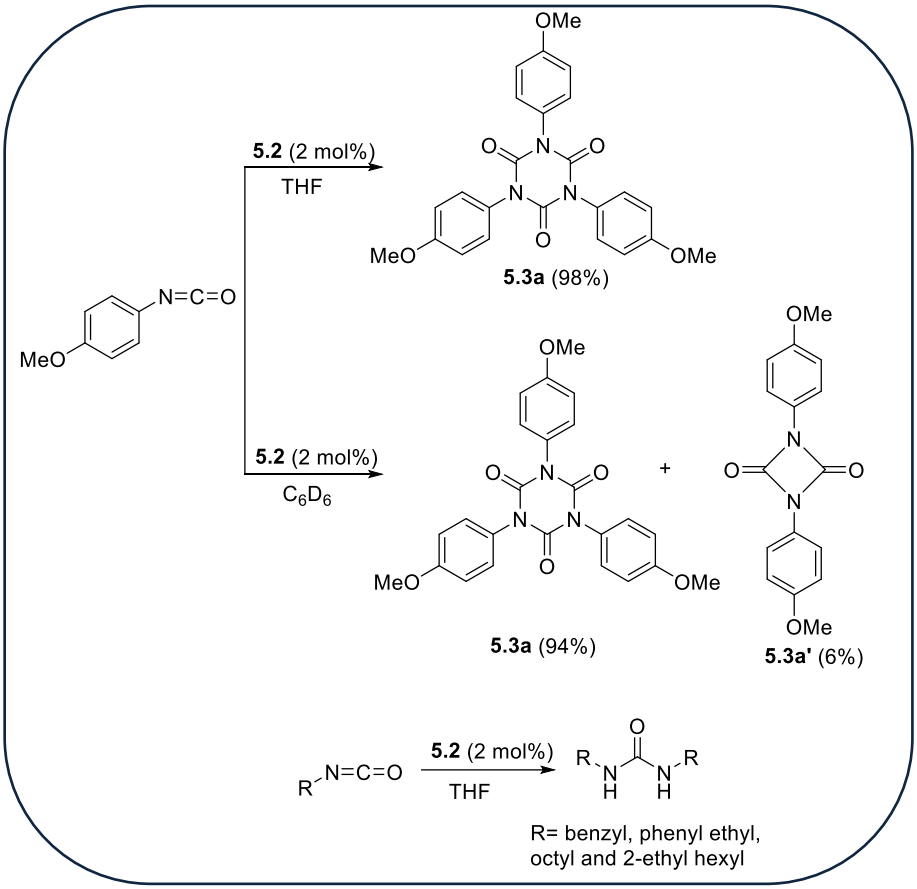

Scheme 5.3: Cyclotrimerization of aryl isocyanate catalysed by compound **5.2** (above); Formation of 1,3-disubstituted urea when alkyl isocyanates were used (below).

Interestingly, when the oligomerization reaction of 4-methoxy phenyl isocyanate was performed in benzene-d_6, the trimerized product (**5.3a**) was obtained almost quantitatively along with the formation of the dimerized product (**5.3a'**) in a very minor amount (Scheme 5.3). Therefore, our catalyst does not suffer from issues of selectivity.[32] Fortuitously, we were able to characterize both these products by single-crystal X-ray diffraction studies (Figure 5.3). There were several studies on the effects of the solvent on the cyclization of phenyl isocyanates,[33] and it has been generally accepted that the trimerization is favored when polar solvents are employed. In the case of alkyl isocyanates, no trimerization product was detected. Because of the lack of conjugation, the C=N bond is probably not activated in alkyl isocyanates. We have probed the reaction with benzyl, phenyl ethyl, octyl and 2-ethyl hexyl isocyanate and observed the formation

of the corresponding 1,3-disubstituted urea, which was confirmed by the HMRS and ^{1}H NMR spectroscopy (Scheme 5.3) and compared to the previously reported samples by Lang and co-workers.[34] It must be stated here that we have also performed the reaction in the neat condition, but found the reaction to be incomplete, presumably due to the heterogeneous nature of the reaction medium.

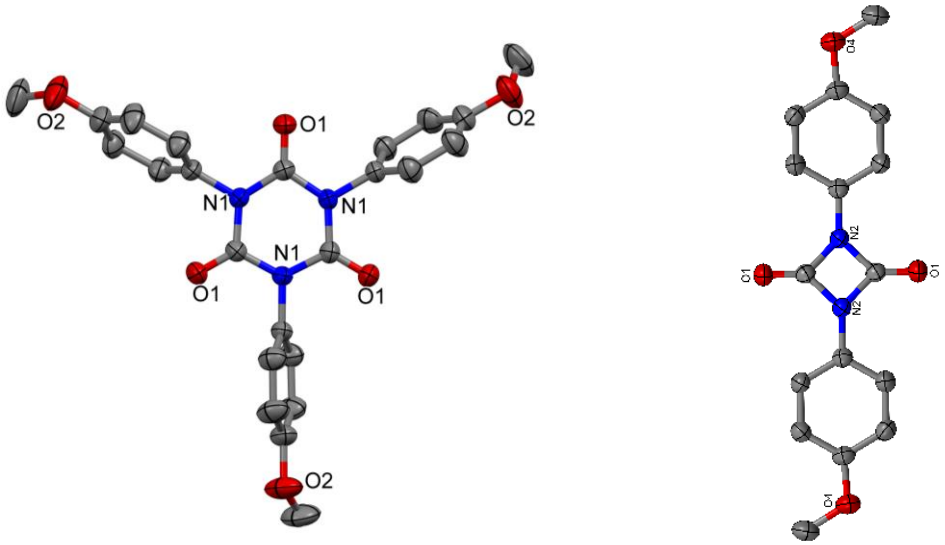

Figure 5.3: The molecular structure of **6a** (left) and **6a´** (right) with parameters of anisotropic displacement shown at the 50% level of probability. [24]

Subsequently, the oligomerization of a wide range of isocyanates was studied. As the reaction was carried out in THF, no dimer formation was observed. Good to excellent yields were observed for isocyanates either having an electron-donating group such as Me (Scheme 5.4, **5.3d** and **5.3g**) or OMe (**5.3a**) or having an electron-withdrawing group such as bromide and chloride (Scheme 5.4, **5.3b**, **5.3e** and **5.3j**). The reaction is a bit sluggish with 2,6-diisopropyl phenyl isocyanate (**5.3c**), and 12 h reaction time is required for productive conversion. The sluggishness can be attributed to the steric hindrance imparted by the isopropyl groups, as the replacement by *i*Pr groups with Me groups or Cl groups results in rapid conversion (**5.3d** and **5.3e**). 4-fluorophenyl isocyanate (Scheme 5.4, **5.3k**) also took 12h to lead to a fruitful conversion, while the reactions were smoother for 4-bromophenyl isocyanate (**5.3b**) and 4-chlorophenyl isocyanate (**5.3j**). This

could be due to the electron-withdrawing nature of the fluorine atom, though the reaction is faster for the nitrile substituent (**5.3i**). The 1-naphthyl isocyanate and the substituted groups at the *ortho* or *meta* position of the aromatic rings were well tolerated, and the respective isocyanurates were separated in excellent yields (**5.3f**-**5.3h**), reflecting that there are no apparent electronic effects in this reaction.

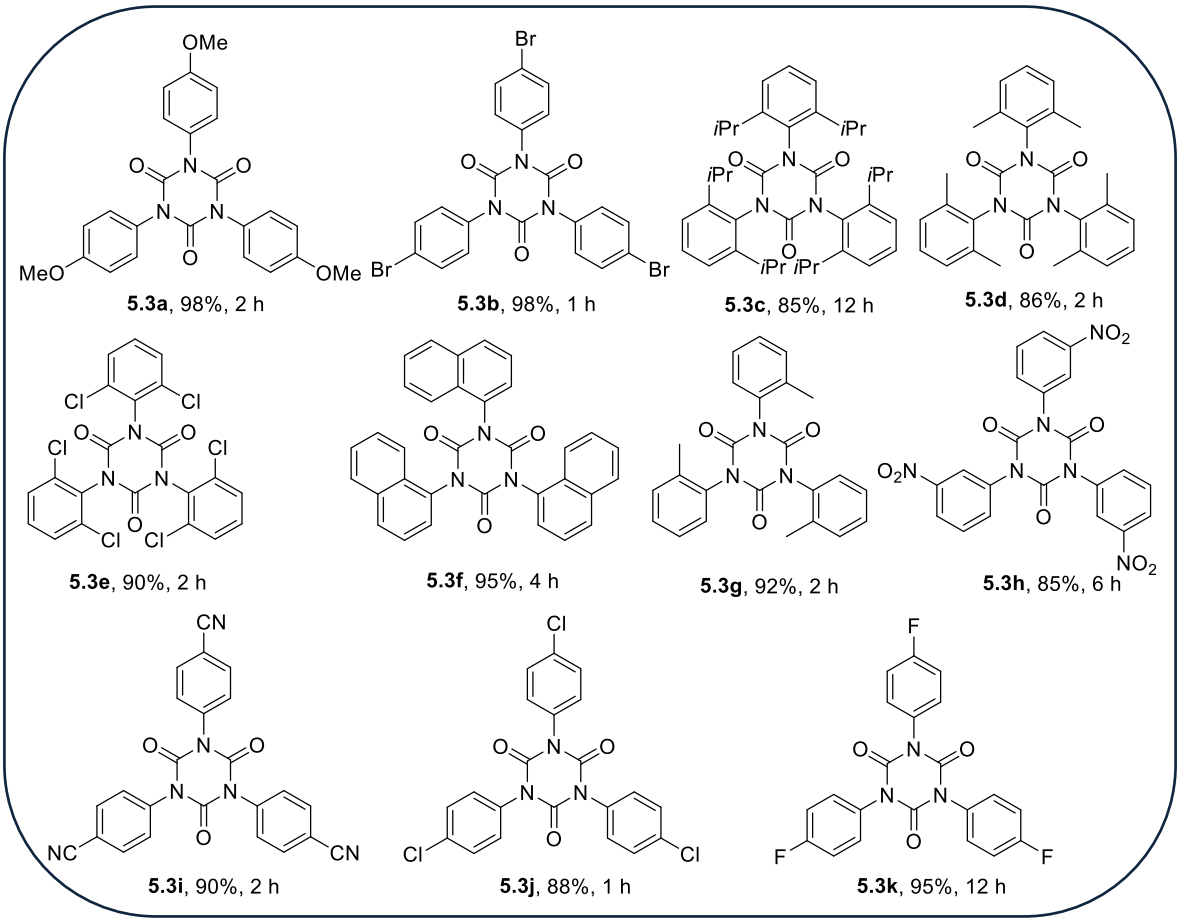

Scheme 5.4: The range of substrates for isocyanate cyclotrimerization. Reaction conditions: isocyanate (3 mmol), catalyst (2 mol%), solvent: THF (3-4 mL), room temperature, 1-12 h unless otherwise mentioned, isolated yield.

We have performed the reactions of 4-methoxyphenyl isocyanate and 4-bromophenyl isocyanate using LiI iodide as the catalyst. However, no product formation was observed even after using 20 mol% of catalyst loading and 24 hours of reaction time (Table 1, entry 2 and 5).

Subsequently, we have employed PhC(N*i*Pr)$_2$CaI[30], which we have previously reported, as a catalyst because no lithium metal is associated with it. Though it was possible to cyclotrimerize 4-methoxyphenyl isocyanate and 4-bromophenyl isocyanate, the catalyst loading is higher and the yields were significantly lesser (entry 3 and 6) than those obtained by using **5.2** as a catalyst (see entry 1 and 3). Similarly, the use of **5.1** as a catalyst afforded the trimerization of 4-methoxyphenyl isocyanate and 4-bromophenyl isocyanate in 78% and 72% yield, respectively. However, we could not prepare 5.2 without LiI coordination; hence it is unclear whether Li has any role in the catalytic cycle.

Table 5.1: Comparative catalytic details for isocyanate trimerization catalyzed by **5.2**, LiI and PhC(N*i*Pr)$_2$CaI in THF.

Entry	Substrate	Catalyst (mol%)	Time (h)	Product & yield (%)
1	4-OMe-C_6H_4NCO	**5.2** (2)	2 h	**5.3a** (98)
2	4-OMe-C_6H_4NCO	LiI (20)	24 h	-
3	4-OMe-C_6H_4NCO	PhC(N*i*Pr)$_2$CaI (5)		**5.3a** (75)
4	4-Br- C_6H_4NCO	**5.2** (2)	1h	**5.3b** (98)
5	4-Br- C_6H_4NCO	LiI (20)	24 h	-
6	4-Br- C_6H_4NCO	PhC(N*i*Pr)$_2$CaI (5)		**5.3b** (75)

We have also compared the performance of our catalyst with other catalysts reported for this transformation. The scope of Kays' Mn and Fe catalysts was limited to aliphatic isocyanates, while ours is restricted to aromatic isocyanates.[14] Cui's yttrium catalyst requires less amount of catalyst loading, but 12 h reaction time.[18] The aluminum-based catalyst reported by Ward's group[24] requires 50 °C and 1-48 h reaction time, but it works for aryl, alkyl, and allyl isocyanates. Interestingly, in the case of 4-chlorophenyl isocyanate and 4-methoxyphenyl isocyanate, 50 °C and 0.5 h and 3.5 h reaction time was required, respectively, for quantitative conversion. In the same amount of time, our catalyst gave excellent yields at room temperature in 1-2 h reaction time

for these two substrates. Nembenna's stannylene catalyst[23] produced excellent yields in 30-60 min with 2 mol% catalyst loading, but the scope was limited to only two aryl isocyanates.

5.4: DFT studies

Although we are not sure about the mechanism and no intermediate was observed spectroscopically, a tentative catalytic cycle for the cyclotrimerization reaction is proposed below. We note here that only the thermodynamics of potential intermediates has been considered, and robust evidence can only be provided by locating the transition states.

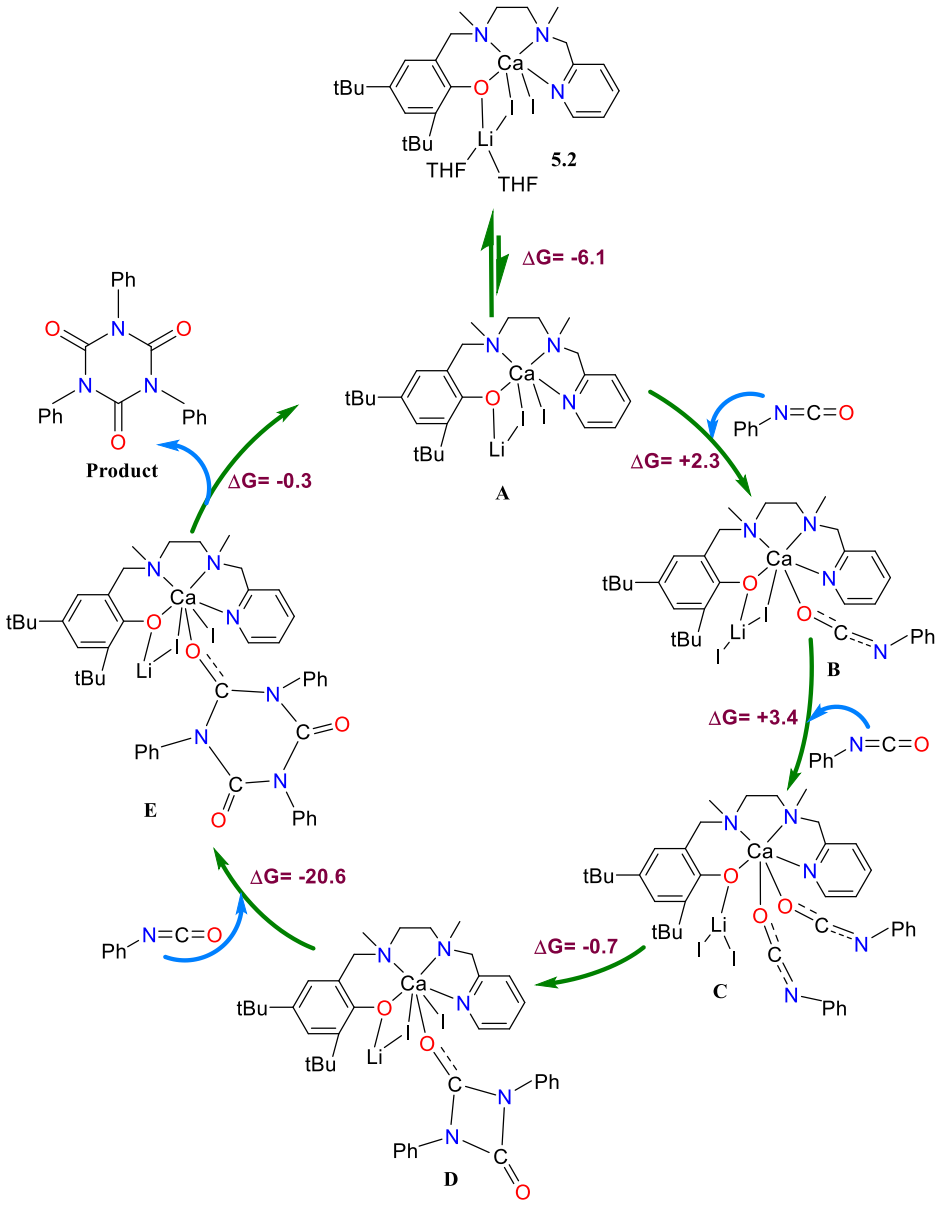

Scheme 5.5. A tentative mechanism for the cyclotrimerization of isocyanates by **5.2**.

The first step of the reaction mechanism is the coordination of aryl isocyanate to the calcium atom of **5.2**, leading to the formation of complex **B** (see Scheme 5.5). Calculations suggest that the ΔG (free energy) change in this step is 2.3 kcal/mol for phenyl isocyanate. Subsequent to this, another molecule of phenyl isocyanate reacts with **B**, leading to the formation of **C**, a process that is endergonic by 3.4 kcal/mol. In upcoming step, complex **C** undergoes dimerization and forms complex **D**, which is exergonic by 1.0 kcal/mol. Furthermore, in the next step, the addition of a third molecule of phenyl isocyanate leads to complex **E**, which is favorable by 20.6 kcal/mol. Dissociation of the bond between the carbonyl group and the calcium center results in the catalyst's regeneration and the generation of the cyclotrimerized product. We have also considered other mechanisms (see Schemes 5.6 and 5.7). However, according to the thermodynamics, these mechanisms are less likely to be operative.

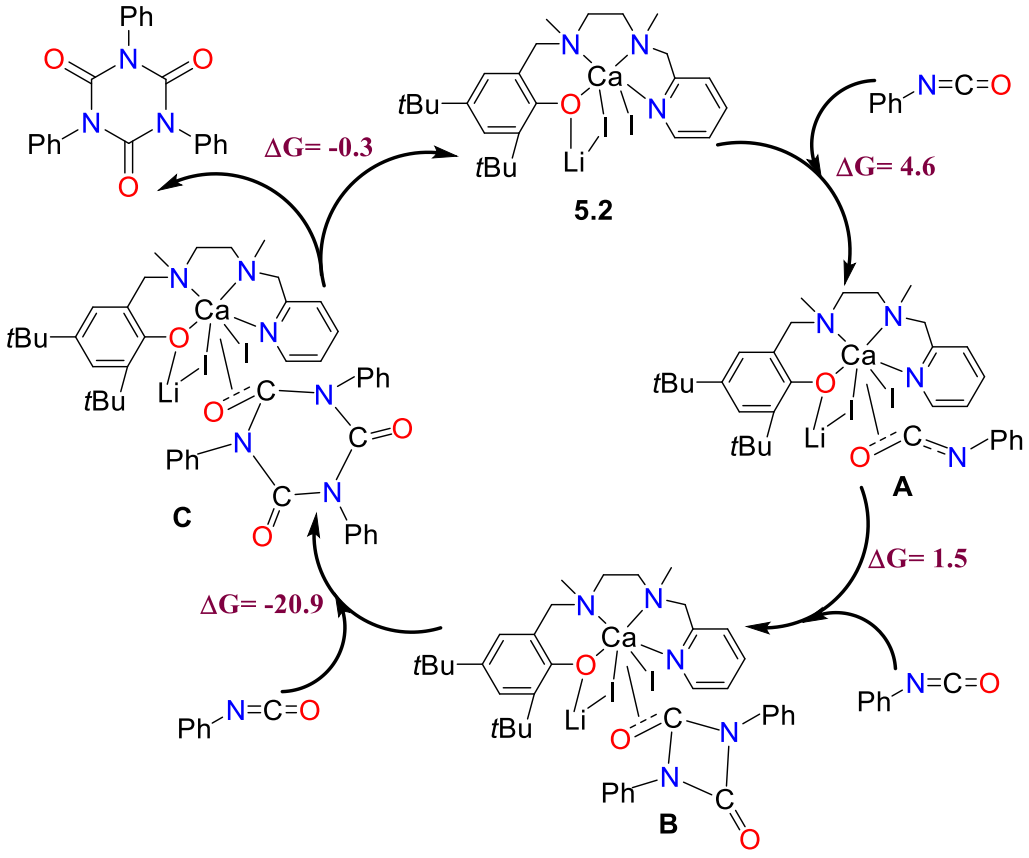

Scheme 5.6: The tentative catalytic cycle for the cyclotrimerization of isocyanates. The free energy values are in kcal/mol. This mechanism is less favorable in terms of thermodynamic potential calculations.

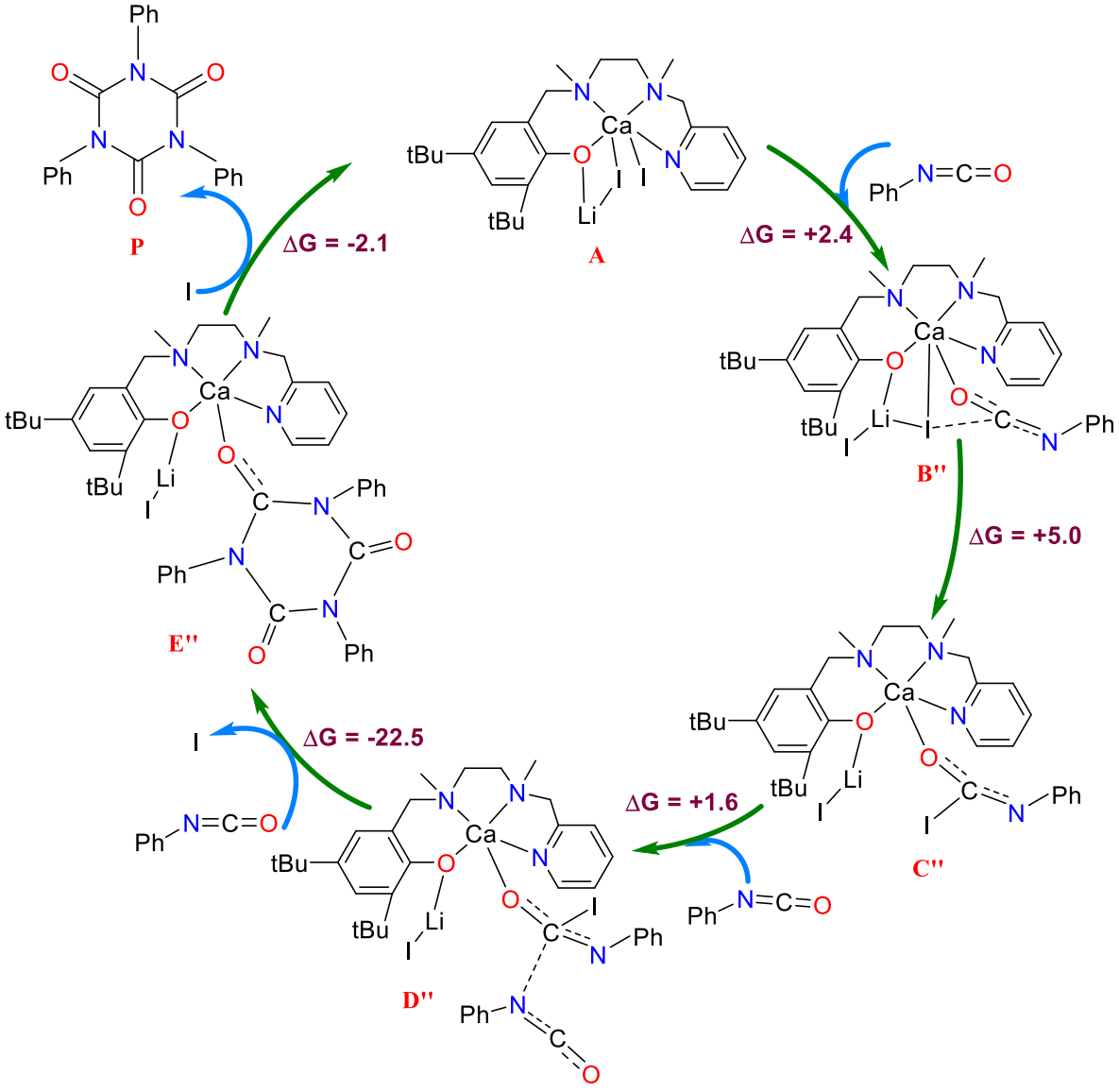

Scheme 5.7: The tentative mechanism for the cyclotrimerization of isocyanates. The free energy values are in kcal/mol. This mechanism is less favorable in terms of thermodynamic potential calculations.

5.5: Conclusions

In summary, we have introduced a novel heterobimetallic lithium-calcium complex (**5.2**) supported by a tetradentate monoanionic ligand, featuring a diaminoethane core and phenolate and pyridine peripheral donors. Subsequently, we have employed **5.2** as a catalyst for the cyclotrimerization of a variety of isocyanates to give the respective isocyanurates in THF under mild reaction conditions. These isocyanurate frameworks could enhance the physical properties of polyurethanes by incorporating them into polymer networks, copolymer resins, and plastic and coating materials, with improved heat and chemical resistance, transparency, water and impact resistance.

5.6: References

[1] D. W. Stephan, *Acc. Chem. Res.*, **2015**, *48*, 306–316.

[2] Editorial in *Nat. Catal.*, **2019**, *2*, 735.

[3] S. Harder, *Chem. Rev.*, **2010**, *110*, 3852–3876.

[4] T. E. Stennett, S. Harder, *Chem. Soc. Rev.*, **2016**, *45*, 1112–1128.

[5] M. S. Hill, D. J. Liptrot, C. Weetman, *Chem. Soc. Rev.*, **2016**, *45*, 972–988.

[6] a) S. Yadav, S. Pahar, S. S. Sen, *Chem. Commun.*, **2017**, *53*, 4562–4564; b) S. Yadav, R. Dixit, K. Vanka, S. S. Sen, *Chem. Eur. J.*, **2018**, *24*, 1269–1273.

[7] Z. Wirpsza, *Polyurethanes: Chemistry, Technology and Application*, Ellis Horwood, London, **1993**.

[8] a) T. S. Leu, *J. Appl. Polym. Sci.*, **2006**, *102*, 2470–2480; b) G. Q. Xiao, S. Q. Gao, X. L. Xie, M. C. Xu, *Polym. Adv. Technol.*, **2009**, *20*, 1157–1162; c) W. Sun, X. Yan, X. Zhu, *J. Appl. Polym. Sci.*, **2011**, *122*, 2359–2367.

[9] Y. Zhang, S. N. Riduan, J. Y. Ying, *Chem. Eur. J.*, **2009**, *15*, 1077–1081.

[10] J. G. Noltes, J. Boersma, *J. Organomet. Chem.*, **1967**, *7*, 6–8.

[11] F. Paul, S. Moulin, O. Piechaczyk, P. Le Floch, J. A. Osborn, *J. Am. Chem. Soc.*, **2007**, *129*, 7294–7304.

[12] S. G. Lee, K. Y. Choi, Y. J. Kim, S. Park, S. W. Lee, *Dalton Trans.*, **2015**, *44*, 6537–6545.

[13] A. Flamini, A. M. Giuliani, N. Poli, *Tetrahedron Lett.*, **1987**, *28*, 2169–2170.

[14] H. R. Sharpe, A. M. Geer, H. E. L. Williams, T. J. Blundell, W. Lewis, A. J. Blakea, D. L. Kays, *Chem. Commun.*, **2017**, *53*, 937—940.

[15] X. C. Zhu, J. X. Fan, Y. J. Wu, S. W. Wang, L. J. Zhang, G. S. Yang, Y. Wei, C. W. Yin, H. Zhu, S. H. Wu, H. T. Zhang, *Organometallics*, **2009**, *28*, 3882–3888.

[16] Y. J. Wu, S. W. Wang, X. C. Zhu, G. S. Yang, Y. Wei, L. J. Zhang, H. B. Song, *Inorg. Chem.*, **2008**, *47*, 5503–5511.

[17] W. Yi, J. Zhang, L. Hong, Z. Chen, X. Zhou, *Organometallics*, **2011**, *30*, 5809–5814.

[18] D. Liu, D. Zhou, H. Yang, J. Li, C. Cui, *Chem. Commun.*, **2019**, *55*, 12324–12327.

[19] H. A. Duong, M. J. Cross, J. Louie, *Org. Lett.*, **2004**, *6*, 4679–4681.

[20] S. M. Raders, J. G. Verkade, *J. Org. Chem.*, **2010**, *75*, 5308–5311.

[21] C. Li, W. Zhao, J. Hea, Y. Zhang, *Chem. Commun.*, **2019**, *55*, 12563–12566.

[22] Z. Guo, Y. Xu, X. Wu, X. Wei, C. Xi, *Dalton Trans*., **2019**, *48*, 8116–8121.

[23] M. K. Barman, A. Baishya, T. Peddarao, S. Nembenna, *J. Organometal. Chem.*, **2014**, 772-773, 265–270.

[24] M. A. Bahili, E. C. Stokes, R.C. Amesbury, D. M. C. Ould, B. Christo, R. J. Horne, B. M. Kariuki, J. A. Stewart, R. L. Taylor, P. A. Williams, M. D. Jones, K. D. M. Harris, B. D. Ward, *Chem. Commun.*, **2019**, *55*, 7679–7682.

[25] L. Orzechowski, S. Harder, *Organometallics*, **2007**, *26*, 2144–2148.

[26] T. Rosen, Y. Popowski, I. Goldberg, M. Kol, *Chem. Eur. J.*, **2016**, *22*, 11533–11536.

[27] S. Yadav, R. Dixit, M. K. Bisai, K. Vanka, S. S. Sen, *Organometallics*, **2018**, *37*, 4576–4584.

[28] R. Kumar, S. Yadav, K. Gour, E. Sangtani, S. R. Dash, A. Raja, K. Vanka, R. G. Gonnade, S. S. Sen, *Chem. Asian J.* **2020**, *15*, 820–827

[29] S. P. Sarish, A. Jana, H. W. Roesky, T. Schulz, D. Stalke, *Organometallics*, **2010**, *29*, 2901–2903.

[30] S. Yadav, V. S. V. S. N. Swamy, R. Gonnade, S. S. Sen, *ChemistrySelect*, **2016**, *5*, 1066–1071.

[31] S. Datta, M. T. Gamer, P. W. Roesky, *Dalton Trans.*, **2008**, 2839–2843.

[32] S. R. Foley, Y. Zhou, G. P. A. Yap, D. S. Richeson, *Inorg. Chem.*, **2000**, *39*, 924–929.

[33] F. Parodi in *Comprehensive Polymer Science and Supplements*, **1989**, *5*, 387-412.

[34] H.-M. Wang, H.-X. Li, X.-Y. Yu, Z.-G. Ren, J.-P. Lang, *Tetrahedron*, **2011**, *67*, 1530–1535.

Appendix: Experimental details, crystallographic data and spectral details

6.2: Chapter 2 experimental details

6.2.1: Synthesis and experimental details of ligand **L2.1**

6.2.2: Synthesis and experimental details of complexes **2.1**, **2.2** and **2.3**

6.2.3: Synthesis and experimental details of ligand **L2.2**

6.2.4: Synthesis and experimental details of complexes **2.4**, **2.5** and **2.6**

6.2.5: Crystal structure details of ligand **L2.1**, and complexes **2.1**, **2.2**, **2.3**, **2.4**, **2.5** and **2.6**

6.2.6: Details of single crystal-XRD and DFT calculations

6.3: Chapter 3 experimental details

6.3.1: Synthesis and experimental details of ligand **L3.1**

6.3.2: Synthesis and experimental details of complexes **3.1**, **3.2, 3.3** and **3.4**

6.3.3: Crystal structure details of complexes **3.1**, **3.2**, **3.3** and **3.4**

6.3.4: General procedure for the hydroboration of alkynes

6.3.5: Spectroscopic data for the hydroborated product of alkynes

6.3.6: Deuterium labeling experiment for diastereoselectivity

6.3.7: General procedure for the hydroboration of alkenes

6.3.8: Spectroscopic data for the hydroborated product of alkenes

6.3.9: General procedure for the hydroboration of terpenes

6.3.10: Spectroscopic data for hydroborated product of terpenes

6.3.11: Competitive experiment for ketone/ester/nitrile/alkyne/alkene hydroboration chemo-selectivity study

6.3.12: Mechanistic investigation for characterization and isolation of intermediate

6.3.13: Kinetic study

6.3.14: Details of DFT calculations

6.4: Chapter 4 experimental details

6.4.1: Synthesis and experimental details of complexes **4.1** and **4.2**

6.4.2: Crystal structure details of complexes **4.1** and **4.2**

6.4.3: Photophysical investigations and quantum yield measurement details

6.4.4: Computational details

6.5: Chapter 5 experimental details

6.5.1: Synthesis and experimental details of complexes **5.1** and **5.2**

6.5.2: Crystal structure details of complexes **5.1** and **5.2**

6.5.3: General procedure for the cyclotrimerization of isocyanates

6.3.4: Spectroscopic data for the cyclotrimerized product of isocyanates

6.5.5: Details of DFT calculations

6.6: References

6.2: Chapter 2 experimental details

6.2.1: Synthesis and experimental details of ligand L2.1

Synthetic procedure and characterization data of ligand L2.1: A mixture of 2-phenylaniline (2.25 g, 13.29 mmol), 2,4-pentanedione (1.33 g, 13.29 mmol), and *p*-toluene sulfonic acid (10 mol%) in toluene was heated to reflux for 24 h using Dean-Stark apparatus. After that, the solvent was removed to afford reddish-yellow sticky compound, which was further treated with an aqueous solution of Na_2CO_3 and extracted with dichloromethane (50 mL). The organic layer was separated, dried with $MgSO_4$, and filtered. The solvent was then removed to leave a red sticky compound. Yield 2.5 g (75 %). ^{1}H NMR (200 MHz, $CDCl_3$, 25 °C): δ 1.56 (s, 3H, CH_3), 1.91 (s, 3H, CH_3), 4.93 (s, 1H, C*H*), 7.10−7.27 (m, 9H, aromatic), 12.19 (s, broad, 1H, N*H*) ppm; ^{13}C NMR (100.56 MHz, $CDCl_3$, 25 °C): δ 19.4 (CH_3), 28.9 (CH_3), 97.0 (γ-CH), 126.8, 127.4, 127.9, 128.3, 129.0, 130.8, 136.0, 138.5 (Ph), 160.8 (C-NH), 195.7 (CH_3-C=O) ppm. Elemental Analysis: calcd. C, 81.29; H, 6.81; N, 5.57; found: C, 80.94; H, 5.95; N, 5.97.

6.2.2: Synthesis and experimental details of complexes 2.1, 2.2 and 2.3

Synthetic procedure and characterization data of complex 2.1: THF (10 mL) was added to a mixture of **L2.1** (0.502 g, 2 mmol) and $KN(SiMe_3)_2$ (0.398 g, 2 mmol). The reaction mixture was stirred for 1 h at room temperature. Subsequently, the solution was transferred to another flask containing MgI_2 (0.56 g, 2 mmol) in THF (10 mL) and the resulting reaction mixture was stirred overnight. It was further filtered through celite, the volatiles were removed under vacuum, and finally extracted with *n*-hexane. Single crystal suitable for X-ray diffraction were obtained by keeping concentrated solution of *n*-hexane at −4 °C for 2 days. Yield (0.21 g, 42%). ^{1}H NMR (200 MHz, $CDCl_3$, 25 °C): δ 1.68 (s, 12H, CH_3), 2.02 (s, 12H, CH_3), 5.03 (s, 4H, C*H*), 7.35−7.41 (m, 36H, aromatic) ppm; ^{13}C NMR (100.56 MHz, $CDCl_3$, 25 °C): δ 30.3 (*C*H_3), 31.5 (*C*H_3), 97.0 (γ-CH), 124.0, 125.8, 127.6, 129.6, 134.4, 136.9, 140.1, 140.6, 147.4, 149.9 (Ph), 160.5 (Me−*C*=N) ppm. In ESI-HRMS, $L1_4Mg_2$ is cleaved into two fragments of composition $L1_2Mg$. ESI-HRMS: calculated for $C_{34}H_{33}N_2O_2Mg$ $[M-C_{34}H_{32}N_2O_2Mg+H]^+$: 525.2387; found: 525.2520. Elemental Analysis: calcd. C, 77.79; H, 6.14; N, 5.34; found: C, 77.94; H, 6.36; N, 5.19.

Synthetic procedure and characterization data of complex 2.2: **L2.1** (0.2 g, .795 mmol) was dissolved in 30 mL of THF and *n*BuLi (0.397 mL, 0.795 mmol, 2.0 M solution in cyclohexane) was added to it drop by drop at –78 °C. The reaction mixture was allowed to come to room temperature and stirred for 4 h. Subsequently, the solution was transferred to a second flask containing MgI_2 (0.221 g, 0.795 mmol) in 30 mL of THF and the reaction mixture was stirred overnight. The solvent was removed under reduced pressure and the residue was extracted with toluene (30 mL) to remove LiCl. Crystallization was performed by keeping the supersaturated solution of toluene at –35 °C in a freezer. Yield: 0.15 g (72%). ^{1}H NMR (200 MHz, C_6D_6, 25 °C): δ 1.05 (s, 6H, CH_3), 1.54 (s, 6H, CH_3), 4.51 (s, 2H, C*H*), 7.03−7.30 (m, 22H, aromatic) ppm; ^{13}C NMR (100.56 MHz, C_6D_6, 25 °C): δ 21.2 (CH_3), 25.5 (CH_3), 98.4 (γ-CH), 124.5, 126.0, 127.2, 127.2, 129.6, 129.9, 131.2, 136.0, 141.0, 143.9, 159.6 (Ph), 175.0 (Me−C=N), 176.2 (Me−C=O) ppm. ESI-HRMS: calculated for $C_{34}H_{33}N_2O_2I_2Mg_2$ $[M+H]^+$: 803.0327; found: 803.0468. Elemental Analysis: calcd. C, 50.47; H, 4.73; N, 3.46; found: C, 49.70; H, 4.56; N, 3.25.

Synthetic procedure and characterization data of complex 2.3: Similar procedure of **2.1** was performed using CaI_2 instead of MgI_2. Yield: 0.22 g (42%). ^{1}H NMR (200 MHz, $CDCl_3$, 25 °C): δ 1.68 (s, 18H, CH_3), 2.02 (s, 18H, CH_3), 5.03 (s, 6H, C*H*), 7.32−7.41 (m, 54H, aromatic) ppm; ^{13}C NMR (100.56 MHz, $CDCl_3$, 25 °C): δ 24.8 (*C*H_3), 30.3 (*C*H_3), 99.07 (γ-CH), 123.7, 124.1, 125.9, 126.5, 127.5, 127.9, 129.4, 135.3, 140.1, 150.2 (Ph), 170.2 (Me−*C*=N), 176.5 (Me−*C*=O) ppm. In ESI-HRMS, L_6Ca_3 cleaved into two fragments of composition L_3Ca_2 and L_3Ca. ESI-HRMS: calculated for $C_{51}H_{49}N_3O_3Ca_2$ $[M-C_{51}H_{48}N_3O_3Ca+H]^+$: 830.2942; found: 830.5477. No satisfactory CHN analysis data has been obtained even after repeated attempts.

6.2.3: Synthesis and experimental details of ligand L2.2

Synthetic procedure and characterization data of ligand L2.2: A mixture of 2,6-diphenylaniline (4.0 g, 16.30 mmol), 2,4-pentanedione (1.63 g, 16.30 mmol) and *p*-toluenesulfonic acid (10 mol%) in toluene was heated to reflux for 24 h using Dean-Stark apparatus. After that, the solvent was removed to afford reddish-yellow sticky compound, which was further treated with an aqueous solution of Na_2CO_3 and extracted with dichloromethane (50 mL). The organic layer was separated, dried with MgSO4, and filtered. The solvent was then

removed to leave a red sticky compound. Yield 4.1 g (77 %). ^{1}H NMR (200 MHz, $CDCl_3$, 25 °C): δ 1.32 (s, 3H, CH_3), 1.95 (s, 3H, CH_3), 4.80 (s, 1H, CH), 7.15−7.45 (m, 13H, aromatic), 12.26 (s, broad, 1H, NH) ppm; ^{13}C NMR (100.56 MHz, CDCl3, 25 °C): δ 18.92 (CH_3), 28.45 (CH_3), 95.78 (γ-CH), 126.92, 127.93, 128.89, 129.68, 133.20, 135.0, 138.70, 140.26 (Ph), 161.29 (C-NH), 195.19 (CH_3-C=O) ppm.

6.2.4: Synthesis and experimental details of complexes 2.4, 2.5 and 2.6

Synthetic procedure and characterization data of complex 2.4: MeLi (1.40 mL, 4.36 mmol, 3.1M solution in diethoxymethane) was added to a stirring solution of **L2.2** (1.3 g, 3.97 mmol) in THF (20 mL) at -78 °C. The reaction mixture was allowed to warm slowly to room temperature and stirred further for 4h. The crystallization was performed by reducing the solution to 5 mL and keeping at –35°C in a freezer for 2 days. Yield 1.2 g (96 %). ^{1}HNMR (200MHz, $CDCl_3$, 25 °C): δ 1.45(s, 6H, CH_3), 1.55 (s, 6H, CH_3), 4.56 (s, 2H, C*H*), 7.09−7.35 (m, 26H, aromatic) ppm; ^{13}C NMR (400MHz, $CDCl_3$, 25 °C): δ 21.12 (CH_3), 23.87 (CH_3), 97.25 (γ-CH), 124.69, 127.0, 129.80, 130.09, 135.4, 137.43, 141.58, 147.90 (Ph), 160.07 (CH_3-C=O) ppm. Elemental Analysis: calcd. C, 79.98; H, 6.96; N, 3.45; found: C, 79.81; H, 6.81; N, 3.49.

Synthetic procedure and characterization data of complex 2.5: Compound **2.4** (0.170 g, 0.5 mmol) was dissolved in THF (10 mL) and subsequently was transferred by a cannula to a suspension of MgI_2 (0.170 g, 0.61 mmol) in THF (5 mL) at –78 °C. Subsequently, degassed water (9 μL, 0.5 mmol) was added to the reaction mixture at –78 °C using a microlitre syringe. The reaction mixture was allowed to warm to room temperature and then stirred for 12 h. The solvent was removed under vacuum and the residue was extracted with toluene (20 mL). Crystallization was performed by further reducing the solution to 4 mL and keeping at –35 °C in a freezer for overnight. Yield (0.18 g, 32%). ^{1}H NMR (200MHz, $CDCl_3$, 25 °C): δ 1.39 (s, 6H, CH_3), 2.00 (s, 6H, CH_3), 4.81 (s, 2H, C*H*), 7.27−7.49 (m, 26H, aromatic), 11.91 (s, broad, 2H, N*H*) ppm; ^{13}C NMR (100.56 MHz, $CDCl_3$, 25 °C): δ 25.58(*C*H_3), 28.81(*C*H_3), 96.20 (γ-CH), 127.30, 128.32, 129.26, 130.07 (Ph), 140.60 (C=O) ppm. ESI-HRMS: calculated for $C_{46}H_{33}O_2N_2MgI_2$ $[M-C_{46}H_{43}O_2N_2I_2Mg+H]^+$: 933.9680; found: 933.1259.

Synthetic procedure and characterization data of complex 2.6: MeLi (3.1 M in diethoxy methane, 0.21 mL, 0.67 mmol) was added to a stirring solution of **L2.2** (0.2 g, 0.61mmol) in

THF (15 mL) at –78 °C. The reaction mixture was allowed to warm slowly to room temperature and stirred further for 4h. Subsequently, the solution was transferred by a cannula to a suspension of CaI_2 (0.179 g, 0.61 mmol) in THF (5 mL) at –78 °C. Subsequently, degassed water (12 μL, 0.67 mmol) was added to the reaction mixture at –78 °C using a micro-litre syringe. The reaction mixture was allowed to warm to room temperature and then stirred for 12 h. The solvent was removed under vacuum and the residue was extracted with toluene (20 mL). Crystallization was performed by keeping the supersaturated solution of toluene and THF mixture at –35 °C in a freezer. Yield: 0.19 g (38 %). ^{1}H NMR (200 MHz, $CDCl_3$, 25 °C): δ 1.38 (s, 3H, CH_3), 2.00 (s, 3H, CH_3), 4.70 (s, 1H, C*H*), 7.20−7.43 (m, 13H, aromatic), 11.29 (s, broad, 1H, N*H*) ppm; ^{13}C NMR (100.56 MHz, $CDCl_3$, 25 °C): δ 20.49 (CH_3), 29.82 (CH_3), 96.56 (γ-CH), 127.19, 128.23, 129.61, 130.27, 132.85, 139.01, 140.41 (Ph), 165.38 (Me−C=N), 195.21 (Me−C=O) ppm. ESI-HRMS: calculated for $C_{35}H_{46}O_4NCaI_2$ [M-$C_{35}H_{46}O_4NCaI_2$+H]$^+$: 837.6350; found: 837.7710.

6.2.5: Crystal structure details of ligand L2.1 and complexes 2.1, 2.2, 2.3, 2.4, 2.5 and 2.6

Crystal data of L2.1: CCDC 1886689, $C_{17}H_{17}NO$, M=251.31, yellow, sphere, 0.23 x 0.15 x 0.10 mm^3, triclinic, space group *P-1*, *a*=7.0312(2)Å, *b*=9.8657(3)Å, *c*=11.1549(3)Å, α=70.0315(10)°, β=89.9490(10)°, γ=70.2790(10)°, *V*=679.36(3)Å^3, *Z*=2, *T*=100(2) K, 2θ_{max}=50.00°, D_{calc} (g cm^{-3})=1.229 , *F*(*000*)=268, μ (mm^{-1})= 0.076, 11442 reflections collected, 2406 unique reflections (R_{int}= 0.0868), 2248 observed ($I > 2\sigma(I)$) reflections, multi-scan absorption correction, T_{min}=0.986, T_{max}=0.992, 179 refined parameters, *S*=1.044, *R*1=0.0357, *wR*2=0.0965 (all data *R*=0.0379, *wR*2=0.0989), maximum and minimum residual electron densities; $\Delta\rho_{max}$=0.222, $\Delta\rho_{min}$=−0.222 (eÅ^{-3}).

Crystal data of 2.1: CCDC 1885674, $C_{68}H_{64}N_4O_4Mg_2$, M=1049.85, yellow, sphere, 0.23 x 0.13 x 0.08 mm^3, triclinic, space group *P-1*, *a*=10.6607(5)Å, *b*=12.4941(5)Å, *c*=12.8303(6)Å, α= 116.5330(10)°, β=109.7540(10)°, γ=94.8030(10)°, *V*= 1381.94(11)Å^3, *Z*=1, *T*=100(2) K, 2θ_{max}=50.00°, D_{calc} (g cm^{-3})=1.262, *F*(*000*)=556, μ (mm^{-1})=0.098, 62189 reflections collected, 4859 unique reflections (R_{int}=0.0927), 4164 observed ($I > 2\sigma(I)$) reflections, multi-scan absorption correction, T_{min}=0.985, T_{max}=0.992, 357 refined parameters, *S*=1.141, *R*1=0.0626, *wR*2=0.1405(all data *R*=0.0746, *wR*2=0.1465), maximum and minimum residual electron densities; $\Delta\rho_{max}$=0.410, $\Delta\rho_{min}$=−0.443(eÅ^{-3}).

Crystal data of 2.2: CCDC 1885678, $C_{38}H_{40}N_2O_3Mg_2I_2 \cdot C_7H_8$ M=967.27, yellow, sphere, 0.26 x 0.19 x 0.10 mm^3, *orthorhombic*, space group *'P 21 2121'*, *a*=10.5891(4)Å, *b*=16.9841(7)Å, *c*=23.9817(10)Å, $\alpha=\beta=\gamma=90°$, *V*=4313.0(3Å^3, *Z*=4, *T*=100(2) K, $2\theta_{max}$=50.00°, D_{calc}(g cm^{-3})=1.490, *F*(*000*)=1944, μ (mm^{-1})=1.528, 71104 reflections collected, 7596 unique reflections (R_{int}=0.0299), 7459 observed ($I > 2\sigma(I)$) reflections, multi-scan absorption correction, T_{min}=0.718, T_{max}=0.852, 492 refined parameters, *S*=1.132, *R*1=0.0193, *wR*2=0.0498(all data *R*= 0.0198, *wR*2=0.0501), maximum and minimum residual electron densities; $\Delta\rho_{max}$=0.614, $\Delta\rho_{min}$=-0.324(e$Å^{-3}$).

Crystal data of 2.3: CCDC 1885782, $C_{102}H_{96}N_6O_6Ca_3$, (C_6H_{12}), M=1708.26, yellow sphere, 0.32 x 0.10 x 0.01 mm^3, triclinic, space group *P-1*, *a*=13.026(2)Å, *b*=13.075(3)Å, *c*=14.739(3)Å, α=79.766(5)°, β=77.702(5)°, γ=73.683(5)°, *V*=2335.2(8)Å^3, *Z*=1, *T*=100(2) K, $2\theta_{max}$=50.00°, D_{calc} (g cm^{-3})=1.215, *F*(*000*)=908, μ (mm^{-1})=0.235, 96355 reflections collected, 8233 unique reflections (R_{int}=0.2855), 5833 observed ($I > 2\sigma(I)$) reflections, multi-scan absorption correction, T_{min}=0.972, T_{max}=0.997, 564 refined parameters, *S*=1.028, *R*1=0.1160, *wR*2=0.2263(all data *R*=0.1585, *wR*2=0.2464), maximum and minimum residual electron densities; $\Delta\rho_{max}$=0.857, $\Delta\rho_{min}$= −0.582 (e$Å^{-3}$).

Crystal data of 2.4: CCDC 1958801, $C_{54}H_{56}Li_2N_2O_4$, M=810.88, colorless,cubic, 0.28 x 0.22 x 0.15 mm^3, triclinic, space group *P-1*, *a*=9.6180(9) Å, *b*=10.0429(10) Å, *c*=13.2348(12) Å, α=70.130(3)°, β=70.791(3)°, γ=74.255(3)°, *V* = 1116.87(19) Å^3, *Z*=1, *T*=100(2) K, $2\theta_{max}$=50.00°, D_{calc} (g cm^{-3})=1.206, *F*(*000*)=432, μ (mm^{-1})=0.074, 65795 reflections collected, 6581 unique reflections (R_{int}=0.0890), 6549 observed ($I > 2\sigma(I)$) reflections, multi-scan absorption correction, T_{min}=0.979, T_{max}=0.989, 282 refined parameters, *S*=0.970, *R*1=0.0639, *wR*2=0.1628 (all data *R*=0.0890, *wR*2=0.1775), maximum and minimum residual electron densities; $\Delta\rho_{max}$=0.347, $\Delta\rho_{min}$= -0.346 (e$Å^{-3}$).

Crystal data of 2.5: CCDC 1959123, $C_{53.25}H_{51.50}I_2MgN_2O_{2.50}$, M = 1037.57, colorless plate, 0.293 x 0.188 x 0.072 mm^3, monoclinic, space group *P21/n*, a = 13.794(5) Å, b = 14.285(4) Å, c = 26.645(9) Å, β = 90.953(13)°, V = 5249(3) Å^3, Z = 4, T = 100(2) K, λ= 0.71073 Å, $2\theta_{max}$ = 59.80°, Dcalc (g cm^{-3}) = 1.313, F(000) = 2092, μ (mm^{-1}) = 1.247, 279949 reflections collected,

15084 unique reflections (R_{int} = 0.0918, R_{sig} = 0.0375), 12366 observed ($I > 2\sigma$ (I)) reflections, multi-scan absorption correction, T_{min} = 0.711, T_{max} = 0.916, 604 refined parameters, Good of Fit = S = 1.030, R1 = 0.0461, wR2 = 0.1169 (all data R = 0.0571, wR2 = 0.1237), maximum and minimum residual electron densities; $\Delta\rho_{max}$= 0.565, $\Delta\rho_{min}$ = -0.927 (eÅ^{-3}).

Crystal data of 2.6: CCDC 1958776, $C_{70}H_{90}Ca_2I_4N_2O_8$, M = 1675.19, colorless plate, 0.418 x 0.323 x 0.094 mm^3, triclinic, space group *P*-1, *a* = 14.8121(10) Å, *b* = 15.9426(11) Å, *c* = 16.2225(11) Å, α = 88.512(4)°, β = 70.441(4)°, γ = 89.970(4)°, *V* = 3608.4(4) Å^3, Z = 2, *T* = 100(2) K, λ = 0.71073 Å,$2\theta_{max}$ = 57.00°, D_{calc} (g cm^{-3}) = 1.542, *F*(*000*) = 1680, μ(mm^{-1}) = 1.921, 53614 reflections collected, 17821 unique reflections (R_{int} = 0.0747, R_{sig} = 0.0977), 13488 observed ($I > 2\sigma$ (*I*)) reflections, multi-scan absorption correction, T_{min} = 0.501, T_{max} = 0.840, 780 refined parameters, Good of Fit = *S* = 1.124, *R*1 = 0.0829, *wR*2 = 0.2350 (all data *R* = 0.1103, *wR*2 = 0.2551), maximum and minimum residual electron densities; $\Delta\rho_{max}$ = 4.555, $\Delta\rho_{min}$ = -1.742 (eÅ^{-3}).

6.2.6: Details of single crystal-XRD and DFT calculations

Details of single crystal-XRD: X-ray intensity data measurements of compound **L1**, **1-9** were carried out on a Bruker SMART APEX II CCD diffractometer with graphite-monochromatized (MoK_α= 0.71073Å) radiation. The X-ray generator was operated at 50 kV and 30 mA. A preliminary set of cell constants and an orientation matrix were calculated from three sets of 36 frames. Data were collected with ω scan width of 0.5° at different settings of φ and 2θ keeping the sample-to-detector distance fixed at 5.00 cm. The X-ray data collection was monitored by APEX2 program (Bruker, 2006).[1] All the data were corrected for Lorentzian, polarization, and absorption effects using SAINT and SADABS programs (Bruker, 2006). SHELX-97 was used for structure solution and full-matrix least-squares refinement on F^2.[2] All the hydrogen atoms were placed in geometrically idealized position and constrained to ride on their parent atoms. An *ORTEP* III[3] views of all compounds were drawn with 50% probability displacement ellipsoids and H atoms omitted for clarity.

Details of DFT calculations: All DFT calculations were performed by using the pbe functional[4] and def-TZVP[5] basis set by employing the Turbomole 7.1 suite of programs.[6] The

resolution of Identity (ri)[7] and multipole accelerated resolution of Identity (marij)[8] approximations with dispersion correction (disp3)[9] were employed for all the calculations. Solvent corrections were incorporated in all calculations using the COSMO model,[10] with THF (dielectric constant, ε = 7.58) as the solvent. The values reported are ΔG values, with zero-point energy corrections, internal energy and entropic contributions included through frequency calculations on the optimized minima, with the temperature 298.15 K. Harmonic frequency calculations were performed for all stationary points to confirm them as a minima.

6.3: Chapter 3 experimental details

6.3.1: Synthesis and experimental details of ligand L3.1

Synthetic procedure and characterization data of Bis(2,6-dibromo-4-methylphenyl) amine & bis(2-bromo-4-methylphenyl) amine: Bromine (10.4 mL, 0.2027 mole) was slowly added over a period of 10 min. to a solution of 10 g. (0.0506 mol) of di-p-tolylamine in 80 ml. of glacial acetic acid at 0 ºC. The reaction mixture was then allowed to warm to room temperature. After stirring for 1 hour, the reaction mixture was hydrolyzed with 100 ml. dilute sodium bisulfite solution. The aqueous solution was cooled in an ice bath and the resulting oily suspension which was filtered. The brownish-yellow solid was crystallized in hot ethanol which gives block shape crystal of bis(2,6-dibromo-4-methylphenyl) amine (yield, 9.7 g, 37.3 %). For further purification, the filtrate part was recrystallized in hexane which gives needle shape crystals of bis(2-bromo-4-methylphenyl) amine (yield, 7.5 g, 41.66 %). Both these crystals are characterized by single crystal-XRD and NMR spectroscopy.

^{1}H NMR ($CDCl_3$, 400 MHz, 298 K) for **Bis(2,6-dibromo-4-methylphenyl) amine**: δ 7.45-7.37 (m, 2H, *Ph*), 7.12-7.10 (d, 1H, *Ph*), 7.02-7.00 (d, 1H, *Ph*), 5.75 (bs, 1H, -*NH*), 2.28 (s, 6H, CH_3) ppm; ^{1}H NMR for **bis(2-bromo-4-methylphenyl) amine:** δ 7.42-7.41 (d, 2H, *Ph*), 7.07-6.96 (m, 4H, *Ph*), 6.20 (bs, 1H, -*NH*), 2.30 (s, 6H, CH_3) ppm.

Synthetic procedure and characterization data of L3.1 (**1,8-bis(dicyclohexylphosphaneyl)-3,6-dimethyl-9H-carbazole**): *n*BuLi (19.98 mL, 39.97 mmol, 2.0 M in cyclohexane) was added to a solution of bis(2,6-dibromo-4-methylphenyl) amine (5.0 g, 9.749 mmol) in diethyl ether at -

78 °C. Reaction mixture was allowed to room temperature and stirred for 3h. After that the reaction mixture was again cooled to -78 °C and chlorodicyclohexyl phosphine (4.53 g, 19.49 mmol) in diethyl ether was added then it was allowed to come to room temperature and stirred for 24 h. All volatiles were removed in vaccum and the solid compound was extracted with toluene followed by frit filtration. Again, the volatiles were removed in vaccum and further washing with iso-octane results in final ligand as orangish yellow solid. Yield: 5.3 g (92.5 %). ^{1}H NMR (C_6D_6, 400 MHz, 298 K): δ 8.26-8.25 (s, 1H, *Ph*), 7.62 (bs, 1H, -*NH*), 7.62 (bs, 1H, *NH*), 7.45-7.37 (m, 2H, *Ph*), 7.03-6.93 (m, 3H, *Ph*), 2.33 (s, 3H, *CH*$_3$), 2.19 (s, 3H, *CH*$_3$), 2.07-1.99 (m, 6H, Cy), 1.71-1.53 (m, 20H, *Cy*), 1.40-1.38 (m, 14H, *Cy*) ppm; ^{13}C{^{1}H} NMR (C_6D_6, 100.5 MHz, 298 K): δ 142.68, 140.73, 134.89, 133.72, 132.23, 131.02, 115.01, 111.59 (*Ph*), 53.65, 34.23, 33.40, 31.45, 30.60, 26.01, 25.28, 23.28 ppm; ^{31}P{^{1}H} NMR (C_6D_6, 400 MHz, 298 K): -21.67 (s, *P*Cy$_2$) ppm.

6.3.2: Synthesis and experimental details of complexes 3.1, 3.2, 3.3 and 3.4

Synthetic procedure and characterization data of complex 3.1: Methyl magnesium bromide (0.62 mL, 1.87 mmol, 3 M in THF) was added to a solution of **L3.1** (1 g, 1.70 mmol) in THF at -78 °C. The reaction mixture was kept stirring for overnight in cooling bath. After that, all volatiles were removed in vaccum and the solid compound was extracted with toluene followed by filtration using frit. Again, all volatiles were removed under vaccum and reaction mixture was kept for crystallization in THF at -36 °C. Yield: 1.1 g (93.22 %).

^{1}H NMR (C_6D_6, 400 MHz, 298 K): δ 8.13 (5, 1H, *Ph*), 7.51-7.49 (m, 2H, *Ph*), 7.41-7.40 (m, 2H, *Ph*), 6.97-6.95 (d, 1H, *Ph*), 2.62 (s, 4H, N*CH*$_2$*CH*$_2$), 2.03-1.57 (m, 40H, *Cy*), -0.74 (s, 3H, Mg*CH*$_3$) ppm; ^{13}C{^{1}H} NMR (C_6D_6, 100.5 MHz, 298 K): δ 138.21, 132.54, 129.66, 126.02, 27.91, 26.92, 21.79, 21.33, 20.48, 14.66, 3.76 ppm; ^{31}P{^{1}H} NMR (C_6D_6, 162 MHz, 298 K): -22.04 (s, *P*Cy$_2$) ppm. ESI-HRMS: calculated for $C_{43}H_{65}MgNOP_2$ $[M^+H]^+$: 698.4392; found: 698.4465.

Synthetic procedure and characterization data of complex 3.2: Ethyl magnesium bromide (0.93 mL, 1.87 mmol, 2 M in THF) was added to a solution of **L3.1** (1 g, 1.70 mmol) in THF at -78 °C. The reaction mixture was kept stirring for overnight in cooling bath. After that, all volatiles were removed in vaccum and the solid compound was extracted with toluene followed

by filtration using frit. Again, all volatiles were removed under vaccum and reaction mixture was kept for crystallization in THF at -36 ºC. Yield: 0.985 g (81.40 %).

^{1}H NMR (C_6D_6, 400 MHz, 298 K): δ 7.48-7.28 (m, 2H, *Ph*), 7.08-7.05 (d, 1H, *Ph*), 6.95-6.92 (d, 1H, *Ph*), 2.48 (s, 3H, *CH*$_3$), 2.19 (s, 3H, *CH*$_3$), 1.71-1.63 (m, 20H, *Cy*), 1.30-1.20 (m, 20H, *Cy*), 0.82-0.78 (t, 3H, Mg-*CH*$_3$), 0.21-0.10 (q, 2H, Mg-*CH*$_2$) ppm; ^{13}C{^{1}H} NMR (C_6D_6, 100.5 MHz, 298 K): δ 133.72, 132.47, 131.02, 130.58, 129.63, 38.91, 34.11, 33.40, 32.32, 29.86, 28.09, 27.65, 27.33, 23.40, 21.32, 14.71, 7.31, 1.75 ppm; ^{31}P{^{1}H} NMR (C_6D_6, 162 MHz, 298 K): -23.87 (s, *P*Cy$_2$), -25.80 (s, *P*Cy$_2$) ppm. ESI-HRMS: calculated for $C_{44}H_{67}MgNOP_2$ $[M+H]^+$: 712.4548; found: 712.4621.

Synthetic procedure and characterization data of complex 3.3: Isopropyl magnesium chloride (0.93 mL, 1.87 mmol, 2 M in THF) was added to a solution of **L3.1** (1 g, 1.70 mmol) in THF at -78 °C. The reaction mixture was kept stirring for overnight in cooling bath. After that, all volatiles were removed in vaccum and the solid compound was extracted with toluene followed by filtration using frit. Again, all volatiles were removed under vaccum and reaction mixture was kept for crystallization in THF at -36 °C. Yield: 1.05 g (85.36 %).

^{1}H NMR (C_6D_6, 500 MHz, 298 K): δ 7.38-7.30 (d, 2H, *Ph*), 7.01-6.94 (d, 1H, *Ph*), 6.87-6.85 (d, 1H, *Ph*), 2.16 (s, 3H, *CH*$_3$), 2.13 (s, 3H, *CH*$_3$), 1.56-1.38 (m, 20H, *Cy*), 1.18-1.02 (m, 20H, *Cy*), 0.25-0.22 (d, 3H, Mg-CH*CH*$_3$), 0.11-0.09 (d, 3H, Mg-CH*CH*$_3$), -0.04- -0.09 (m, 1H, Mg-*CH*CH$_3$) ppm; ^{13}C{^{1}H} NMR (C_6D_6, 126 MHz, 298 K): δ 135.4, 134.9, 133.0, 132.6, 131.9, 33.0, 31.7, 28.2, 27.8, 27.7, 27.1, 23.2, 21.1, 14.5, 1.5 ppm; ^{31}P{^{1}H} NMR (C_6D_6, 202 MHz, 298 K): -23.9 (s, *P*Cy$_2$), -25.8 (s, *P*Cy$_2$) ppm. ESI-HRMS: calculated for $C_{45}H_{69}MgNOP_2$ $[M+H]^+$: 726.4705; found: 726.4778.

Synthetic procedure and characterization data of complex 3.4: Dibutyl magnesium (1.87 mL, 1.87 mmol, 1 M in heptane) was added to a solution of **L3.1** (1 g, 1.70 mmol) in THF at -78 °C. The reaction mixture was kept stirring for overnight in cooling bath. After that, all volatiles were removed in vaccum and the solid compound was extracted with toluene followed by filtration using frit. Again, all volatiles were removed under vaccum and reaction mixture was kept for crystallization in THF at -36 °C. Yield: 0.92 g (73.01 %).

^{1}H NMR (C_6D_6, 400 MHz, 298 K): δ 7.06-7.03 (d, 2H, *Ph*), 6.94-6.93 (d, 1H, *Ph*), 6.87-6.85 (d, 1H, *Ph*), 2.10 (s, 6H, *CH*$_3$), 1.94-1.90 (m, 10H, *Cy*), 1.53-1.52 (m, 10H, *Cy*), 1.40-1.36 (m, 10H, *Cy*), 1.20-1.16 (m, 10H, *Cy*), 0.22-0.19 (t, 3H, Mg-$CH_2CH_2CH_2$*CH*$_3$), 0.12-0.06 (m, 4H, Mg-CH_2*CH*$_2$*CH*$_2$$CH_3$), -0.18− -0.20 (t, 2H, Mg-*CH*$_2$$CH_2CH_2CH_3$) ppm; ^{13}C{^{1}H} NMR (C_6D_6, 126 MHz, 298 K): δ 133.9, 133.4, 33.2, 33.0, 32.3, 32.1, 31.4, 31.3, 31.2, 30.9, 30.2, 29.8, 29.7, 28.8, 28.2, 27.8, 27.7, 27.4, 27.3, 26.9, 26.7, 23.4, 21.1, 15.0, 14.9, 14.7, 14.5, 11.8, 8.7 ppm; ^{31}P{^{1}H} NMR (C_6D_6, 162 MHz, 298 K): -21.08 (s, *P*Cy_2) ppm. ESI-HRMS: calculated for $C_{46}H_{71}MgNOP_2$ $[M+H]^+$: 740.4861; found: 740.4934.

6.3.3: Crystal structure details of complexes 3.1, 3.2, 3.3 and 3.4

Crystal data of 3.1: CCDC number- 2144879, $C_{49}H_{77}MgNO_{2.50}P_2$, M=806.36, colorless, block, 0.32 x 0.24 x 0.17 mm^3, monoclinic, space group *P21/n*, *a*=13.9627(8) Å, *b*=17.9245(10) Å, *c*=19.5392(9) Å, α=90°, β=104.734(2)°, γ=90°, *V*=4729.4(4) Å^3 , *Z*=4, *T*=100(2) K, $2\theta_{max}$=50.00°, *Dcalc* (g cm^{-3})=1.132 , *F*(*000*)=1760, μ (mm^{-1})=0.140, 11765 reflections collected, 6955 unique reflections (R_{int}=0.0769), 5186 observed ($I > 2\sigma$ (I)) reflections, multi-scan absorption correction, T_{min}=0.976, T_{max}=0.955, 501 refined parameters, *S*=1.020, *R*1=0.0769, *wR*2=0.1619 (all data *R*=0.1432, *wR*2=0.1619), maximum and minimum residual electron densities; $\Delta\rho_{max}$=0.706, $\Delta_{\rho min}$=-0.630 (eÅ^{-3}).

Crystal data of 3.2: CCDC number- 2144880, $C_{51}H_{79}MgNO_2P_2$, M=824.40, colourless, block, 0.28 x 0.19 x 0.12 mm^3, monoclinic, space group *P21/n*, *a*=13.8104(14) Å, *b*=17.8763(17) Å, *c*=19.802(2) Å, α=90°, β=102.877(3)°, γ=90°, *V*=4765.7(8) Å^3 , *Z*=4, *T*=100(2) K, $2\theta_{max}$=50.00°, D_{calc}(g cm^{-3})=1.149, *F*(*000*)=1800, μ(mm^{-1})= 0.143, 8591 reflections collected, 6282 unique reflections (R_{int}=0.1255), 6018 observed ($I > 2\sigma$ (I)) reflections, multi-scan absorption correction, T_{min}=0.983, T_{max}=0.961, 499 refined parameters, *S*=1.192, *R*1=0.1255, *wR*2=0.2448 (all data *R*=0.1644, *wR*2=0.2671), maximum and minimum residual electron densities; $\Delta\rho_{max}$=0.787, $\Delta\rho_{min}$=-0.735 (eÅ^{-3}).

Crystal data of 3.3: CCDC number- 2144881, $C_{52}H_{80}MgNO_2P_2$, M=837.42, colourless, plate, 0.34 x 0.23 x 0.14 mm^3, monoclinic, space group *P21/n*, *a*=13.9968(9) Å, *b*=17.7759(10) Å, *c*=19.8548(14) Å, *α*=90°, β=101.171(2)°, *γ*=90°, *V*= 4846.4(5) $Å^3$, *Z*=4, *T*=100(2) K, $2\theta_{max}$=50.00°, D_{calc}(g cm^{-3})=1.148 , *F*(*000*)=1828, μ(mm^{-1})=0.142, 14216 reflections collected, 9328 unique reflections (R_{int}=0.0768), 9766 observed ($I > 2\sigma(I)$) reflections, multi-scan absorption correction, T_{min}=0.980, T_{max}=0.953, 501 refined parameters, *S*=1.028, *R*1=0.0768, *wR*2=0.1816 (all data *R*=0.1184, *wR*2=0.1995), maximum and minimum residual electron densities; $\Delta\rho_{max}$=1.189, $\Delta\rho_{min}$=-1.024 ($eÅ^{-3}$).

Crystal data of 3.4: CCDC number- 2144882, $C_{53}H_{85}MgNO_2P_2$, M=854.46, colourless, block, 0.32 x 0.22 x 0.12 mm^3, monoclinic, space group *P21/n*, *a*=13.8849(8) Å, *b*=17.7489(10) Å, *c*=20.1618(13) Å, *α*=90°, β=101.449(2)°, *γ*=90°, *V*=4869.8(5) $Å^3$, *Z*=4, *T*=100(2) K, $2\theta_{max}$=50.00°, D_{calc}(g cm^{-3})=1.165, *F*(*000*)=1872, μ(mm^{-1})= 0.142, 9543 reflections collected, 6442 unique reflections (R_{int}=0.0960), 9766 observed ($I > 2\sigma(I)$) reflections, multi-scan absorption correction, T_{min}=0.956, T_{max}=0.983, 522 refined parameters, *S*=1.038, *R*1=0.0960, *wR*2=0.2282 (all data *R*=0.1384, *wR*2=0.2563), maximum and minimum residual electron densities; $\Delta\rho_{max}$=1.303, $\Delta\rho_{min}$=-0.621 ($eÅ^{-3}$).

6.3.4: General procedure for the hydroboration of alkynes

Alkyne (0.250 mmol), pinacolborane (1.1 equiv., 0.275 mmol), catalyst (**3.1**, 5.0 mol%) were charged in a Schlenk tube/ nmr tube inside the glove box. The reaction mixture was allowed to heat at 80 °C for 18 h. Upon completion of the reaction, the solvent was removed using vacuum in a Schlenk line and mesitylene (0.25 mmol) was added as the internal standard, while making the NMR in appropriate deuterated solvent. The progress of the reaction was monitored by the ^{1}H NMR spectroscopy, which indicated the completion of the reaction by the disappearance of alkyne (RC≡C*H*) proton and the appearance of a new C*H*=C*H* resonance.

6.3.5: Spectroscopic data for hydroborated product of alkynes

(E)-4,4,5,5-tetramethyl-2-styryl-1,3,2-dioxaborolane (3.5a): ^{1}H NMR ($CDCl_3$, 400 MHz, 298 K): δ 7.37-7.35 (m, 2H, Ar*H*), 7.20-7.15 (m, 4H, Ar*H* and ArC*H*), 6.08-6.04 (d, 1H, $^{3}J_{H\text{-}H}$ = 19.89 Hz, ArCHC*H*), 1.19 (s, 12H, CH_3) ppm; ^{13}C{^{1}H} NMR ($CDCl_3$, 100.28 MHz, 298 K): δ 149.44, 128.78, 128.45, 83.20, 24.69 ppm.

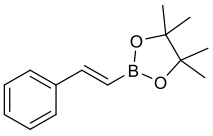

(E)-2-(4-methoxystyryl)-4,4,5,5-tetramethyl-1,3,2-dioxaborolane (3.5b): ^{1}H NMR ($CDCl_3$, 200 MHz, 298 K): δ 7.50-7.46 (m, 3H, Ar*H*), 6.92-6.90 (m, 2H, Ar*H* and ArC*H*), 6.12-6.07 (d, 1H, $^{3}J_{H\text{-}H}$ = 18.39 Hz, ArCHC*H*), 3.83 (s, 3H, -OCH_3), 1.37 (s, 12H, CH_3) ppm; ^{13}C{^{1}H} NMR ($CDCl_3$, 50.28 MHz, 298 K): δ 160.19, 148.97, 130.26, 128.30, 113.82, 82.99, 54.99, 24.66 ppm.

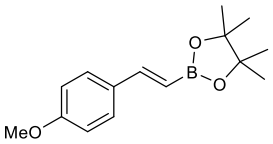

(E)-2-(4-(tert-butyl) styryl)-4,4,5,5-tetramethyl-1,3,2-dioxaborolane (3.5c): ^{1}H NMR ($CDCl_3$, 200 MHz, 298 K): δ 7.40-7.25 (m, 5H, Ar*H* and ArC*H*), 6.14-6.05 (d, 1H, $^{3}J_{H\text{-}H}$ = 18.44 Hz, ArCHC*H*), 1.25 (s, 9H, C(C$H_{3)3}$), 1.22 (s, 12H, CH_3) ppm; ^{13}C{^{1}H} NMR ($CDCl_3$, 50.28 MHz, 298 K): δ 151.97, 149.37, 134.77, 131.80, 125.39, 125.12, 83.12, 34.58, 31.16, 24.72 ppm.

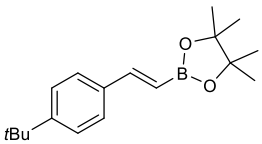

(E)-2-(4-fluorostyryl)-4,4,5,5-tetramethyl-1,3,2-dioxaborolane (3.5d): ^{1}H NMR ($CDCl_3$, 500 MHz, 298 K): δ 7.53-7.41 (d, 3H, Ar*H* and ArC*H*), 7.09-7.05 (m, 2H, Ar*H*), 6.17-6.13 (d, 1H, $^{3}J_{H\text{-}H}$ = 18.39 Hz, ArCHC*H*), 1.38 (s, 12H, CH_3) ppm; ^{13}C{^{1}H} NMR ($CDCl_3$, 100.28 MHz, 298 K): δ 164.27, 161.60, 148.06, 133.67, 128.63, 115.32, 82.23, 24.67 ppm.

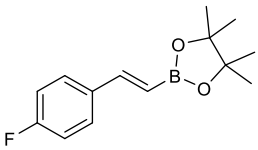

(E)-2-(4-bromostyryl)-4,4,5,5-tetramethyl-1,3,2-dioxaborolane (3.5e): ^{1}H NMR ($CDCl_3$, 400 MHz, 298 K): δ 7.51-7.37 (m, 5H, Ar*H* and ArC*H*), 6.24-6.19 (d, 1H, $^{3}J_{H\text{-}H}$ = 18.39 Hz, ArCHC*H*), 1.37 (s, 12H, CH_3) ppm; ^{13}C{^{1}H} NMR ($CDCl_3$, 100.28 MHz, 298 K): δ 147.63, 135.98, 133.42, 131.31, 128.06, 122.45, 82.98, 24.37 ppm.

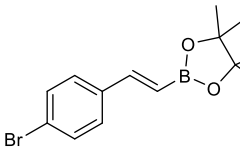

(E)-4,4,5,5-tetramethyl-2-(4-pentylstyryl)-1,3,2-dioxaborolane (3.5f): ^{1}H NMR ($CDCl_3$, 100 MHz, 298 K): δ 7.51-7.47 (m, 3H, Ar*H* and ArC*H*),

7.23-7.21 (m, 2H, Ar*H*), 6.25-6.20 (d, 1H, $^{3}J_{H-H}$ = 18.51 Hz, ArCHC*H*), 2.69-2.65 (t, 2H, CH_3), 1.73-1.67 (m, 3H, CH_2), 1.39-1.34 (m, 16H, CH_3 & CH_2), 1.00-0.97 (t, 3H, CH_3) ppm; $^{13}C\{^{1}H\}$ NMR ($CDCl_3$, 100.28 MHz, 298 K): δ 149.44, 143.84, 134.93, 128.50, 83.05, 35.64, 31.38, 30.90, 24.67, 22.43, 13.89 ppm.

The spectroscopic data is consistent with the literature data. [11]

(E)-4,4,5,5-tetramethyl-2-(4-methylstyryl)-1,3,2-dioxaborolane (3.5g): ^{1}H NMR ($CDCl_3$, 500 MHz, 298 K): δ 7.51-7.46 (m, 3H, Ar*H* and ArC*H*), 7.22-7.20 (d, 2H,$^{3}J_{H-H}$ = 7.88 Hz, Ar*H*), 6.25-6.19 (d, 1H, $^{3}J_{H-H}$= 18.39 Hz, ArCHC*H*), 2.42 (s, 3H, ArCH_3), 1.40 (s, 12H, CH_3) ppm; $^{13}C\{^{1}H\}$ NMR ($CDCl_3$, 100.28 MHz, 298 K): δ 149.40, 138.76, 134.74, 129.18, 126.9, 83.09, 24.69 ppm.

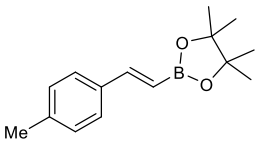

(E)-2-(2-(cyclohex-1-en-1-yl)vinyl)-4,4,5,5-tetramethyl-1,3,2-dioxaborolane (3.5h): ^{1}H NMR ($CDCl_3$, 500 MHz, 298 K): δ 7.11-7.06 (d, 1H, $^{3}J_{H-H}$ = 18.26 Hz, RC*H*CH), 6.00 (s, 1H, Internal-C*H*), 5.51-5.46 (d, 1H, $^{3}J_{H-H}$ = 18.26 Hz, RCHC*H*), 2.19 (br, 4H, -CH_2), 1.73-1.62 (br, 4H, -CH_2), 1.32 (s, 12H, CH_3) ppm; $^{13}C\{^{1}H\}$ NMR ($CDCl_3$, 100.28 MHz, 298 K): δ 153.12, 137.06, 134.02, 82.85, 26.06, 24.65, 23.67, 22.33 ppm.

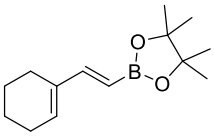

The spectroscopic data is consistent with the literature data. [11]

(E)-4,4,5,5-tetramethyl-2-(2-(thiophen-3-yl)vinyl)-1,3,2-dioxaborolane (3.5i): ^{1}H NMR ($CDCl_3$, 500 MHz, 298 K): δ 7.40-7.36 (d, 1H, $^{3}J_{H-H}$ = 18.39 Hz, ArC*H*CH), 7.24-7.20 (m, 3H, ArC*H*), 5.97-5.92 (d, 1H, $^{3}J_{H-H}$ = 18.39 Hz, RCHC*H*), 1.29 (s, 12H, CH_3) ppm; $^{13}C\{^{1}H\}$ NMR ($CDCl_3$, 100.28 MHz, 298 K): δ 143.05, 141.12, 125.98, 124.87, 124.70, 83.12, 24.67, 22.59 ppm.

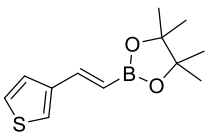

(E)-N,N-dimethyl-4-(2-(4,4,5,5-tetramethyl-1,3,2-dioxaborolan-2-yl)vinyl)aniline (3.5j): ^{1}HNMR ($CDCl_3$, 500 MHz, 298 K): δ 7.44-7.36 (m, 3H, Ar*H* and ArC*H*), 6.70-6.68 (d, 2H, $^{3}J_{H-H}$ = 8.88 Hz, ArH), 5.99-5.94 (d, 1H, $^{3}J_{H-H}$ = 18.39 Hz, ArCHC*H*), 3.00 (s, 3H, -NMe_2), 2.93 (s, 3H, -NMe_2), 1.34 (s, 12H, CH_3) ppm; $^{13}C\{^{1}H\}$ NMR ($CDCl_3$, 100.28 MHz, 298 K): δ 150.86, 149.74, 128.29, 128.3, 125.81, 82.89, 40.16, 24.72 ppm.

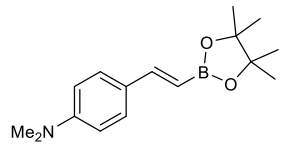

(E)-4,4,5,5-tetramethyl-2-(2-(thiophen-3-yl)vinyl)-1,3,2-dioxaborolane (3.5k): ^{1}H NMR

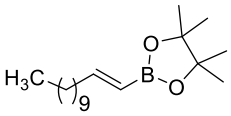

(CDCl$_3$, 500 MHz, 298 K): δ 6.73-6.65 (m, 1H, RC*H*CH), 5.50-5.46 (d, 1H, $^{3}J_{H\text{-}H}$ = 17.89 Hz, RCHC*H*), 2.20-2.17 (quat, 2H, -C*H*$_2$), 1.47-1.43 (br, 4H, -C*H*$_2$), 1.31 (bs, 36H, -CH$_2$ & C*H*$_3$), 0.95-0.92 (s, 3H, C*H*$_3$) ppm; ^{13}C{^{1}H} NMR (CDCl$_3$, 100.28 MHz, 298 K): δ 154.68, 82.82, 35.78, 31.87, 29.58, 29.19, 28.19, 24.69, 22.63, 14.04 ppm.

(E)-2-(but-1-en-1-yl)-4,4,5,5-tetramethyl-1,3,2-dioxaborolane (3.5l): ^{1}H NMR (CDCl$_3$, 500

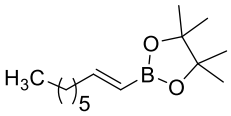

MHz, 298 K): δ 6.73-6.66 (m, 1H, RC*H*CH), 5.51-5.46 (d, 1H, $^{3}J_{H\text{-}H}$ = 18.01 Hz, RCHC*H*), 2.22-2.17 (quat, 2H, -C*H*$_2$), 1.48-1.43 (br, 4H, -C*H*$_2$), 1.31 (s, 12H, C*H*$_3$), 1.28-1.23 (m, 4H, -CH$_2$), 0.95-0.92 (s, 3H, C*H*$_3$) ppm; ^{13}C{^{1}H} NMR (CDCl$_3$, 100.28 MHz, 298 K): δ 154.59, 82.77, 35.73, 31.64, 28.83, 28.11, 24.64, 22.50, 13.96 ppm.

(E)-2-(but-1-en-1-yl)-4,4,5,5-tetramethyl-1,3,2-dioxaborolane (3.5m): ^{1}H NMR (CDCl$_3$, 500

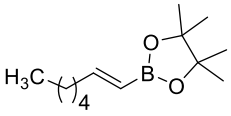

MHz, 298 K): δ 6.72-6.66 (m, 1H, RC*H*CH), 5.51-5.46 (d, 1H, $^{3}J_{H\text{-}H}$ = 17.89 Hz, RCHC*H*), 2.22-2.17 (quat, 2H, -C*H*$_2$), 1.49-1.45 (br, 4H, -C*H*$_2$), 1.31 (s, 12H, C*H*$_3$), 1.28-1.24 (m, 6H, -CH$_2$), 0.95-0.92 (s, 3H, C*H*$_3$) ppm; ^{13}C{^{1}H} NMR (CDCl$_3$, 100.28 MHz, 298 K): δ 154.64, 82.82, 35.70, 31.34, 27.83, 24.67, 22.44, 13.89 ppm.

(Z)-2-(1,2-diphenylvinyl)-4,4,5,5-tetramethyl-1,3,2-dioxaborolane (3.5n): ^{1}H NMR (CDCl$_3$,

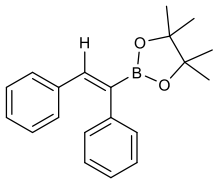

500 MHz, 298 K): δ 7.40-7.37 (m, 2H, ArH), 7.18-7.04 (m, 5H, ArH), 7.01 (s, 1H), 6.96-6.92 (m, 3H, ArH), 1.12 (s, 12H) ppm; ^{13}C{^{1}H} NMR (CDCl$_3$, 100.28 MHz, 298 K): δ 143.09, 140.33, 131.45, 129.82, 128.1, 128.72, 128.19, 127.71, 126.11, 123.19, 89.27, 83.57, 83.07, 81.74, 24.73, 22.59 ppm.

(Z)-2-(hex-3-en-3-yl)-4,4,5,5-tetramethyl-1,3,2-dioxaborolane (3.5o): ^{1}H NMR (CDCl$_3$, 400

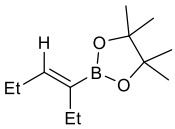

MHz, 298 K): δ 6.51-6.47 (t, 1H, EtC*H*), 2.33-2.18 (m, 2H, C*H*$_2$CH$_3$), 1.47-1.42 (t, 3H, CH$_2$*CH*$_3$), 1.08-0.93 (m, 5H, *CH*$_2$*CH*$_3$), 1.12 (s, 12H, C*H*$_3$), 1.05 (m, 6H, CH$_2$C*H*$_3$) ppm; ^{13}C{^{1}H} NMR (CDCl$_3$, 100.28 MHz, 298 K): δ 146.84, 140.15, 83.11, 81.78, 29.98, 24.77, 22.61, 13.89 ppm.

6.3.6: Deuterium labelling experiment for diastereoselectivity

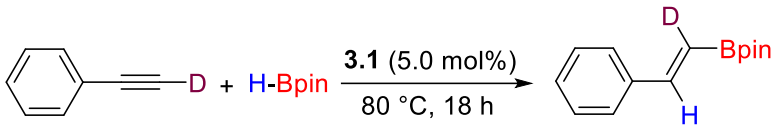

Phenylacetylene-d_1 (25.75 mg, 0.25 mmol), pinacolborane (35.2 mg, 0.275 mmol), catalyst (5.0 mol% for **3.1**) were charged in a screw cap NMR tube inside the glove box. The reaction mixture was heated at 80 °C for 18 h. The progress of the reaction was monitored by the ^{2}H NMR. After dissolving in CD_3CN, the spectrum shows a peak at δ = 6.20 ppm, which indicates a *cis* orientation of deuterium and phenyl group.

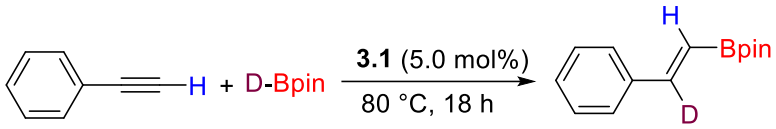

Phenylacetylene (25.53 mg, 0.25 mmol), pinacolborane-d_1 (36 mg, 0.275 mmol), catalyst (5.0 mol% for **3.1**) were charged in a screw cap NMR tube inside the glove box. The reaction mixture was heated at 80 °C for 18 h. The progress of the reaction was monitored by ^{2}H NMR after dissolving in CD_3CN, which indicated the peak at δ = 7.24 ppm, due to the *cis* orientation of deuterium and Bpin unit.

6.3.7: General procedure for the hydroboration of alkenes

Alkene (0.250 mmol), pinacolborane (1.1 equiv, 0.275 mmol), catalyst (**3.1**, 10 mol%) were mixed together in a Schlenk tube/ nmr tube inside the glove box. The reaction mixture was allowed to heat at 100 °C for 12 h in neat condition. Volatiles of the mixture were removed under reduced pressure and mesitylene (0.25 mmol) as an internal standard, was added while making the NMR in appropriate deuterated solvent. The progress of the reaction was monitored by ^{1}H NMR, which indicated the completion of the reaction by the disappearance of alkene (RCH=CH_2) proton and appearance of a new RCH_2CH_2Bpin resonance.

6.3.8: Spectroscopic data for hydroborated product of alkenes

4,4,5,5-tetramethyl-2-phenethyl-1,3,2-dioxaborolane (3.6a): ^{1}H NMR ($CDCl_3$, 500 MHz, 298 K): δ 7.30-7.17 (m, 5H, Ar*H*), 2.82-2.78 (t, 2H, ArC*H*$_2$CH$_2$), 1.26 (s, 12H, C*H*$_3$), 1.22-1.18 (t, 2H, ArCH$_2$C*H*$_2$) ppm; ^{13}C{^{1}H} NMR ($CDCl_3$, 100.28 MHz, 298 K): δ 144.28, 128.91, 128.06, 127.90, 125.38, 82.95, 29.86, 24.68 ppm.

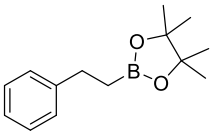

4,4,5,5-tetramethyl-2-(4-methylphenethyl)-1,3,2-dioxaborolane (3.6b): ^{1}H NMR ($CDCl_3$, 400 MHz, 298 K): δ 7.23-7.16 (m, 4H, Ar*H*), 2.85-2.81 (t, 2H, ArC*H*$_2$CH$_2$), 2.41 (s, 3H, Ar*CH*$_3$), 1.33 (s, 12H, C*H*$_3$), 1.27-1.23 (t, 3H, ArCH$_2$*CH*$_2$) ppm; ^{13}C{^{1}H} NMR ($CDCl_3$, 100.28 MHz, 298 K): δ 141.27, 134.65, 128.75, 127.74, 82.90, 29.43, 25.35, 24.69 ppm.

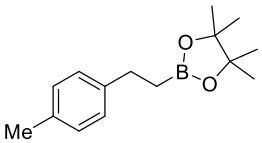

2-(4-methoxyphenethyl)-4,4,5,5-tetramethyl-1,3,2-dioxaborolane (3.6c): ^{1}H NMR ($CDCl_3$, 400 MHz, 298 K): δ 7.21-7.19 (d, 2H, Ar*H*), 6.89-6.88 (d, 2H, Ar*H*), 3.82 (s, 3H, -*OMe*), 2.79-2.75 (t, 2H, ArC*H*$_2$CH$_2$), 1.29 (s, 12H, C*H*$_3$) 1.22-1.18 (t, 2H, ArCH$_2$C*H*$_2$), ppm; ^{13}C{^{1}H} NMR ($CDCl_3$, 100.28 MHz, 298 K): δ 157.46, 136.40, 128.74, 113.46, 82.90, 55.02, 28.96, 24.69 ppm.

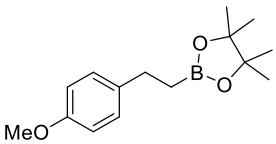

2-(4-(tert-butoxy)phenethyl)-4,4,5,5-tetramethyl-1,3,2-dioxaborolane (3.6d): ^{1}H NMR ($CDCl_3$, 500 MHz, 298 K): δ 7.19-7.17 (d, 2H, Ar*H*), 6.97-6.95 (m, 2H, Ar*H*), 2.82-2.79 (t, 2H, ArC*H*$_2$CH$_2$), 1.39 (s, 9H, -*OtBu*), 1.26 (s, 12H, C*H*$_3$), 1.24-1.21 (t, 2H, ArCH$_2$C*H*$_2$) ppm; ^{13}C{^{1}H} NMR ($CDCl_3$, 100.28 MHz, 298 K): δ 152.63, 137.17, 127.92, 123.57, 82.54, 77.39, 28.85, 28.41, 25.05, 24.36 ppm.

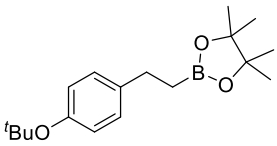

4,4,5,5-tetramethyl-2-(2,4,6-trimethylphenethyl)-1,3,2-dioxaborolane (3.6e): ^{1}H NMR ($CDCl_3$, 400 MHz, 298 K): δ 6.97 (s, 1H, Ar*H*), 6.95 (s, 1H, Ar*H*), 2.85-2.81 (t, 2H, ArC*H*$_2$CH$_2$), 2.45 (s, 3H, ArC*H*$_3$), 2.38 (s, 3H, ArC*H*$_3$), 2.33 (s, 3H, ArC*H*$_3$), 1.41 (s, 12H, C*H*$_3$), 1.14-1.10 (t, 2H, ArCH$_2$C*H*$_2$) ppm; ^{13}C{1H} NMR ($CDCl_3$, 100.56 MHz, 298 K): δ 142.34, 138.07, 135.15, 134.14, 128.41, 128.12, 118.58, 82.62, 25.06, 24.43, 20.36, 19.23 ppm.

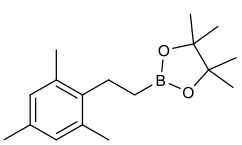

2-(2-bromophenethyl)-4,4,5,5-tetramethyl-1,3,2-dioxaborolane (3.6f): ^{1}H NMR ($CDCl_3$, 400 MHz, 298 K): δ 7.45-7.43 (d, 1H, Ar*H*), 7.24-7.22 (d, 1H, Ar*H*), 7.17-7.13 (t, 1H, Ar*H*), 6.97-6.95 (t, 1H, Ar*H*), 2.84-2.80 (t, 2H, ArCH_2CH_2), 1.19 (s, 12H, CH_3), 1.13-1.09 (s, 3H, ArCH$_2$CH_2), ppm; ^{13}C{^{1}H} NMR ($CDCl_3$, 100.28 MHz, 298 K): δ 143.39, 132.53, 129.66, 127.15, 124.25, 83.02, 30.35, 25.36, 24.72 ppm.

2-(4-chlorophenethyl)-4,4,5,5-tetramethyl-1,3,2-dioxaborolane (3.6g): ^{1}H NMR ($CDCl_3$, 400 MHz, 298 K): δ 7.21-7.19 (d, 2H, ArH), 7.13-7.11 (d, 2H, ArH), 2.72-2.68 (t, 2H, ArCH_2CH$_2$), 1.20 (s, 12H, CH_3), 1.13-1.09 (t, 2H, ArCH$_2$CH_2) ppm; ^{13}C{^{1}H} NMR ($CDCl_3$, 100.56 MHz, 298 K): δ 142.72, 131.07, 129.29, 128.12, 83.04, 29.25, 25.36, 24.69 ppm.

2-(4-(chloromethyl)phenethyl)-4,4,5,5-tetramethyl-1,3,2-dioxaborolane (3.6h): ^{1}H NMR ($CDCl_3$, 400 MHz, 298 K): δ 7.29-7.11 (m, 4H, Ar*H*), 4.55 (s, 2H, ArCH_2Cl), 2.78-2.74 (t, 2H, ArCH_2CH$_2$), 1.28 (s, 12H, CH_3), 1.17-1.12 (t, 2H, ArCH$_2$CH_2) ppm; ^{13}C{^{1}H} NMR ($CDCl_3$, 100.28 MHz, 298 K): δ 144.75, 134.60, 128.77, 128.44, 83.04, 63.83, 46.19, 29.59, 24.78, 22.59 ppm.

2-(4-bromophenethyl)-4,4,5,5-tetramethyl-1,3,2-dioxaborolane (3.6i): ^{1}H NMR ($CDCl_3$, 500 MHz, 298 K): δ 7.47-7.44 (d, 2H, Ar*H*), 7.19-7.17 (d, 2H, Ar*H*), 2.82-2.78 (t, 2H, ArCH_2CH$_2$), 1.31 (s, 12H, CH_3), 1.23-1.19 (t, 2H, ArCH$_2$CH_2) ppm; ^{13}C{^{1}H} NMR ($CDCl_3$, 100.56 MHz, 298 K): δ 143.24, 131.07, 129.72, 119.09, 83.05, 29.31, 25.36, 24.70 ppm.

2-(2-([1,1'-biphenyl]-4-yl)ethyl)-4,4,5,5-tetramethyl-1,3,2-dioxaborolane (3.6j): ^{1}H NMR ($CDCl_3$, 200 MHz, 298 K): δ 7.44-7.35 (m, 4H, Ar*H*), 7.29-7.15 (m, 5H, Ar*H*), 2.69-2.65 (t, 2H, ArCH_2CH$_2$), 1.13 (s, 12H, CH_3), 1.03-0.98 (t, 2H, ArCH$_2$CH_2) ppm; ^{13}C{^{1}H} NMR ($CDCl_3$, 100.56 MHz, 298 K): δ 143.16, 140.83, 138.06, 128.25, 128.03, 82.69, 29.20, 24.46 ppm.

4,4,5,5-tetramethyl-2-(3-phenylpropyl)-1,3,2-dioxaborolane (3.6k): ^{1}H NMR ($CDCl_3$, 400 MHz, 298 K): δ 7.36-7.24 (m, 5H, Ar*H*), 2.73-2.69 (t, 2H, ArC*H*$_2$CH$_2$CH$_2$), 1.88-1.80 (m, 2H, ArCH$_2$*CH*$_2$CH$_2$), 1.33 (t, 12H, C*H*$_3$), 0.95-0.91 (s, 2H, ArCH$_2$CH$_2$*CH*$_2$) ppm; ^{13}C{^{1}H} NMR ($CDCl_3$, 100.28 MHz, 298 K): δ 142.54, 128.43, 128.04, 125.44, 82.76, 38.48, 26.01, 25.34, 24.70 ppm.

4,4,5,5-tetramethyl-2-(2-(naphthalen-2-yl)ethyl)-1,3,2-dioxaborolane (3.6l): ^{1}H NMR ($CDCl_3$, 500 MHz, 298 K): δ 7.86-7.51 (m, 7H, Ar*H*), 3.06-3.02 (t, 2H, ArC*H*$_2$CH$_2$), 1.33 (s, 12H, C*H*$_3$), 1.02-0.98 (t, 2H, ArCH$_2$C*H*$_2$), ppm; ^{13}C{^{1}H} NMR ($CDCl_3$, 100.28 MHz, 298 K): δ 141.83, 133.57, 131.84, 127.58, 127.45, 127.31, 127.15, 125.59, 124.79, 82.98, 30.05, 25.36, 24.7 ppm.

4,4,5,5-tetramethyl-2-(2-(1,2,3,4-tetrahydronaphthalen-2-yl)ethyl)-1,3,2-dioxaborolane (3.6m): ^{1}H NMR ($CDCl_3$, 400 MHz, 298 K): δ 7.37-7.17 (m, 4H, Ar*H*), 2.99-2.95 (t, 2H, ArC*H*$_2$CH$_2$), 1.59 (m, 4H, Cy*CH*$_2$), 1.45-142 (bs, 14H, Cy*CH*$_2$ & C*H*$_3$), 1.32-1.29 (t, 2H, ArCH$_2$C*H*$_2$), ppm; ^{13}C{^{1}H} NMR ($CDCl_3$, 100.28 MHz, 298 K): δ 135.29, 134.00, 128.43, 127.71, 126.30, 125.76, 83.10, 81.78, 27.38, 24.75, 23.06, 22.59 ppm.

2-(2-cyclohexylethyl)-4,4,5,5-tetramethyl-1,3,2-dioxaborolane (3.6n): ^{1}H NMR ($CDCl_3$, 400 MHz, 298 K): δ 1.79-1.67 (m, 4H), 1.57-1.45 (m, 6H), 1.29 (s, 12H, CH_3), 1.21-1.16 (m, 4H), 0.83-0.79 (t, 2H) ppm; ^{13}C{^{1}H} NMR ($CDCl_3$, 100.28 MHz, 298 K): δ 82.69, 62.71, 39.88, 32.92, 31.31, 26.69, 26.37, 24.71 ppm.

2-cyclohexyl-4,4,5,5-tetramethyl-1,3,2-dioxaborolane (3.6o): ^{1}H NMR ($CDCl_3$, 400 MHz, 298 K): δ 1.77-1.53 (m, 5H), 1.30-1.15 (m, 17H, CH_3 and CH_2), 0.92 (bm, 1H) ppm; ^{13}C{^{1}H} NMR ($CDCl_3$, 100.28 MHz, 298 K): δ 83.14, 81.81, 27.92, 27.24, 26.44, 24.79, 22.62, 17.22 ppm.

2-(3-bromopropyl)-4,4,5,5-tetramethyl-1,3,2-dioxaborolane (3.6p): ^{1}H NMR ($CDCl_3$, 400 MHz, 298 K): δ 3.47-3.43 (t, 2H, C*H*$_2$Br), 2.02-1.97 (q, 2H, C*H*$_2$), 1.31 (s, 12H, C*H*$_3$), 0.99-0.94 (t, 2H, C*H*$_2$) ppm; ^{13}C{^{1}H} NMR ($CDCl_3$, 100.28 MHz,

298 K): δ 83.22, 69.72, 36.03, 27.44, 24.77, 22.62 ppm.

2-(3,3-dimethylbutyl)-4,4,5,5-tetramethyl-1,3,2-dioxaborolane (3.6q): ^{1}H NMR ($CDCl_3$, 500 MHz, 298 K): δ 1.43 (bs, 3H), 1.31 (s, 12H, C*H*$_3$), 1.29-1.28 (mt, 2H, C*H*$_2$), 1.17-1.16 (t, 2H, C*H*$_2$), 0.93 (bs, 3H, C*H*$_3$) ppm; ^{13}C{^{1}H} NMR ($CDCl_3$, 100.28 MHz, 298 K): δ 83.13, 37.67, 28.76, 25.35, 24.78, 24.34, 17.21 ppm.

4,4,5,5-tetramethyl-2-(4-methylpentyl)-1,3,2-dioxaborolane (3.6r): ^{1}H NMR ($CDCl_3$, 500 MHz, 298 K): δ 1.44 (bs, 3H), 1.32-1.28 (m, 14H, CH_2 & C*H*$_3$), 0.93-0.91 (d, 3H, C*H*$_3$), 0.83-0.79 (t, 2H, CH_2) ppm; ^{13}C{^{1}H} NMR ($CDCl_3$, 100.28 MHz, 298 K): δ 83.15, 41.88, 34.72, 27.73, 25.37, 24.78, 22.56, 17.22 ppm.

2-hexyl-4,4,5,5-tetramethyl-1,3,2-dioxaborolane (3.6s): ^{1}H NMR ($CDCl_3$, 400 MHz, 298 K): δ 1.46-1.43 (t, 3H, CH_3), 1.33-1.32 (m, 4H, CH_2), 1.29 (s, 12H, CH_3), 0.94-0.91 (m, 4H, C*H*$_3$), 0.84-0.80 (t, 2H, CH_2) ppm; ^{13}C{^{1}H} NMR ($CDCl_3$, 100.28 MHz, 298 K): δ 82.69, 32.02, 31.58, 25.35, 24.70, 23.90, 22.51, 13.99 ppm.

4,4,5,5-tetramethyl-2-octyl-1,3,2-dioxaborolane (3.6t): ^{1}H NMR ($CDCl_3$, 400 MHz, 298 K): δ 1.48-1.45 (t, 3H, CH_3), 1.32-1.31 (m, 8H, CH_2), 1.29 (s, 12H, CH_3), 0.95-0.92 (m, 4H, C*H*$_3$), 0.85-0.81 (t, 2H, CH_2) ppm; ^{13}C{^{1}H} NMR ($CDCl_3$, 100.28 MHz, 298 K): δ 82.67, 32.37, 31.85, 29.20, 24.70, 23.93, 22.61, 14.02 ppm.

2-decyl-4,4,5,5-tetramethyl-1,3,2-dioxaborolane (3.6u): ^{1}H NMR ($CDCl_3$, 500 MHz, 298 K): δ 1.48-1.45 (t, 3H, CH_3), 1.32-1.31 (m, 12H, CH_2), 1.29 (s, 12H, CH_3), 0.96-0.92 (m, 4H, C*H*$_3$), 0.85-0.81 (t, 2H, CH_2) ppm; ^{13}C{^{1}H} NMR ($CDCl_3$, 100.28 MHz, 298 K): δ 82.68, 32.39, 31.89, 29.64, 24.72, 23.96, 22.64, 14.04 ppm.

2-dodecyl-4,4,5,5-tetramethyl-1,3,2-dioxaborolane (3.6v): ^{1}H NMR ($CDCl_3$, 500 MHz, 298 K): δ 1.48-1.45 (t, 3H, CH_3), 1.32-1.31 (m, 16H, CH_2), 1.29 (s, 12H, CH_3), 0.96-0.92 (m, 4H, C*H*$_3$), 0.85-0.81 (t, 2H, CH_2) ppm; ^{13}C{^{1}H} NMR ($CDCl_3$, 100.28 MHz, 298 K): δ 82.66, 32.40, 31.90, 29.68, 24.72, 23.96, 22.65, 14.05 ppm.

2-(2-bromo-2-phenylethyl)-4,4,5,5-tetramethyl-1,3,2-dioxaborolane (3.6w): ^{1}H NMR

($CDCl_3$, 400 MHz, 298 K): δ 7.53-7.51 (d, 2H, Ar*H*), 7.27-7.25 (m, 3H, Ar*H*), 3.83-3.80 (t, 1H, Ar*CH*Br), 3.37-3.34 (d, 2H, ArCHBr*CH*$_2$), 1.20-1.08 (s, 12H, C*H*$_3$) ppm; $^{13}C\{^1H\}$ NMR ($CDCl_3$, 100.28 MHz, 298 K): δ 138.40, 130.89, 128.97, 128.16, 127.18, 117.52, 83.22, 63.70, 33.35, 28.95, 24.76, 24.31 ppm.

4,4,5,5-tetramethyl-2-(2-phenylpropyl)-1,3,2-dioxaborolane (3.6x): ^1H NMR ($CDCl_3$, 400 MHz, 298 K): δ 7.23-7.13 (m, 5H, Ar*H*), 3.18-3.05 (sextet, 1H, ArC*H*Me), 1.33-1.31 (d, 2H, C*H*$_2$) 1.29 (bs, 12H, C*H*$_3$), 1.18 (d, 3H, CH_3) ppm; $^{13}C\{^1H\}$ NMR ($CDCl_3$, 100.28 MHz, 298 K): δ 149.36, 128.22, 126.43, 126.56, 82.82, 81.77, 36.45, 35.73, 25.88, 24.77, 24.40, 22.62 ppm.

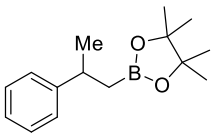

2-(2,2-diphenylethyl)-4,4,5,5-tetramethyl-1,3,2-dioxaborolane (3.6y): ^1H NMR ($CDCl_3$, 400 MHz, 298 K): δ 7.24-6.88 (m, 10H, Ar*H*), 4.23-4.20 (t, 1H, ArC*H*Ph), 1.89-1.87 (d, 1H, ArCH(Me)C*H*$_2$), 1.54-1.51 (d, 1H, ArCH(Me)C*H*$_2$), 1.16 (s, 12H, C*H*$_3$), ppm; $^{13}C\{^1H\}$ NMR ($CDCl_3$, 100.28 MHz, 298 K): δ 149.71, 146.49, 141.11, 128.08, 127.87, 127.31, 125.49, 113.84, 82.84, 46.89, 25.07, 24.49, 23.72 ppm.

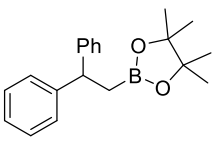

2-(2-methoxypropyl)-4,4,5,5-tetramethyl-1,2-oxaborolane (3.6z): ^1H NMR ($CDCl_3$, 400 MHz, 298 K): δ 3.61 (s, 3H, -OMe), 1.49-1.45 (d, 3H, CH_3), 1.28 (s, 12H, CH_3), 0.96-0.94 (d, 2H, C*H*$_2$), 0.80-0.77 (t, 1H, Me*CH*) ppm; $^{13}C\{^1H\}$ NMR ($CDCl_3$, 100.28 MHz, 298 K): δ 83.07, 52.39, 24.72, 24.45, 22.55, 17.32 ppm.

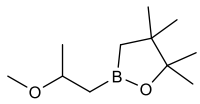

6.3.9: General procedure for the hydroboration of terpenes

Terpene (0.25 mmol), pinacolborane (1.1 equiv., 0.275 mmol), catalyst (10.0 mol% for **3.1**) were mixed together in a Schlenk tube with a magnetic bead inside the glove box. The reaction mixture was allowed to stir at 100 °C for 18 h in neat condition. Volatiles of the mixture were removed under reduced pressure and mesitylene (0.25 mmol) was added while making the NMR in appropriate deuterated solvent. The progress of the reaction was monitored by the ^1H NMR spectroscopy, which indicated the completion of the reaction by the disappearance of alkene (RCH=C*H*$_2$) proton and the appearance of a new RC*H*$_2$C*H*$_2$Bpin resonance.

6.3.10: Spectroscopic data for hydroborated product of terpenes

4,4,5,5-tetramethyl-2-((S)-2-((R)-4-methylcyclohex-3-en-1-yl)propyl)-1,3,2-dioxaborolane

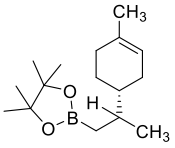

(3.7a): ^{1}H NMR ($CDCl_3$, 400 MHz, 298 K): δ 5.43-5.39 (t, 1H), 1.68 (s, 3H), 1.55-1.40 (m, 1H), 1.40-1.38 (d, 3H), 1.29-1.27 (bs, 16H, CH_3 & CH_2), 1.15-1.14 (d, 2H) ppm; $^{13}C\{^{1}H\}$ NMR ($CDCl_3$, 100.28 MHz, 298 K): δ 149.67, 133.20, 120.21, 107.95, 82.47, 81.92, 40.63, 30.36, 30.14, 27.47, 25.00, 24.07, 23.01, 20.35 ppm.

4,4,5,5-tetramethyl-2-((S)-2-((R)-4-methylcyclohex-3-en-1-yl)propyl)-1,3,2-dioxaborolane

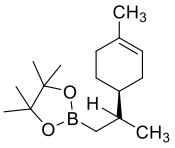

(3.7b): ^{1}H NMR ($CDCl_3$, 400 MHz, 298 K): δ 5.45-5.44 (t, 1H), 1.77 (s, 3H), 1.70-1.69 (d, 3H), 1.42 (m, 2H), 1.31-1.27 (m, 19H, CH_3 & CH_2), 1.17-1.16 (d, 2H) ppm; $^{13}C\{^{1}H\}$ NMR ($CDCl_3$, 100.28 MHz, 298 K): δ 150.02, 133.53, 120.59, 108.33, 83.12, 81.78, 41.02, 30.76, 30.52, 27.85, 24.78, 24.42, 23.37, 22.62, 20.70 ppm.

4,4,5,5-tetramethyl-2-(7-methyl-3-methyleneoct-6-en-1-yl)-1,3,2-dioxaborolane (3.7c): ^{1}H

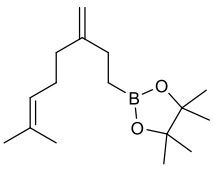

NMR ($CDCl_3$, 400 MHz, 298 K): δ 6.47-6.40 (m, 1H), 5.32-5.28 (m, 1H), 5.24-5.17 (m, 1H), 5.12-5.06 (m, 1H), 2.29-2.25 (t, 2H), 1.76 (s, 3H), 1.67 (s, 3H), 1.47-1.45 (d, 2H), 1.29 (s, 12H, CH_3), 1.19-1.17 (t, 2H) ppm; $^{13}C\{^{1}H\}$ NMR ($CDCl_3$, 100.28 MHz, 298 K): δ 145.98, 138.88, 13.48, 124.06, 115.51, 112.83, 83.04, 82.57, 81.73, 79.34, 31.32, 25.54, 24.74, 22.58, 17.53 ppm.

2-(((1S,2S,5S)-6,6-dimethylbicyclo[3.1.1]heptan-2-yl)methyl)-4,4,5,5-tetramethyl-1,3,2-

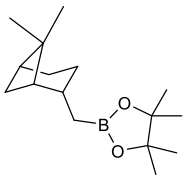

dioxaborolane (3.7d): The ^{1}H NMR spectrum of **3.7d** was not very clean since the proton resonances overlap with the other diastereomer and unreacted starting materials. $^{13}C\{^{1}H\}$ NMR ($CDCl_3$, 100.28 MHz, 298 K): δ 82.73, 82.30, 81.41, 48.37, 40.90, 39.22, 38.38, 36.89, 31.28, 30.77, 27.90, 26.50, 25.01, 24.43, 24.06, 22.26, 19.75, 19.62 ppm.

6.3.11: Competitive experiment for ketone/ester/nitrile/alkyne/alkene hydroboration-chemoselectivity study

Selective hydroboration of acetophenone over styrene in presence of 1 equiv. HBpin:

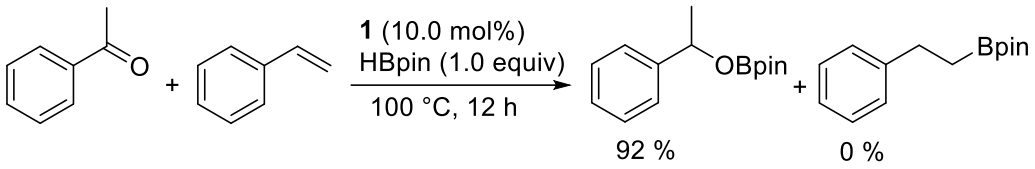

Acetophenone (30.03 mg, 0.25 mmol), styrene (26.03 mg, 0.25 mmol), pinacolborane (32 mg, 0.25 mmol), catalyst (10.0 mol% for **3.1**) were charged in a Schlenk tube inside the glove box. The reaction mixture was stirred for 12 hours at 100 °C after in neat conditions. Upon completion of the reaction, the progress of the reaction was monitored by ^{1}H NMR after addition of mesitylene (0.25 mmol) as an internal standard in $CDCl_3$. A quartet resonance at δ = 5.42-5.36 ppm indicates for the formation of hydroboration product from acetophenone.

Selective hydroboration of ethyl benzoate over styrene in presence of 2 equiv. HBpin:

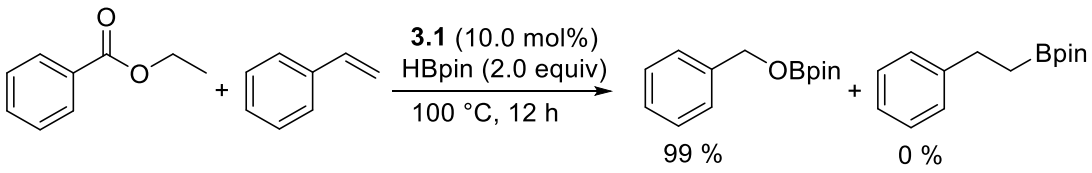

Ethyl benzoate (37.54 mg, 0.25 mmol), styrene (26.03 mg, 0.25 mmol), pinacolborane (32 mg, 0.25 mmol), catalyst (10.0 mol% for **3.1**) were charged in a Schlenk tube inside the glove box. The reaction mixture was stirred for 12 hours at 100 °C after in neat conditions. Upon completion of the reaction, the progress of the reaction was monitored by ^{1}H NMR after addition of mesitylene (0.25 mmol) as an internal standard in $CDCl_3$. A sharp singlet resonance at δ = 4.81 ppm indicates for the formation of hydroboration product from ethyl benzoate.

Hydroboration of phenylacetylene and styrene in presence of 1 equiv. HBpin:

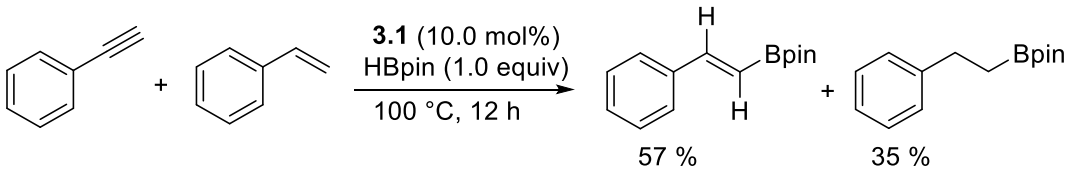

Phenyl acetylene (25.53 mg, 0.25 mmol), styrene (26.03 mg, 0.25 mmol), pinacolborane (32 mg, 0.25 mmol), catalyst (10.0 mol% for **3.1**) were charged in a Schlenk tube inside the glove box. The reaction mixture was stirred for 12 hours at 100 °C after in neat conditions. Upon completion of the reaction, the progress of the reaction was monitored by ^{1}H NMR after addition of mesitylene (0.25 mmol) as an internal standard in $CDCl_3$. Formation of the hydroboration product was identified from the doublet resonanceat δ = 5.90-5.86 ppm for alkyne and triplet resonance at δ = 2.94-2.90 ppm for alkene.

Hydroboration of phenylacetylene and styrene in presence of 2 equiv. HBpin:

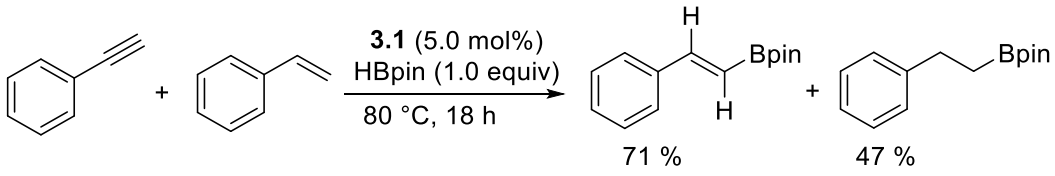

Phenyl acetylene (25.53 mg, 0.25 mmol), styrene (26.03 mg, 0.25 mmol), pinacolborane (32 mg, 0.25 mmol), catalyst (5.0 mol% for **3.1**) were charged in a Schlenk tube inside the glove box. The reaction mixture was stirred for 18 hours at 80 °C after in neat conditions. Upon completion of the reaction, the progress of the reaction was monitored by ^{1}H NMR after addition of mesitylene (0.25 mmol) as an internal standard in $CDCl_3$. Formation of the hydroboration product was identified from the doublet resonanceat δ = 6.10-6.05 ppm for alkyne and triplet resonance at δ = 2.67-2.63 ppm for alkene.

Selective hydroboration of acetophenone over phenyl acetylene in presence of one equiv. HBpin:

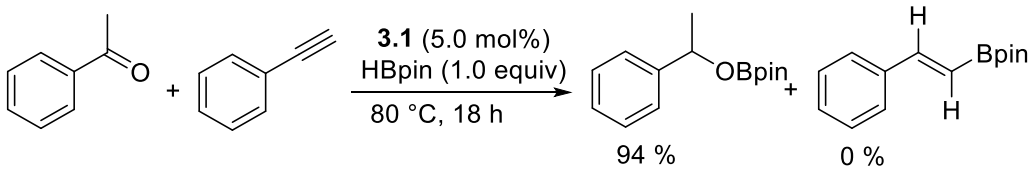

Acetophenone (30.03 mg, 0.25 mmol), phenyl acetylene (25.53 mg, 0.25 mmol), pinacolborane (32 mg, 0.25 mmol), catalyst (5.0 mol% for **3.1**) were charged in a Schlenk tube inside the glove box. The reaction mixture was stirred for 18 hours at 80 °C after in neat conditions. Upon completion of the reaction, the progress of the reaction was monitored by ^{1}H NMR after addition of mesitylene (0.25 mmol) as an internal standard in $CDCl_3$. A quartet resonance at δ = 5.17-5.12 ppm indicates for the formation of hydroboration product from acetophenone.

Selective hydroboration of ethyl benzoate over phenyl acetylene in presence of two equiv. HBpin:

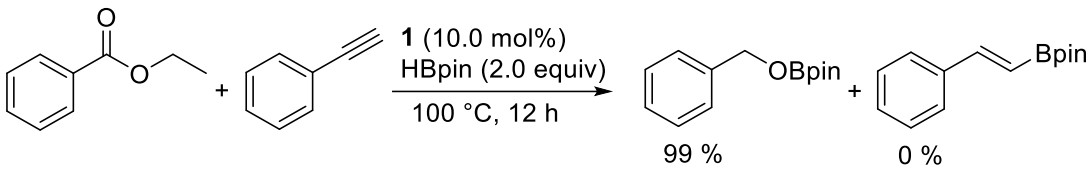

Ethyl benzoate (37.54 mg, 0.25 mmol), phenyl acetylene (25.53 mg, 0.25 mmol), pinacolborane (32 mg, 0.25 mmol), catalyst (10.0 mol% for **3.1**) were charged in a Schlenk tube inside the glove box. The reaction mixture was stirred for 18 hours at 80 °C after in neat conditions. Upon completion of the reaction, the progress of the reaction was monitored by ^{1}H NMR after addition of mesitylene (0.25 mmol) as an internal standard in $CDCl_3$. A sharp singlet resonance at δ = 4.81 ppm indicates for the formation of hydroboration product from ethyl benzoate.

Hydroboration of styrene and benzonitrile in presence of one equiv. HBpin:

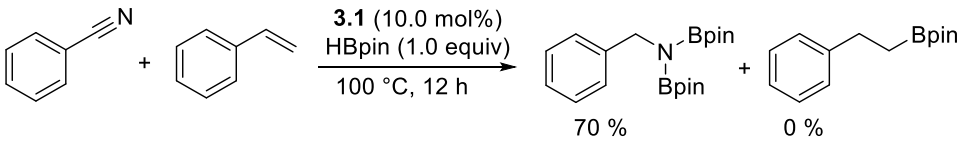

Benzonitrile (25.76 mg, 0.25 mmol), styrene (26.03 mg, 0.25 mmol), pinacolborane (35 mg, 0.27 mmol), catalyst (10.0 mol% for **3.1**) were charged in a Schlenk tube inside the glove box. The reaction mixture was stirred for 12 hours at 100 °C after in neat conditions. Upon completion of the reaction, the progress of the reaction was monitored by ^{1}H NMR after addition of mesitylene (0.25 mmol) as an internal standard in $CDCl_3$. A sharp singlet resonance at δ = 4.22 ppm indicates for the formation of hydroboration product from benzonitrile.

Hydroboration of phenyl acetylene and benzonitrile in presence of one equiv. HBpin:

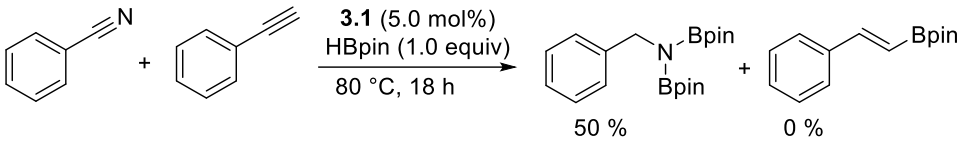

Benzonitrile (25.76 mg, 0.25 mmol), phenyl acetylene (25.53 mg, 0.25 mmol), pinacolborane (35 mg, 0.27 mmol), catalyst (5.0 mol% for **3.1**) were charged in a Schlenk tube inside the glove box. The reaction mixture was stirred for 18 hours at 80 °C after in neat conditions. Upon completion of the reaction, the progress of the reaction was monitored by ^{1}H NMR after addition of mesitylene (0.25 mmol) as an internal standard in $CDCl_3$. A sharp singlet resonance at δ = 4.22 ppm indicates for the formation of hydroboration product from benzonitrile.

6.3.12: Mechanistic investigation for characterization and isolation of intermediate

The stoichiometric reaction of catalyst 3.1 and HBpin:

A solution of HBpin (64/128 mg, 0.50/1.0 mmol) in THF/C_6D_6 was added drop by drop to the THF/C_6D_6 solution of **3.1** (315 mg, 0.50 mmol) at room temperature or inside the glove box. The reaction mixture was stirred/heated for overnight at 80 °C. The reaction mixture was subjected for characterization. ^{1}H NMR (C_6D_6, 400 MHz, 298 K): ^{1}H NMR spectra is not very clean hence it is very difficult to conclude anything from it. The ^{11}B NMR indicates that the Bpin moiety is coordinated to the Mg centre through one of the O-atoms. ^{11}B NMR (C_6D_6, 128 MHz, 298 K): δ 33.38 (s, Me-Bpin), 29.06 (d, J= 173.14 Hz for unreacted HBpin), 22.41 (s, for **INT-8**), 43.75 (s, for zwitter ionic species **INT-7**) ppm.

Reaction of HBpin and 10 mol % of catalyst 3.1:

HBpin (128 mg, 1.0 mmol) was added to the screw cap NMR tube of **3.1** (62.61 mg, 0.1 mmol) at room temperature or inside the glove box. The reaction mixture was stirred/heated for overnight at 100 °C. The reaction mixture was subjected for characterization. Interestingly, ^{11}B NMR shows the same peaks like for the stoichiometric reaction of catalyst **3.1** and HBpin. ^{1}H NMR ($CDCl_3$, 400 MHz, 298 K): Here also, ^{1}H NMR spectra is not very clean hence it is very difficult to conclude anything from it. The ^{11}B NMR is same as stoichiometric reaction of **3.1**

with HBpin; ^{11}B NMR ($CDCl_3$, 128 MHz, 298 K): δ 34.0 (s, Me-Bpin), 28.90 (d, J= 180.33 Hz for unreacted HBpin), 21.92 (s, for **INT-8**), 45.11 (s, for zwitter ionic species) ppm.

Stoichiometric reaction of 3.1 with phenylacetylene or styrene:

No reaction was observed when an equimolar amount of **3.1** was treated separately with phenylacetylene or styrene in THF/toluene solvent at room temperature and at 60-100 °C. Further heating at 80-100 °C overnight in neat conditions also does not indicate any appreciable changes in the ^1H NMR spectra.

Hydroboration of styrene in presence of 10 mol % of TMEDA:

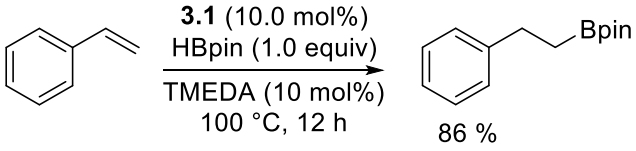

To identify whether the BH_3 is behaving as hidden catalyst in the hydroboration of benzamide or not, we performed the reaction in presence of *N,N,N′,N′*-Tetramethylethylenediamine (TMEDA) as a BH_3 scavenger. A Screw cap NMR tube was charged with HBpin (32 mg, 0.25 mmol, 1.0 equiv), and TEMDA (0.35 mg, 10 mol%) inside the argon-filled glovebox. Subsequently styrene (26.03 mg, 0.25 mmol, 1.0 equiv), was added to the reaction mixture and heated at 100 °C for 12 hours in an oil bath. After completion of the reaction 0.25 mmol mesitylene was added as an internal standard prior to the NMR measurement in $CDCl_3$ solvent. For the mentioned reaction, 86% NMR yield (93% for without TMEDA) for the corresponding borylated product was observed. Which clearly suggest for the non-involvement or very less influence of BH_3 as an active catalyst for the hydroboration of benzamide.

6.3.13: Kinetic study

Kinetics of hydroboration for alkenes/alkynes was studied by performing NMR scale reactions. Styrene is used as substrate for the kinetic study because it is the simplest compound of aromatic alkenes.

The reaction was monitored by ^{1}H NMR analysis at time interval of 20 min and the reaction was performed at 100 °C. The kinetic data was obtained by the proton integral of -CH_2 peak relative to CH_3 protons of mesitylene (internal standard).

General procedure for the rate determination

In argon atmosphere, required amount of HBpin and styrene were taken along with mesitylene. NMR was recorded at room temperature considering it at T= 0 min (no product was observed). Then NMR tube was kept in oil bath at 100 °C temperature and spectra was recorded at the interval of 20 min.

HBpin rate order assessment

Varying concentration of HBpin while keeping styrene concentration constant.

HBpin [M]	Styrene [M]	Rate (M/min)	R^2
0.75	0.25	$8.43\times 10^{-4} \pm 1.67 \times 10^{-5}$	0.99803
0.50	0.25	$14.2 \times 10^{-4} \pm 2.76 \times 10^{-5}$	0.9981
0.25	0.25	$7.78 \times 10^{-4} \pm 9.67 \times 10^{-5}$	0.99923

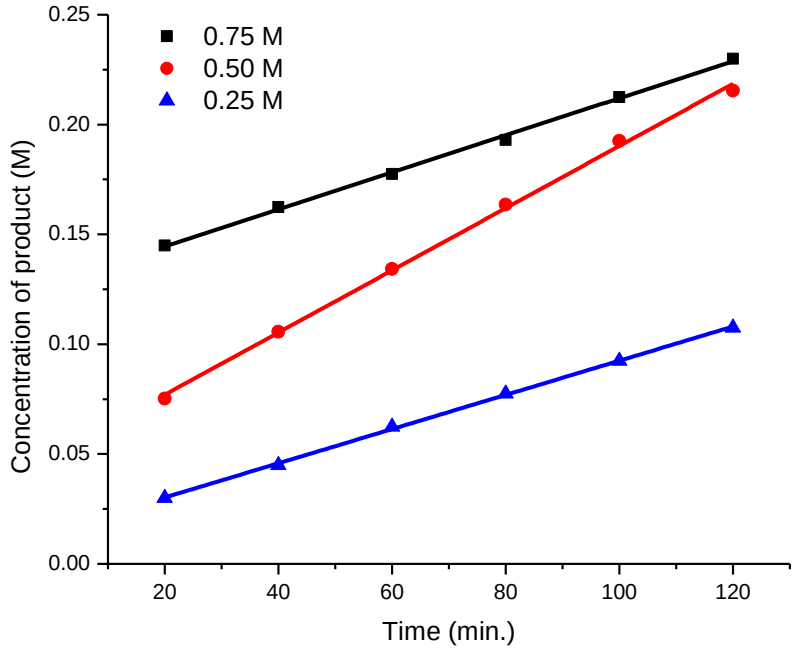

Plot of conc. of product vs. time at different HBpin concentrations.

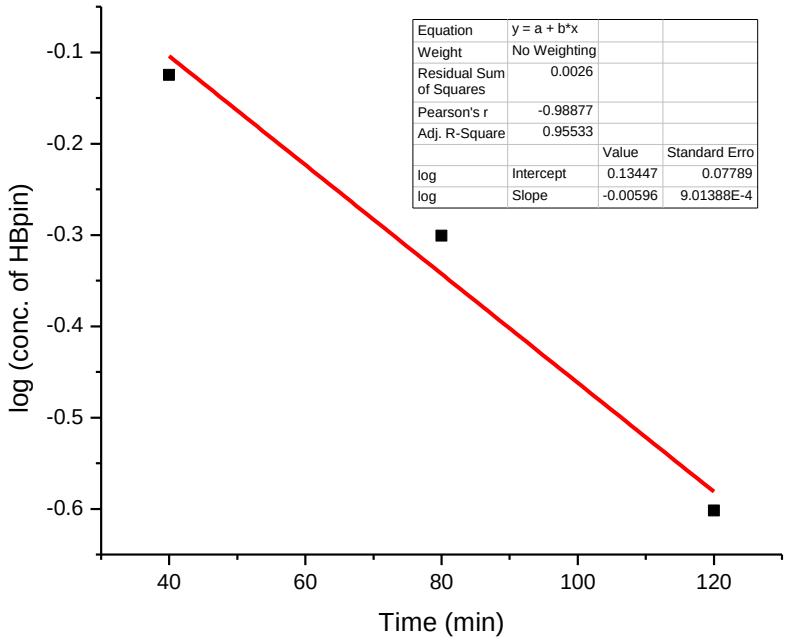

Plot of log (conc. of HBpin) vs. time (min.). This shows first order dependence over HBpin.

Styrene rate order assessment

Varying concentration of styrene while keeping HBpin concentration constant.

HBpin [M]	Styrene [M]	Rate (M/min)	R^2
0.25	0.50	$4.33 \times 10^{-4} \pm 8.42 \times 10^{-6}$	0.99812
0.25	0.25	$7.78 \times 10^{-4} \pm 9.67 \times 10^{-6}$	0.99923
0.25	0.125	$7.51 \times 10^{-4} \pm 9.00 \times 10^{-6}$	0.99928

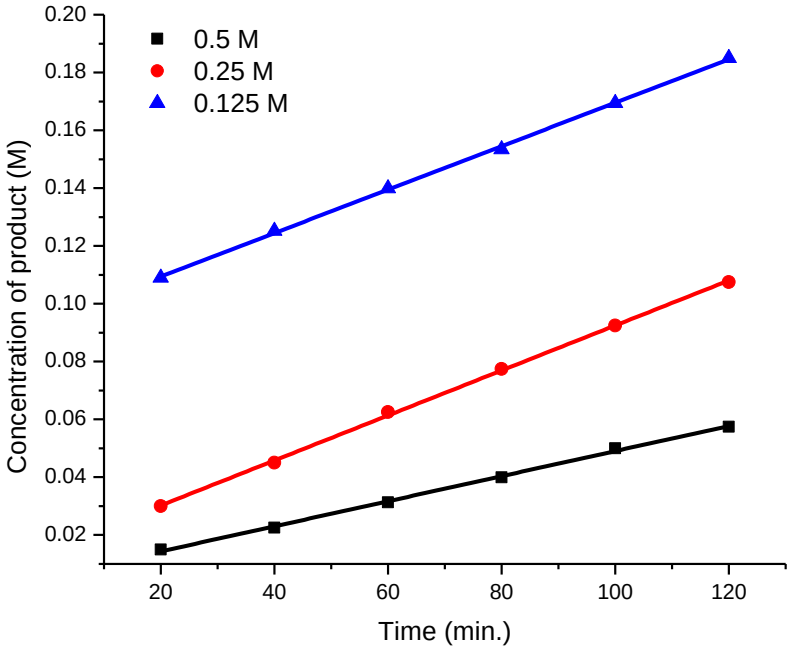

Plot of conc. of product vs. time at different styrene concentrations.

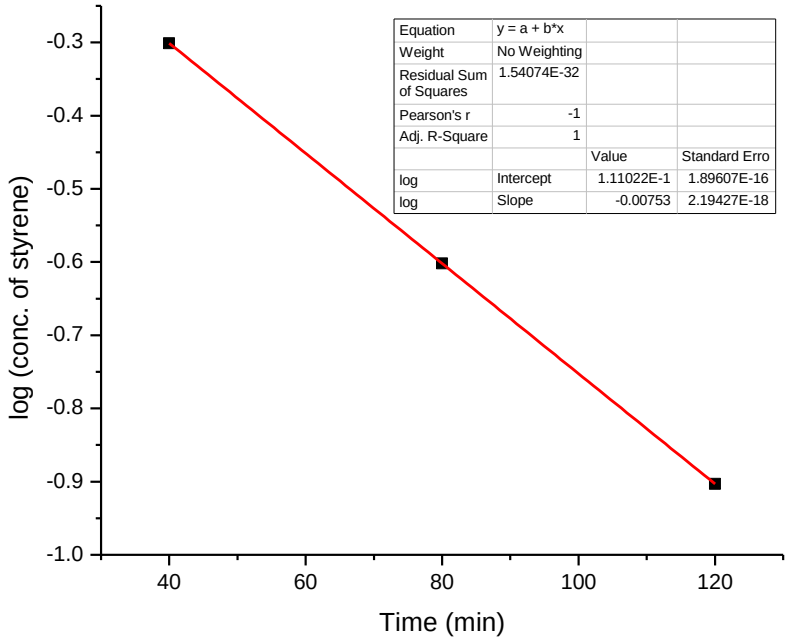

Plot of log (conc. of styrene) vs. time (min.). This shows first order dependence over styrene.

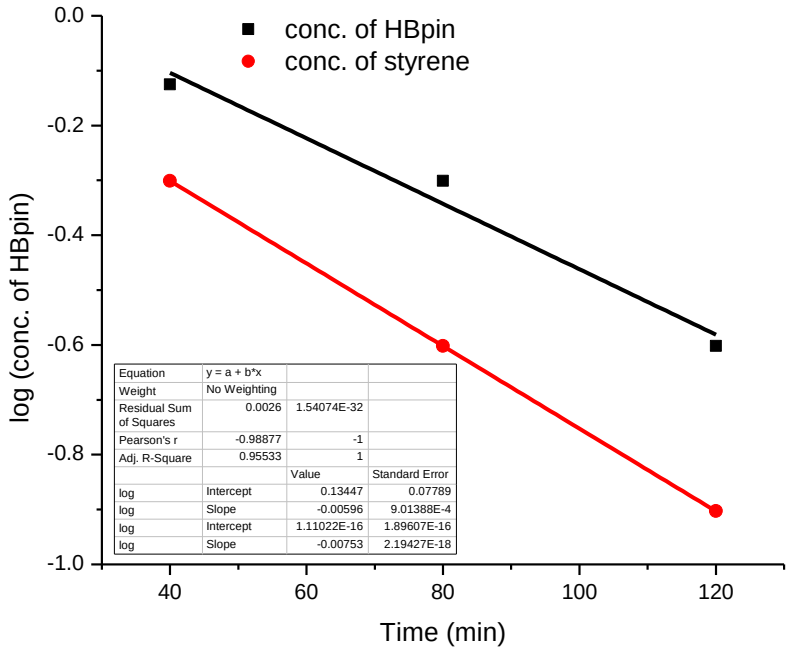

Equation	y = a + b*x		
Weight	No Weighting		
Residual Sum of Squares	0.0026	1.54074E-32	
Pearson's r	-0.98877	-1	
Adj. R-Square	0.95533	1	
		Value	Standard Error
log	Intercept	0.13447	0.07789
log	Slope	-0.00596	9.01388E-4
log	Intercept	1.11022E-16	1.89607E-16
log	Slope	-0.00753	2.19427E-18

Plot of log (conc. of HBpin) *vs* time by varying the concentration of styrene. This indicates that the reaction is second order of the form.

The overall rate law for the hydroboration is presented in equation below:

Rate= k[Styrene][HBPin]

Activation energy of the reaction

In argon atmosphere, equimolar amount of HBpin, catalyst and styrene were taken along with mesitylene in four NMR tubes. ^{1}H NMR was recorded at room temperature considering it at T= 0 min (no product was observed). The NMR tubes were heated at a temperature of 80 °C, 90 °C and 110 °C respectively and ^{1}H NMR spectra was recorded at an interval of 20 minutes up to 2 hours. [styrene]$^{-1}$ *vs* time was plotted and the rate constant at different temperatures were obtained using the second order rate law. Through the obtained rate constants, Arrhenius equation was used to obtain the activation energy of the reaction.

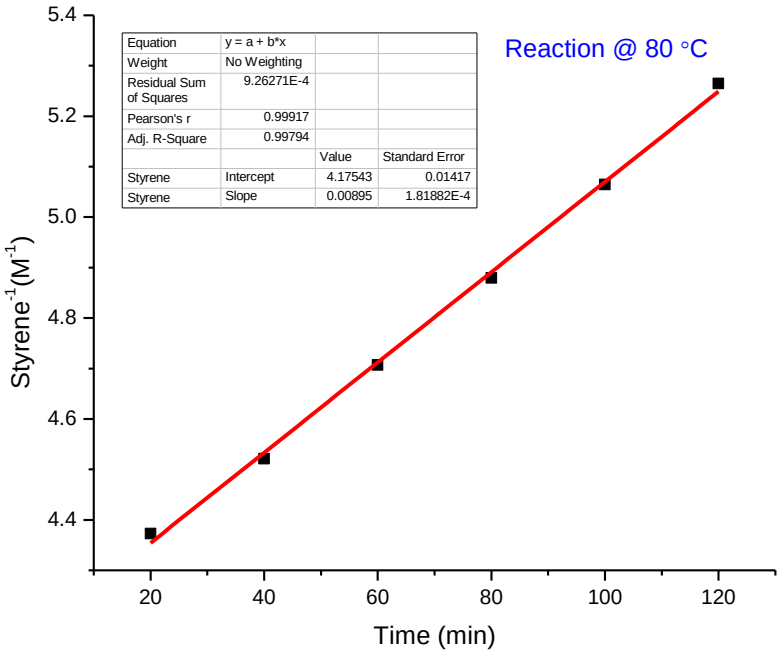

Kobs = 0.00895/(M*min.)

Equimolar reaction between **1**, styrene and HBpin at 80 °C.

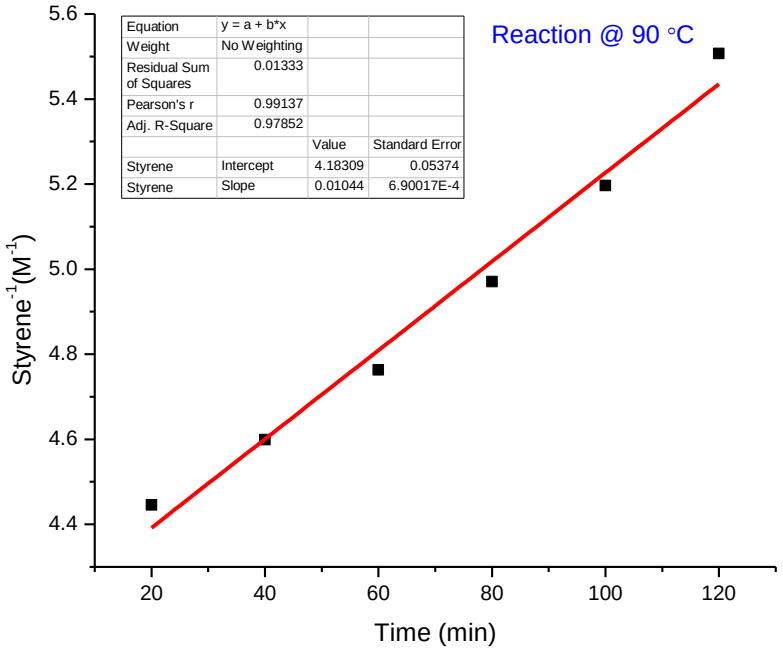

Kobs = 0.01044/(M*min.)

Equimolar reaction between **1**, styrene and HBpin at 90 °C.

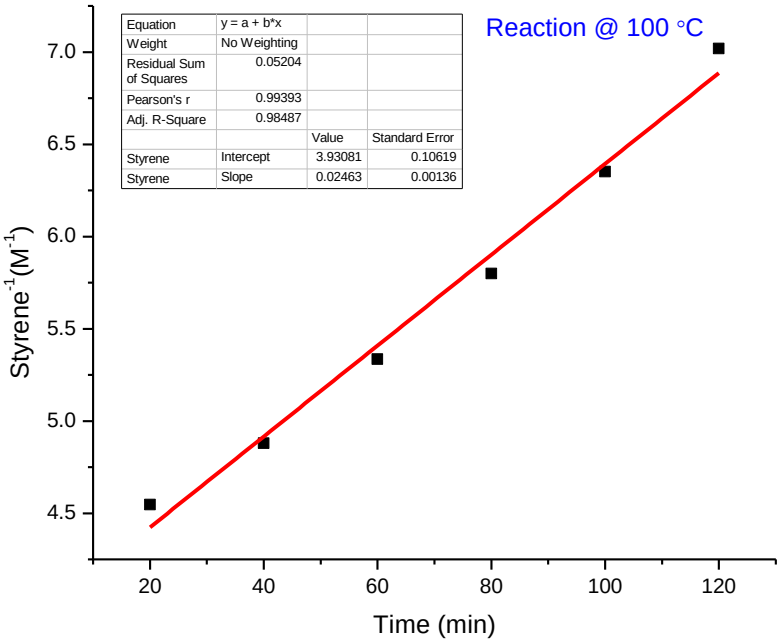

Kobs = 0.02463/(M*min.)

Equimolar reaction between **1**, styrene and HBpin at 100 °C.

Now using Arrhenius equation, a plot of ln(k_{obs}) *vs.* (1/T) was made whose slope will give -Ea/R.

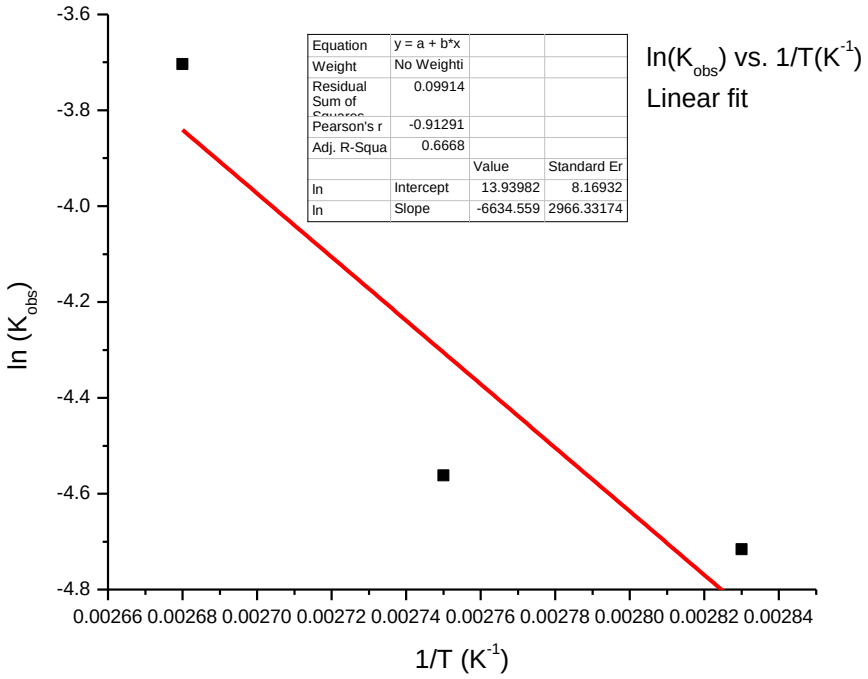

Arrhenius plot of $\ln(K_{obs})$ *vs*. 1/T (K^{-1}).

Slope of Arrhenius plot = -6634.56

-Ea/R = -6634.56

Ea = 55.16 kJ/mol or 13.2 kcal/mol

6.3.14: Details of DFT calculations

Computations were carried out employing density functional theory (DFT) implemented in the Gaussian 09 suite of programs.[12] Geometry optimizations were carried out using gradient-corrected BP86 functional[13] in conjunction with Ahlrichs' split valence plus polarization basis set (def2-SVP)[14] for all the atoms. No symmetry constraints were imposed during structural optimizations. The frequency analyses were executed on the optimized geometries at the same level to ascertain the nature of stationary points on the potential energy surface either as minima or the transition states characterized by first-order saddle points and also to obtain the thermochemical energy values. The minima were identified by having a full set of real frequencies, whereas the transition states possess only one imaginary frequency. The transition states were searched using the linear synchronous transit (LST) method,[15] and subsequent optimizations were performed by utilizing the default Berny algorithm, implemented in the Gaussian 09 code. Intrinsic reaction coordinate (IRC) calculations were enforced to ensure that the transition state connects the corresponding real minima.[16] Furthermore, to improve the accuracy of the energies obtained at the R-BP86/def2-SVP level, single-point calculations were performed on the optimized geometries with the Truhlar's meta-hybrid functional, M06-2X,[17] employing the triple-ζ valence plus polarization basis set (def2-TZVP)[14] for all the atoms. Tight wave function convergence criteria and "ultrafine" (99,950) grid were used in numerical integration during single-point calculations. Additionally, to incorporate the London dispersion effects, we used Grimme's D3 empirical correction.[18] All the reported energy values (ΔG_L) were obtained at the R-M06-2X-D3/def2-TZVP//R-BP86/def2-SVP level.

Moreover, to enrich our understanding towards the origin of activation barriers, distortion–interaction analysis[19] was performed on the optimized geometries of selected transition states.

The distortion–interaction model allows for partitioning the activation barrier of a transition state ($\Delta^{\ddagger}E$) into two physically meaningful terms:

$$\Delta^{\ddagger}E = \Delta^{\ddagger}E_{dist} + \Delta^{\ddagger}E_{int} \qquad (Eq.\ 1)$$

In *Eq.* 1, the destabilizing distortion energy term $\Delta^{\ddagger}E_{dist}$ accounts for the energy required to promote the reactants from their equilibrium geometries to the geometries in the transition state. In contrast, the stabilizing interaction energy term $\Delta^{\ddagger}E_{int}$ corresponds to the energy change upon interaction of the two distorted fragments. Optimized geometries were rendered using CYLview[20] visualization software.

6.4: Chapter 4 experimental details

6.4.1: Synthesis and experimental details of complexes 4.1 and 4.2

Synthetic procedure and characterization data of complex 4.1: Isopropyl magnesium chloride (1.6 mL, 3.19 mmol, 2.0 M in THF) was added to a stirring solution of ligand (**PyPyrH**) (500 mg, 2.90 mmol) in THF (20 mL) at –78 °C. The reaction mixture was kept in cooling bath for 2 hour and then allowed to warm slowly to room temperature and stirred further for 12 h at this temperature. The solvent was removed under vacuum and the residue was extracted with toluene (30 mL). Crystallization was performed in toluene at 4 °C in a freezer. Yield: 1.26 g {94.0 % (without THF molecules) and 64.2 % (with THF molecules). ^{1}H NMR (C_6D_6, 500 MHz, 298 K): δ 9.02 (bs, 2H, *Py*), 7.40-7.38 (d, 2H, *Py*), 7.07-7.03 (t, 2H, *Py*), 6.37-6.33 (t, 2H, *Py*), 6.28 (s, 2H, *Pyr*), 2.93 (bs, 6H, Pyr*CH*$_3$), 2.51 (s, 6H, Pyr*CH*$_3$) ppm; ^{13}C{^{1}H} NMR (C_6D_6, 100.5 MHz, 298 K): δ 158.78, 148.63, 138.16, 131.86, 124.25, 117.67, 115.99, 115.38 (*Py* & *Pyr*), 17.93, 16.23 (*CH*$_3$) ppm. ESI-HRMS: calculated for $C_{50}H_{76}K_2N_6O_2$ $[M+H]^+$: 677.2648; found: 677.5099.

Synthetic procedure and characterization data of complex 4.2: **Method (i)** Isopropyl magnesium chloride (1.6 mL, 3.19 mmol, 2.0 M in THF) was added to a stirring solution of ligand (**PyPyrH**) (500 mg, 2.90 mmol) in THF (20 mL) at –78 °C. The reaction mixture was kept

in cooling bath for 2 hour and then allowed to warm slowly to room temperature and stirred further for 12 h at this temperature. The solvent was removed under vacuum and the residue was extracted with toluene (30 mL). Crystallization was performed in toluene at 4 °C in a freezer. Yield: 0.920 g {86.8 % (without THF molecule) and 72.4 % (with THF molecule). ^{1}H NMR (C_6D_6, 500 MHz, 298 K): δ 8.97 (bs, 2H, *Py*), 7.39-7.37 (d, 2H, *Py*), 7.03-7.00 (t, 2H, *Py*), 6.29 (bs, 4H, *Py* & *Pyr*), 2.78 (bs, 6H, Pyr*CH*$_3$), 2.54 (s, 6H, Pyr*CH*$_3$) ppm; ^{13}C{^{1}H} NMR (C_6D_6, 100.5 MHz, 298 K): δ 157.09, 148.63, 138.54, 132.17, 124.45, 117.88, 115.73 (*Py* & *Pyr*), 17.70, 16.07 (*CH*$_3$) ppm. ESI-HRMS: calculated for $C_{50}H_{76}K_2N_6O_2$ $[M+H]^+$: 439.2270; found: 439.6562.

Method (ii) *n*BuLi (1.6 mL, 3.19 mmol, 2.0 M solution in cyclohexane) was added to a stirring solution of ligand (**PyPyrH**) (500 mg, 2.90 mmol) in THF (20 mL) at –78 °C. The reaction mixture was kept in cooling bath for 30 min and then allowed to warm slowly to room temperature and stirred further for 4 h at this temperature. Again, reaction mixture was cooled to -78 C and methyl magnesium bromide (1.03 mL, 3.19 mmol, 3.1 M in THF) was added at this temperature. The reaction mixture was kept in cooling bath for 2 hours and then allowed to warm slowly to room temperature and stirred further for 4 h at this temperature. The solvent was removed under vacuum and the residue was extracted with toluene (30 mL). Crystallization was performed in toluene at 4 °C in a freezer.

Method (iii) *n*BuLi (1.6 mL, 3.19 mmol, 2.0 M solution in cyclohexane) was added to a stirring solution of ligand (**PyPyrH**) (500 mg, 2.90 mmol) in THF (20 mL) at –78 °C. The reaction mixture was kept in cooling bath for 30 min and then allowed to warm slowly to room temperature and stirred further for 4 h at this temperature. Again, the reaction mixture was cooled to -78 C and isopropyl magnesium chloride (1.6 mL, 3.19 mmol, 2.0 M in THF) was added at this temperature. The reaction mixture was kept in cooling bath for 2 hours and then allowed to warm slowly to room temperature and stirred further for 4 h at this temperature. The solvent was removed under vacuum and the residue was extracted with toluene (30 mL). Crystallization was performed in toluene at 4 °C in a freezer. Compared to method (i), a little discrepancy was observed in the yield of compound **4.2** with these methods (ii) and (iii).

6.4.2: Crystal structure details of complexes 4.1 and 4.2

Crystal data of 4.1: CCDC number- 2189747, $C_{34}H_{43}Cl_2Mg_2N_4O_3$, M=675.24, green, block, 0.32 x 0.21 x 0.15 mm^3, monoclinic, space group *Cc*, *a*=8.8994(7)Å, *b*=24.393(3)Å, *c*=16.1873(14)Å, *α*= 90°, β=105.719(3)°, *γ*=90°, *V*=3382.6(5)$Å^3$, *Z*=4, *T*=100(2) K, 2θmax=50.00°, *Dcalc* (g cm^{-3})=1.326, *F*(*000*)=1428, μ (mm^{-1})=0.270, 10000 reflections collected, 9221 unique reflections (*R*int=0.0552), 9625 observed ($I > 2\sigma$ (*I*)) reflections, multi-scan absorption correction, *T*min=0.917, *T*max=0.960, 440 refined parameters, *S*=1.148, *R*1=0.0552, *wR*2=0.1406 (all data *R*=0.0611, *wR*2=0.1452), maximum and minimum residual electron densities; *Δ*ρmax=0.587, *Δ*ρmin=-0.352 ($eÅ^{-3}$).

Crystal data of 4.2: CCDC number- 2189748, $C_{26}H_{30}MgN_4O$, M=438.85, green, block, 0.33 x 0.25 x 0.12 mm^3, monoclinic, space group *Pc*, *a*=9.1371(8)Å, *b*=16.8002(17)Å, *c*= 8.3053(8)Å, *α*=90°, β=116.752(3)°, *γ*=90°, *V*=1138.44(19)$Å^3$, *Z*=2, *T*=100(2) K, 2θmax=50.00°, *Dcalc* (g cm^{-3})=1.280, *F*(*000*)=468, μ (mm^{-1})=0.104, 4542 reflections collected, 3863 unique reflections (*R*int=0.0824), 4503 observed ($I > 2\sigma$ (*I*)) reflections, multi-scan absorption correction, *T*min=0.966, *T*max=0.988, 543 refined parameters, *S*=1.141, *R*1=0.0824, *wR*2=0.1595 (all data *R*=0.0970, *wR*2=0.1662), maximum and minimum residual electron densities; *Δ*ρmax=0.464, *Δ*ρmin=-0.238 ($eÅ^{-3}$).

6.4.3: Photophysical investigations and quantum yield measurement details

A Shimadzu UV−vis−IR (UV3600 Plus) spectrophotometer was used for optical absorption measurements. Absorption measurements of solid compounds were carried out with the help of an integrating sphere (ISR-603), attached to a Shimadzu UV-3600 Plus spectrophotometer. Steady-state emission spectra were collected in a Fluoromax-4 spectrofluorometer (Horiba, Jobin Yvon, USA). A spectrofluorometer FS5 (Edinburgh Instruments) was used for lifetime measurements of solid compounds using their SC-05 and SC-10 attachments (EPLED-330 picosecond pulsed diode LASER).

Absolute quantum yield was estimated by using the integrating sphere method in a Fluoromax-4 spectrofluorometer (Horiba, Jobin Yvon, USA).

6.4.4: Computational details

All the calculations were performed with Gaussian 09 program package.[12] Geometry of the ligand PyPyrH, **4.1** and **4.2** were optimized by employing B3LYP-D3/def2-SVP level of theory.[21-25] The optimized geometries were confirmed to be true minima by performing harmonic vibrational frequency calculations. The B3LYP-D3/def2-SVP optimized geometries were further used to carry out single point time-dependent density functional theory (TD-DFT) calculations to obtain the absorption spectra at the triple-ζ (def2-TZVPP) level of theory along with B3LYP[21-24], BP86[26,27], cam-B3LYP[28], M06-2X[29], ωb97XD[30], PBE0[31], and B97D3[25,32] functionals. To obtain the emission spectra, TD-DFT calculations were performed to optimize the excited S_1 states by employing B3LYP-D3/def2-SVP level of theory. These optimized S_1 states were further used to generate the fluorescence spectra by carrying out single point calculations at different level of theories whose absorption spectra (λ^{abs}) were close to the experimentally obtained values (Table-S3). To gain further insights, natural transition orbitals (NTOs) associated with the $S_1 \rightarrow S_0$ emission were evaluated at the M06-2X/def2-TZVPP//B3LYP-D3/def2-SVP level of theory.

The reorganization energies (λ^{RE}) were also calculated at the M06-2X/def2-TZVPP//B3LYP-D3/def2-SVP level of theory. The λ^{RE} consist of the external and internal reorganization energy.[33,34] The external reorganization energy caused by the polarization of the medium can be negligible.[35,36] The internal reorganization energy is caused by the geometrical deformation in the Franck–Condon vertical absorption transition and radiative process, and the value can be estimated as the following.[37,38]

6.5: Experimental details of chapter 5

6.5.1: Synthesis and experimental details of complex 5.1 and 5.2

Synthesis and characterization data for complex 5.1: Potassium bis(trimethylsilyl) amide (0.75 g, 3.78 mmol) in THF was added to a stirring solution of ligand (**L5.1**) (1.5 g, 3.78 mmol) in THF (20 mL) at –78 °C. The reaction mixture was allowed to warm slowly to room

temperature and stirred further for 12 h at this temperature. The reaction mixture was allowed to warm to room temperature and then stirred for overnight. The solvent was removed under vacuum and the residue was extracted with toluene (30 mL) to remove LiI. Crystallization was performed in toluene at –35 °C in a freezer. Yield: 2.10 g (64.01 %). ^{1}H NMR ($CDCl_3$, 400 MHz, 298 K): *δ* 8.54-8.53 (d, 1H, *Ph*), 7.65-7.56 (m, 2H, *Ph*), 7.22-7.14 (m, 2H, *Ph*), 6.83 (d, 1H, *Ph*), 3.69 (s, 4H, N*CH*$_2$*CH*$_2$), 2.66 (s, 4H, Ph*CH*$_2$*CH*$_2$Py), 2.27 (s, 3H, *CH*$_3$), 2.25 (s, 3H, *CH*$_3$), 1.43 (s, 9H, *t*Bu), 1.29 (s, 9H, *t*Bu) ppm; ^{13}C{^{1}H} NMR ($CDCl_3$, 100.5 MHz, 298 K): *δ* 159.41, 151.06, 154.10, 148.87, 140.24, 136.44, 135.31, 128.99, 128.18, 123.32, 123.18, 122.71, 122.91, 121.34 (*Ph*), 64.45, 61.99, 55.12, 54.25, 42.41, 41.56, 38.41, 34.07, 31.67, 29.55 ppm. ESI-HRMS: calculated for $C_{50}H_{76}K_2N_6O_2$ $[M+H]^+$: 870.5304; found: 398.3157 (Compound was decomposed and only ligand mass came).

Synthesis and characterization data for compound 5.2: MeLi (1.34 mL, 4.15 mmol, 3.1 M solution in diethoxy methane) was added to a stirring solution of ligand (**L5.1**) (1.5 g, 3.78 mmol) in THF (20 mL) at –78 °C. The reaction mixture was allowed to warm slowly to room temperature and stirred further for 2 h at this temperature. This solution was transferred by a cannula to a suspension of CaI_2 (1.1 g, 3.78 mmol) in THF (15 mL) at –78 °C. The reaction mixture was allowed to warm to room temperature and then stirred for overnight. The solvent was removed under vacuum and the residue was extracted with toluene (30 mL) to remove LiI. Crystallization was performed in THF:toluene mixture (1:4) –35 °C in a freezer. Yield: 2.21 g {84.03 % (without THF molecules), 69.71 % (with THF molecules). ^{1}H NMR ($CDCl_3$, 400 MHz, 298 K): *δ* 7.75-7.72 (m, 1H, *Ph*), 7.25-7.16 (m, 4H, *Ph*), 2.35 (s, 4H, N*CH*$_2$*CH*$_2$), 2.29 (s, 3H, N*CH*$_3$), 2.10 (s, 3H, N*CH*$_3$), 1.49 (s, 9H, *t*Bu), 1.30 (s, 9H, *t*Bu) ppm; ^{13}C{^{1}H} NMR ($CDCl_3$, 100.5 MHz, 298 K): *δ* 157.66, 151.06, 150.22, 138.16, 137.77, 128.95, 128.14, 125.21, 123.10, 122.87 (*Ph*), 68.27, 62.86, 43.14, 34.72, 34.33, 31.47, 30.49, 25.41, 21.38 ppm. ESI-HRMS: calculated for $C_{33}H_{54}CaI_2LiN_3O_3$ $[M+H]^+$: 841.2040; found: 841.9728.

6.5.2: Crystal structure details of complex 5.1 and 5.2

Crystal data of 5.1. CCDC number- 2111877, $C_{50}H_{76}K_2N_6O_2$, M=870.53, colourless, cubic, 0.31 x 0.22 x 0.15 mm^3, triclinic, space group *P-1*, *a*=11.138(5)Å, *b*=11.145(4)Å, *c*=12.916(7)Å, α= 111.710(15)°, β=101.123(19)°, γ=96.150(18)°, *V*=1433.4(11)$Å^3$, *Z*=1, *T*=100(2) K, $2\theta_{max}$=50.00°, D_{calc} (g cm^{-3})=1.132 , *F*(*000*)=526, μ (mm^{-1})= 0.209, 7131 reflections collected, 6328 unique reflections (R_{int}=0.0576), 9829 observed (*I* > 2σ (*I*)) reflections, multi-scan absorption correction, T_{min}=0.936, T_{max}=0.939, 313 refined parameters, *S*=1.388, *R*1=0.0576, *wR*2=0.1802 (all data *R*=0.0654, *wR*2=0.1929), maximum and minimum residual electron densities; $\Delta\rho_{max}$=0.741, $\Delta\rho_{min}$=-0.836 ($eÅ^{-3}$).

Crystal data of 5.2. CCDC number- 2111874, $C_{33}H_{54}CaI_2LiN_3O_3$, M=841.20, colourless, cubic, 0.32 x 0.21 x 0.14 mm^3, triclinic, space group *P-1*, *a*=9.9041(6)Å, *b*=10.6928(7)Å, *c*=20.8692(13)Å, α=85.481(2)°, β=89.389(2)°, γ=86.494(2)°, *V*=2199.1(2)$Å^3$, *Z*=2, *T*=100(2) K, $2\theta_{max}$=50.00°, D_{calc} (g cm^{-3})=1.410 , *F*(*000*)=952, μ (mm^{-1})=1.583, 12920 reflections collected, 10925 unique reflections (R_{int}= 0.0311), 9593 observed (*I* > 2σ (*I*)) reflections, multi-scan absorption correction, T_{min}=0.631, T_{max}=0.809, 460 refined parameters, *S*=0.996, *R*1=0.0311, *wR*2=0.1154 (all data *R*=0.0412, *wR*2=0.1262), maximum and minimum residual electron densities; $\Delta\rho_{max}$=1.250, $\Delta\rho_{min}$=-1.194 ($eÅ^{-3}$).

6.5.3: General procedure for the cyclotrimerization of isocyanates

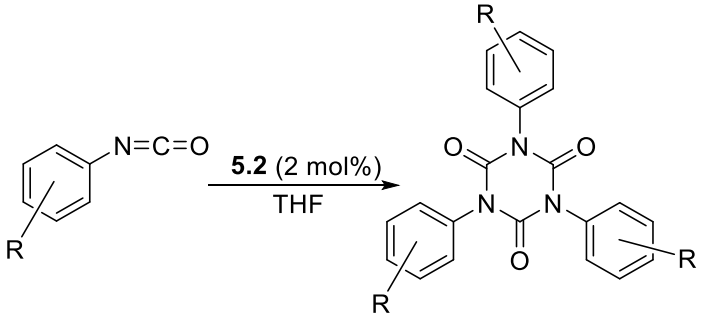

Cyclotrimerization of isocyanates catalysed by compound **5.2**.

A 50 mL Schlenk tube was charged with calcium compound **5.2** (2 mol%), 3 mL of tetrahydrofuran was added, and then aryl isocyanate (3 mmol) was added dropwise through a

syringe with stirring. The solution became cloudy gradually and the white suspension was stirred at room temperature for 1-12 h depending on the substrate after the addition was completed. The resulting suspension was concentrated under reduced pressure and washed with diethyl ether (3 × 10 mL), which gave the corresponding isocyanurate as a white solid. All of the products were characterized by NMR spectroscopy, mass spectrometry and some of the compounds by single crystal XRD.

6.3.4: Spectroscopic data for cyclotrimerized product of isocyanates

5.3a: 1,3,5-Tris(4-methoxyphenyl)-1,3,5-triazinane-2,4,6-trione

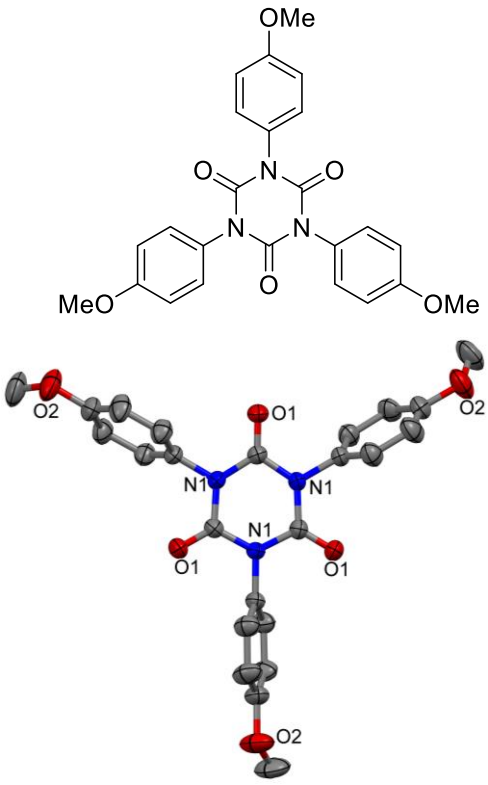

Molecular structure of **5.3a** with anisotropic displacement parameters depicted at the 50 % probability level. Hydrogen atoms are not shown for clarity.

White solid, yield: 98%. ^{1}H NMR (400 MHz, $CDCl_3$) δ 7.12-7.10 (d, 2H), 6.81-6.79 (d, 2H), 3.64 (s, 3H). ^{13}C NMR (100.28 MHz, $CDCl_3$) δ 159.83, 149.09, 129.37, 126.23, 114.53, 55.43. ESI-HRMS: calculated for $C_{24}H_{21}N_3O_3$ $[M+H]^+$: 448.1430; found: 448.1490.

Interestingly, when reaction of 4-methoxy phenyl isocyanate was performed in C_6D_6, then both the dimerized (**5.3a'**) as well as trimerized (**5.3a**) products were observed which were characterized by single crystal X-ray diffraction. But when reaction was performed in THF, only trimerized product was observed.

5.3a': 1,3-bis(4-methoxyphenyl)-1,3-diazetidine-2,4-dione

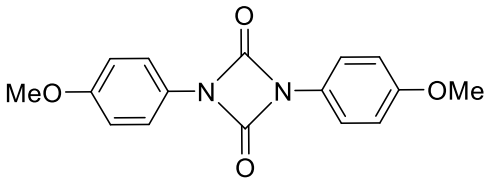

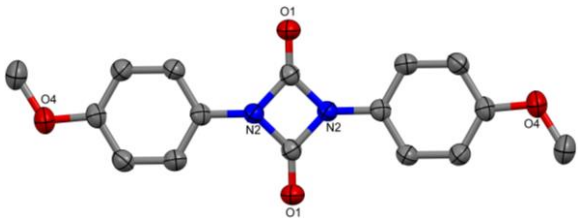

Molecular structure of **5.3a'** with anisotropic displacement parameters depicted at the 50 % probability level. Hydrogen atoms are not shown for clarity.

White solid: 4% yield. ^{1}H NMR (400 MHz, C_6D_6) δ 6.56-6.54 (d, 2H), 6.47-6.44 (d, 2H), 3.17 (s, 3H). ^{13}C NMR (100.28 MHz, $CDCl_3$) δ 157.83, 128.85, 115.01, 55.02.

5.3b: 1,3,5-tris(4-bromophenyl)-1,3,5-triazinane-2,4,6-trione

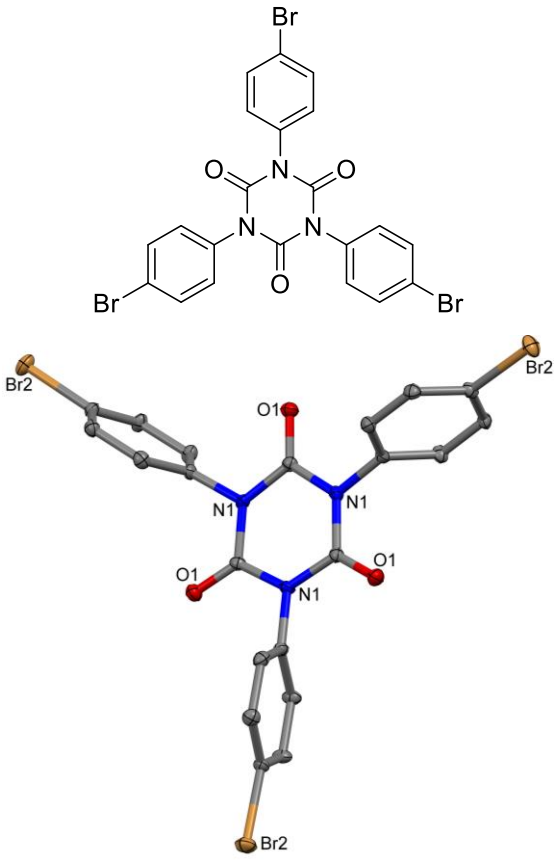

Molecular structure of **5.3b** with anisotropic displacement parameters depicted at the 50 % probability level. Hydrogen atoms are not shown for clarity.

White solid, yield: 98%. ^{1}H NMR (400 MHz, $CDCl_3$) δ 7.56-7.54 (d, 2H), 7.19-7.17 (d, 2H). ^{13}C NMR (100.28 MHz, $CDCl_3$) δ 147.98, 132.88, 130.01, 123.66. ESI-HRMS: calculated for $C_{21}H_{12}Br_3N_3O_3$ $[M+H]^+$: 591.8429; found: 591.8486.

5.3c: 1,3,5-tris(2,6-diisopropylphenyl)-1,3,5-triazinane-2,4,6-trione

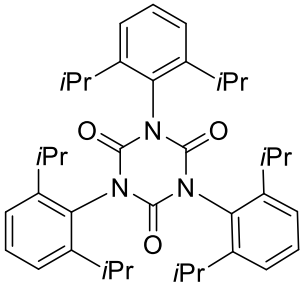

White solid, yield: 85%. ^{1}H NMR (400 MHz, $CDCl_3$) δ 7.48-7.39 (dd, 1H), 7.31-7.30 (d, 2H), 3.40-3.33 (sept, 2H), 1.41-1.39 (d, 12H). ^{13}C NMR (100.28 MHz, $CDCl_3$) δ 147.60, 146.19, 143.01, 130.27 128.60, 126.05, 123.34, 29.51, 28.68, 28.55, 22.84. ESI-HRMS: calculated for $C_{39}H_{51}N_3O_3$ $[M+H]^+$: 610.3930; found: 610.3994.

5.3d: 1,3,5-tris(2,6-dimethylphenyl)-1,3,5-triazinane-2,4,6-trione

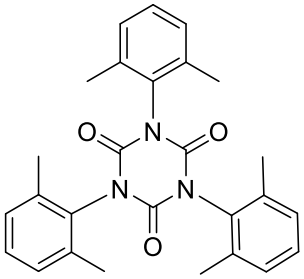

White solid, yield: 86%. ^{1}H NMR (400 MHz, $CDCl_3$) δ 7.66-7.64 (d, 2H), 7.31-7.29 (d, 2H), 1.43 (s, 3H), 1.31 (s, 3H). ^{13}C NMR (100.28 MHz, $CDCl_3$) δ 148.03, 132.67, 130.06, 123.63, 51.63, 31.65, 29.59. ESI-HRMS: calculated for $C_{27}H_{27}N_3O_3$ $[M+H]^+$: 442.2052; found: 442.3051.

5.3e: 1,3,5-tris(2,4-dichlorophenyl)-1,3,5-triazinane-2,4,6-trione

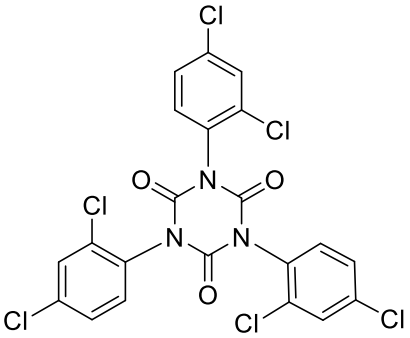

White solid, yield: 90%. ^{1}H NMR (400 MHz, $CDCl_3$) δ 8.20-8.18 (d, 1H), 7.70 (s, 1H), 7.51 (s, 1H), 7.39 (s, 1H). ^{13}C NMR (100.28 MHz, $CDCl_3$) δ 151.67, 132.97, 132.25, 131.28, 128.88, 127.89, 124.38, 122.44. ESI-HRMS: calculated for $C_{21}H_9Cl_6N_3O_3$ $[M+H]^+$: 560.8775; found: 561.8793

5.3f: 1,3,5-tri(naphthalen-1-yl)-1,3,5-triazinane-2,4,6-trione

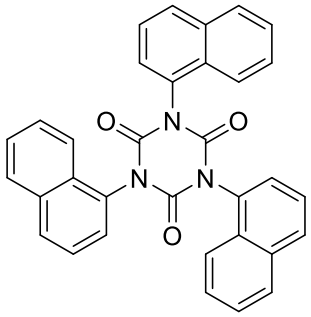

White solid, yield: 95%. ^{1}H NMR (400 MHz, $CDCl_3$) δ 7.99-7.94 (m, 3H), 7.72-7.70 (d, 2H), 7.59-7.57 (d, 2H). ^{13}C NMR (100.28 MHz, $CDCl_3$) δ 148.73, 134.49, 130.27, 128.92, 127.71, 127.27, 126.53, 125.40, 122.63, 121.95, 120.76. ESI-HRMS: calculated for $C_{33}H_{21}N_3O_3$ $[M+H]^+$: 507.1583; found: 508.1631.

5.3g: 1,3,5-tri-o-tolyl-1,3,5-triazinane-2,4,6-trione

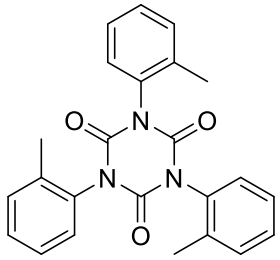

White solid, yield: 92%. ^{1}H NMR (400 MHz, $CDCl_3$) δ 7.24-7.23 (d, 2H), 7.19-7.17 (d, 1H), 7.11-7.10 (d, 1H), 2.24 (s, 3H). ^{13}C NMR (100.28 MHz, $CDCl_3$) δ 147.92, 135.63, 132.67, 131.15, 129.73, 128.57, 127.18, 118.53, 114.86, 51.58. ESI-HRMS: calculated for $C_{24}H_{21}N_3O_3$ $[M+H]^+$: 399.1583; found: 400.1649.

5.3h: 1,3,5-tris(3-nitrophenyl)-1,3,5-triazinane-2,4,6-trione

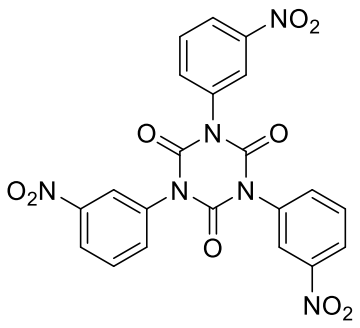

White solid, yield: 85%. ^{1}H NMR (400 MHz, $CDCl_3$) δ 7.60-7.58 (d, 2H), 7.50 (s, 1H), 7.31-7.29 (d, 1H), 6.97-6.94 (d, 1H). ^{13}C NMR (100.28 MHz, $CDCl_3$) δ 129.91, 120.58, 113.19, 109.04. ESI-HRMS: calculated for $C_{21}H_{12}N_6O_9$ $[M+H]^+$: 492.0666; found: 493.0730.

5.3i: 4,4',4''-(2,4,6-trioxo-1,3,5-triazinane-1,3,5-triyl) tribenzonitrile

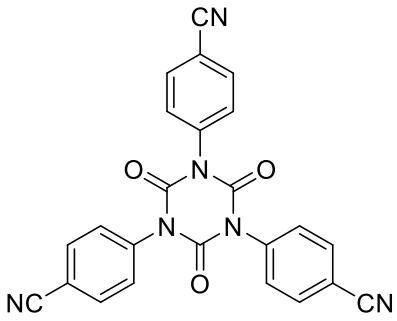

White solid, yield: 90%. ^{1}H NMR (400 MHz, $CDCl_3$) δ 7.84-7.82 (d, 2H), 7.56-7.53 (d, 2H). ^{13}C NMR (100.28 MHz, $CDCl_3$) δ 133.84, 133.38, 129.05, 128.14, 114.46. ESI-HRMS: calculated for $C_{24}H_{12}N_6O_3$ $[M+H]^+$: 432.0971; found: 433.2458.

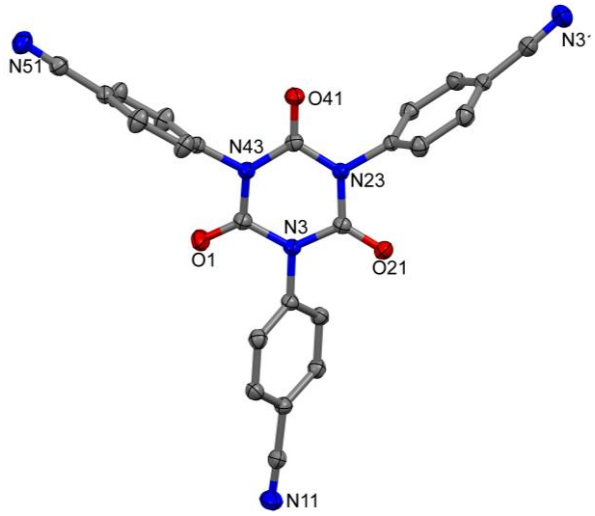

Molecular structure of **5.3i** with anisotropic displacement parameters depicted at the 50 % probability level. Hydrogen atoms are not shown for clarity.

5.3j: 1,3,5-tris(4-chlorophenyl)-1,3,5-triazinane-2,4,6-trione

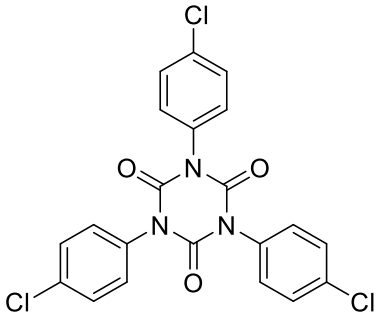

White solid, yield: 88%. ^{1}H NMR (400 MHz, $CDCl_3$) δ 7.50-7.47 (d, 2H), 7.34-7.32 (d, 2H). ^{13}C NMR (100.28 MHz, $CDCl_3$) δ 148.13, 135.59, 131.71, 129.72. ESI-HRMS: calculated for $C_{21}H_{12}Cl_3N_3O_3$ $[M+H]^+$: 458.9944; found: 459.9982.

5.3k: 1,3,5-tris(4-fluorophenyl)-1,3,5-triazinane-2,4,6-trione

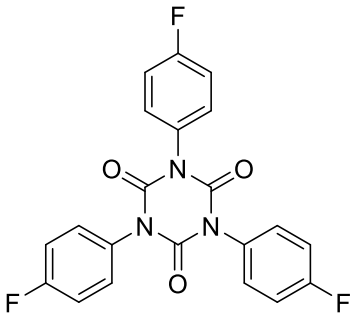

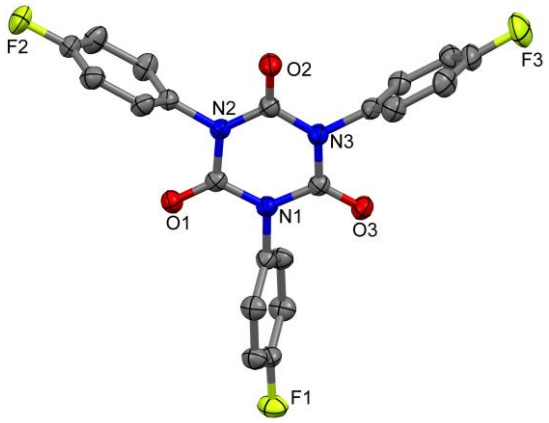

Molecular structure of **5.3k** with anisotropic displacement parameters depicted at the 50 % probability level. Hydrogen atoms are not shown for clarity.

White solid, yield: 95%. ^{1}H NMR (400 MHz, $CDCl_3$) δ 7.39-7.36 (d, 2H), 7.19-7.17 (d, 2H). ^{13}C NMR (100.28 MHz, $CDCl_3$) δ 163.98, 161.50, 148.51, 130.18, 129.21, 116.63, 116.40. ESI-HRMS: calculated for $C_{21}H_{12}F_3N_3O_3$ $[M+H]^+$: 411.0831; found: 412.0892.

6.5.5: Details of DFT calculations

The quantum chemical calculations have been performed using density functional theory (DFT), as a tool with the aid of the Turbomole 7.0 suite of programs. The PBE functional, and the TZVP basis set has been employed. The resolution of identity (RI), along with the multipole accelerated resolution of identity (marij) approximations have been used for an accurate and efficient treatment of the electronic Coulomb term in the DFT calculations. Solvent correction were incorporated with optimization calculations using the COSMO model, with tetrahydrofuran (THF, ε = 7.58) as the solvent. The option "disp" provided in the Turbomole package (DFT-D3) was employed for dispersion-corrected DFT calculations. The values reported are ΔG values, with zero point energy corrections, internal energy and entropic contributions included through frequency calculations on the optimized minima with the temperature taken to be 298.15 K. Harmonic frequency calculations were performed for all stationary points to confirm them as a local minima. The translational entropy term in the calculated structures was corrected through a free volume correction introduced by Mammen et al.

6.6: References

[1] Bruker (2006). APEX2, SAINT and SADABS. Bruker AXS Inc., Madison, Wisconsin, USA.

[2] G. M. Sheldrick, *Acta Crystallogr., Sect. A*, **2008**, *64*, 112–122.

[3] L. J. Farrugia, *J. Appl. Cryst.* **1997**, *30*, 565–565.

[4] J. P. Perdew, K. Burke, M. Ernzerhof, *Phys. Rev. Lett*. **1996**, *77*, 3865–3868.

[5] F. Weigend, R. Ahlrichs, *Phys. Chem. Chem. Phys*. **2005**, *7*, 3297-3305.

[6] R. Ahlrichs, M. Bar, M. Häser, H. Horn, C. Kölmel, *Chem. Phys. Lett.* **1989**, *162*, 165−169.

[7] K. Eichkorn, O. Treutler, H. Öhm, M. Häser, R. Ahlrichs, *Chem. Phys. Lett*. **1995**, *240*, 283-289.

[8] M. Sierka, A. Hogekamp, R. Ahlrichs, *J. Chem. Phys*. **2003**, *118*, 9136-9148.

[9] (a) J. Hepburn, G. Scoles, R. Penco, *Chem. Phys. Lett.* **1975**, *36*, 451–456; (b) S. Grimme, J. Antony, S. Ehrlich, H. Krieg, *Chem. Phys.* **2010**, *132*, 154104(1)–154104(19).

[10] A. Klamt, G. Schürmann, *J. Chem. Soc., Perkin Trans*. **1993**, *2*, 799-805.

[11] M. Magre, B. Maity, A. Falconnet, L. Cavallo, M. Rueping, *Angew. Chem. Int. Ed.* **2019**, *58*, 7025–7029.

[12] M. J. Frisch, G. W. Trucks, H. B. Schlegel, G. E. Scuseria, M. A. Robb, J. R. Cheeseman, G. Scalmani, V. Barone, B. Mennucci, G. A. Petersson, G. H. Nakatsuji, M. Caricato, X. Li, H. P. Hratchian, A. F. Izmaylov, J. Bloino, G. Zheng, J. L. Sonnenberg, M. Hada, M. Ehara, K. Toyota, R. Fukuda, J. Hasegawa, M. Ishida, T. Nakajima, Y. Honda, O. Kitao, H. Nakai, T. Vreven, J. A. Montgomery, Jr., J. E. Peralta, F. Ogliaro, M. Bearpark, J. J. Heyd, E. Brothers, K. N. Kudin, V. N. Staroverov, R. Kobayashi, J. Normand, K. Raghavachari, A. Rendell, J. C. Burant, S. S. Iyengar, J. Tomasi, M. Cossi, N. Rega, J. M. Millam, M. Klene, J. E. Knox, J. B. Cross, V. Bakken, C. Adamo, J. Jaramillo, R. Gomperts, R. E. Stratmann, O. Yazyev, A. J. Austin, R. Cammi, C. Pomelli, J. W. Ochterski, R. L. Martin, K. Morokuma, V. G. Zakrzewski, G. A. Voth, P. Salvador, J. J. Dannenberg, S. Dapprich, A. D. Daniels , O. Farkas, J. B. Foresman, J. V. Ortiz, J. Cioslowski, D. J. Fox, *Gaussian 09, Revision D.01*; Gaussian, Inc., Wallingford, CT, **2013**.

[13] (a) A. D. Becke, *Phys. Rev. A: At., Mol., Opt. Phys.*, **1988**, *38*, 3098−3100; (b) J. P. Perdew, *Phys. Rev. B: Condens. Matter Mater. Phys.*, **1986**, *33*, 8822−8824.

[14] (a) F. Weigend, R. Ahlrichs, *Phys. Chem. Chem. Phys.*, **2005**, *7*, 3297−3305; (b) F. Weigend, *Phys. Chem. Chem. Phys.*, **2006**, *8*, 1057−1065.

[15] T. A. Halgren, W. N. Lipscomb, *Chem. Phys. Lett.*, **1977**, *49*, 225−232.

[16] (a) H. P. Hratchian, H. B. Schlegel, *J. Chem. Phys.*, **2004**, *120*, 9918−9924; (b) K. Fukui, *Acc. Chem. Res.*, **1981**, *14*, 363−368.

[17] Y. Zhao, D. G. Truhlar, *Theor. Chem. Acc.*, **2008**, *120*, 215−241.

[18] S. Grimme, J. Antony, S. Ehrlich, H. Krieg, *J. Chem. Phys.*, **2010**, *132*, 154104−154122.

[19] (a) K. Kitaura, K. Morokuma, *Int. J. Quantum Chem.*, **1976**, *10*, 325−340; (b) F. M. Bickelhaupt, K. N. Houk, *Angew. Chem. Int. Ed.*, **2017**, *56*, 10070−10086.

[20] C. Y. Legault, *CYLView*, *1.0b*, Université de Sherbrooke, **2009**, http://www.cylview.org.

[21] S. H. Vosko, L. Wilk, M. Nusair, *J. Phys.*, **1980**, *58*, 1200–1211.

[22] C. Lee, W. Yang, R. G. Parr, *Phys. Rev. B Condens. Matter*, **1988**, *37*, 785–789.

[23] A. D. Becke, *J. Chem. Phys.*, 1993, **98**, 5648–5652.

[24] P. J. Stephens, F. J. Devlin, C. F. Chabalowski, M. J. Frisch, *J. Phys. Chem*., *A*, **1994**, *98*, 11623–11627.

[25] S. Grimme, J. Antony, S. Ehrlich, H. Krieg, *J. Chem. Phys*., **2010**, *132*, 154104.

[26] J. P. Perdew, *Phys. Rev. B*, **1986**, *33*, 8822–8824.

[27] A. D. Becke, *Phys. Rev. A*, **1988**, *38*, 3098–3100.

[28] T. Yanai, D. P. Tew, N. C. Handy, *Chem. Phys. Lett.*, **2004**, *393*, 51–57.

[29] Y. Zhao, D. G. Truhlar, *Theor. Chem. Acc.*, **2008**, *120*, 215–241.

[30] J.-D. Chai, M. Head-Gordon, *Phys. Chem. Chem. Phys.*, **2008**, *10*, 6615–6620.

[31] J. P. Perdew, K. Burke, M. Ernzerhof, *Phys. Rev. Lett.*, **1996**, *77*, 3865–3868.

[32] S. Grimme, *J. Comput. Chem.*, **2006**, *27*, 1787–1799.

[33] B. S. Brunschwig, J. Logan, M. D. Newton, N. Sutin, *J. Am. Chem. Soc.*, **1980**, *102*, 5798.

[34] J. L. Bredas, D. Beljonne, V. Coropceanu, J. Cornil, *Chem. Rev.*, **2004**, *104*, 4971–5004.

[35] J. E. Norton, J. L. Bredas, *J. Am. Chem. Soc.*, **2008**, *130*, 12377–12384.

[36] S. Di Motta, E. Di Donato, F. Negri, G. Orlandi, D. Fazzi, C. Castiglioni, *J. Am. Chem. Soc.*, **2009**, *131*, 6591–6598.

[37] B. Zhang, Y.-H. Kan, Y. Geng, Y.-A. Duan, H.-B. Li, J. Hua, Z.-M. Su, *Org. Electron*., **2013**, *14*, 1359–1369.

[38] F. Liu, Z. Cheng, L. Wan, Z. Feng, H. Liu, H. Jin, L. Gao, P. Lu, W. Yang, *Small*, **2021**, *18*, 2106462(1-9).

ABSTRACT

Name of the Student: Rohit Kumar **Registration No.:** 10CC17A26023

Faculty of Study: Chemical Sciences **Year of Submission:** 2022

AcSIR Academic Centre/CSIR Lab: CSIR-National Chemical Laboratory **Name of the Supervisor(s):** Dr. Sakya Singha Sen

Title of the thesis: Synthesis and Molecular Catalysis with Organo-Alkaline Earth Metal Complexes.

This thesis covers the work to develop cheap and biocompatible metal complexes that can be used as an alternative to transition metal complexes. Transition metal chemistry forms the heart of catalysis due to the availability of partially filled d-orbitals, allowing fast and reversible changes in the metal's oxidation states. However, these metals are expensive, and their byproducts are hazardous. The current trend in chemistry is to move towards cheaper alternatives. The last two decades have witnessed that main group metal complexes, especially alkaline earth metal complexes, were used as the alternative to transition metal complexes because these metals are cheap in price and biocompatible in nature. **Chapter 1** discusses the history and development of organo-alkaline earth metals/complexes as the organo alkaline earth metal chemistry was started more than a century ago. In 1901, Grignard synthesized organomagnesium halides (Grignard reagents), which proved to be a milestone in organometallic chemistry. But the higher analog of magnesium has several synthetic challenges that can be solved using a suitable ligand. **Chapter 2** presents the synthesis and characterization of N,O-ketiminato ligand stabilized homoleptic and heteroleptic magnesium and calcium complexes. Single crystal XRD studies determined the structural and the bonding arrangement of all the complexes. Furthermore, DFT studies support the different reactivity of two N,O-ketiminato ligands with biphenyl and terphenyl substituents on the nitrogen atom. **Chapter 3** contains the synthesis of various monomeric magnesium alkyl complexes prepared using bis(phosphino)carbazole framework. Among them, magnesium-methyl has been used as a catalyst for hydroboration of alkenes and alkynes with pinacolborane (HBpin). A broad variety of aromatic and aliphatic alkenes and alkynes were efficiently reduced. Anti-Markovnikov regioselective hydroboration of alkenes and alkynes was achieved, which was confirmed by deuterium-labelling experiments. Finally, the hydroboration protocol was extended to biologically important terpenes. **Chapter 4** contains the synthesis and structural characterization of well-defined 2,2'-pyridylpyrrolide (PyPyrH) ligand stabilized two magnesium complexes. Both the complexes show bright luminescence with a quantum yield of 22% and 16% in the solid state. Theoretical calculations reveal that the emissive properties is originated from the intra- and inter-ligand charge transfer. **Chapter 5** accounts the synthesis and structural characterization of a calcium complex bearing a monoanionic tetradentate ligand. Further, calcium complex was found to be an efficient catalyst for the cyclotrimerization of a variety of aromatic isocyanates under mild conditions.

List of publication(s) in SCI Journal(s) (published & accepted) emanating from the thesis work, with complete bibliographic details

1. **R. Kumar**, S. Yadav, K. Gour, E. Sangtani, S. R. Dash, A. Raja, K. Vanka, R. G. Gonnade, and S. S. Sen* A Tale of Biphenyl and Terphenyl Substituents for Structurally Diverse Ketiminato Magnesium, Calcium and Germanium Complexes, *Chem. Asian. J.*, **2020**, *15*, 820-827.
2. **R. Kumar**, V. Sharma, S. Jain, K. Vanka, S. S. Sen*, A Well-Defined Calcium Compound Catalyzes Trimerization of Arylisocyanates into 1,3,5-Triarylisocyanurates, *ChemCatChem*, **2022**, *14*, e202101788(1-6).
3. **R. Kumar**, S. Datta, V. Sharma, P. P. Singh, R. G. Gonnade, D. Koley, S. S. Sen*, Monomeric Magnesium-Catalyzed Alkene and Alkyne Hydroboration, *Chem. Eur. J.*, **2022**, *28*, e202201896-(1-8).
4. **R. Kumar**, S. Pahar, J. Chatterjee, S. R. Das, R. G. Gonnade, K. Vanka, S. S. Sen, Luminescent Magnesium Complexes with Intra- and Inter-Ligand Charge Transfer, *Chem. Commun.*, **2022**, *58*, 11843-11846.

Other publications:

1. **R. Kumar**, M. Bisai, S. Jain, K. Vanka, S. S. Sen*, Deoxygenative Hydroboration of Primary and Secondary Amides: a Catalyst-Free and Solvent-Free Approach, *Chem Comm.*, **2021**, *57*, 10596-10599.
2. S. Yadav, **R. Kumar**, K. V. Raj, P. Yadav, K. Vanka and S. S. Sen*, Amidinato Germylene-Zinc Complexes: Synthesis, Bonding, and Reactivity, *Chem. Asian. J.*, **2020**, *15*, 3116-3121.
3. **R. Kumar**, V. Sharma, S. Banerjee, K. Vanka, S. S. Sen*, Controlled Reduction of Isocyanates to Formamides using a Monomeric Magnesium Compound (manuscript submitted).

List of papers with abstract presented (oral/poster) at national/international conferences/seminars with complete details

1. Awarded "***NCL-Research Foundation Dr. Paul Ratnasamy and Dr. Suneeta B. Kulkarni award***" for the "***best published research paper in Catalysis***" from CSIR-National Chemical Laboratory with the highest impact factor for the year 2021.
2. Presented a research poster in ***"#RSC-IISER Desktop Webinar Twitter Conference 2022"*** held during May 9th – 12th, 2022 on Twitter. The title of the poster was ***"A Well-Defined Calcium Compound Catalyzes Trimerization of Arylisocyanates into 1,3,5-Triarylisocyanurates"***.
3. Presented a research poster in ***"#RSCPoster Twitter Conference 2022"*** held during March 1st - 2nd, 2022 on Twitter. The title of the poster was ***"Low Coordinate Monomeric Magnesium-Catalyzed Alkene and Alkyne Hydroboration"***.
4. Presented a research poster in ***"#LatinXChem Twitter Conference 2021"*** held during September 20th, 2021 on Twitter. The title of the poster was ***"Deoxygenative Hydroboration of Primary and Secondary Amides: A Catalyst-Free and Solvent-Free Approach"***.
5. Presented a research poster at ***"#RSC Poster Twitter Conference 2021"*** held on March 2-3, 2021 on Twitter. The title of the poster was ***"Amidinato Germylene-Zinc Complexes: Synthesis, Bonding, and Reactivity"***.
6. Presented and selected as one of the Top 500 best posters in ***"#LatinXChem Twitter Conference 2020"*** for presenting research poster, held during September 7th, 2020 on Twitter. The title of the poster was ***"Amidinato Germylene-Zinc Complexes: Synthesis, Bonding, and Reactivity"***.
7. Presented a research poster at "***International Conference on Recent Trends in Catalysis (RTC-2020)***" held during 26-29 February 2020 at NIT Calicut, Kerala. The title of the poster was ***"A Tale of Biphenyl and Terphenyl Substituents for Structurally Diverse Ketiminato Magnesium, Calcium and Germanium Complexes"***.
8. Gave a talk at "***Hindi Science Seminar"*** held on 25th Sep 2019 at CSIR-NCL, Pune. The presentation title was ***"Structurally Diverse Hydrocarbon Soluble Calcium and Magnesium Complexes"***.
9. Presented a research poster at "***International Conference on Structural and Inorganic Chemistry-II (ICSIC-II)***" held during March- 2019 at IISER, Pune. The title of the poster was ***"Structural Diversity in Ketoiminato Calcium and Magnesium Complexes"***.
10. Presented a research poster at "***Science Day***" held during 25-28 February 2019 at CSIR-NCL, Pune. The title of the poster was ***"Structural Diversity in Ketoiminato Calcium and Magnesium Complexes"***.

About the Author

Mr. Rohit Kumar, son of Premchand and Satyaviri Devi, was born in Nan village of Hapur district, Uttar Pradesh, India, in 1994. He completed his B.Sc. Chemistry from S. S. V. (P.G.) College, Hapur affiliated with Choudhary Charan Singh University, Meerut. He obtained his master's degree from Chaudhary Charan Singh University Campus, Meerut. After qualifying CSIR-National Eligibility Test (NET-JRF) examination, he moved to Catalysis and Inorganic Chemistry Division, CSIR-National Chemical Laboratory, Pune, India to pursue his Ph.D. degree under the guidance of Dr. Sakya Singha Sen. His research area lies on "*Synthesis and Molecular Catalysis with Organo-Alkaline Earth Metal Complexes*."

Education and Research Experience:

Ph.D.: From July 2017 to till date, working under the supervision of Dr. Sakya Singha Sen at CSIR- National Chemical Laboratory. I will be completing my doctoral work by May 2022.

UGC-JRF: Qualified in chemical sciences, 2017 with all India rank 40.

CSIR-JRF: Qualified in chemical sciences, 2016 with all India rank 60.

M.Sc.: (2013-2015) from Choudhary Charan Singh University Campus, Meerut, India.

B.Sc.: (2010-2013) S. S. V. (P.G.) College, Hapur affiliated with Choudhary Charan Singh University, Meerut, India

List of Scientific Contributions:

Publications

1. **R. Kumar**, S. Yadav, K. Gour, E. Sangtani, S. R. Dash, A. Raja, K. Vanka, R. G. Gonnade, and S. S. Sen* A Tale of Biphenyl and Terphenyl Substituents for Structurally Diverse Ketiminato Magnesium, Calcium and Germanium Complexes, *Chem. Asian. J.*, **2020**, *15*, 820. (**Thesis related**)

2. S. Yadav, **R. Kumar**, K. V. Raj, P. Yadav, K. Vanka and S. S. Sen*, Amidinato Germylene-Zinc Complexes: Synthesis, Bonding, and Reactivity, *Chem. Asian. J.*, **2020**, *15*, 3116.

3. **R. Kumar**, M. Bisai, S. Jain, K. Vanka, S. S. Sen*, Deoxygenative hydroboration of primary and secondary amides: a catalyst-free and solvent-free approach, *Chem Comm.*, **2021**, *57*, 10596.

4. **R. Kumar**, V. Sharma, S. Jain, K. Vanka, S. S. Sen*, A Well-Defined Calcium Compound Catalyzes Trimerization of Arylisocyanates into 1,3,5-Triarylisocyanurates, *ChemCatChem*, **2022**, *14*, e202101788(1-6). (**Thesis related**)

5. **R. Kumar**, S. Datta, V. Sharma, P. P. Singh, R. G. Gonnade, D. Koley, S. S. Sen*, Monomeric Magnesium-Catalyzed Alkene and Alkyne Hydroboration *Chem. Eur. J.*, 2022, (DOI: 10.1002/chem.202201896). (**Thesis related**)

6. **R. Kumar,** S. Pahar, J. Chatterjee, S. R. Das, R. G. Gonnade, K. Vanka, S. S. Sen, Luminescent Magnesium Complexes with Intra- and Inter-Ligand Charge Transfer (*Manuscript submitted*).

Symposia Attended

National conferences:	2 (Participation)
	1 (Oral presentation)
International conferences:	3 (Participation)
	2 (Poster presentation)
	5 (Poster presentation: Virtual mode)

ACES Asian Chemical Editorial Society

DOI: 10.1002/asia.201901801

CHEMISTRY AN ASIAN JOURNAL Full Paper

Special Collection

A Tale of Biphenyl and Terphenyl Substituents for Structurally Diverse Ketiminato Magnesium, Calcium and Germanium Complexes

Rohit Kumar[+],[a, b] Sandeep Yadav[+],[a, b] Kritika Gour,[a, b] Ekta Sangtani,[b, c] Soumya Ranjan Dash,[b, c] Abhishekram Raja,[d] Kumar Vanka,[b, c] Rajesh G. Gonnade,[b, c] and Sakya S. Sen*[a, b]

Abstract: In this paper, we have used two N,O-ketiminato ligands (**L1** and **L2**) with biphenyl and terphenyl substituent on the nitrogen atom. Deprotonation of **L1** with $KN(SiMe_3)_2$ and subsequent reaction with MgI_2 led to a homoleptic dinuclear magnesium complex (**1**) with a Mg_2O_2 four-membered ring. Deprotonation with *n*BuLi and subsequent reaction with MgI_2 afforded a unusual dinuclear magnesium complex (**2**) with a Mg_2O_2 ring. Extension of the ligand for calcium resulted in a trinuclear calcium complex (**3**) with six four-membered Ca_2O_2 rings. We could not isolate any chelating complex when **L2** was used as a ligand, and only oxygen bound magnesium (**4**) and calcium (**5**) adducts were isolated. DFT studies were performed to understand this dissimilar behavior. More diverse results were obtained when lithiated **L1** and **L2** were treated with germanium dichloride. We were able to stabilize a monomeric germylene monochloride (**7**) with **L1**. However, with **L2**, an unusual ligand scrambling, and a C–C coupling take place, leading to the formation of a secondary carbocation with $GeCl_3$- as a counter-anion (**8**). Besides, a germanium dichloride adduct (**9**) bound to the oxygen center of the ligand was obtained as the minor product.

Introduction

Monoanionic bidentate ligand systems such as amidinate $[RC\{NR\}_2]^-$,[1] guanidinate $[RNC(NR_2)NR]^-$,[1] trizenide $[(R_2N_3)]^v$,[2] β-diketiminate $[(R)NC(Me)C(H)C(Me)N(R)]^-$,[3] diboxmethanide $[(4,6\text{-}R\text{-}NCOC_6H_2)_2CH]^-$,[4,5] silylated aminopyridinato $[(2\text{-}R_3SiNH\text{-}6\text{-}MeC_5H_3N)]^-$[6] have featured prominently in the development of main group metal chemistry. Such ligands provide greater stability to the metal center by occupying additional coordination site and offer easy manipulation of their steric and electronic properties. In β-diketiminate ligand system, further replacement of an NDipp moiety (Dipp = 2,6-*i*$Pr_2C_6H_3$) with an oxygen atom leads to the formation of a N,O-ketiminato ligand. This replacement reduces the steric protection from the ligand system and provides a more open side to the metal center. As a result, the ketiminato moieties have not found expanding use as ligands for stabilization of the main group complexes. Nevertheless, following the initial studies on the preparation of aluminum ketiminato complexes and their reactivity towards ring-opening polymerization of ε-caprolactone by Huang and coworkers,[7] the synthesis of main group complexes using N,O-ketiminato ligand has received renewed interest. Subsequently, the synthesis of aluminum, gallium, and especially zinc complexes containing N,O ketiminato ligands and their applications in ring opening polymerization of lactides have been accomplished of late.[8–12] The germanium compounds using N,O ketiminato ligands have recently been reported by the group of Ghosh,[13] who further described elegant cyclometallation of these germylenes upon reacting with the transition metal complexes. The same group[13] as well as Schulz and coworkers[14] independently reported analogous tin complexes using the same N,O-ketiminato ligand. The isolation of alkaline earth metal complexes, especially magnesium with N,O-ketiminato ligands were also achieved, thanks to extensive works from the groups of Huang, Reddy, Wang, and others.[15–20]

In this paper, we have prepared a new N,O-ketiminato ligand (**L1**) by introducing "biphenyl" moiety on the nitrogen atoms and prepared structurally diverse complexes with magnesium (**1** and **2**), calcium (**3**), and germanium (**7**). Furthermore, to investigate the influence of the sterics on the structures of the corresponding complexes, the substitution of the "biphenyl" group with "terphenyl" moiety was accomplished (**L2**). While both magnesium and calcium do not form a chelating complex with **L2**, germanium undergoes a very unusual ligand scrambling and C–C coupling reaction, leading

[a] R. Kumar,[+] Dr. S. Yadav,[+] K. Gour, Dr. S. S. Sen
Inorganic Chemistry and Catalysis Division
CSIR-National Chemical Laboratory
Dr. Homi Bhabha Road, Pashan, Pune 411008 (India)
E-mail: ss.sen@ncl.res.in

[b] R. Kumar,[+] Dr. S. Yadav,[+] K. Gour, E. Sangtani, S. Ranjan Dash, Dr. K. Vanka, Dr. R. G. Gonnade, Dr. S. S. Sen
Academy of Scientific and Innovative Research (AcSIR)
Ghaziabad-201002 (India)

[c] E. Sangtani, S. Ranjan Dash, Dr. K. Vanka, Dr. R. G. Gonnade
Physical and Material Chemistry Division
CSIR-National Chemical Laboratory
Dr. Homi Bhabha Road, Pashan, Pune 411008 (India)

[d] A. Raja
Mountain View College
4849 W. Illinois Avenue, Dallas, TX 5211 (United States)

[+] The first two authors contributed equally for the manuscript

Supporting information for this article is available on the WWW under https://doi.org/10.1002/asia.201901801

Special Collection This manuscript is part of a special collection in honor of the 2nd International Conference on Organometallics and Catalysis (ICOC-2020). Click here to see the Table of Contents of the special collection.

to the formation of a carbocation with $GeCl_3^-$ as a counter-anion (**8**). Our results are reported herein.

Results and Discussion

Ligand **L1** can be prepared by reacting 1:1 ratio of 2,4-pentanedione and 2-phenylaniline in toluene with catalytic amount of *p*-toluenesulfonic acid (Scheme 1). The formation of **L1** was confirmed by NMR spectroscopy and single-crystal X-ray studies (Figure 1). Two methyl groups resonate at δ 1.56 and 1.91 ppm, while the γ proton resonates at δ 4.93 ppm. **1** crystallizes in the triclinic space group *P*$\bar{1}$.

Deprotonation of **L1** with $KN(SiMe_3)_2$ in THF at room temperature and subsequent reaction with MgI_2 led to a homoleptic complex of composition $L1_4Mg_2$ (**1**) (Scheme 2) containing a four-membered Mg_2O_2 ring, where the oxygen atoms of the two ligands participate in the ring formation. **1** crystallizes in the triclinic space group *P*$\bar{1}$.[21] Each magnesium atom is connected by two ligand moieties and another oxygen atom of the third ligand, resulting a penta-coordinate magnesium atom with a distorted square pyramidal geometry (Figure 2). The η^2-ketiminato ligands coordinate to the magnesium atom with a bite angle of 87.89(8)°, which is lower than that reported by Huang and coworkers presumably due to ring strain.[15] The Mg-$O_{Ketiminato}$ bond lengths are 1.9436(19), 2.0263(18), and 2.0433(19) Å, which are longer than those reported by Huang and coworkers (1.8955(15) Å).[15] The ^{1}H NMR spectrum of **1** displays a singlet resonance at δ 5.03 ppm for the methine protons of the ketiminato backbones, which has been shifted downfield compared to the free ketimine ligands (δ 4.93 ppm). In addition, complex **1** exhibits two singlet resonances for the methyl groups at δ 1.68 and 2.02 ppm of the ketiminato backbones integrating each for 12 protons. This indicates that the four ligands attached to the magnesium centers are equivalent but the two methyl groups on a particular ligand are not equivalent. In the HRMS, only half fragment was detected with the highest relative intensity at *m/z* 525.2520. Due to the sensitivity of the system, we could never obtain a very clean ^{13}C NMR and always accomanied with free ligand resonances.

Next, we lithiated **L1** with *n*BuLi in THF and subsequently added this solution to the MgI_2 suspension in THF (Scheme 3). The reaction led to the formation of an unusual magnesium compound (**2**) with a four-membered Mg_2O_2 cycle (Figure 3). However, the coordination environment of the two magnesium atoms is different. Although a similar dinuclear Zn complex with two differently coordinated Zn atoms was previously reported,[22] to our knowledge, analogous alkaline earth metal complexes are not known. **2** is extremely sensitive towards air and moisture. Despite several attempts, a full spectroscopic characterization of **2** could not be obtained. Most of the time, the resonances for the NH peak was observed, resulting presumably from the decomposition of **2**. However, in the HRMS, the molecular ion peak at *m/z* 803.0468 was detected with the highest relative intensity. The constitution was authenticated by single-crystal X-ray study. **2** crystallizes in the orthorhombic space group $P2_12_12_1$. The relevant bond length and angles are given in the legend of the Figure 3. One magnesium atom is coordinated to two ligand moieties and

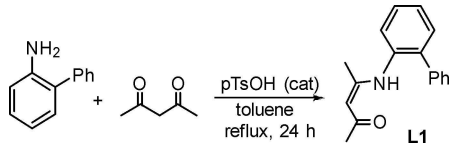

Scheme 1. Synthesis of ligand, **L1**.

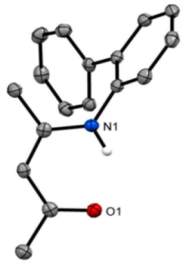

Figure 1. The molecular structure of **L1** with the anisotropic displacement parameters depicted at the 50% probability level. Hydrogen atoms (except the one bound to N) are omitted for clarity.

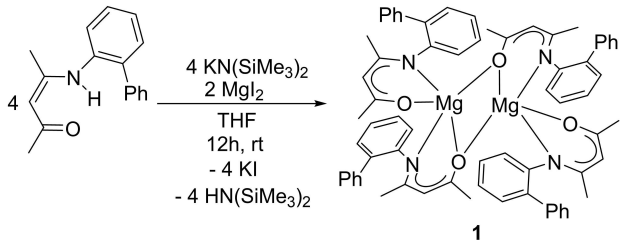

Scheme 2. Synthesis of dinuclear magnesium complex, **1**.

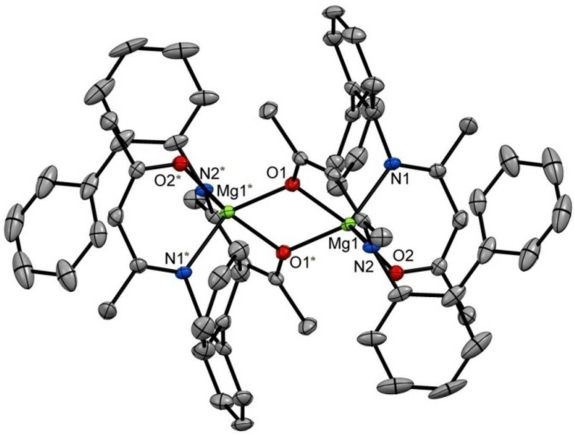

Figure 2. The molecular structure of **1** with anisotropic displacement parameters depicted at the 50% probability level. Hydrogen atoms are omitted for clarity. Symmetry generator *: 1-x, 1-y, 1-z. Selected bond lengths [Å] or angles [deg]: Mg1–O2 1.9436(19), Mg1–O1 2.0263(18), Mg1–O1 2.0433(19), Mg1–N1 2.148(2), Mg1–N2 2.154(2),), O1–Mg1 2.0433(19); O2–Mg1–O1 96.16(8) and 170.48(8), O1–Mg1–O1 78.16(8), O2–Mg1–Mg1 134.59(7), O1–Mg1–Mg1 38.89(5) and 39.28(5), N1–Mg1–Mg1 117.59(7), N2–Mg1–Mg1 106.86(7), Mg1–O1–Mg1 101.84(8).

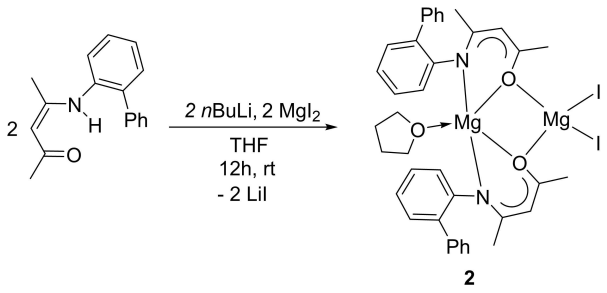

Scheme 3. Synthesis of **2**, where two Mg centers are differently coordinated.

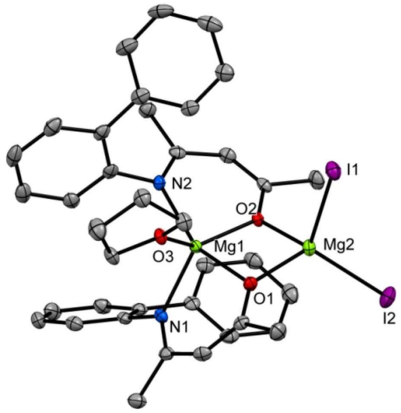

Figure 3. The molecular structure of **2**·toluene in the solid-state with anisotropic displacement parameters depicted at the 50% probability level. Hydrogen atoms and the toluene molecule are omitted for clarity. Selected bond lengths [Å] or angles [deg]: I1–Mg2 2.6909(12), I2–Mg2 2.6643(13), Mg1–O2 2.012(3), Mg1–O1 2.039(3), Mg1–O3 2.092(3), Mg1–N1 2.123(3), Mg1–N2 2.162(3), Mg1–Mg2 3.0782(17), Mg2–O1 1.958(3), Mg2–O2 1.985(3); O2–Mg1–O1 77.24(11), O2–Mg1–O3 134.13(11), O1–Mg1–O3 87.92(11), O2–Mg1–Mg2 39.32(8), O1–Mg1–Mg2 38.68(8), O3–Mg1–Mg2 110.23(8), N1–Mg1–Mg2 116.45(10), N2–Mg1–Mg2 120.44(10), O1–Mg2–O2 79.77(11), O2–Mg2–Mg1 39.95(8), I1–Mg2–Mg1 107.53(5), Mg2–O2–Mg1 100.73(12).

one THF molecule. It has the tau parameter value $\tau_5 = 0.497$, indicating the geometry around the Mg is intermediate between the idealized square-pyramidal and trigonal-bipyramidal.[23] The Mg–O_{thf} bond length is 2.092(3) Å, which is longer than the other Mg–O bonds (2.012(3) and 2.039(3) Å). The second magnesium center is connected to the two oxygen atoms of the ligand systems and two iodine atoms, giving tau parameter value $\tau_4 = 0.832$, which indicates a trigonal pyramidal geometry around the Mg center.[24] No THF molecule is coordinated to the second magnesium atom. The Mg–O bond lengths (1.958(3) and 1.985(3) Å) are shorter than the Mg–O bond lengths in compound **1**. The Mg–I bond lengths in **2** are 2.6643(13) and 2.6909(12) Å, which are in good agreement with those in the four-coordinate $(Et_2O)_2MgI_2$ (2.654(3) Å), independently reported by the groups of Schnöckel and Eaborn.[25,26] The Mg–I bond length is shorter than that in the solid-state structure of MgI_2 (2.9183(5) Å)[27] but longer than the Mg–I bond length in di-coordinate magnesium diiodide in the gas phase (2.52 ± 0.03 Å),[28] as measured by electron diffraction studies.

Subsequently, we have treated **L1** with $KN(SiMe_3)_2$ and further reacted with CaI_2. The reaction led to an interesting trinuclear calcium complex (**3**) stabilized by six N,O-ketiminato ligands (Scheme 4). **3** crystallizes in the triclinic system space group Pī (Figure 4). The single-crystal X-ray diffraction studies showed that the two calcium atoms are connected with three ligand moieties in the usual ketiminate bonding mode, leading to an octahedral geometry around the calcium atoms. However, the octahedral coordination sphere of the third calcium atom is saturated by the oxygen atom of each six ligands. The γ-H for all six ligands appear at δ 5.03 ppm, while the methyl groups resonate at δ 1.68 and 2.02 ppm. In spite of several efforts, only relatively poor quality crystals of **3** could be obtained by crystallization. Although the X-ray diffraction study leaves no doubt about the constitution, the bond precision is limited. The absolute values for the bond lengths might, therefore be not as

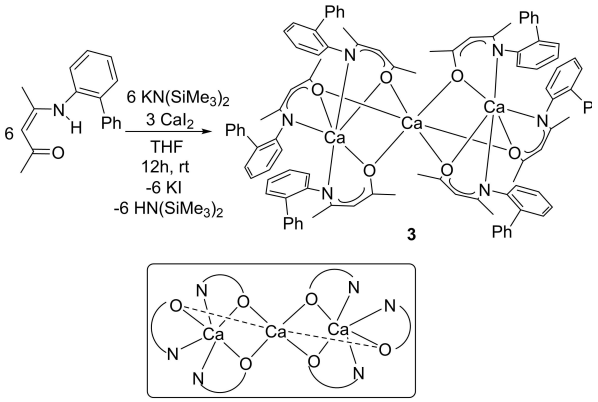

Scheme 4. Synthesis of trinuclear calcium complex, **3**.

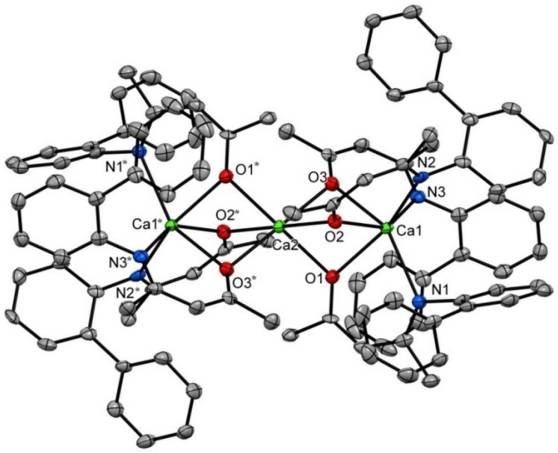

Figure 4. The molecular structure of **3** in the solid-state with anisotropic displacement parameters depicted at the 50% probability level. Hydrogen atoms are omitted for clarity. Symmetry generator *: 1-x, 1-y, 1-z. Selected bond lengths [Å] or angles [deg]: Ca2–O3 2.315(4) and 2.316(4), Ca2–O2 2.347(4) and 2.347(4), Ca2–O1 2.361(4) and 2.361(4), Ca2–Ca1 3.3307(12), Ca1–O2 2.333(4), Ca1–O1 2.342(4), Ca1–O3 2.359(4); O3–Ca2–O3 180.0, O3–Ca2–O2 105.26(13) and 74.74(13), O2–Ca2–O2 180.0, O3–Ca2–O1 104.09(13), 105.24(13), 74.76(13) and 75.91(13), O3–Ca2–O1 75.91(13) and 104.09(13), O2–Ca2–O1 74.76(13) and 105.24(13), O1–Ca2–O1 180.0,, Ca1–Ca2–Ca1 180.0, O2–Ca1–O1 75.35(14), O2–Ca1–O3 74.17(13), O1–Ca1–O3 75.43(13).

reliable as their standard deviations indicate and hence we refrain from discussing any structural parameters.

Subtle modification in the ligand skeletons may have a striking influence on the structure of the corresponding complexes. We decided to modify the ligand by replacing the biphenyl group with the terphenyl moiety to see if the extra phenyl group indeed stabilize the heteroleptic alkaline earth metal complexes. The synthesis of ligand **L2** was accomplished by the following method shown in Scheme 5. **L2** was characterized by the state of the art spectroscopic tools.

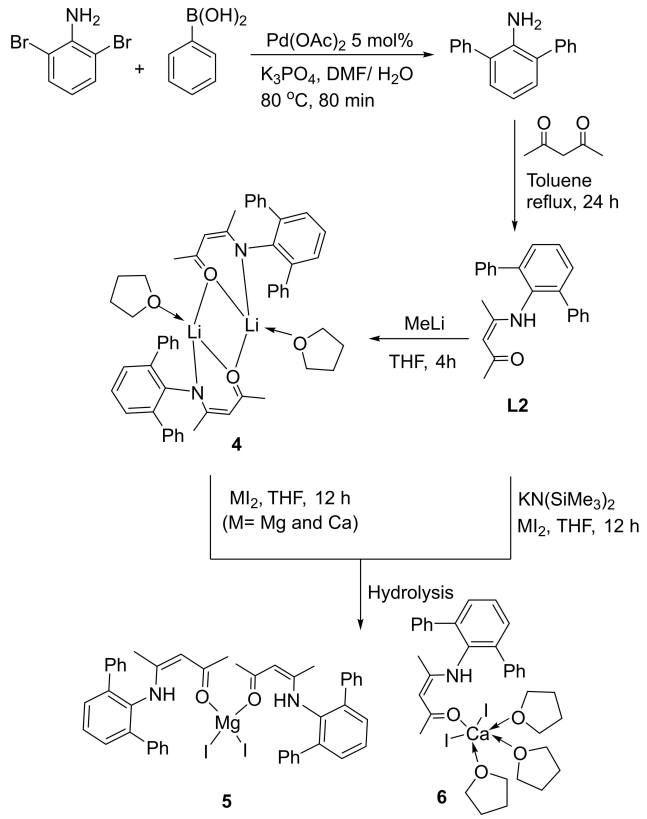

Scheme 5. Synthesis of ligand (**L2**) and preparation of **4**–**6** from **L2**.

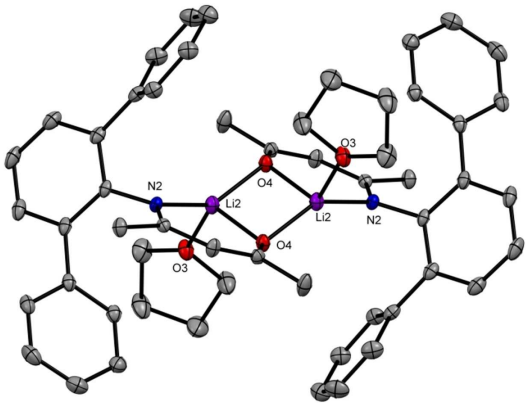

Figure 5. The molecular structure of **4** in the solid-state with anisotropic displacement parameters depicted at the 50% probability level. Hydrogen atoms are omitted for clarity. Selected bond lengths [Å] or angles [deg]: C24–O3 1.436(2), C24–C25 1.511(3), C27–O3 1.427(2), C33–O4 1.2864(18), C36–N2 1.3068(19), Li2–O4 1.892(3), Li2–O3 1.993(3), Li–N2 2.020(3), O4–Li2-O4$^{\#1}$92.80(13), O4–Li2–O3 109.78(15), O4$^{\#1}$–Li2-O3 100.88(13), O4–Li2-N2 95.42(13), O4–Li2–N2 95.42(13), O4$^{\#1}$–Li2–N2 144.98(17), O3–Li2–N2 108.11(14), O4–Li2–Li2$^{\#1}$ 46.99(9), O4$^{\#1}$–Li2–Li2$^{\#1}$ 45.81(9).

The reaction of **L2** with *n*BuLi led to 75–80% deprotonation. Hence, we have deprotonated **L2** with MeLi at −78 °C to get the lithiated compound (**4**) in almost quantitative yield (Scheme 5). **4** is a dimeric compound with a Li_2O_2 four-membered ring (Figure 5) and having a Li–N bond length 2.020(3) Å, which is slightly less than the sum of covalent radii of Li and N i.e. 2.09 Å and Li2-O3 1.993(3) Å. The Li atoms in **4** are tetracoordinate with one nitrogen and one oxygen atoms of the ketiminato ligand, one oxygen atom from another ketiminato ligand, and one oxygen atom of the coordinated THF molecule, and this arrangement leads to a distorted tetrahedral geometry around them. The ^{1}H NMR shows two singlet peaks for methyl protons at δ 1.45 ppm and 1.55 ppm, while the γ-proton appears at δ 4.56 ppm, which comes slightly upfield compared to ligand i.e. 4.66 ppm, due to coordination of the solvent to the lithium atom.

Consequently, we have sought to prepare magnesium and calcium complexes with **L2**. The reaction of **4** with MgI_2/CaI_2 or metallation with $KN(SiMe_3)_2$ and subsequent reaction with MgI_2/CaI_2 led to **5** and **6**, where magnesium and calcium are found to bind with the oxygen atom of the ligand without entering into the ligand pocket (Scheme 5). This is presumably due to the sterics of the additional phenyl ring that inhibits the chelation. It is also assumed that an unintended hydrolysis is taking place during the reaction or crystallization. It is surprising though that when no base is used, the adduct formation was not observed, even after heating conditions (See Figure S30 in the Supporting Information). However, even after several attempts, we were not able to prevent the hydrolysis. The source of the hydrogen ion is most likely the leakage of moisture during the reaction or crystallization. Hence, we have attempted deliberate synthesis of **5** and **6** using with a stoichiometric amount of degassed water in THF at −78 °C. Both **5** and **6** have been structurally characterized. While the magnesium atom in **5** exhibits a tetrahedral geometry, the calcium atom in **6** posses an octahedral geometry. The difference in their coordination geometries can be attributed to their difference in the ionic radii.

The unit cell of compound **5** contains two molecules of tetrahydrofuran, which have been treated as a diffuse contribution to the overall scattering without specific atomic positions by squeeze/platon.[29] However, it has been considered in the molecular formula unit for correct molecular weight, crystal density and F(000) computations. The molecular structure of **5** is depicted in Figure 6. The Mg–I bond lengths are 2.6898(12) and 2.7022(11) Å, which are in good agreement with those in **2**. The molecular structure of **6** is depicted in Figure 7. The Ca–I bond lengths are 3.136(2) and 3.099(2) Å, which are in good agreement with the Ca–I bond length in [(thp)$_4$Ca(I)(Ph)] (thp = tetrahydropyran).[30]

DFT calculations were carried out to find the possibility of chelated binding models of Mg and Ca with the ligand (**L2**). **5A**, **6A** and **6B** were found to be the plausible structures for the binding of Mg and Ca respectively (Figure 8). However, all these

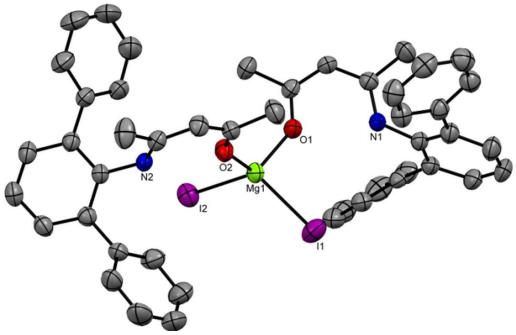

Figure 6. The molecular structure of **5** in the solid-state with the anisotropic displacement parameters depicted at the 50% probability level. Hydrogen atoms are omitted for clarity. Selected bond lengths [Å] or angles [deg]: Mg1–I1 2.6898(12), Mg1–I2 2.7022(11), Mg1–O2 1.936(2), Mg1–O1 1.945(2), N1–C4 1.326(3), N2–C27 1.321(3), O1–C2 1.279(3), O2–C25 1.280(3), O2–Mg1–O1 110.45(9), O2–Mg1–I1 109.98(8), O1–Mg1–I1 100.17(6), O2–Mg1–I2 99.58(7), O1–Mg1–I2 115.00(7), I1–Mg1–I2 121.76(4), C4–N1–C6 124.8(2), C4–N1–H1 117.6, C6–N1–H1 117.6, C27–N2–C29 124.1(2).

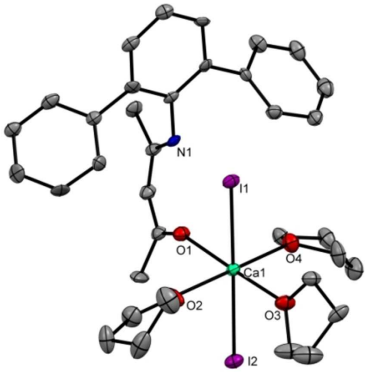

Figure 7. The molecular structure of **6** in the solid-state with anisotropic displacement parameters depicted at the 50% probability level. Hydrogen atoms are omitted for clarity. Selected bond lengths [Å] or angles [deg]: Ca1–I1 3.136(2), Ca1–I2 3.099(2), Ca1–O1 2.312(8), Ca1–$O2_{thf}$ 2.334(8), Ca1–$O3_{thf}$ 2.404(8), Ca1–$O4_{thf}$ 2.367(7), O1–C1 1.257(13), N1–C3 1.313(14), C1–C2 1.438(13), O1–Ca1–O2 89.4(3), O1–Ca1–O4 87.4(3), O2–Ca1–O4 175.4(3), O1–Ca1–O3 175.4(3), O2–Ca1–O3 88.9(4), O4–Ca1–O3 94.5(3), O1–Ca1–I2 85.57(18), O2–Ca1–I2 89.0(2), O4–Ca1–I2 93.9(2), O3–Ca1–I2 90.15(19), O1–Ca1–I1 95.84(19), O2–Ca1–I1 88.9(2), O4–Ca1–I1 88.2(2), O3–Ca1–I1 88.38(19), I2–Ca1–I1 177.53(7).

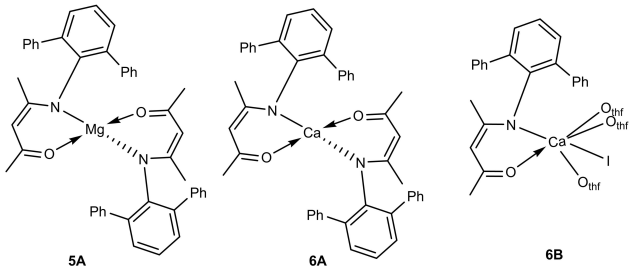

Figure 8. Possible chelated model complexes of Mg and Ca.

model complexes were found to be higher in energy than **5** and **6**. For example, **5A** was found to be +44.9 kcal/mol higher in energy than compound **5**. Similarly **6A** and **6B** were found to be +52.9 kcal/mol and +33.0 kcal/mol higher than **6**, respectively. The energy difference can be attributed to the presence of the extra phenyl group, which sterically hinders the complex formation and does not permit the metal ion to be in a position for the chelation with both nitrogen and oxygen. The steric crowding upon probable chelation can be clearly observed in the optimized models (Figure 9).

More divergent results were obtained from the reaction of $GeCl_2$ with lithiated **L1** and **L2**. The reaction of **L1** with *n*BuLi in THF at −78 °C, followed by salt metathesis reaction with $GeCl_2$.dioxane in THF resulted in the formation of germylene chloride, **7** (Scheme 6).

7 crystallizes in the monoclinic system with $P2_1$ space group (Figure 10). The three-coordinate germanium center in **7** features a distorted trigonal-pyramidal geometry with a lone pair on its apex; a feature that has been witnessed in various germylene monochloride complexes.[31] The Ge–N bond length in **7** is of 2.009(16) Å and the Ge–O bond length is of 1.877(18) Å, which are in good agreement with those of Ge–N or Ge–O bond lengths reported in the literature.[13,32–34] The Ge–Cl bond length was determined to be 2.317(7) Å, which is slightly longer than that in [(Dipp)NCMeCHCOMe-GeCl] (2.306(3) Å)[13] and Roesky's amidinato germylene chloride, $PhC(NtBu)_2GeCl$ (2.2572(13) Å),[32] shorter than Nagendran's aminotroponiminato germylene chloride, $[(tBu)_2ATI]GeCl$ (2.362(1) Å),[33] but matches well with that in Khan's acyclic α-phosphinoamido-germylene (2.302(4) Å).[34]

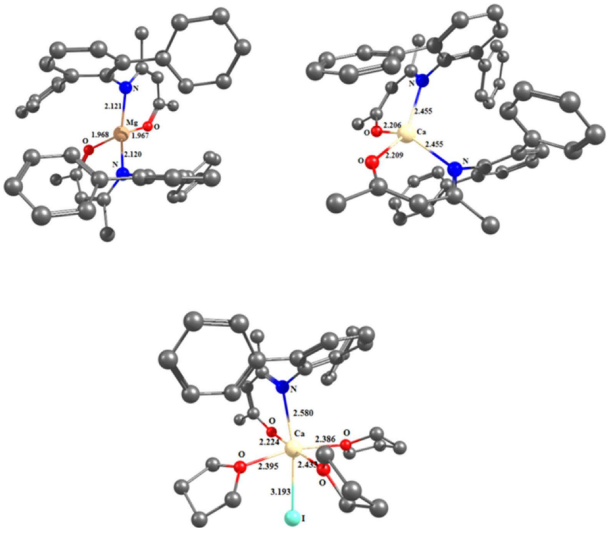

Figure 9. Probable chelated models for Mg and Ca with ligand **L2: 5A** (above left), **6A** (above right) and **6B** (below) (Optimized using Turbomole 7.1 by employing pbe functional and def-TZVP basis set).

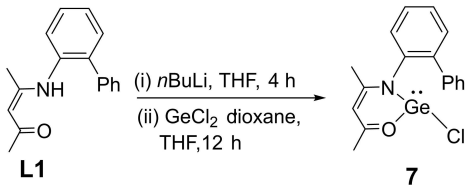

Scheme 6. Synthesis of germylene chloride, **7**.

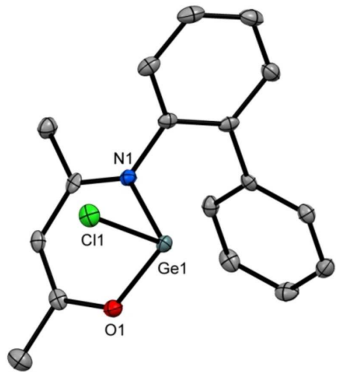

Figure 10. The molecular structure of **7** in the solid-state with anisotropic displacement parameters depicted at the 50% probability level. Hydrogen atoms are omitted for clarity. Selected bond lengths [Å] or angles [deg]: Ge1–O1 1.8776(18), Ge1–N1 2.0091(16), Ge1–Cl1 2.3168(7); O1–Ge1–N1 90.92(9), O1–Ge1–Cl1 95.07(6), N1–Ge1–Cl1 90.78(6).

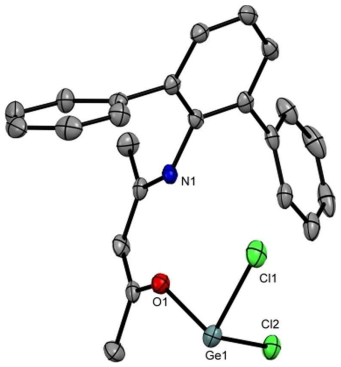

Figure 12. The molecular structure of **9** in the solid-state with anisotropic displacement parameters depicted at the 50% probability level. Hydrogen atoms are omitted for clarity. Selected bond lengths [Å] or angles [deg]: Ge (1)–Cl(1) 2.3122(6), Ge(1)–Cl(2) 2.2942(6), Ge(1)–O(1) 1.9689(15); Cl(1)–Ge(1) –Cl(2) 96.04(2), O(1)–Ge(1) –Cl(1) 85.86(4), O(1)–Ge(1)–Cl(2) 92.53(5).

The N–Ge–Cl bond angles (90.78(6)° in **7** is shorter than that in [(Dipp)NMeCHCOMeGeCl] (95.52(16)°) and this may be due to the presence of the phenyl ring which enforces a puckered six-membered ring. Further, to avoid the steric repulsion, the chloride atom bends away from the biphenyl moiety. The ^{1}H NMR spectrum of **7** displays a singlet at δ 5.24 ppm for the methine protons of the ketiminato backbones and two singlet resonances for the methyl groups at δ 1.66 and 1.90 ppm, which are shifted downfield compared to **L1**. The most abundant ion peak in the HRMS spectrum appeared at *m/z* 360.1761.

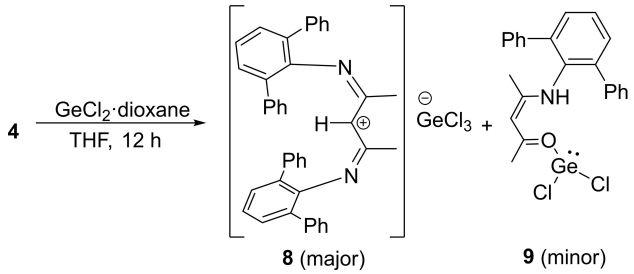

Scheme 7. Formation of C–C coupled product (**8**).

The reaction of **4** with $GeCl_2$ leads to ligand scrambling and a C–C coupled secondary carbocation with a $GeCl_3^-$ as the counter anion (**8**) (Scheme 7). Ligand oxygen bound germylene adduct, **9** was also formed as a minor product. **8** crystallizes in the *P*-1 space group of the triclinic crystal system (Figure 11) with a C–N bond length of 1.344(2) Å and 1.338(2) Å, suggesting that the C–N bonds have double bond character. The stability of the carbocation **8** can be attributed to the delocalization from the two adjacent C=N bonds. The Ge–Cl bond lengths range from 2.2465(7) to 2.3711(5) Å, which are in good agreement with our recently reported Ge(II) dication with two $GeCl_3^-$ as the counter-anions. The ^{1}H NMR of the crystals shows one resonance for the six methyl protons at δ 1.84 ppm and for the γ-proton at δ 4.48 ppm. The ^{13}C NMR shows a downfield peak at δ 190.93 ppm for the γ-carbon due to having a positive charge on carbon. Although **9** was obtained at a very low yield, we were able to crystallize it from the saturated toluene solution. **9** crystallizes in the *P*21/n space group of monoclinic crystal system (Figure 12) with the Ge–O bond length of 1.9689(15)Å and the Ge–Cl bond lengths of 2.3122(6) and 2.2942(6) Å.

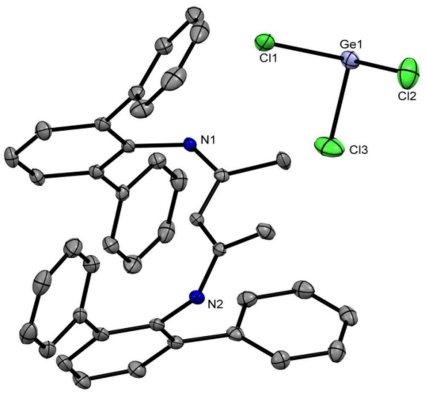

Figure 11. The molecular structure of **8** in the solid-state with anisotropic displacement parameters depicted at the 50% probability level. Hydrogen atoms are omitted for clarity. Selected bond lengths [Å] or angles [deg]: C20–N2 1.344(2), C20–C21 1.390(2), C21–C22 1.397(2), C22–N(1) 1.338(2), Cl1–Ge1 2.3711(5), Cl2–Ge1 2.2465(7), Cl3–Ge1 2.2688(6), Cl1–Ge1–Cl3 96.88(3), Cl1–Ge1–Cl2 98.18(2), Cl3–Ge1-Cl2 95.02(2), C22–N1–C24 121.40(14),C20–N2–C12 123.99(15).

Conclusion

N,O-ketiminato ligand (**L1**) featuring sterically demanding 2-biphenyl substituent on the nitrogen atom has been used to stabilize structurally diverse magnesium (**1** and **2**) and calcium complexes (**3**). We have also attempted several catalytic reaction using **1**–**3** such as hydrosilylation, Tischenko reaction etc., however due to homoleptic nature they are found to be catalytically impotent and only moderate yields were obtained. We have also isolated a monomeric germylene

monochloride, **7** using **L1**. Slightly modified ligand (**L2**) was prepared by substituting the "biphenyl" group by "terphenyl" moiety and it has a profound effect on the structures of the corresponding complexes. Magnesium and calcium only form O-bound adducts (**5** and **6**) with **L2**. DFT studies shed light why **L1** forms chelated complexes and **L2** forms simple adduct. When lithiated **L2** (**4**) was reacted with $GeCl_2$, it does not form any germylene chloride, but led to the formation of a secondary carbocation with $GeCl_3-$ as a counter-anion (**8**) through ligand scrambling and subsequent C–C coupling. Comparing the previous reports on N,O-ketiminate main group compounds with our results, it can be said that the coordination environment of the resulting main group compounds can be varied by changing the substituents on the nitrogen atom of the ligand.

Experimental Section

Please see Supporting Information for the synthesis, characterization, and structural data for **L1**, **L2**, and **1**–**9**. Complete computational details and relevant NMR spectra are also provided in the supporting information.

Acknowledgements

This work was supported by Ramanujan Research Grant (SB/S2/RJN-073/2014) and CSIR-Young Scientist Contingency Grant (YSA000726). R. K., S. Y., K. G., and E. S. thank CSIR, India for their research fellowships. The first two authors have contributed equally to this work.

Conflict of Interest

The authors declare no conflict of interest.

Keywords: Ligand · X-ray Structure · Germylene · Calcium · Magnesium

[1] a) G. J. Moxey, F. Ortu, L. G. Sidley, H. N. Strandberg, A. J. Blake, W. Lewis, D. L. Kays, *Dalton Trans.* **2014**, *43*, 4838–4846; b) R. J. Schwamm, B. M. Day, N. E. Mansfield, W. Knowelden, P. B. Hitchcock, M. P. Coles, *Dalton Trans.* **2014**, *43*, 14302–14314; c) B. M. Day, W. Knowelden, M. P. Coles, *Dalton Trans.* **2012**, *41*, 10930–10933; d) J. Schwamm, M. P. Coles, *Organometallics* **2013**, *32*, 5277–5280; e) S. Yadav, V. S. V. S. N. Swamy, R. G. Gonnade, S. S. Sen, *ChemistrySelect* **2016**, *1*, 1066–1071; f) B. M. Day, N. E. Mansfield, M. P. Coles, P. B. Hitchcock, *Chem. Commun.* **2011**, *47*, 4995–4997; g) C. Jones, *Coord. Chem. Rev.* **2010**, *254*, 1273–1289; h) C. Glock, C. Loh, H. Goerls, S. Krieck, M. Westerhausen, *Eur. J. Inorg. Chem.* **2013**, 3261–3269; i) M. K. Barman, A. Baishya, S. Nembenna, *J. Organomet. Chem.* **2015**, *785*, 52–60.

[2] a) S.-O. Hauber, F. Lissner, G. B. Deacon, M. Niemeyer, *Angew. Chem. Int. Ed.* **2005**, *44*, 5871–5875; *Angew. Chem.* **2005**, *117*, 6021–6025; b) A. G. M. Barrett, M. R. Crimmin, M. S. Hill, P. B. Hitchcock, G. Kociok-Köhn, P. A. Procopiou, *Inorg. Chem.* **2008**, *47*, 7366–7376; c) H. S. Lee, S.-O. Hauber, D. Vinduš, M. Niemeyer, *Inorg. Chem.* **2008**, *47*, 4401–4412; d) A. R. Leverett, V. Diachenko, M. L. Cole, A. I. McKay, *Dalton Trans.* **2019**, *48*, 13197–13204.

[3] a) S. Nembenna, H. W. Roesky, S. Nagendran, A. Hofmeister, J. Magull, P.-J. Wilbrandt, M. A. Hahn, *Angew. Chem. Int. Ed.* **2007**, *46*, 2512–2514; *Angew. Chem.* **2007**, *119*, 2564–2566; b) A. G. M. Barrett, M. R. Crimmin, M. S. Hill, P. B. Hitchcock, P. A. Procopiou, *Angew. Chem. Int. Ed.* **2007**, 46, 6339–6342; *Angew. Chem.* **2007**, *119*, 6455–6458; c) C. Ruspic, S. Harder, *Inorg. Chem.* **2007**, *46*, 10426–10433; d) M. Westerhausen, M. H. Digeser, C. Gückel, H. Nöth, J. Knizek, W. Ponikwar, *Organometallics* **1999**, *18*, 2491–2496; e) S. P. Sarish, A. Jana, H. W. Roesky, T. Schulz, M. John, D. Stalke, *Inorg. Chem.* **2010**, *49*, 3816–3820; f) S. Yadav, R. Dixit, M. K. Bisai, K. Vanka, S. S. Sen, *Organometallics* **2018**, *37*, 4576–4584; g) S. P. Sarish, S. Nembenna, S. Nagendran, H. W. Roesky, *Acc. Chem. Res.* **2011**, *44*, 157–170.

[4] a) I. Koehne, R. Herbst-Irmer, D. Stalke, *Eur. J. Inorg. Chem.* **2017**, 3322—3326; b) I. Koehne, S. Bachmann, T. Niklas, R. Herbst-Irmer, D. Stalke, *Chem. Eur. J.* **2017**, *23*, 13141–13149.

[5] I. Koehne, N. Graw, T. Teuteberg, R. Herbst-Irmer, D. Stalke, *Inorg. Chem.* **2017**, *56*, 14968–14978.

[6] a) F. Ortu, G. J. Moxey, A. J. Blake, W. Lewis, D. L. Kays, *Inorg. Chem.* **2013**, *52*, 12429–12439; b) N. Sen, S. Pal, V. V. Khade, S. Khan, *Eur. J. Inorg. Chem.* **2019**, *41*, 4450–4454.

[7] a) R.-C. Yu, C.-H. Hung, J.-H. Huang, H.-Y. Lee, J.-T. Chen, *Inorg. Chem.* **2002**, *41*, 6450–6455.

[8] H-C. Huang, B. Wang, X.-L. Chen, L. Pan, Y.-S. Li, *J. Polymer. Chem. A.* **2019**, *57*, 973–981.

[9] B. Jana, W. Uhl, *Inorg. Chim. Acta* **2017**, *455*, 61–69.

[10] C. C. Roberts, B. R. Barnett, D. B. Green, J. M. Fritsch, *Organometallics* **2012**, *31*, 4133–4141.

[11] C. Di Iulio, M. Middleton, G. Kociok-Köhn, M. D. Jones, A. L. Johnson, *Eur. J. Inorg. Chem.* **2013**, 1541–1554.

[12] C. Scheiper, D. Dittrich, C. Wölper, D. Bläser, J. Roll, S. Schulz, *Eur. J. Inorg. Chem.* **2014**, 2230–2240.

[13] K. Bakthavachalam, S. Dutta, C. Arivazhagan, B. Raghavendra, A. Haridas, S. S. Sen, D. Koley, S. Ghosh, *Dalton Trans.* **2018**, *47*, 15835–15844.

[14] J. Wiederkehr, C. Wolper, S. Schulz, *Z. Naturforsch. Sect. B* **2017**, *72*, 813–820.

[15] W.-Yi Lee, H.-H. Hsieh, C.-C. Hsieh, H. M. Lee, G.-H. Lee, J.-H. Huang, T.-C. Wu, S.-H. Chuang, *J. Organomet. Chem.* **2007**, *692*, 1131–1137.

[16] S.-M. Ho, C.-S. Hsiao, A. Datta, C. H. Hung, L.-C. Chang, T.-Y. Lee, J.-H. Huang, *Inorg. Chem.* **2009**, *48*, 8004–8011.

[17] L.-F. Hsueh, N.-T. Chuang, C.-Y. Lee, A. Datta, J.-H. Huang, T.-Y. Lee *Eur. J. Inorg. Chem.* **2011**, 5530–5537.

[18] B. Raghavendra, P. V. S. Shashank, M. K. Pandey, N. D. Reddy, *Organometallics* **2018**, *37*, 1656–1664.

[19] X.-L. Chen, B. Wang, L. Pan, Y.-S. Li, *Appl. Organomet. Chem.* **2019**, *33*, e4770-e4781.

[20] J. Gao, D. Zhu, W. Zhang, G. A. Solan, Y. Ma, W.-H. Sun, *Inorg. Chem. Front.*, **2019**, *6*, 2619–2652.

[21] a) T. Kottke, D. Stalke, *J. Appl. Crystallogr.* **1993**, *26*, 615–619; b) D. Stalke, *Chem. Soc. Rev.* **1998**, *27*, 171–178; c) T. Schulz, K. Meindl, D. Leusser, D. Stern, J. Graf, C. Michaelsen, M. Ruf, G. M. Sheldrick, D. Stalke, *J. Appl. Crystallogr.* **2009**, *42*, 885–891; d) L. Krause, R. Herbst-Irmer, G. M. Sheldrick, D. Stalke, *J. Appl. Crystallogr.* **2015**, *48*, 3–10; e) L. Krause, R. Herbst-Irmer, D. Stalke, *J. Appl. Crystallogr.* **2015**, *48*, 1907–1913. CCDC 1886689 (**L1**), 1885674 (**1**), 1885678 (**2**), 1885782 (**3**), 1958801 (**4**), 1959123 (**5**), 1958776 (**6**), 1885671 (**7**), 1958777 (**8**), 1962641 (**9**) contain the supplementary crystallographic data for this paper. These data can be obtained free of charge from The Cambridge Crystallographic Data Centre.

[22] R. Olejník, M. Bílek, Z. Růžičková, Z. Hoštálek, J. Merna, A. Růžička, *J. Organomet. Chem.* **2015**, *794*, 237–246.

[23] L. Yang, D. R. Powell, R. P. Houser, *Dalton Trans.* **2007**, 955–964.

[24] A. W. Addison, T. N. Rao, J. Reedijk, J. v. Rijn, G. C. Verschoor, *J. Chem. Soc. Dalton Trans.* **1984**, 1349—1356.

[25] A. Ecker, C. Üffing, H. Schnöckel, *Chem. Eur. J.* **1996**, *2*, 1112–1114.

[26] C. Eaborn, P. B. Hitchcock, A. Kowalewska, Z.-R. Lu, D. J. Smith, W. A. Stanczyk, *J. Organomet. Chem.* **1996**, *521*, 113–120.

[27] M. A. Brogan, A. J. Blake, C. Wilson, D. H. Gregory, *Acta Crystallogr.* **2003**, *C59*, i136–i138.

[28] P. A. Akishin, V. P. Spiridonov, *Zh. Fiz. Khim.* **1958**, *32*, 1682–1683.

[29] A. L. Spek, *Acta Crystallogr.* **2015**, *C71*, 9–18.

[30] J. Langer, S. Krieck, R. Fischer, H. Görls, M. Westerhausen, *Z. Anorg. Allg. Chem.* **2010**, *636*, 1190–1198.

[31] S. Nagendran, H. W. Roesky, *Organometallics* **2008**, *37*, 457–492.

[32] S. Nagendran, S. S. Sen, H. W. Roesky, D. Koley, H. Grubmuller, A. Pal, R. Herbst-Irmer, *Organometallics* **2008**, *27*, 5459–5463.

[33] R. K. Siwatch, S. Kundu, D. Kumar, S. Nagendran, *Organometallics* **2011**, *30*, 1998–2005.
[34] S. Pal, R. Dasgupta, S. Khan, *Organometallics* **2016**, 35, 3635–3640.

Manuscript received: December 23, 2019
Revised manuscript received: January 29, 2020
Accepted manuscript online: February 3, 2020
Version of record online: February 18, 2020

Chemistry
A European
Journal

Chemistry Europe
European Chemical Societies Publishing

Cover Feature:
R. G. Gonnade, D. Koley, S. S. Sen and co-workers
Monomeric Magnesium-Catalyzed Alkene and Alkyne Hydroboration

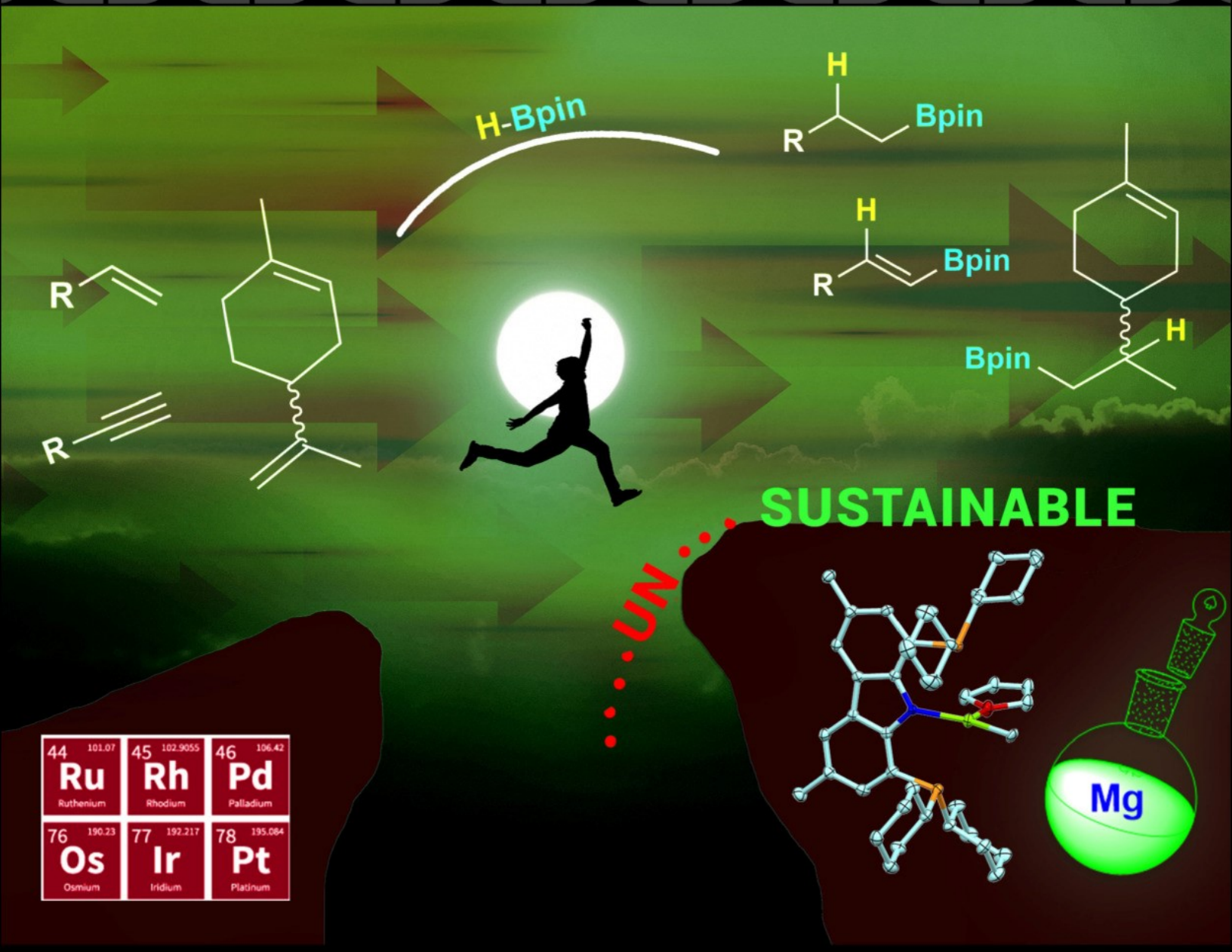

WILEY-VCH

00/2022

Chemistry–A European Journal
Research Article
doi.org/10.1002/chem.202201896
Chemistry Europe
European Chemical Societies Publishing
www.chemeurj.org

Monomeric Magnesium Catalyzed Alkene and Alkyne Hydroboration

Rohit Kumar[+],[a, b] Sayan Dutta[+],[c] Vishal Sharma,[a, b] Praval P. Singh,[c] Rajesh G. Gonnade,*[b, d] Debasis Koley,*[c] and Sakya S. Sen*[a, b]

Dedicated to Professor Holger Braunschweig on the occasion of his 60th birthday.

Abstract: In this work, two monomeric magnesium alkyl complexes (**1** and **2**) were prepared using bis(phosphino)carbazole framework and among them **1** has been used as a catalyst for hydroboration of alkenes and alkynes with pinacolborane (HBpin). A broad variety of aromatic and aliphatic alkenes and alkynes were efficiently reduced. Anti-Markovnikov regioselective hydroboration of alkenes and alkynes was achieved, which was confirmed by deuterium-labelling experiments. The work represents the first example of the use of magnesium in homogeneous catalytic hydroboration of alkene with broad substrate scope. Experimental mechanistic investigations and DFT calculations provided insights into the reaction mechanism. Finally, the hydroboration protocol was extended to terpenes.

Introduction

Increased focus on sustainable catalytic methods has brought a shift of emphasis toward catalysis with more earth-abundant elements.[1] In this regard, the alkaline-earth metal-based compounds have recently come forth as alternatives to the traditional transition metal or lanthanide-based catalysts for the hydroelementation of the unsaturated bonds. Magnesium is the eighth most abundant element in the Earth's crust, magnesium compounds are readily accessible, and their byproducts are easily decomposed, and non-hazardous. The well-defined magnesium compounds have achieved remarkable advances as homogeneous catalysts in recent years for the hydroboration of polarized unsaturated bonds such as aldehydes, ketones, nitriles, isonitriles carbodiimides, isocyanates, carbonates, thanks to ground-breaking works from the groups of Hill, Sadow, Okuda, Rueping and others.[2–14] By contrast, the hydroboration of alkynes and alkenes, which has applications in fine chemicals, perfumes, medicines etc.,[15] lags far behind in implementing magnesium based catalysts, perhaps owing to the less/non-polarized nature of the C–C multiple bond. Stoichiometric hydroboration of functionalized alkynes and alkenes using excess pinacolborane (HBpin) was reported by the group of Knochel,[16] and in recent years several catalysts based on *p*-block elements have been reported to mediate this transformation, thanks to stimulating works by the groups of Thomas, Ingleson, Roesky, Melen and others.[17] However, it was only recently that Rueping and co-workers reported the hydroboration of terminal and internal alkynes catalyzed by Bu_2Mg (Scheme 1).[18] The only report of magnesium-catalyzed hydroboration of alkenes came from Parkin and co-workers, who

[a] *R. Kumar,[+] V. Sharma, Dr. S. S. Sen*
Inorganic Chemistry and Catalysis Division
CSIR-National Chemical Laboratory
Dr. Homi Bhabha Road, Pashan, Pune 411008 (India)
E-mail: ss.sen@ncl.res.in
Homepage: http://academic.ncl.res.in/ss.sen

[b] *R. Kumar,[+] V. Sharma, Dr. R. G. Gonnade, Dr. S. S. Sen*
Academy of Scientific and Innovative Research (AcSIR)
Ghaziabad-201002 (India)

[c] *Dr. S. Dutta,[+] P. P. Singh, Prof. D. Koley*
Department of Chemical Sciences
Indian Institute of Science Education and Research (IISER) Kolkata
Mohanpur, 741246 (India)
E-mail: koley@iiserkol.ac.in
Homepage: http://www.iiserkol.ac.in/~koley/

[d] *Dr. R. G. Gonnade*
Physical and Materials Chemistry Catalysis Division
CSIR-National Chemical Laboratory
Dr. Homi Bhabha Road, Pashan, Pune 411008 (India)
E-mail: rg.gonnade@ncl.res.in
Homepage: http://academic.ncl.res.in/rg.gonnade

[+] *These authors contributed equally for this manuscript.*

Supporting information for this article is available on the WWW under https://doi.org/10.1002/chem.202201896

Magnesium catalyzed alkyne hydroboration: (Cavallo & Rueping, 2019)[18]

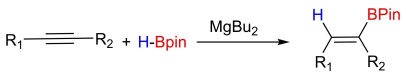

Magnesium catalyzed alkyne & alkene hydroboration: (This work)

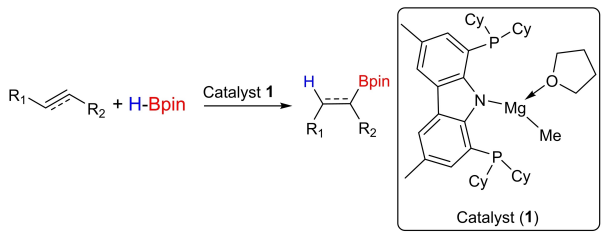

Scheme 1. Mg-catalyzed hydroboration of alkyne (known) and alkenes (unknown).

employed a five-coordinate magnesium hydride, [TismPriBenz]MgH [TismPriBenz = tris[(1-isopropylbenzimidazol-2-yl)-dimethylsilyl)]methyl] as a catalyst for hydroboration of styrene,[19a] however the substrate scope was not elaborated. Besides, in a seminal work Harder and co-workers described that in [DIPPnacnacCaH·(THF)]$_2$ catalyzed alkene hydroboration, the organocalcium compound catalyzes the decomposition of HBcat to mainly $B_2(cat)_3$ and BH_3 (or B_2H_6), and the latters are the bonafide catalysts.[19b]

Despite the synthetic utility and widespread application of Grignard reagents, only a handful of well-defined magnesium alkyl complexes are known to date and a closer look at their molecular structures reveals that the magnesium center in these compounds is mostly four or higher coordinate.[20] Here, we describe the preparation of a series of quasi three-coordinate magnesium alkyl complexes using bis(phosphino)carbazolido ligand, and their activity as catalysts for the hydroboration of alkenes and alkynes.

Results and Discussion

For the design of well-defined magnesium alkyl complexes, we have turned our attention towards bis(phosphino)carbazole-based frameworks due to the push-pull electronic environment provided by a π-acidic phosphine and a π-donating carbazolido ligand. Moreover, these scaffolds combine "hard" amido and "soft" phosphine donors. Particularly interesting to us in this regard is the recent report by Munz and co-workers, who have isolated a luminescent magnesium bromide complex supported by carbazolyl bridged pincer-type NHC. However, the compound was not structurally authenticated presumably due to solubility issue.[21] We have developed here a new and convenient synthetic procedure to access bis(phosphino)carbazole ligand. We could start with relatively cheap di-*p*-tolylamine instead of 3,6-bromo-9*H*-carbazole and avoid the use of hazardous *tert*-butyllithium.

The preparation of **LH** requires only two steps in comparison to multi-step synthesis reported by Gibson and co-workers[22] (i) bromination of di-p-tolyl amine using bromine in acetic acid and (ii) lithiation of the brominated compound using *n*BuLi and subsequent addition of chlorodicyclohexyl phosphine in diethyl ether, which led to the formation of PNP-donor ligand (Scheme 2). Treatment of **LH** with Grignard reagents such as MeMgBr, or $MgBu_2$ in THF gives corresponding magnesium methyl (**1**) and butyl (**2**) complexes. The ^{1}H NMR of **1** show the chemical shift for the methyl protons bound to Mg at −0.74 ppm. It must be stated here that despite repeated attempts, we are unable to get very pure spectra of **1** and **2** mainly due to solubility issue. The additional peaks in their respective spectrum originate from the coordinated THF molecules and toluene solvent which has been used during work up and sometimes isooctane (in case of **2**). The molecular structures of **1** and **2**, are given in Figures 1 and 2, respectively, which demonstrate that they exist as monomeric species with a terminal alkyl ligand. The phosphine moieties did not coordinate to the magnesium centers of **1** and **2**. The Mg–P

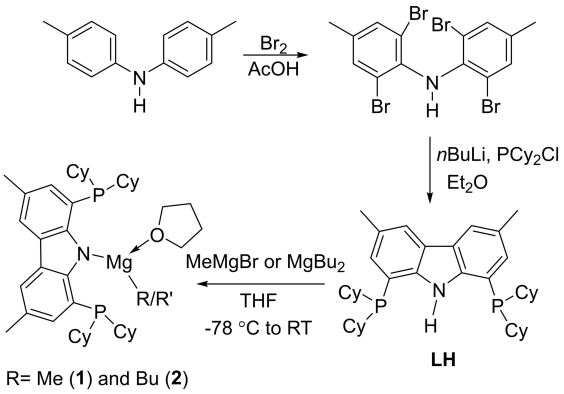

Scheme 2. Synthesis of **1** and **2** starting from di-p-tolylamine.

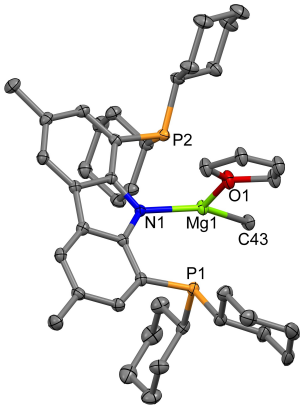

Figure 1. The molecular structure of **1** with anisotropic displacement parameters depicted at the 50% probability level. Hydrogen atoms are not shown for clarity. Selected distances (Å) and angles (deg): P1-Mg1 2.8461(13), P2-Mg1 2.8094(13), Mg1-O1 2.027(3), Mg1-N1 2.081(3), Mg1-C43 2.164(3); O1-Mg1-N1 98.56(10), O1-Mg1-C43 112.87(12), N1-Mg1-C43 148.50(13), O1-Mg1-P2 96.43(8), N1-Mg1-P2 74.75(7), C43-Mg1-P2 102.65(9), O1-Mg1-P1 96.19(8), N1-Mg1-P1 74.30(7), C43-Mg1-P1 99.33(9), P2-Mg1-P1 147.94(5).

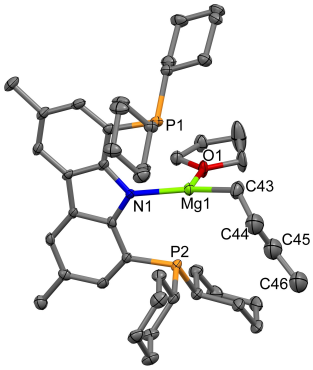

Figure 2. The molecular structure of **2** with anisotropic displacement parameters depicted at the 50% probability level. Hydrogen atoms are not shown for clarity. Selected distances (Å) and angles (deg): P1-Mg1 2.8307(18), P2-Mg1 2.8428(18), Mg1-O1 2.031(3), Mg1-N1 2.085(3), Mg1-C43 2.142(5); O1-Mg1-N1 97.80(13), O1-Mg1-C43 111.05(18), N1-Mg1-C43 150.63(19), O1-Mg1-P1 98.09(11), N1-Mg1-P1 74.16(10), C43-Mg1-P1 95.80(15), O1-Mg1-P2 95.03(11), N1-Mg1-P2 74.30(10), C43-Mg1-P2 107.33(15), P1-Mg1-P2 147.14(6).

interactions in these compounds vary within the range of 2.8094(13)–2.8428(18) Å, which are longer than the predicted covalent value (2.65 Å) and other mononuclear and dinuclear magnesium phosphanides for example [BuMg{P(CH-(SiMe$_3$)$_2$)(C$_6$H$_4$-2-OMe)}]$_2$ (2.5760(8) and 2.5978(8) Å), Mg[P{CH-(SiMe$_3$)$_2$}{C$_6$H$_4$-2-CH$_2$NMe$_2$}]$_2$ (2.556(1) Å) and [Mg{[O,O′-(Me$_2$PCH$_2$)$_2$C$_6$H$_3$]$_2$}$_2$] 2.761(1) and 2.770(1) Å).[23] However, there might be weak interaction between the phosphorus and magnesium atom as the angles N1-Mg1-C43, N1-Mg1-O1, O1-Mg1-C43 are 148.5°, 98° and 112°. The Mg-N$_{carbazole}$ bond lengths are 2.081(3) and 2.085(3) Å in **1** and **2**, which are longer than Mg–N bond lengths in β-diketiminato magnesium complexes[20b] and those of three-coordinate amido magnesium alkyl complexes [1.997(3), 1.9973(12), 2.046(2) Å] reported by Ma and co-workers.[20h] During the preparation of our manuscript, the groups of Westerhausen and Tan independently reported the carbazolyl Hauser bases, [(thf)$_3$Mg(Carb)Br] (**3**) and [(OEt$_2$){3,6-*t*Bu$_2$-1,8-bis(10-phenylanthracen-9-yl)Carb}MgI] (**4**), where the Mg-N$_{carbazole}$ bonds were determined to be 2.045(3) (for **3**) and 2.038(3) Å (for **4**), slightly shorter than those in **1** and **2**.[24] The slightly elongated Mg–N bond lengths in **1** and **2** are more in line with the quasi-coordination of the phosphine units to the Mg centers. The terminal Mg–C bond lengths in **1** and **2** are of 2.164(3) and 2.142(5) Å, which are in good agreement with those reported by Ma and co-workers [2.114(4), 2.1844(16), 2.173(4) Å].[20h]

Having established simple strategies to obtain magnesium alkyl complexes based on bis(phosphino)carbazolido ligand, the catalytic utility of these derivatives was further studied. Because hydroboration by compounds with main-group elements has become a hot topic in recent years, hydroboration of alkyne was chosen for further investigation. Initial catalyst evaluation for the hydroboration of alkynes was carried out with **1** and **2**, and phenyl acetylene as model substrate and HBpin. Results suggest that compound **1** shows better catalytic activity than **2**. Performing the reaction with **1** at 80 °C for 18 h afforded the corresponding (E)-vinyl boronate **5a** in 91 % yield and excellent selectivity. Using the optimized reaction conditions (see Table S1 for optimization), both aliphatic and aromatic alkynes underwent hydroboration to form the corresponding vinyl-boronates in good to excellent yields (Scheme 3), reflecting the high efficiency of the catalyst. Smooth hydroboration of aromatic alkynes with electron-donating (**5b**, **5c**, **5f**, **5g**) or withdrawing (**5d** and **5e**) substituents was observed. 1-Ethenyl cyclohexene was found to react exclusively with the alkyne functionality in good yield (**5h**), with no apparent reduction of the alkene moiety. Overall, the protocol is comparable with that reported by Rueping and co-workers,[18] though in our case the catalyst mol % is less, and no solvent is needed. In fact, scaling up the reaction to 5 mmol for phenylacetylene revealed almost no drop in yield. Internal alkynes such as diphenyl acetylene and 3-hexyne underwent hydroboration (**5n** and **5o**) though in moderate yields. Deuterium labelling experiments were carried out to understand the stereoselectivity (Scheme 4). A resonance at δ 6.20 ppm in the ^{2}H NMR for the catalytic reduction of PhC≡CD with HBpin designates a cis configuration of the deuterium and phenyl ring (Scheme 4, above). Similarly, the

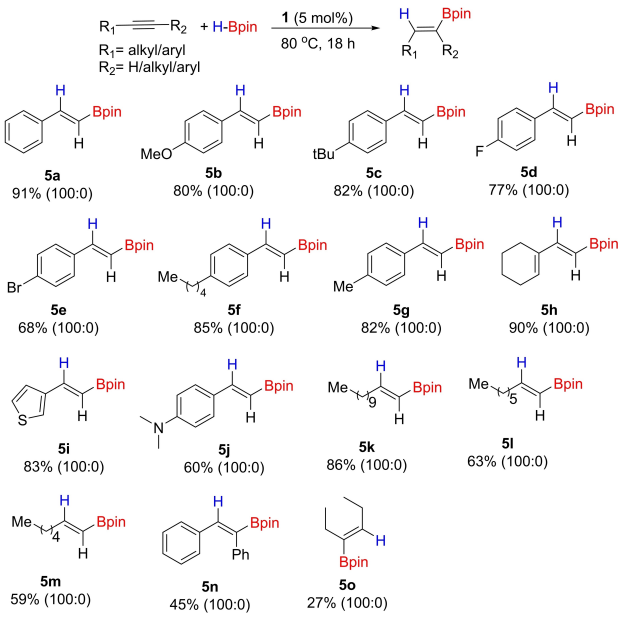

Scheme 3. Hydroboration scope with alkyne substrates. Reaction conditions: Alkyne (0.25 mmol), HBpin (0.275 mmol, 1.1 equiv), 5 mol % catalyst, 18 h reaction at 80 °C temperature in neat condition. Yields were determined by the ^{1}H NMR integration relative to mesitylene. Ratios in parentheses report the ratio of regioisomers (linear vs. branched).

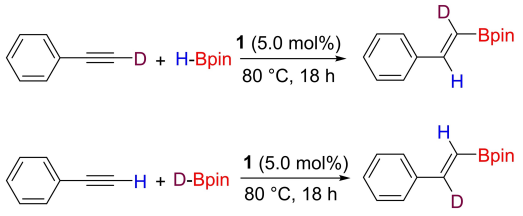

Scheme 4. Deuterium labelling experiment: Hydroboration of phenylacetylene-D with HBpin (above) and (b) Hydroboration of phenylacetylene with DBpin (below).

reaction of PhC≡CH and DBpin (Scheme 4, below) exhibits a resonance at δ 7.24 ppm in the ^{2}H NMR spectrum (see Schemes S11 and S12, and Figures S109 and S110), demonstrating evidence in favor of a 1,2-*cis*-hydroboration.

Subsequently, we were interested in the hydroboration of alkenes, which is more challenging compared to alkynes. For hydroboration of alkenes, catalyst loadings were increased up to 10 mol %, and the reactions were over around 12 h upon heating at 100 °C. Simple aryl- and alkyl-substituted terminal alkenes proceeded to the hydroboration products (Scheme 5). Notably, the isomer ratio for all substrates was 95–99 : 5–1 towards the anti-Markovnikov product. The substrate scope revealed that the reduction of both electron-rich styrene derivatives (**6b**–**6e**) and electron-poor derivatives (**6f**, **6g**, **6i**) afforded the corresponding boronates in excellent yields. Sterically encumbered 2,4,6-trimethylphenyl substituted styrene performed well (**6e**), explicating that the steric parameters have little effect on the catalyst activity. Analysis of the scope for aliphatic alkenes has shown high reactivity for a large number

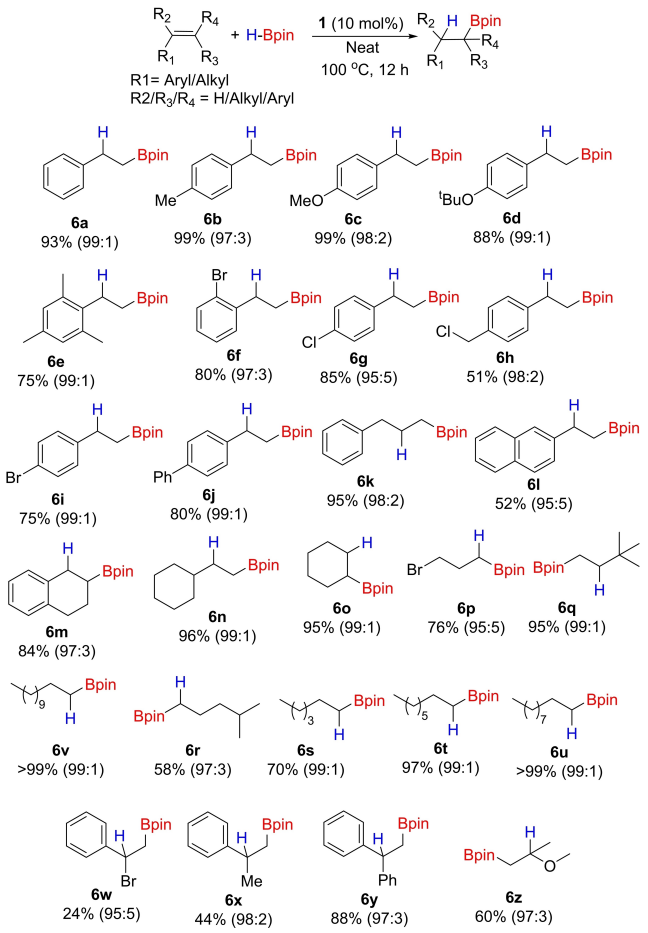

Scheme 5. Hydroboration Scope with alkene substrates. Reaction conditions: Alkene (0.25 mmol), HBpin (0.275 mmol, 1.1 equiv.), 10 mol% catalyst, 12 h reaction at 100 °C temperature in neat condition. Yields were determined by the ^{1}H NMR integration relative to mesitylene. Ratios in parentheses report the ratio of regioisomers (linear vs. branched).

of alkyl substrates. While a recently reported Mn(I) catalyst was unreactive towards hydroboration of cyclohexene,[25] **1** can selectively reduce cyclohexene (**6o**) in quantitative yield. Similarly, Oestreich and co-workers found only traces for hydroboration of 4-methoxy styrene[17i] with BAr^F_3 (Ar^F = 3,5-bis(trifluoromethyl)phenyl), while **1** gives quantitative yield for the same. In case of internal alkenes, the reactions were sluggish with α-bromo (**6w**) and α-methyl (**6x**) groups. However, the reaction was smooth for α-phenyl styrene, which gives 88% conversion (**6y**). Gratifyingly, the alkene hydroboration reaction was also scaled up to 5 mmol under the same conditions with almost no compromise of the yields.

Recently Thomas and cowokers have shown that nucleophiles such as NaO*t*Bu,[26] *n*BuLi,[27] nBu$_2$Mg[18] etc. actually promote the formation of BH_3 from HBpin and the generated BH_3 does the catalysis.[28,29] To ascertain whether BH_3 was involved in hidden catalysis, we have carried out the same reaction in the presence of 10 mol% TMEDA, which led to the formation of the corresponding borylated alkane with 86% yield (Scheme S14, Figure S117) for styrene with a 7% yield drop. The ^{11}B NMR of the reaction in presence of TMEDA reveals no prominent resonance at −10 ppm (Figure S118), which is characteristics for TMEDA·BH_3 adduct.[28] However, the inspection of the ^{11}B NMR spectrum arisen from the reaction of HBpin with **1** reveals the generation of BH_3 in very minor quantity (Figure 3, magnified section and Figure S114). Hence, we cannot exclude unequivocally the possibility of hidden borohydride catalysis.[28–30]

In a bid to expand the scope of catalysis by **1**, naturally occurring terpenes such as R- or S-limonene, myrcene and β-pinene have been subjected for the selective hydroboration of their olefinic bond. Interestingly, good yields were obtained for all cases with excellent selectivity (Scheme 6), which could not be afforded with our previously reported lithium based catalyst.[31] In case of limonene, only terminal double bond was selectively reduced.[32] Interestingly, Ritter and co-workers reported the analogous hydroboration of myrcene with HBpin, which was catalyzed by the iminopyridine-iron(II) complex (5 mol%) in the presence of magnesium metal (10%),[33] while in our case no transition metal or elemental magnesium is needed.

To further evaluate the chemoselective hydroboration, a series experiments were carried out (Scheme 7). The competing experiment involving a mixture of (i) acetophenone and styrene and (ii) ethyl benzoate and styrene resulted in almost quantitative hydroboration of ketone/ester and complete recycle of styrene. Similarly, equimolar amounts of acetophenone or ethyl benzoate and phenylacetylene were reacted with HBpin to produce the corresponding boronate esters of ketone or ester. Similar chemoselectivity was observed for nitriles over alkene and alkyne. In another competition study, where

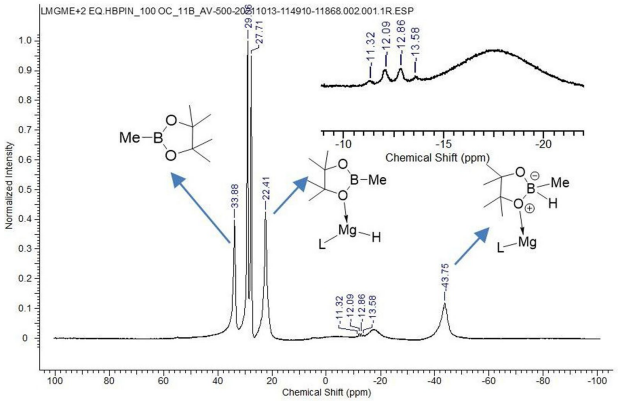

Figure 3. ^{11}B NMR spectrum of the reaction of **1** with HBpin.

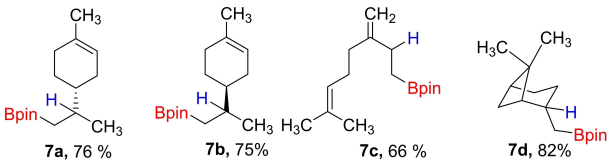

Scheme 6. Selective alkene hydroboration for terpenes: *R*- or *S*- limonene, myrcene, and β-pinene.

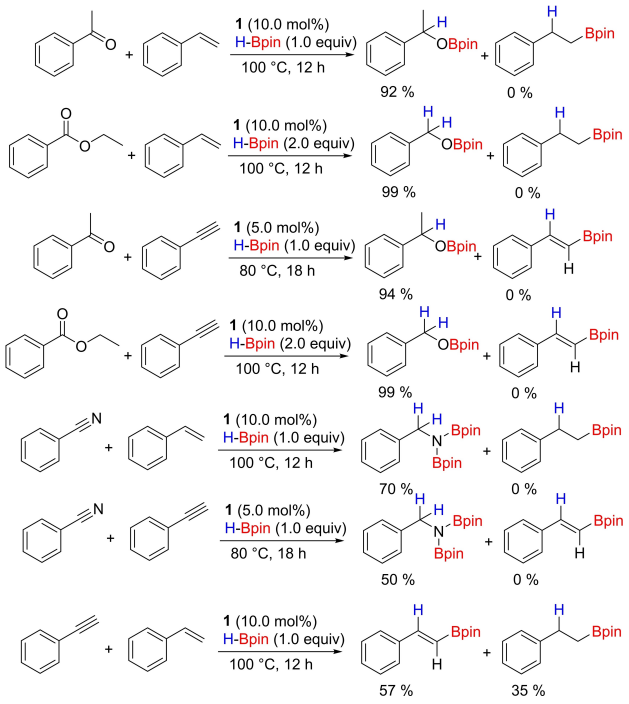

Scheme 7. Competitive experiments for chemoselective hydroboration.

equimolar styrene and phenylacetylene are allowed to compete for 1.0 equiv of HBpin, marginal preference for alkyne hydroboration was witnessed, reaching 57% conversion of phenylacetylene and only 35% conversion of styrene. The details of the competitive experiments are given in the Supporting Information (Scheme S3–S10, Figure S103–S110).

The hydroboration of styrene with **1** was monitored in situ by ^{1}H NMR spectroscopy. Reactions were initially carried out employing identical concentrations of **1** and different styrene concentrations. A graph of ln[styrene] versus time (Figure S123), revealed that the reaction is first order with respect to styrene. The same sets of experiments were performed with varying concentration of HBpin and the resulting plot indicated first-order rate dependence with respect to HBpin (Figure S121). Arrhenius analysis afforded an activation of ca. 13 (± 6) kcal mol^{-1} (Figure S128).

A detailed theoretical exploration of the catalytic efficiency of the monomeric magnesium alkyl complexes in hydroboration reactions is performed to unravel the complete mechanistic scenario. Quantum chemical calculations were performed at the R-M06-2X-D3/def2-TZVP//R-BP86/def2-SVP level[34] to explore the mechanistic avenues in Mg-catalyzed hydroboration of styrene. Theoretical calculations suggest the initiation of the reaction with σ-bond metathesis between the H-Bpin and Mg–Me bonds following *Pathway-A* via the transition state **TS-1** (Figure 4), leading to the formation of a slightly more stable intermediate **INT-1** that serves as the active catalyst. This step

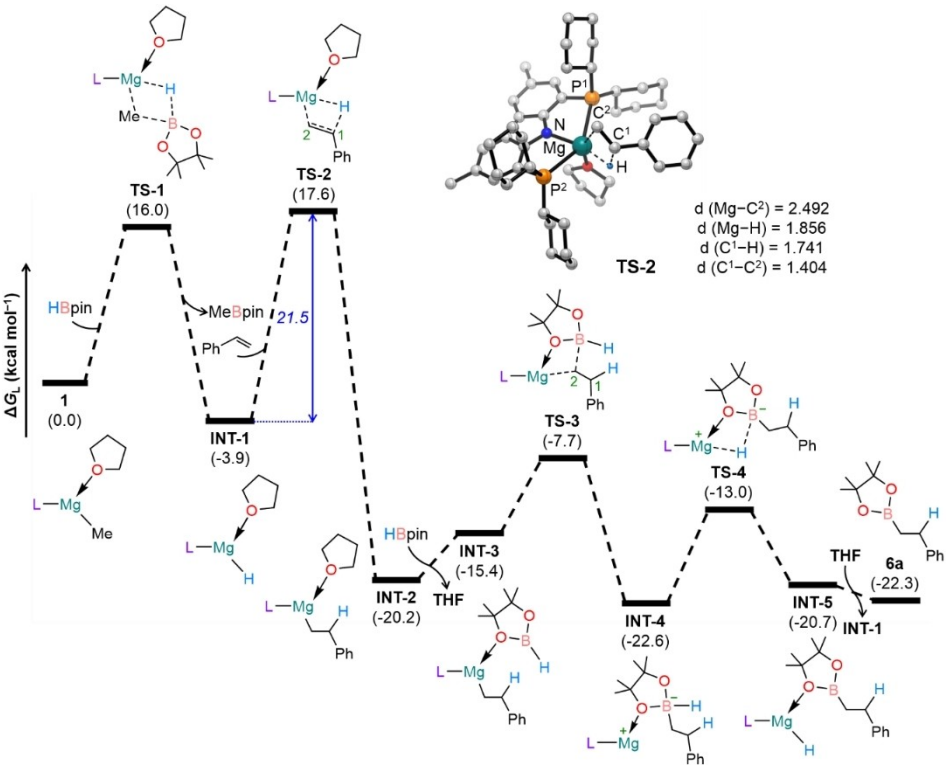

Figure 4. Energy profile for the Mg-catalyzed hydroboration of styrene following *Pathway-A*. Optimized geometry of the transition state **TS-2** with important geometrical parameters is also provided. Bond distances (d) are in angstroms (Å). Only key hydrogen atom is shown for clarity. L = 1,8-bis(phosphino)carbazolide anion.

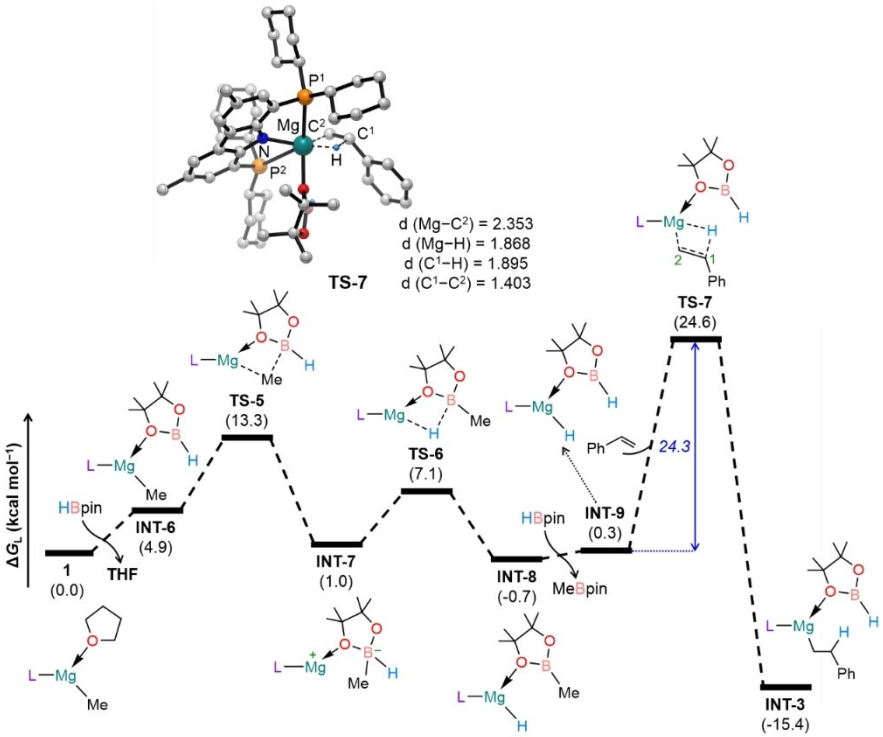

Figure 5. Energy profile for the Mg-catalyzed hydroboration of styrene following *Pathway-B*. Optimized geometry of the transition state **TS-7** with important geometrical parameters is also provided. Bond distances (d) are in angstroms (Å). Only key hydrogen atoms are shown for clarity. L = 1,8-bis(phosphino)carbazolide anion.

needs to overcome an energy barrier of 16.0 kcal mol^{-1}. The insertion of styrene into the Mg–H bond in **INT-1** furnishes an appreciably stable intermediate **INT-2**, surmounting the rate-limiting energy barrier of 21.5 kcal mol^{-1}. The substitution of the coordinated THF in **INT-2** with HBpin followed by the nucleophilic migration of the phenethyl group to the boron center results in the zwitterionic intermediate **INT-4**. The generation of **INT-4** is supported by the ^{11}B NMR resonance at −43.75 ppm arising from the stoichiometric reaction of **1** and HBpin (Figure S114), which is in good agreement with that reported by Cavallo and Rueping.[18] The subsequent hydride transfer from boron to magnesium generates **INT-5** via **TS-4**. Finally, the desired hydroboration product (**6a**) is liberated from **INT-5** to regenerate the active catalyst **INT-1** for the next catalytic cycle.

We have also investigated the alternative route, *Pathway-B*, concerning the HBpin coordinated magnesium hydride species (**INT-9**) as the active catalyst (Figures 5 and S129).[18] Though the generation of **INT-9** demands an appreciably lower energy barrier than that of **INT-1** by 2.7 kcal mol^{-1}, similar insertion of styrene into the Mg–H bond in **INT-9** requires a slightly higher energy barrier of 24.3 kcal mol^{-1} to afford **INT-3**. Hence, of the two competing routes for the generation of **INT-3**, *Pathway-A* prevails over *Pathway-B* on the kinetic ground. However, monitoring the stoichiometric reaction of **1** with HBpin by ^{11}B NMR revealed three resonances at 33.9 (MeBpin),[29] 22.4 (**INT-8**), and −43.7 (zwitterionic species **INT-7**) ppm (Figure 3), which are in good agreement with those reported by Cavallo and Rueping.[18] Additionally, given the fact that HBpin was used in stoichiometric amount, **INT-9** may dominate the reaction course. These data prefer *Pathway-B* over *Pathway-A*. Furthermore, distortion-interaction analyses[35] of the key transition states **TS-2**/**TS-7** considering **INT-1**/**INT-9** and styrene as the interacting fragments reveal the activation barriers to be solely governed by the distortion energies of the **INT-1**/**INT-9** fragments (Tables S6 and S7).[36] We have also investigated *Pathway-C* involving direct insertion of styrene into the B–H bond in **INT-6**, as depicted in Figure S131. However, the corresponding transition state **TS-9** exhibits a drastically high energy barrier of 44.2 kcal mol^{-1}; therefore, this route can be safely discarded.

Conclusion

We have introduced bis(phosphino)carbazolido ligand to develop monomeric magnesium alkyl species through a convenient synthetic route. We have further demonstrated that the easily prepared magnesium methyl compound **1** may be applied to the efficient hydroboration of a variety of alkenes and alkynes as well as few biologically important terpenes. The methodology proceeds with the syn addition of HBpin and good regioselectivity for unsymmetrical alkenes and alkynes. Extensive DFT studies have been carried out to have an insight the mechanism. Future investigations will look at expanding the

scope of this magnesium catalyst for other unsaturated substrates.

Experimental Section

Please see Supporting Information for the synthesis, characterization, and structural data for **LH** and **1** and **2**. Complete computational details and relevant NMR spectra for hydroborated product of alkenes and alkynes are also provided in the Supporting Information.

Deposition Number(s) 2144879 (for **1**), 2144882 (for **2**) contain(s) the supplementary crystallographic data for this paper. These data are provided free of charge by the joint Cambridge Crystallographic Data Centre and Fachinformationszentrum Karlsruhe Access Structures service.

Acknowledgements

This work was supported by the Scheme for Translational and Advanced Research in Sciences (STARS), the Ministry of Education, and the Government of India (Grant MoE-STARS/STARS-1/255) (S.S.S. and D.K.). R.K., S.D., V.S., and P.P.S. thank CSIR, India, for their research fellowships. D.K. and S.D. acknowledge IISER Kolkata for the computational facility. We are thankful to the reviewers for their critical inputs to improve the manuscript.

Conflict of Interest

The authors declare no conflict of interest.

Data Availability Statement

The data that support the findings of this study are available in the supplementary material of this article.

Keywords: carbazole · magnesium · monomeric complexes · phosphorous · X-ray structure

[1] R. M. Bullock, J. G. Chen, L. Gagliardi, P. J. Chirik, O. K. Farha, C. H. Hendon, C. W. Jones, J. A. Keith, J. Klosin, S. D. Minteer, R. H. Morris, A. T. Radosevich, T. B. Rauchfuss, N. A. Strotman, A. Vojvodic, T. R. Ward, J. Y. Yang, Y. Surendranath, *Science* **2020**, *369*, eabc3183 (1-10).
[2] M. Arrowsmith, T. J. Hadlington, M. S. Hill, G. Kociok-Köhn, *Chem. Commun.* **2012**, *48*, 4567–4569.
[3] M. Arrowsmith, M. S. Hill, G. Kociok-Köhn, *Chem. Eur. J.* **2013**, *19*, 2776–2783.
[4] D. Mukherjee, A. Ellern, A. D. Sadow, *Chem. Sci.* **2014**, *5*, 959–964.
[5] C. Weetman, M. S. Hill, M. F. Mahon, *Chem. Commun.* **2015**, *51*, 14477–14480.
[6] N. L. Lampland, M. Hovey, D. Mukherjee, A. D. Sadow, *ACS Catal.* **2015**, *5*, 4219–4226.
[7] C. Weetman, M. D. Anker, M. Arrowsmith, M. S. Hill, G. Kociok-Köhn, D. J. Liptrot, M. F. Mahon, *Chem. Sci.* **2016**, *7*, 628–641.
[8] D. Mukherjee, S. Shirase, T. P. Spaniol, K. Mashima, J. Okuda, *Chem. Commun.* **2016**, *52*, 13155–13158.
[9] Y. Yang, M. D. Anker, J. Fang, M. F. Mahon, L. Maron, C. Weetman, M. S. Hill, *Chem. Sci.* **2017**, *8*, 3529–3537.
[10] S. Yadav, R. Dixit, M. K. Bisai, K. Vanka, S. S. Sen, *Organometallics* **2018**, *37*, 4576–4584.
[11] Y. K. Jang, M. Magre, M. Rueping, *Org. Lett.* **2019**, *21*, 8349–8352.
[12] M. Szewczyk, M. Magre, V. Zubar, M. Rueping, *ACS Catal.* **2019**, *9*, 11634–11639.
[13] M. S. Hill, D. J. Liptrot, C. Weetman, *Chem. Soc. Rev.* **2016**, *45*, 972–988.
[14] M. Magre, M. Szewczyk, M. Rueping, *Chem. Rev.* **2022**, *122*, 9, 8261–8312.
[15] J. V. Obligacion, P. J. Chirik, *Nat. Chem. Rev.* **2018**, *2*, 15–34.
[16] C. E. Tucker, J. Davidson, P. Knochel, *J. Org. Chem.* **1992**, *57*, 3483–3485.
[17] Selected references for alkyne hydroboration by compounds with *p*-block elements, please see: a) Z. Yang, M. Zhong, X. Ma, K. Nijesh, S. De, P. Parameswaran, H. W. Roesky, *J. Am. Chem. Soc.* **2016**, *138*, 2548–2551; b) A. Bismuto, S. P. Thomas, M. J. Cowley, *Angew. Chem.* **2016**, *128*, 15582–15585; *Angew. Chem. Int. Ed.* **2016**, *55*, 15356–15359; c) J. S. McGough, S. M. Butler, I. A. Cade, M. J. Ingleson, *Chem. Sci.* **2016**, *7*, 3384–3389; d) J. R. Lawson, L. C. Wilkins, R. L. Melen, *Chem. Eur. J.* **2017**, *23*, 10997–11000; e) J. L. Carden, L. J. Gierlichs, D. F. Wass, D. L. Browne, R. L. Melen, *Chem. Commun.* **2019**, *55*, 318–321; f) S. Pahar, V. Sharma, S. Tothadi, S. S. Sen, *Dalton Trans.* **2021**, *50*, 16678–16684; g) A. Harinath, I. Banerjee, J. Bhattacharjee, T. K. Panda, *New J. Chem.* **2019**, *43*, 10531–10536. For alkene hydroboration:; h) A. Prokofjevs, A. Boussonnihre, L. Li, H. Bonin, E. Lacite, D. P. Curran, E. Vedejs, *J. Am. Chem. Soc.* **2012**, *134*, 12281–12288; i) Q. Yin, S. Kemper, H. F. T. Klare, M. Oestreich, *Chem. Eur. J.* **2016**, *22*, 13840–13844; j) A. Bismuto, M. J. Cowley, S. P. Thomas, *ACS Catal.* **2018**, *8*, 2001–2005.
[18] M. Magre, B. Maity, A. Falconnet, L. Cavallo, M. Rueping, *Angew. Chem.* **2019**, *131*, 7099–7103; *Angew. Chem. Int. Ed.* **2019**, *58*, 7025–7029.
[19] a) M. Rauch, S. Ruccolo, G. Parkin, *J. Am. Chem. Soc.* **2017**, *139*, 13264–13267; b) S. Harder, J. Spielmann, *J. Organomet. Chem.* **2012**, *698*, 7–14.
[20] a) P. Ghosh, G. Parkin, *Inorg. Chem.* **1996**, *35*, 1429–1430; b) V. C. Gibson, J. A. Segal, A. J. P. White, D. J. Williams, *J. Am. Chem. Soc.* **2000**, *122*, 7120–7121; c) A. P. Dove, V. C. Gibson, P. Hormnirun, E. L. Marshall, J. A. Segal, A. J. P. White, D. J. Williams, *Dalton Trans.* **2003**, 3088–3097; d) L. F. Sánchez-Barba, A. Garcés, M. Fajardo, C. Alonso-Moreno, J. Fernández-Baeza, A. Otero, A. Antiñolo, J. Tejeda, A. Lara-Sánchez, M. I. López-Solerag, *Organometallics* **2007**, *26*, 6403–6411; e) S. E. Baillie, V. L. Blair, T. D. Bradley, W. Clegg, J. Cowan, R. W. Harrington, A. Hernan-Gómez, A. R. Kennedy, Z. Livingstone, E. Hevia, *Chem. Sci.* **2013**, *4*, 1895–1905; f) V. Balasanthiran, M. H. Chisholm, K. Choojun, C. B. Durr, P. M. Wambua, *Polyhedron* **2016**, *103*, 235–240; g) S. Ruccolo, M. Rauch, G. Parkin, *Chem. Sci.* **2017**, *8*, 4465–4474; h) M. Ma, J. Li, X. Shen, Z. Yu, W. Yao, S. A. Pullarkat, *RSC Adv.* **2017**, *7*, 45401–45407; i) J. Langer, I. Kosygin, R. Puchta, J. Pahl, S. Harder, *Chem. Eur. J.* **2016**, *22*, 17425–17435.
[21] P. Pinter, C. M. Schüßlbauer, F. A. Watt, N. Dickmann, R. Herbst-Irmer, B. Morgenstern, A. Grünwald, T. Ullrich, M. Zimmer, S. Hohloch, D. M. Guldi, D. Munz, *Chem. Sci.* **2021**, *12*, 7401–7410.
[22] V. C. Gibson, S. K. Spitzmesser, A. J. P. White, D. J. Williams, *Dalton Trans.* **2003**, 2718–2727.
[23] a) S. Blair, K. Izod, W. Clegg, R. W. Harrington, *Eur. J. Inorg. Chem.* **2003**, 3319–3324; b) S. Blair, K. Izod, W. Clegg, *Inorg. Chem.* **2002**, *41*, 3886–3893; c) A. Pape, M. Lutz, G. Müller, *Angew. Chem.* **1994**, *106*, 2372–2375; *Angew. Chem. Int. Ed. Engl.* **1994**, *33*, 2281–2284; d) M. M. Meinholz, S. K. Pandey, S. M. Deuerlein, D. Stalke, *Dalton Trans.* **2011**, *40*, 1662–1671.
[24] a) P. Schüler, S. Sengupta, S. Zaubitzer, F. Fiesinger, S. Dongmo, H. Görls, M. Wohlfahrt-Mehrens, M.v.d. Borg, D. Gaissmaier, S. Krieck, M. Marinaro, T. Jacob, M. Westerhausen, *Eur. J. Inorg. Chem.* **2022**, e202200149 (1–6); b) J. Pan, L. Zhang, Y. He, Q. Yu, G. Tan, *Organometallics* **2021**, *40*, 3365–3369.
[25] S. Weber, D. Zobernig, B. Stöger, L. F. Veiros, K. Kirchner, *Angew. Chem.* **2021**, *133*, 24693–24697; *Angew. Chem. Int. Ed.* **2021**, *60*, 24488–24492.
[26] J. H. Docherty, J. Peng, A. P. Dominey, S. P. Thomas, *Nat. Chem.* **2017**, *9*, 595–600.
[27] Z.-C. Wang, M. Wang, J. Gao, S.-L. Shi, Y. Xu, *Org. Chem. Front.* **2019**, *6*, 2949–2953.
[28] A. D. Bage, T. A. Hunt, S. P. Thomas, *Org. Lett.* **2020**, *22*, 4107–4112.
[29] A. D. Bage, K. Nicholson, T. A. Hunt, T. Langer, S. P. Thomas, *ACS Catal.* **2020**, *10*, 13479–13486.

[30] N. W. J. Ang, C. S. Buettner, S. Docherty, A. Bismuto, J. R. Carney, J. H. Docherty, M. J. Cowley, S. P. Thomas, *Synthesis* **2018**, *50*, 803–808.
[31] M. K. Bisai, S. Yadav, T. Das, K. Vanka, S. S. Sen, *Chem. Commun.* **2019**, *55*, 11711–11714.
[32] W. N. Palmer, T. Diao, I. Pappas, P. J. Chirik, *ACS Catal.* **2015**, *5*, 622–626.
[33] J. Y. Yu, B. Moreau, T. Ritter, *J. Am. Chem. Soc.* **2009**, *131*, 12915–12917.
[34] a) D. Sarkar, S. Dutta, C. Weetman, E. Schubert, D. Koley, S. Inoue, *Chem. Eur. J.* **2021**, *27*, 13072–13078; b) S. Dutta, K. Singh, D. Koley, *Chem. Asian J.* **2021**, *16*, 3492–3508.
[35] a) K. Kitaura, K. Morokuma, *Int. J. Quantum Chem.* **1976**, *10*, 325–340; b) F. M. Bickelhaupt, K. N. Houk, *Angew. Chem.* **2017**, *129*, 10204–10221; *Angew. Chem. Int. Ed.* **2017**, *56*, 10070–10086.
[36] S. Dutta, S. De, S. Bose, E. Mahal, D. Koley, *Eur. J. Inorg. Chem.* **2020**, 638–655.

Manuscript received: June 20, 2022
Accepted manuscript online: July 21, 2022
Version of record online: August 17, 2022

ChemComm

COMMUNICATION

View Article Online
View Journal | View Issue

Cite this: *Chem. Commun.*, 2022, **58**, 11843

Received 25th July 2022,
Accepted 22nd September 2022

DOI: 10.1039/d2cc04142a

rsc.li/chemcomm

Luminescent magnesium complexes with intra- and inter-ligand charge transfer†

Rohit Kumar,[ab] Sanjukta Pahar,[ab] Joy Chatterjee,[c] Soumya Ranjan Dash,[bd] Rajesh G. Gonnade,[bd] Kumar Vanka[bd] and Sakya S. Sen*[ab]

Herein, we report two 2,2′-pyridylpyrrolide (PyPyrH) ligand supported magnesium complexes (1 and 2), which demonstrate bright luminescence with a quantum yield of 22% and 14% in the solid state, respectively. Theoretical calculations reveal that their emissive properties originate from the intra- and inter-ligand charge transfer.

Molecular photosensitizers typically consist of electron-rich metals from the 2nd or 3rd row of the transition metal series, combined with electron-deficient ligands.[1–3] Such a combination allows metal-to-ligand charge transfer (MLCT), leading to long-lived emissive excited states. However, increased emphasis on sustainable and economic systems has shifted the focus to developing photosensitizers based on earth-abundant elements. Keeping the photo-induced charge separation by MLCT intact, a range of first row late transition metals have been explored to replace the precious metals.[4] In the same vein, luminescent magnesium complexes are desirable targets due to the high abundance of magnesium in the Earth's crust, and they are primarily non-toxic and inexpensive. However, due to the electron-deficient nature of magnesium, it can be conceived that they need an electron-rich ligand and rely on alternative mechanisms such as ligand to metal charge transfer (LMCT) or ligand to ligand or intra-ligand charge transfer (LLCT/ILCT). While there are some reports on luminescent group 1 metal complexes,[5–7] analogous well-defined magnesium complexes have remained largely underexplored despite the first report that came in 2005 from the group of Chandrasekhar.[8] However, two recent landmark studies on luminescent magnesium species by the groups of Roesky[9] and Munz[7] could revolutionize the field. Roesky's team reported N-supported phosphine complexes of magnesium with a quantum yield of 27–34%.[9] Munz and coworkers showed that lithium and magnesium complexes based on a carbazolide bridged mesoionic bis-carbene pincer ligand exhibit bright luminescence with quantum yields of up to 14%;[7] however, the magnesium compound was not structurally authenticated, presumably due to solubility issues. Hence, it is apparent from the aforementioned discussion that studies on the photophysical properties of well-defined magnesium complexes have been rather cursory, but have started to attract some attention.

In order to search for an electron-rich ligand, we turned our attention toward 2,2′-pyridylpyrrolide (PyPyrH). Inspiration comes from the increased luminescent properties shown by a good number of transition metal complexes such as Zn, Pd, Ir, Hf, and Zr based on this ligand,[10–13] while the protonated ligand is slightly fluorescent. The fluorescent properties in most cases emanate from the π–π* transition (HOMO–LUMO). Main-group compounds composed of the 2,2′-pyridylpyrrolide system have been less explored,[14] and we surmise it could be due to the lack of kinetic support provided by the ligand. Nonetheless, we have recently prepared a series of germanium and tin compounds using this system.[15,16] Here, we have prepared two magnesium complexes (**1** and **2**) based on the 2,2′-pyridylpyrrolide ligand. Interestingly, both **1** and **2** are luminescent, and their luminescent properties originate from the inter/intra-ligand charge transfer. The quantum yields of **1** and **2** are 22% and 14% in the solid state, which are significantly more than that of **C**, but less than that of **B**.

The synthetic procedure to access the **PyPyrH** ligand involves the condensation of 2-aminomethylpyridine and 1,3-diketone.[17] Treatment of **PyrPyH** with iPrMgCl in THF gives a chloride bridged dimeric magnesium complex (**1**) (Scheme 1). The dimerization presumably takes place to satisfy the electrophilicity of the magnesium centres, a phenomenon common in alkaline earth metal chemistry.[18] Here it is important to mention that the

[a] *Inorganic Chemistry and Catalysis Division, CSIR-National Chemical Laboratory, Dr. Homi Bhabha Road, Pashan, Pune 411008, India. E-mail: ss.sen@ncl.res.in*
[b] *Academy of Scientific and Innovative Research (AcSIR), Ghaziabad-201002, India*
[c] *Department of Chemistry, Indian Institute of Science, Education, and Research (IISER)-Pune, Dr. Homi Bhabha Road, Pashan, Pune 411008, India*
[d] *Physical and Material Chemistry Division, CSIR-National Chemical Laboratory, Dr. Homi Bhabha Road, Pashan, Pune 411008, India*

† Electronic supplementary information (ESI) available: Synthetic procedures, spectroscopic data, details on crystal structure determination and crystal structure data (CIF). CCDC 2189747 (**1**) and 2189748 (**2**). For ESI and crystallographic data in CIF or other electronic format see DOI: https://doi.org/10.1039/d2cc04142a

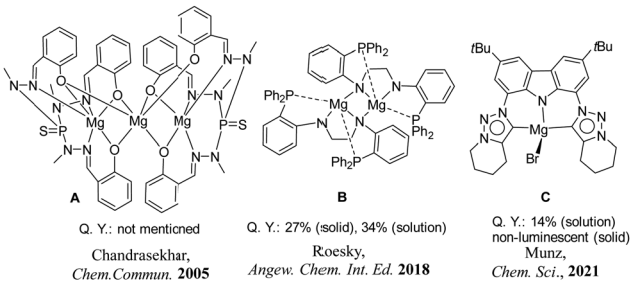

Scheme 1 Reported luminescent magnesium complexes.

group of Kays performed a similar reaction (with a diphenylpyrrolide instead of a dimethyl variant) with MeMgI in the presence of TMEDA, which led to a green coloured monomeric magnesium iodide complex due to chelation from TMEDA;[14] however, the photophysical properties of this compound have not been reported so far. **1** crystallizes in the monoclinic space group C_2/c and the magnesium centres adopt a distorted octahedral geometry (Fig. 1). The Mg–Cl bond lengths found for **1** are 2.48–2.50 Å, slightly longer than those of the nacnac-based magnesium chloride dimer, *i.e.*, 2.3926–2.4091 Å.[14] The Mg–N bond lengths are 2.063–2.075 Å, marginally shorter than the Mg–N bond lengths in β-diketiminato magnesium complexes.[15] Interestingly, there are three THF molecules in the asymmetric unit. Each magnesium centre is coordinated by a THF molecule. The third THF molecule coordinates to both magnesium atoms and plays the role of a bridging ligand.

Replacement of iPrMgCl with less bulky EtMgX (X = Cl, Br) led to the formation of a homoleptic magnesium complex (**2**), where two PyPyr moieties stabilize the magnesium center along with one THF molecule (Scheme 2). **2** crystallizes in the P_2/c space group of the monoclinic crystal system and the magnesium center adopts a distorted trigonal bipyramidal geometry (Fig. 2). The Mg–N bond lengths are 2.080–2.087 Å, which are longer than those in **1**. When **PyPyrH** was deprotonated with *n*BuLi and subsequently treated with MeMgBr and iPrMgCl, it only led to compound **2**.

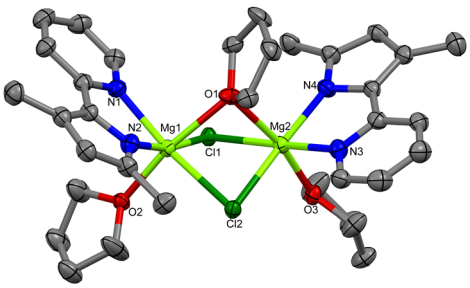

Fig. 1 The molecular structure of **1** with anisotropic displacement parameters depicted at the 50% probability level. Hydrogen atoms are not shown for clarity. Selected bond lengths (Å) and bond angles (°): Cl1 Mg2 2.4874(17), Cl1 Mg1 2.4956(17), Cl2 Mg1 2.4881(17), Cl2 Mg2 2.4936(17), Mg1 N2 2.072(4), Mg1 O2 2.074(3), Mg1 N1 2.176(4), Mg1 O1 2.328(4), Mg2 N4 2.069(4), Mg2 O3 2.077(3), Mg2 N3 2.174(4), Mg2 O1 2.343(4); Mg2 Cl1 Mg1 80.09(5), Mg1 Cl2 Mg2 80.12(5), N2 Mg1 O2 93.52(15), N2 Mg1 N1 78.93(16), O2 Mg1 N1 94.34(14), N2 Mg1 O1 95.73(15), O2 Mg1 O1 168.87(14).

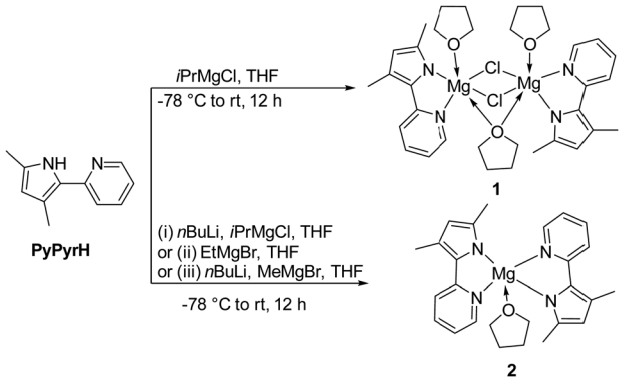

Scheme 2 Synthesis of magnesium complexes **1** and **2**.

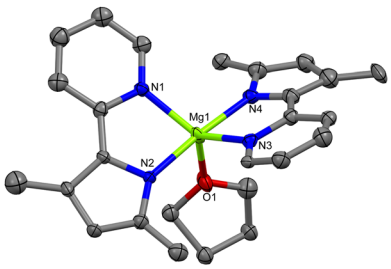

Fig. 2 The molecular structure of **2**. Anisotropic displacement parameters are depicted at the 50% probability level. Hydrogen atoms are omitted for clarity. Selected bond distances (Å) and bond angles (°): selected bond lengths (Å) and bond angles (°): N1 Mg1 2.083(14), N2 Mg1 2.02(2), Mg1 N4 2.07(5), Mg1 O1 2.078(5), Mg1 N3 2.107(14); N2 Mg1 N1 83.1(7); N4 Mg1 N1 101.4(13); N2 Mg1 N3 98.4(7); N4 Mg1 N3 79.8(14).

We have also collected the experimental powder X-ray diffraction (PXRD) data on both compounds and compared with their simulated powder X-ray diffraction patterns from the single crystal X-ray diffraction (SC-XRD) data. The overlay of both the experimental and simulated PXRD data revealed a good match. The experimental PXRD profile of **1** showed good crystallinity as the diffraction peaks are very sharp, similar to the simulated PXRD pattern. Conversely, the experimental PXRD data of **2** revealed broader diffraction peaks; however they showed a good match with the simulated PXRD profile (Fig. S11 and S12, ESI†).

Solid-state absorption studies reveal that both **1** and **2** display a broad absorption band with a peak at 413 nm (Fig. 3a and b). Due to the closed-shell electronic configuration of Mg^{2+}, the possibility of MLCT can be safely excluded.[10,19] Hence, the broad absorption peaks are observed to originate from the intra-ligand and/or inter-ligand π–π* and n–π* transitions. Similar interligand charge transfer was reported by Wagler and coworkers for hexa-coordinate silicon complexes.[20] The emission spectra of both the complexes show peaks at ∼515 nm (Fig. 3a and b) with a significant difference in the full-width-half-maximum (FWHM) value. The FWHM values of the emission bands were found to be 112 nm and 71 nm for **1** and **2**, respectively.

In order to carry out molecular level investigation, TD-DFT calculations were performed at different level of theories

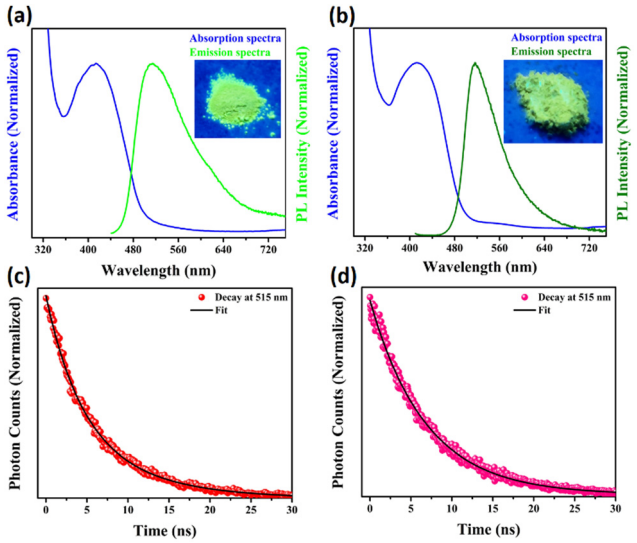

Fig. 3 (a) Absorption spectra and emission spectra (excited at 400 nm) of **1** along with the solid state compound image under UV light, (b) absorption spectra and emission spectra (excited at 400 nm) of **2** along with the solid state compound image under UV light, (c) emission decay profile of **1**, and (d) emission decay profile of **2**.

(for details, please see the ESI†). The orbitals were generated from the TD-DFT calculation at the M06-2X/def2-TZVPP//B3LYP-D3/def2-SVP level of theory, where the HOMO and LUMO are shown in Fig. S14 (ESI†) with corresponding energy levels. For the ligand, the HOMO has a larger electron density at the pyrrole moiety, and the LUMO shares a larger electron density over the pyridine moiety (Fig. S14a, ESI†). However, both the orbitals have a reasonable spatial overlap with each other. However, in the complexes, the HOMO–LUMO transition exhibits a significant charge flow from one coordinated ligand to another. Interestingly, complex **2** shares a larger HOMO–LUMO overlap (Fig. S14c, ESI†), and complex **1** has significant spatial separation between the HOMO and LUMO (Fig. S14b, ESI†). To further elaborate on the nature of the excited state processes in the complexes and to obtain the emission spectra, the first excited states (S_1) were optimized (details in the ESI†), and natural transition orbital (NTO) calculations were conducted for the S_1–S_0 transition in both complexes. It was observed that for **2** during the emission (S_1 to S_0 transition) h-NTO shares a large electron density localized over one coordinated ligand, and in e-NTO the electron density is distributed over another ligand (Fig. 4b). This indicates the formation of an emissive inter-ligand charge transfer excited state. This was also predicted from the excitation to the S_1 state involving the HOMO to LUMO transition (Table S2 and Fig. S13, ESI†) for **2** (f^{osc} = 0.1040, $^{calcd}\lambda^{abs}$ = 361 nm, $^{exp}\lambda^{abs}$ = 413 nm). On the other hand, for complex **1**, the electron density distribution is entirely different in the first excited state (S_1). In this case, during the emission process (S_1 to S_0 transition) e-NTO has a larger electron density on the pyridine moiety of one ligand, and h-NTO has a higher electron density on the pyrrole moiety of the same ligand (Fig. 4a). As the electron density during the emission gets shifted within the same ligand, the S_1 to S_0 transition here is regarded as an emission from an intra-ligand charge transfer excited state. Similar behaviour was also predicted from the excitation to the S_1 state involving the HOMO−1 to LUMO transition (Table S2 and Fig. S13, ESI†) for **1** (f^{osc} = 0.0115, $^{calcd}\lambda^{abs}$ = 355 nm, $^{exp}\lambda^{abs}$ = 413 nm).

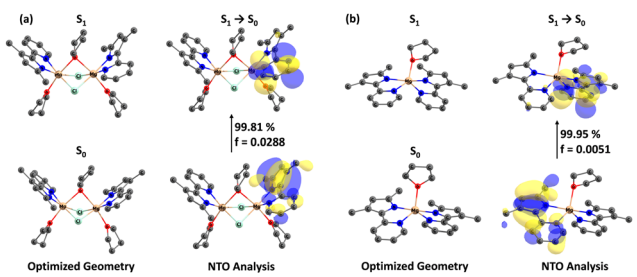

Fig. 4 (a) Optimized geometry of **1** in the ground state and excited state along with NTO analysis for emission and (b) optimized geometry of **2** in the ground state and excited state along with NTO analysis for emission.

The different charge transfer excited states for **1** and **2** can also be characterized from the emission bandwidth. Band broadening in solid state emission significantly depends upon the reorganization energy, the charge transfer character of the complexes and the electron–phonon scattering.[21,22] The bandwidth of the individual vibrational coarse structure in the emission spectra increases with increasing reorganization energy and charge transfer character of the complex, leading to a structureless broad emission.[23] To explain the difference between the emission bandwidths of the two complexes, excited state energies need to be investigated. Hence, the reorganization energies (λ^{RE}) were calculated at the M06-2X/def2-TZVPP//B3LYP-D3/def2-SVP level of theory (computational details in the ESI†). It was observed that **1** has a higher reorganization energy (20.8 kcal mol^{-1}) compared to **2** (15.5 kcal mol^{-1}), which explains why the emission spectrum of **1** has a larger bandwidth than that of **2**.[24–26]

The calculated emission from the S_1 state for **1** (f^{osc} = 0.0288, $^{calcd}\lambda^{em}$ = 479 nm, $^{exp}\lambda^{em}$ = 515 nm) and for **2** (f^{osc} = 0.0051, $^{calcd}\lambda^{em}$ = 447 nm, $^{exp}\lambda^{em}$ = 515 nm) was also found to be in good agreement with the experimental observation (Table S3, ESI†). This also gives insights into the higher quantum yield of **1** (22%) than that of **2** (14%) (quantum yield measurements in the ESI†), which can be attributed to the approx. 5.6 times higher oscillator strength (f) of **1** than that of **2** (Fig. 4a and b). In TD-DFT calculations, the higher oscillator strength of the S_1 to S_0 transition in **1** can be explained in terms of the electron density of e-NTO and h-NTO. In this case, the extent of spatial overlap between e-NTO and h-NTO is greater due to its intra-ligand charge transfer character (Fig. 4a). On the other hand, due to the inter-ligand charge transfer process being predominant in **2**, the spatial overlap between e-NTO and h-NTO becomes minimal (Fig. 4b). Therefore, the S_1 to S_0 transition probability is higher in **1**, and so is the oscillator strength and the quantum yield. Moreover, the intra-ligand charge transfer in **1** may increase the vibronic coupling among the excited states,[27] thereby enhancing the internal conversion (IC) as well. However, excited state lifetimes for both the complexes were

found to be similar. For **1**, the emission decay profile has two components with lifetime values of 4.14 and 9.37 ns having relative contributions of 0.63 and 0.38, respectively (Fig. 3c; refer the lifetime table in the ESI†). For **2**, the emission transient is composed of two components, 6.20 and 8.12 ns, having a relative contribution of 0.64 and 0.33, respectively (Fig. 3d; refer the lifetime table in the ESI†). As the lifetime of the complexes lies within the range of a few nanoseconds, the possibility of delayed emission or phosphorescence is eliminated and the emission is predominantly fluorescence.

As we have observed an intra-ligand charge transfer in PyMgCl involving a minimal role of Mg^{2+}, it is also important to carry out a comparative study of the ligand. The ligand shows broad emission features with a peak at ~420 nm (for more details, see the ESI†). Despite a ligand restricted charge transfer in both **1** and **2**, their emissive behaviours are entirely different. TD-DFT studies were performed to address this intriguing observation. We observed that, in the case of the ligand, the frontier orbital transition contributing to the S_1 state is HOMO-to-LUMO with an excitation energy of 4.19 eV (S_0 to S_1). On the other hand, in **1**, the S_1 state is mainly composed of HOMO to LUMO+1 (46.65%) and HOMO−1 to LUMO (51.52%) transitions with an excitation energy of 3.49 eV (S_0 to S_1). This illustrates that the electronic structure of the emissive state in PyPyrH has been modulated upon complex formation. The Franck–Condon (FC) energy of **1** has also been found to be decreased by 4.19 − 3.49 = 0.6 eV. This decrease in FC energy accounts for the large emission band shift of **1** compared to the free ligand.

The molecular orbitals derived from NTO and TD-DFT calculations show almost zero electron density over the Mg atom. Therefore, we hypothesize that the magnesium atoms in **1** and **2** play a structural connectivity role, but not an electronic role.[28] For **2**, both the ligands are connected to a single Mg atom, and therefore this single connectivity allows the electron density to switch from one ligand to another. However, in **1**, the ligands are separated by two Mg and Cl atoms, making the inter-ligand charge transfer process unfeasible.

In conclusion, we have employed the PyPyrH ligand to obtain two well-defined pyridylpyrrole magnesium complexes (**1** and **2**), which exhibit fluorescence with quantum yields of 22% and 14% in the solid state. Detailed theoretical studies rationalize that the luminescent properties arise due to inter- and intra-ligand charge transfer.

Financial assistance from SJF Grant SB/SJF/2021-22/06, GOI is acknowledged. R. K. and S. P. thank CSIR, India and DST-INSPIRE, India (IF160314) for their research fellowships, respectively. J. C. is indebted to IISER Pune for the fellowship. The support and the resources provided by 'PARAM Brahma Facility' under the National Supercomputing Mission, GOI at the IISER Pune are acknowledged.

Conflicts of interest

There are no conflicts to declare.

Notes and references

1 A. Juris, V. Balzani, F. Barigelletti, S. Campagna, P. Belser and A. von Zelewsky, *Coord. Chem. Rev.*, 1988, **84**, 85–277.
2 V. Balzani and A. Juris, *Coord. Chem. Rev.*, 2001, **211**, 97–115.
3 I. M. Dixon, J.-P. Collin, J.-P. Sauvage, L. Flamigni, S. Encinas and F. Barigelletti, *Chem. Soc. Rev.*, 2000, **29**, 385–391.
4 C. Wegeberg and O. S. Wenger, *JACS Au*, 2021, **1**, 1860–1876.
5 O. Back, C. Förster, T. Basché and K. Heinze, *Chem. – Eur. J.*, 2019, **25**, 6542.
6 T. J. Feuerstein, B. Goswami, P. Rauthe, R. Köppe, S. Lebedkin, M. M. Kappes and P. W. Roesky, *Chem. Sci.*, 2019, **10**, 4742.
7 P. Pinter, C. M. Schüßlbauer, F. A. Watt, N. Dickmann, R. Herbst-Irmer, B. Morgenstern, A. Grünwald, T. Ullrich, M. Zimmer, S. Hohloch, D. M. Guldi and D. Munz, *Chem. Sci.*, 2021, **12**, 7401–7410.
8 V. Chandrasekhar, R. Azhakar, J. F. Bickley and A. Steiner, *Chem. Commun.*, 2005, 459–461.
9 S. Bestgen, C. Schoo, B. L. Neumeier, T. J. Feuerstein, C. Zovko, R. Köppe, C. Feldmann and P. W. Roesky, *Angew. Chem., Int. Ed.*, 2018, **57**, 14265–14269.
10 J. J. Klappa, S. A. Geers, S. J. Schmidtke, L. A. MacManus-Spencer and K. McNeill, *Dalton Trans.*, 2004, 883–891.
11 (*a*) A. Ionescu, N. Godbert, R. Termine, M. La Deda, M. Amati, F. Lelj, A. Crispini, A. Golemme, M. Ghedini, P. Garcia-Orduña and I. Aiello, *Inorg. Chem.*, 2021, **60**, 9287–9301; (*b*) T. F. Mastropietro, M. La Deda, N. Godbert, L. Ricciardi, E. I. Szerb, M. Ghedini and I. Aiello, *J. Organomet. Chem.*, 2015, **786**, 55–62.
12 Y. Zhang, N. G. Akhmedov, J. L. Petersen and C. Milsmann, *Chem. – Eur. J.*, 2019, **25**, 3042–3052.
13 P. M. N. Đô, N. G. Akhmedov, J. L. Petersen, B. S. Dolinar and C. Milsmann, *Chem. Commun.*, 2020, **56**, 5397–5400.
14 A. C. A. Ried, L. J. Taylor, A. M. Geer, H. E. L. Williams, W. Lewis, A. J. Blake and D. L. Kays, *Chem. – Eur. J.*, 2019, **25**, 6840–6846.
15 S. Pahar, V. S. V. S. N. Swamy, T. Das, R. G. Gonnade, K. Vanka and S. S. Sen, *Chem. Commun.*, 2020, **56**, 11871–11874.
16 S. Pahar, V. Sharma, S. Tothadi and S. S. Sen, *Dalton Trans.*, 2021, **50**, 16678–16684.
17 J. J. Klappa, A. E. Rich and K. McNeill, *Org. Lett.*, 2002, **4**, 435–437.
18 S. P. Sarish, S. Nembenna, S. Nagendran and H. W. Roesky, *Acc. Chem. Res.*, 2011, **44**, 157–170.
19 Y. Hai, J.-J. Chen, P. Zhao, H. Lv, Y. Yu, P. Xu and J.-L. Zhang, *Chem. Commun.*, 2011, **47**, 2435–2437.
20 J. Wagler, D. Gerlach, U. Böhme and G. Roewer, *Organometallics*, 2006, **25**, 2929–2933.
21 J.-W. Huang, Y.-C. Hsu, X. Wu, S. Wang, X.-Q. Gan, W.-Q. Zheng, H. Zhang, Y.-Z. Gong, W.-Y. Hung, P.-T. Chou and W. Zhu, *J. Mater. Chem. C*, 2022, **10**, 7866–7874.
22 X.-K. Chen, V. Coropceanu and J.-L. Bredas, *Nat. Commun.*, 2018, **9**, 5295.
23 X. Wen, P. Yu, Y.-R. Toh, X. Ma, S. Huang and J. Tang, *Nanoscale*, 2013, **5**, 10251–10257.
24 F. Liu, Z. Cheng, L. Wan, Z. Feng, H. Liu, H. Jin, L. Gao, P. Lu and W. Yang, *Small*, 2022, **18**, 2106462.
25 X.-F. Song, Z.-W. Li, W.-K. Chen, Y.-J. Gao and G. Cui, *Inorg. Chem.*, 2022, **61**, 7673–7681.
26 Z. Pei, Q. Ou, Y. Mao, J. Yang, A. d l Lande, F. Plasser, W. Liang, Z. Shuai and Y. Shao, *J. Phys. Chem. Lett.*, 2021, **12**, 2712–2720.
27 W.-C. Chen, P.-T. Chou and Y.-C. Cheng, *J. Phys. Chem. C*, 2019, **123**, 10225–10236.
28 C. L. Ramírez, C. N. Pegoraro, O. Filevich, A. Bruttomeso, R. Etchenique and A. R. Parise, *Inorg. Chem.*, 2012, **51**, 1261–1268.

ChemCatChem

Research Article
doi.org/10.1002/cctc.202101788

Chemistry Europe
European Chemical Societies Publishing

www.chemcatchem.org

A Well-Defined Calcium Compound Catalyzes Trimerization of Arylisocyanates into 1,3,5-Triarylisocyanurates

Rohit Kumar,[a, c] Vishal Sharma,[a, c] Shailja Jain,[b] Himanshu Sharma,[b, c] Kumar Vanka,[b, c] and Sakya S. Sen*[a, c]

We report the synthesis of a calcium complex (**2**) bearing a tetradentate monoanionic ligand with a diaminoethane core and phenolate and pyridine peripheral donors. Single crystal X-ray studies on **2** revealed that LiI was also co-crystallized, leading to a four-membered ring with four different elements. **2** was found to be an efficient catalyst for the cyclotrimerization of a variety of aromatic isocyanates under mild conditions.

Introduction

There has been a trend in chemistry for some time of using compounds with main-group elements in the place of platinum group metals (PGM: Ru, Os, Rh, Ir, Pd, and Pt) for molecular catalysis.[1,2] The main factor driving this trend to switch from PGMs is their expenses and low-terrestrial abundances. Besides, there is a growing apprehension about the health and environmental impact of the residual metal that is retained in the products. Among main-group elements, calcium complexes have attracted considerable attention due to the high terrestrial abundance (3.4 wt%; calcium is the fifth most abundant element) and biocompatibility of calcium. Organocalcium compounds have been shown to catalyze important organic transformations such as hydroamination, hydrophosphination, hydrosilylation, hydroboration, hydrogenation, the cyanosilylation of unsaturated organic compounds, as well as polymerization.[3–6]

Cyclotrimerization of isocyanate derivatives is an important and atom-economical transformation to access isocyanurates, which have industrial and commercial applications, as they have excellent thermal stability and flame resistance properties. Hence, incorporation of isocyanurate frameworks into polymer networks could enhance the physical properties of polyurethanes, copolymer resins, and plastic and coating materials, with increased thermal and chemical resistance, water-resistance, transparency, as well as impact resistance.[7,8] Besides, isocyanurates are essential units for the synthesis of microporous (poly)isocyanurate, which has been applied as a support in heterogeneous catalysis.[9] Examples of catalysts that have been used for this important transformation include transition metals,[10–14] rare earth metals,[15–18] and Lewis bases like N-heterocyclic carbenes,[19] phosphines,[20] and N-heterocyclic olefins.[21] However, less attention has been paid to employing main-group elements, though there are some recent reports on the cyclotrimerization of isocyanates by K, Al, Ge, and Sn compounds.[22–24] Despite such progress, these approaches have significant limitations, including high temperatures, prolonged reaction time, by-product formation, and subsequent difficulties in separation.

In 2007, Orzechowski and Harder reported the catalytic trimerization of PhNCO by a calcium carbene complex with iminophosphorane ligands.[25] However, no further substrate scope was studied. Herein, we report the synthesis of an {ONNN}-type tetradentate ligand-based new heteroleptic calcium iodide (**2**), which is found to be quite an efficient catalyst for the trimerization reaction.

Results and Discussion

The tetradentate ligand (**LH**) was prepared according to the literature procedure.[26] The ligand consists of a diaminoethane group as core and pyridine and di-*tert*-butyl-phenolate as peripheral moieties. We reasoned that such a ligand might be appropriate for the calcium atom, because it provides a high coordination number around the metal center, and thereby could hinder the formation of a homoleptic compound.[27,28] The reaction between **LH** and $KN(TMS)_2$ in THF led to a dimeric potassium complex (**1**) (Scheme 1). Lithiation of the ligand by MeLi, with the subsequent addition of CaI_2, afforded a hexacoordinate calcium complex (**2**) (Scheme 1). Both **1** and **2** were characterized by NMR spectroscopy and single-crystal X-ray analysis. Compound **1** features a dimeric centrosymmetric structure where the two halves of the dimer are linked through a four-membered K_2O_2 ring (Figure 1). The potassium atoms are penta-coordinated with a distorted trigonal pyramidal geome-

[a] *R. Kumar, V. Sharma, Dr. S. S. Sen*
Inorganic Chemistry and Catalysis Division
CSIR-National Chemical Laboratory
Dr. Homi Bhabha Road, Pashan, Pune 411008 (India)
E-mail: ss.sen@ncl.res.in
[b] *Dr. S. Jain, H. Sharma, Dr. K. Vanka*
Physical and Material Chemistry Division
CSIR-National Chemical Laboratory
Dr. Homi Bhabha Road, Pashan, Pune 411008 (India)
[c] *R. Kumar, V. Sharma, H. Sharma, Dr. K. Vanka, Dr. S. S. Sen*
Academy of Scientific and Innovative Research (AcSIR)
Ghaziabad-201002 (India)

Supporting information for this article is available on the WWW under https://doi.org/10.1002/cctc.202101788

This publication is part of a joint Special Collection with EurJIC on "Main Group Catalysis". Please check the ChemCatChem homepage for more articles in the collection.

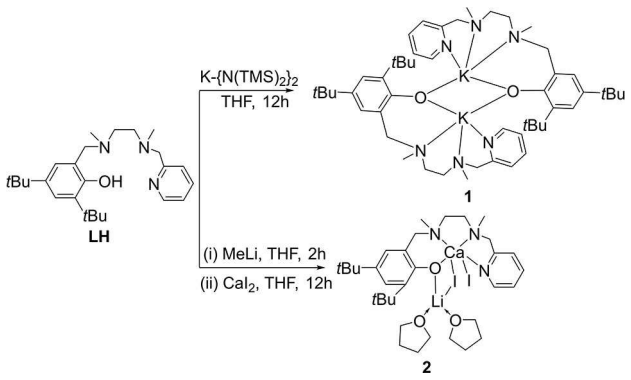

Scheme 1. Synthesis of potassium (**1**) and calcium iodide (**2**) complexes.

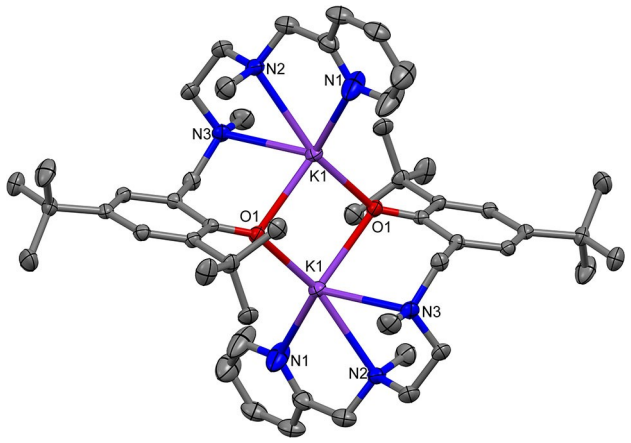

Figure 1. The molecular structure of **1** with anisotropic displacement parameters depicted at the 50% probability level. Hydrogen atoms are not shown for clarity. Selected distances (Å) and angles (deg): K1–O1, 2.5589(17); K1–O1, 2.5997(15); K1–N1, 2.851(2); K1–N3 2.8605(18); K1–N2, 2.8792(18); K1–C1, 3.367(2); K1–C16, 3.423(2); K1–C19, 3.496(3); K1–K1 3.7291 and O1–K1–O1, 87.41(5); O1–K1–N1, 120.38(6); O1–K1–N1, 130.48(7); O1–K1–N3, 111.33(5); O1–K1–N3, 73.31(5), N1–K1–N3, 121.89(6); O1–K1–N2, 159.84(4).[35]

try. The K–O and K–N bond lengths are 2.55–2.59 Å and 2.85–2.86 Å, respectively, which are shorter than the sum of their covalent radii. Compound **2** contains a hexacoordinated calcium center, and it adopts a distorted octahedral geometry. Interestingly, lithium iodide is also co-crystallized along with calcium iodide (Figure 2), resulting in an unprecedented Ca-O–Li-I four-membered ring with four different atoms. The terminal Ca–I bond length in **2** is 3.078(5) Å, which is marginally shorter than the previously reported terminal Ca–I bond (3.084–3.166 Å).[29–31]

Following its preparation, **2** was screened as a potential catalyst for the cyclotrimerization of isocyanates (Scheme 2). No reaction was observed in the absence of the catalyst. The reaction was performed in THF with 2 mol% of catalyst loading. Compound **2** was found to be effective for aryl isocyanates, but in the case of alkyl isocyanates, no cyclotrimerization was observed due to the absence of C=N bond activation by the conjugation of the aryl ring like in aryl isocyanates. The NMR

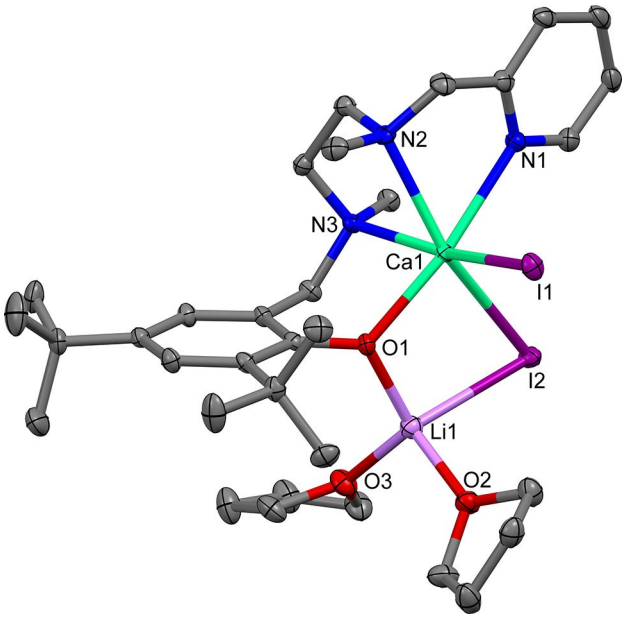

Figure 2. The molecular structure of **2** with anisotropic displacement parameters depicted at the 50% probability level. Hydrogen atoms are not shown for clarity. Selected distances (Å) and angles (deg): Ca1–O1, 2.2529(17); Ca1–N2, 2.507(2); Ca1–N1 2.522(2); Ca1–N3, 2.527(2); Ca1–I1, 3.0780(5); Ca1–I2, 3.0814(5); Ca1–Li1, 3.298(5); I2–Li1, 2.877(5); Li1–O1, 1.921(5); Li1–O2, 1.937(5); Li1–O3, 1.952(5) and C15–N3–Ca1, 108.35(14); C1–O1–Li1, 115.5(2); C1–O1–Ca1, 126.58(15); Li1–O1–Ca1, 104.09(16); C30–O2–C33 106.8(2); C30–O2–Li1, 124.7(2); C33–O2–Li1, 126.5(2).[35]

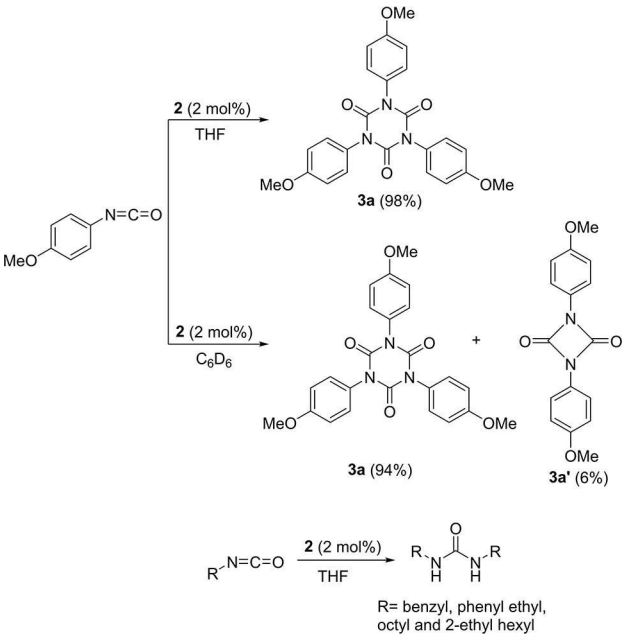

Scheme 2. Cyclotrimerization of aryl isocyanate catalysed by compound **2** (above); Formation of 1,3-disubstituted urea when alkyl isocyanates were used (below).

and mass spectra indicate that the crude product mixture is pure (only trimer is detected), and that the bulk product was characterized by single-crystal X-ray diffraction in the cases of

4-methoxyphenyl isocyanate (**3a**), 4-bromophenyl isocyanate (**3b**), 4-cyano phenyl isocyanate (**3i**), and 4-fluorophenyl isocyanate (**3k**). Interestingly, when the oligomerization reaction of 4-methoxy phenyl isocyanate was performed in benzene-d_6, the trimerized product (**3a**) was obtained almost quantitatively along with the formation of the dimerized product (**3a'**) in a very minor amount (Scheme 2). Therefore, our catalyst does not suffer from issues of selectivity.[32] Fortuitously, we were able to characterize both these products by single-crystal X-ray diffraction studies (Figure 3). There were several studies on the effects of the solvent on the cyclization of phenyl isocyanates,[33] and it has been generally accepted that the trimerization is favored when polar solvents are employed. In case of alkyl isocyanates, no trimerization product was observed. Due to the lack of conjugation, the C=N bond is probably not activated in alkyl isocyanates. We have probed the reaction with benzyl, phenyl ethyl, octyl and 2-ethyl hexyl isocyanate and observed the formation of the corresponding 1,3-disubstituted urea, which was confirmed by the HMRS and ^{1}H NMR spectroscopy (See Scheme 2, below and the Supporting Information, Figures S50–57) and compared to the previously reported samples by Lang and co-workers.[34] It must be stated here that we have also performed the reaction in the neat condition, but found the reaction to be incomplete, presumably due to the heterogeneous nature of the reaction medium.

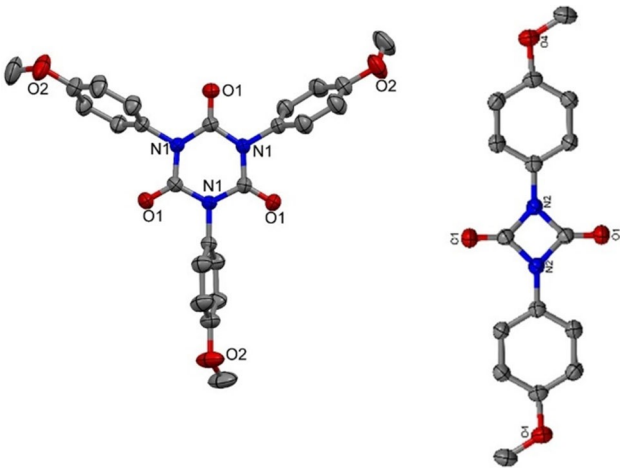

Figure 3. The molecular structure of **3a** (left) and **3a'** (right) with anisotropic displacement parameters depicted at the 50% probability level.[24]

Subsequently, the oligomerization of a wide range of isocyanates were studied. As the reaction was carried out in THF, no dimer formation was observed. Good to excellent yields were observed for isocyanates either having an electron-donating group such as Me (Table 1, entry 8 and 11) or OMe (entry 1) or having an electron-withdrawing group such as bromide and chloride (entries 4, 9 and 14). The reaction is a bit sluggish with 2,6-diisopropyl phenyl isocyanate (entry 7) and 12 h reaction time is required for productive conversion. The sluggishness is due to the steric hindrance imparted by the isopropyl groups, as the replacement by *i*Pr groups with Me groups or Cl groups results in rapid conversion (entry 8 and 9). 4-fluorophenyl isocyanate (Table 1, entry 15) also took 12 h to lead to a fruitful conversion, while the reactions were smoother for 4-bromophenyl isocyanate (entry 4) and 4-chlorophenyl isocyanate (entry 14). This could be due to the electron withdrawing nature of the fluorine atom, though the reaction is faster for the nitrile substituent (entry 13). The substituent groups at the *ortho* or *meta* position of the aryl ring, as well as 1-naphthyl isocyanate, were well tolerated, and the corresponding isocyanurates were isolated in excellent yields (entry 10–12), reflecting that there are no apparent electronic effects in this reaction.

We have performed the reactions of 4-methoxyphenyl isocyanate and 4-bromophenyl isocyanate using LiI iodide as the catalyst. However, no product formation was observed even after using 20 mol% of catalyst loading and 24 hours of reaction time (Table 1, entry 2 and 5). Subsequently, we have employed PhC(N*i*Pr)$_2$CaI,[30] which we have previously reported, as a catalyst because there is no lithium metal associated with it. Though it was possible to cyclotrimerize 4-methoxyphenyl isocyanate and 4-bromophenyl isocyanate, the catalyst loading is higher and the yields were significantly lesser (entry 3 and 6) than those obtained by using **2** as a catalyst (see entry 1 and 3).

Table 1. Catalytic data for the trimerization of isocyanates catalysed by **2** in THF.

Entry	Substrate	Catalyst [mol%]	Time [h]	Product & yield [%]
1	4-OMe–C_6H_4NCO	**2** (2)	2 h	**3a** (98)
2	4-OMe–C_6H_4NCO	LiI (20)	24 h	–
3	4-OMe–C_6H_4NCO	PhC(N*i*Pr)$_2$CaI (5)		**3a** (75)
4	4-Br–C_6H_4NCO	**2** (2)	1 h	**3b** (98)
5	4-Br–C_6H_4NCO	LiI (20)	24 h	–
6	4-Br–C_6H_4NCO	PhC(N*i*Pr)$_2$CaI (5)		**3b** (75)
7	2,6-*i*Pr$_2$$C_6H_3$NCO	**2** (2)	12 h	**3c** (85)
8	2,6-Me$_2$$C_6H_3$NCO	**2** (2)	2 h	**3d** (86)
9	2,6–Cl$_2$$C_6H_3$NCO	**2** (2)	2 h	**3e** (90)
10	1-naphthyl-NCO	**2** (2)	4 h	**3f** (95)
11	2-Me–C_6H_4NCO	**2** (2)	2 h	**3g** (92)
12	3-NO_2–C_6H_4NCO	**2** (2)	6 h	**3h** (85)
13	4-CN–C_6H_4NCO	**2** (2)	2 h	**3i** (90)
14	4-Cl–C_6H_4NCO	**2** (2)	1 h	**3j** (88)
15	4-F–C_6H_4NCO	**2** (2)	12 h	**3k** (95)

Reaction conditions: isocyanate (3 mmol), solvent: THF (3–4 mL), room temperature, 1–12 h unless otherwise mentioned, isolated yield.

Similarly, the use of **1** as a catalyst afforded the trimerization of 4-methoxyphenyl isocyanate and 4-bromophenyl isocyanate in 78% and 72% yield, respectively. However, we were not able to prepare **2** without LiI coordination; hence it is not clear whether Li has any role in the catalytic cycle.

We have also compared the performance of our catalyst with other catalysts reported for this transformation. The scope of Kays' Mn and Fe catalysts was limited to aliphatic isocyanates, while ours is restricted to aromatic isocyanates.[14] Cui's yttrium catalyst requires less amount of catalyst loading, but 12 h reaction time.[18] The aluminum based catalyst reported by Ward's group[24] requires 50 °C and 1–48 h reaction time, but it works for aryl, alkyl, and allyl isocyanates. Interestingly, in the case of 4-chlorophenyl isocyanate and 4-methoxyphenyl isocyanate, 50 °C and 0.5 h and 3.5 h reaction time was required, respectively, for quantitative conversion. In the same amount of time, our catalyst gave excellent yields at room temperature in 1–2 h reaction time for these two substrates. Nembenna's stannylene catalyst[23] produced excellent yields in 30–60 min time with 2 mol% catalyst loading, but the scope was limited to only two aryl isocyanates.

Although we are not sure about the mechanism and no intermediate was observed spectroscopically, a tentative catalytic cycle for the cyclotrimerization reaction is proposed below. We note here that only the thermodynamics of potential intermediates has been considered, and robust evidence can only be provided by locating the transition states. The first step of the reaction mechanism is the coordination of aryl isocyanate to the calcium atom of **2**, leading to the formation of complex **B** (Figure 4). Calculations suggest that the free energy (ΔG) change for this step is 2.3 kcal/mol for phenyl isocyanate. Subsequent to this, another molecule of phenyl isocyanate reacts with **B**, leading to the formation of **C**, a process that is endergonic by 3.4 kcal/mol. In the next step, complex **C** undergoes dimerization and forms complex **D**, which is exergonic by 1.0 kcal/mol. Furthermore, in the next step, the addition of a third molecule of phenyl isocyanate leads to complex **E**, which is favorable by 20.6 kcal/mol. Dissociation of the bond between the carbonyl group and the calcium center leads to the formation of the cyclotrimerized product and the regeneration of the catalyst. We have also considered other mechanisms (please see Schemes S3 and S4 in the ESI). However, according to the thermodynamics, these mechanisms are less likely to be operative.

Conclusions

In summary, we have introduced a novel heterobimetallic lithium-calcium complex (**2**) supported by a tetradentate monoanionic ligand, featuring a diaminoethane core and phenolate and pyridine peripheral donors. Subsequently, we have employed **2** as a catalyst for the cyclotrimerization of a variety of isocyanates to give the respective isocyanurates in THF under mild reaction conditions. Further catalytic exploration with **2** is currently ongoing and will be published in due course.

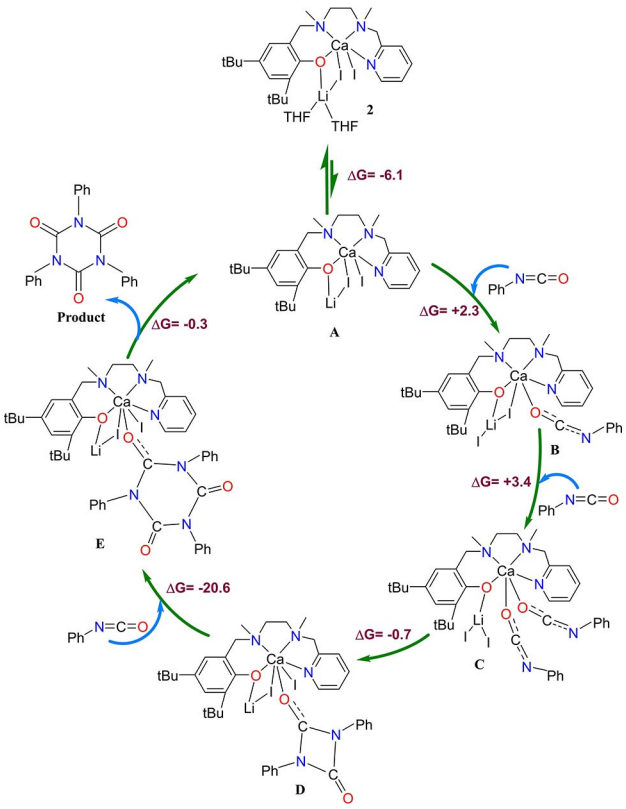

Figure 4. Tentative mechanism for the cyclotrimerization of isocyanates by **2**.

Experimental Section

Please see Supporting Information for the synthesis, characterization, and structural data for **1** and **2**. General catalytic procedure for the cyclotrimerization of isocyanates, analytical data of the corresponding isocyanurates, their representative NMR spectra, and details of theoretical calculations are provided in the supporting information.

Acknowledgements

This work was supported by the Scheme for Translational and Advanced Research in Sciences (STARS), the Ministry of Education, and the Government of India (Grant MoE/STARS-1/255). R.K., V.S., and H.S. thank CSIR, India, for their research fellowships. S.J. thanks DST Inspire for providing a research fellowship. The support and the resources provided by 'PARAM Brahma Facility' under the National Supercomputing Mission, Government of India at the IISER Pune are gratefully acknowledged. We are thankful to the reviewers for their critical comment to improve the quality of the manuscript.

Conflict of Interest

The authors declare no conflict of interest.

Data Availability Statement

The data that support the findings of this study are available in the supplementary material of this article.

Keywords: Calcium · Tetradentate ligand · Cyclotrimerization · Isocyanurates

[1] D. W. Stephan, *Acc. Chem. Res.* **2015**, *48*, 306–316.
[2] Editorial in *Nat. Catal.* **2019**, *2*, 735.
[3] S. Harder, *Chem. Rev.* **2010**, *110*, 3852–3876.
[4] T. E. Stennett, S. Harder, *Chem. Soc. Rev.* **2016**, *45*, 1112–1128.
[5] M. S. Hill, D. J. Liptrot, C. Weetman, *Chem. Soc. Rev.* **2016**, *45*, 972–988.
[6] a) S. Yadav, S. Pahar, S. S. Sen, *Chem. Commun.* **2017**, *53*, 4562–4564; b) S. Yadav, R. Dixit, K. Vanka, S. S. Sen, *Chem. Eur. J.* **2018**, *24*, 1269–1273.
[7] Z. Wirpsza, *Polyurethanes: Chemistry*, *Technology and Application*, Ellis Horwood, London, **1993**.
[8] a) T. S. Leu, *J. Appl. Polym. Sci.* **2006**, *102*, 2470–2480; b) G. Q. Xiao, S. Q. Gao, X. L. Xie, M. C. Xu, *Polym. Adv. Technol.* **2009**, *20*, 1157–1162; c) W. Sun, X. Yan, X. Zhu, *J. Appl. Polym. Sci.* **2011**, *122*, 2359–2367.
[9] Y. Zhang, S. N. Riduan, J. Y. Ying, *Chem. Eur. J.* **2009**, *15*, 1077–1081.
[10] J. G. Noltes, J. Boersma, *J. Organomet. Chem.* **1967**, *7*, 6–8.
[11] F. Paul, S. Moulin, O. Piechaczyk, P. Le Floch, J. A. Osborn, *J. Am. Chem. Soc.* **2007**, *129*, 7294–7304.
[12] S. G. Lee, K. Y. Choi, Y. J. Kim, S. Park, S. W. Lee, *Dalton Trans.* **2015**, *44*, 6537–6545.
[13] A. Flamini, A. M. Giuliani, N. Poli, *Tetrahedron Lett.* **1987**, *28*, 2169–2170.
[14] H. R. Sharpe, A. M. Geer, H. E. L. Williams, T. J. Blundell, W. Lewis, A. J. Blakea, D. L. Kays, *Chem. Commun.* **2017**, *53*, 937–940.
[15] X. C. Zhu, J. X. Fan, Y. J. Wu, S. W. Wang, L. J. Zhang, G. S. Yang, Y. Wei, C. W. Yin, H. Zhu, S. H. Wu, H. T. Zhang, *Organometallics* **2009**, *28*, 3882–3888.
[16] Y. J. Wu, S. W. Wang, X. C. Zhu, G. S. Yang, Y. Wei, L. J. Zhang, H. B. Song, *Inorg. Chem.* **2008**, *47*, 5503–5511.
[17] W. Yi, J. Zhang, L. Hong, Z. Chen, X. Zhou, *Organometallics* **2011**, *30*, 5809–5814.
[18] D. Liu, D. Zhou, H. Yang, J. Li, C. Cui, *Chem. Commun.* **2019**, *55*, 12324–12327.
[19] H. A. Duong, M. J. Cross, J. Louie, *Org. Lett.* **2004**, *6*, 4679–4681.
[20] S. M. Raders, J. G. Verkade, *J. Org. Chem.* **2010**, *75*, 5308–5311.
[21] C. Li, W. Zhao, J. Hea, Y. Zhang, *Chem. Commun.* **2019**, *55*, 12563–12566.
[22] Z. Guo, Y. Xu, X. Wu, X. Wei, C. Xi, *Dalton Trans.* **2019**, *48*, 8116–8121.
[23] M. K. Barman, A. Baishya, T. Peddarao, S. Nembenna, *J. Organomet. Chem.* **2014**, *772–773*, 265–270.
[24] M. A. Bahili, E. C. Stokes, R. C. Amesbury, D. M. C. Ould, B. Christo, R. J. Horne, B. M. Kariuki, J. A. Stewart, R. L. Taylor, P. A. Williams, M. D. Jones, K. D. M. Harris, B. D. Ward, *Chem. Commun.* **2019**, *55*, 7679–7682.
[25] L. Orzechowski, S. Harder, *Organometallics* **2007**, *26*, 2144–2148.
[26] T. Rosen, Y. Popowski, I. Goldberg, M. Kol, *Chem. Eur. J.* **2016**, *22*, 11533–11536.
[27] S. Yadav, R. Dixit, M. K. Bisai, K. Vanka, S. S. Sen, *Organometallics* **2018**, *37*, 4576–4584.
[28] R. Kumar, S. Yadav, K. Gour, E. Sangtani, S. R. Dash, A. Raja, K. Vanka, R. G. Gonnade, S. S. Sen, *Chem. Asian J.* **2020**, *15*, 820–827.
[29] S. P. Sarish, A. Jana, H. W. Roesky, T. Schulz, D. Stalke, *Organometallics* **2010**, *29*, 2901–2903.
[30] S. Yadav, V. S. V. S. N. Swamy, R. Gonnade, S. S. Sen, *ChemistrySelect* **2016**, *5*, 1066–1071.
[31] S. Datta, M. T. Gamer, P. W. Roesky, *Dalton Trans.* **2008**, 2839–2843.
[32] S. R. Foley, Y. Zhou, G. P. A. Yap, D. S. Richeson, *Inorg. Chem.* **2000**, *39*, 924–929.
[33] F. Parodi, in *Comprehensive Polymer Science and Supplements*, **1989**, *5*, 387–412.
[34] H.-M. Wang, H.-X. Li, X.-Y. Yu, Z.-G. Ren, J.-P. Lang, *Tetrahedron* **2011**, *67*, 1530–1535.
[35] Deposition Numbers 2111877 (for **1**) and 2111874 (for **2**) contain the supplementary crystallographic data for this paper. These data are provided free of charge by the joint Cambridge Crystallographic Data Centre and Fachinformationszentrum Karlsruhe Access Structures service www.ccdc.cam.ac.uk/structures.

Manuscript received: December 23, 2021
Revised manuscript received: March 7, 2022
Accepted manuscript online: March 9, 2022
Version of record online: April 6, 2022